

# **Cellular Mechanisms During Vascular Development**

## **Inauguraldissertation**

zur  
Erlangung der Würde eines Doktors der Philosophie  
vorgelegt der  
Philosophisch-Naturwissenschaftlichen Fakultät  
der Universität Basel  
von

Yannick Ernst Henri Blum  
aus  
Basel, Schweiz

Basel, im März 2012

Genehmigt von der Philosophisch-Naturwissenschaftlichen Fakultät  
auf Antrag von

Prof. Dr. Markus Affolter  
(Dissertationsleiter)

Prof. Dr. Rolf Zeller  
(Koreferent)

Basel, den 14.12.2010

Prof. Dr. Martin Spiess  
(Dekan)



## Attribution-Noncommercial-No Derivative Works 2.5 Switzerland

---

**You are free:**



to Share — to copy, distribute and transmit the work

**Under the following conditions:**



**Attribution.** You must attribute the work in the manner specified by the author or licensor (but not in any way that suggests that they endorse you or your use of the work).



**Noncommercial.** You may not use this work for commercial purposes.



**No Derivative Works.** You may not alter, transform, or build upon this work.

- For any reuse or distribution, you must make clear to others the license terms of this work. The best way to do this is with a link to this web page.
- Any of the above conditions can be waived if you get permission from the copyright holder.
- Nothing in this license impairs or restricts the author's moral rights.

**Your fair dealing and other rights are in no way affected by the above.**

This is a human-readable summary of the Legal Code (the full license) available in German:  
<http://creativecommons.org/licenses/by-nc-nd/2.5/ch/legalcode.de>

**Disclaimer:**

The Commons Deed is not a license. It is simply a handy reference for understanding the Legal Code (the full license) — it is a human-readable expression of some of its key terms. Think of it as the user-friendly interface to the Legal Code beneath. This Deed itself has no legal value, and its contents do not appear in the actual license. Creative Commons is not a law firm and does not provide legal services. Distributing of, displaying of, or linking to this Commons Deed does not create an attorney-client relationship.

# 1 Table of content

<b>1</b>	<b>TABLE OF CONTENT</b> .....	<b>1</b>
<b>2</b>	<b>LIST OF ABBREVIATIONS</b> .....	<b>3</b>
<b>3</b>	<b>ABSTRACT</b> .....	<b>5</b>
<b>4</b>	<b>INTRODUCTION</b> .....	<b>6</b>
<b>4.1</b>	<b>Structure and formation of biological tubes</b> .....	<b>7</b>
4.1.1	Epithelial and endothelial cell polarity .....	7
4.1.2	Tube architectures .....	8
4.1.3	Tube formation mechanisms .....	8
<b>4.2</b>	<b>Vascular development</b> .....	<b>10</b>
4.2.1	The vascular system and the zebrafish as a model system .....	10
4.2.2	Vasculogenesis .....	11
4.2.2.1	<i>Origin and differentiation of endothelial cells</i> .....	11
4.2.2.2	<i>Dorsal Aorta, Cardinal Vein formation and arterial venous differentiation</i> .....	12
4.2.2.3	<i>Lumen formation during vasculogenesis</i> .....	13
4.2.2.4	<i>More anterior vessels</i> .....	14
4.2.3	Angiogenesis .....	15
4.2.3.1	<i>Sprout formation</i> .....	16
4.2.3.2	<i>Vessel outgrowth and guidance</i> .....	19
4.2.3.3	<i>Vessel anastomosis</i> .....	21
4.2.3.4	<i>Lumen formation</i> .....	22
4.2.3.5	<i>Vessel stabilization and integrity</i> .....	24
4.2.3.6	<i>Vessel remodeling</i> .....	25
<b>4.3</b>	<b>Aim of this thesis</b> .....	<b>27</b>
<b>5</b>	<b>MATERIALS AND METHODS</b> .....	<b>28</b>
<b>5.1</b>	<b>Molecular biology protocols</b> .....	<b>29</b>
5.1.1	Standard protocol .....	29
5.1.1.1	<i>Restriction enzyme digestion</i> .....	29
5.1.1.2	<i>Dephosphorylation with Alkaline Phosphatase</i> .....	29
5.1.1.3	<i>PCR mix</i> .....	29
5.1.1.4	<i>Agarose Gel</i> .....	29
5.1.1.5	<i>Gel extraction</i> .....	30
5.1.1.6	<i>Ligation</i> .....	30
5.1.1.7	<i>Transformation</i> .....	30
5.1.1.8	<i>Miniprep</i> .....	30
5.1.1.9	<i>Midiprep</i> .....	30
5.1.2	Plasmids.....	31
<b>5.2</b>	<b>Fish protocols</b> .....	<b>31</b>
5.2.1	Maintenance and strain.....	31
5.2.2	DNA and morpholino injecting.....	32
5.2.3	Generation of <i>flkl:EGFP-NLS</i> transgenic fish line.....	32
<b>5.3</b>	<b>Immunofluorescence and Live imaging</b> .....	<b>32</b>



5.3.1	Ab stainings.....	32
5.3.1.1	<i>Mounting and confocal microscopy of Ab stained embryos</i> .....	33
5.3.2	Live imaging (Leica Sp1 confocal microscope).....	33
5.3.3	Single cell labeling using Kaede .....	33
5.3.4	Live imaging with <i>fli1:GFF; UAS:EGFP-hZO1; UAS:RFP</i> embryos (Leica Sp5) .....	34
5.3.4.1	<i>QD-injection</i> .....	34
<b>6</b>	<b>RESULTS .....</b>	<b>35</b>
<b>6.1</b>	<b>Chapter I: Blum et al., 2008 .....</b>	<b>36</b>
<b>6.2</b>	<b>Chapter II: Distribution of different tube architecture in ISVs and the DLAV .....</b>	<b>37</b>
<b>6.3</b>	<b>Chapter III: Cellular mechanisms during ISV formation and anastomosis.....</b>	<b>41</b>
6.3.1	Cellular mechanisms during anastomosis .....	41
6.3.1.1	<i>Initial contact formation</i> .....	45
6.3.1.2	<i>Intracellular lumen formation</i> .....	45
6.3.1.3	<i>Extracellular lumen formation</i> .....	48
6.3.1.4	<i>Blood pressure is not important for initial contact formation and extracellular lumen formation but might be important for intracellular lumen formation</i> .....	50
6.3.2	Other mechanisms observed during ISV formation .....	51
6.3.2.1	<i>EGFP-hZO1 during cell division</i> .....	51
6.3.2.2	<i>Endothelial cells undergo intercalation and cell self fusion</i> .....	54
<b>7</b>	<b>DISCUSSION .....</b>	<b>57</b>
<b>7.1</b>	<b>Different tube architectures in ISVs .....</b>	<b>58</b>
<b>7.2</b>	<b>Cellular mechanisms during sprouting angiogenesis and anastomosis .....</b>	<b>59</b>
7.2.1	Some considerations on using <i>fli1:GFF; UAS:EGFP-hZO1</i> transgenic fish .....	59
7.2.2	Contact formation.....	60
7.2.3	Lumen formation.....	62
7.2.3.1	<i>Intracellular lumen formation</i> .....	62
7.2.3.2	<i>Extracellular lumen formation</i> .....	64
7.2.4	Cell division during vascular development .....	66
7.2.5	Intercalation and cell self fusion.....	70
<b>7.3</b>	<b>Conclusions .....</b>	<b>71</b>
<b>8</b>	<b>ACKNOWLEDGMENT .....</b>	<b>72</b>
<b>9</b>	<b>APPENDIX.....</b>	<b>73</b>
<b>10</b>	<b>REFERENCES.....</b>	<b>74</b>

## 2 List of abbreviations

A	Adenin
AA	Aortic arches
Ab	Antibody
AJ	Adherens junctions
ALPM	Anterior lateral plate mesoderm
Ang	Angiopoetin
ASIM	Apical membrane initiation site
Bmp	Bone morphogenetic protein
BSA	Bovine serum albumine
C	Cytosin
CCM	Cerebral cavernous malformations
CDH-5	Vascular endothelial cadherin
CXCL	CXC (motif) chemokine ligand
CXCR	CXC (motif) receptor
DA	Dorsal aorta
DLAV	Dorsal longitudinal anastomotic vessel
Dll	Delta like
DNA	Deoxyribonucleic acid
dpf	Days post fertilization
EC	Endothelial cell
ECM	Extracellular matrix
E. coli	Escherichia coli
Efnb2	EphrinB2
EGFP	Enhanced GFP
EPC	Endothelial precursor cell (angioblast)
Ephb4	Ephrin receptor B4
ERM	Ezrin, radixin and moesin
Fli	Friend leukemia integration
Flk	Fetal liver kinase
Flt	fms related tyrosin kinase
G	Guanosine
GFP	Green florescent protein
HIF	Hypoxia inducible factor
hpf	Hours post fertilization
HUVEC	Human umbilical vein endothelial cells
IA	Intussusceptive angiogenesis
ISV	Intersegmental vessel
Kdr	Kinase insert domain receptor
LDA	Lateral dorsal aorta
LPM	Lateral plate mesoderm
MAPK	Mitogen-activated protein kinase
MCS	Multiple cloning site
MDCK	Madin-Darby canine kidney (cells)
MMP	Matrix metalloproteinases
MO	Morpholino
MOC	Midbrain organizing center
NEB	New England Biolab
NGS	Normal goat serum
NLS	Nuclear localization signal
<i>obd</i>	<i>out of bound</i>
PAP	Pre-apical patch
PAR	Partitioning defective

---

PBS	Phosphate-buffered saline
PBST	Phosphate-buffered saline-Tween 20
PBSTX	Phosphate-buffered saline-Tween 20- Triton-X 100
PCR	Polymerase chain reaction
PCV	Posterior cardinal vein
PDXL	Podocalyxin
PFA	Paraformaldehyde
PHD	Prolyl hydroxylase domain
PKC	Protein kinase C
plcg1	Phospholipase C $\gamma$
PLGF	Placental growth factor
PLPM	Posterior lateral plate mesoderm
PTU	Propylthiouracil
QD	Quantum dots
Q-H <sub>2</sub> O	Quartz water
RFP	Red fluorescent protein
ROC	Rostral organizing center
RTK	Receptor tyrosine kinase
SAP	Shrimp Alkaline Phosphatase
scl	Stem-cell leukaemia
Shh	Sonic hedgehog
<i>sih</i>	<i>silent heart</i>
SV40	Simian virus 40
T	Thymin
TEM	Transmission electron microscopy
Tie	Tyrosine kinase with immunoglobulin-like and EGF-like domains
TJ	Tight junctions
UAS	Upstream activating sequence
UV	Ultra violet
VE-cadherin	Vascular endothelial cadherin
VEGF	Vascular endothelial growth factor
VEGFR	Vascular endothelial growth factor receptor
Vpf	Vascular permeability factor
ZO	Zonula occludens

### 3 Abstract

The vascular system is an essential organ in vertebrate animals and provides the organism with enough oxygen and nutrients. It is composed of an interconnected network of blood vessels, which form using a number of different morphogenetic mechanisms. Angiogenesis describes the formation of new blood vessels from preexisting vessels. A number of molecular pathways have been shown to be essential during angiogenesis. However, cellular architecture of blood vessels as well as cellular mechanisms involved during vessel formation and anastomosis have remained largely unknown.

The intersegmental vessels (ISVs) of the developing zebrafish embryo have served as a paradigm to study angiogenesis *in vivo*. ISVs sprout bilaterally from the dorsal aorta (DA) in the zebrafish trunk, grow dorsally and ultimately connect with adjacent ISVs on the dorsal side of the trunk forming the dorsal longitudinal anastomotic vessel (DLAV).

We used antibody labeling of endothelial cell-cell junctions, single cell labeling and live-imaging of junctions to investigate cellular architecture and mechanisms during ISV formation and anastomosis. In contrast to previous studies, we found that a large part of ISVs consist of multicellular tubes where the lumen is surrounded by several cells. Seamless tubes with an intracellular lumen are predominantly found in the DLAV. In addition, we found distinct cellular mechanisms to be involved in ISV anastomosis, forming seamless or multicellular tubes respectively. These results show that endothelial cells are rather plastic and can use different mechanisms to form functional blood vessels.

# 4 Introduction

## 4.1 Structure and formation of biological tubes

Biological tubes are found in many different varieties in the animal kingdom, such as the gut, the lung, the kidney, the vascular system or the tracheal system of insects. Even though these tubes fulfill different tasks, they all consist of polarized epithelial or endothelial tubes and many of them undergo branching morphogenesis.

### 4.1.1 Epithelial and endothelial cell polarity

Cells building a polarized tube have different membrane compartments. The apical membrane is facing the inside of the tube (the lumen). The basal membrane is facing the outside, often forming a basal lamina consisting of a dense network of extracellular matrix (ECM) proteins. The lateral membrane is where epithelial cells are interconnected via several types of junctional complexes. For some specialized epithelium such as the endothelium, where cells do not have the typical cuboidal shape but are rather elongated and thin, the lateral membrane is nonexistent and apical and basal membrane are only separated by junctional proteins (Dejana et al., 2009). The different types of junctions can be located more to the apical or more to the basal side of the lateral membrane. For most epithelia, adherens junctions (AJ) are located to the basal side, whereas tight junctions (TJ) are located towards the apical side. One exception are epithelia of *Drosophila melanogaster*, where AJ are subapical and TJ, in *Drosophila* termed septate junctions, basal to the AJs (Figure 4.1 A and B; (Andrew and Ewald, 2010)). In endothelial cells (EC) AJs and TJs are thought to be intermingled and not clearly separated (Figure 4.1C; (Bazzoni and Dejana, 2004)).

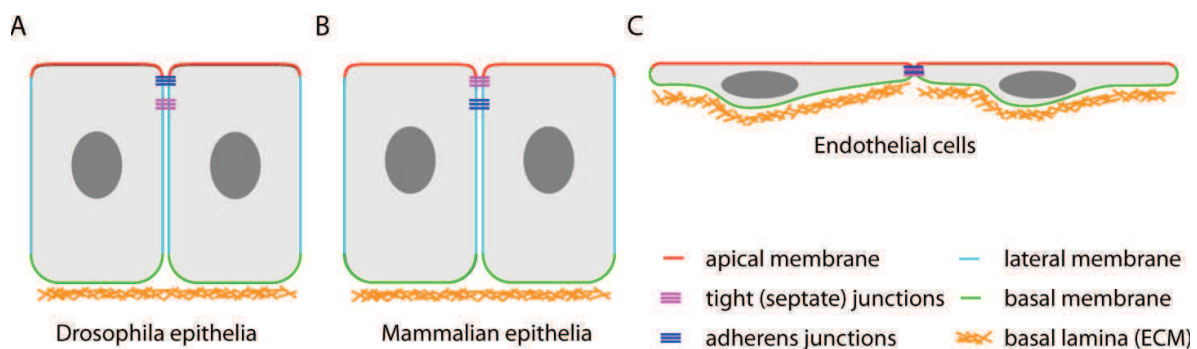


**Figure 4.1**

**Epithelial cells:** Scheme shows basic distribution of membranes and junctions in epithelial and endothelial cells. While epithelial cells have a rather cuboidal shape (A and B), endothelial cells have a flat and elongated shape (C). The apical membrane (red) is facing the lumen and the basal membrane (green) is facing the outside and often contacts a basal lamina (orange). Epithelial cells have a lateral membrane (blue) between the apical and the basal membrane. Due to their thin morphology EC lack the lateral membrane. AJ and TJ maintain integrity and control permeability of the epithelium. In mammalian epithelia TJ are located to the apical side and AJ to the basal side, whereas in epithelia of *Drosophila melanogaster* AJ are located towards the apical side. It is thought that junctions between EC are intermingled without a clear border between AJ and TJ.

### 4.1.2 Tube architectures

Different types of tubes and different mechanisms to form these have been described in the past (Lubarsky and Krasnow, 2003). The most prominent tube morphology is the multicellular tube where several cells are organized around the lumen resulting in an extensive network of junctions connecting these cells (Figure 4.2 A). Two types of unicellular tubes (only one cell around the lumen) have been described. In tubes with autocellular junctions, one cell reaches around the lumen and makes contact with itself. This is then seen as a single line of junctions (Figure 4.2 B). Such tubes are found in the tracheal system of *Drosophila melanogaster* (Ribeiro et al., 2004) and in a few specialized cells of the excretory tract in *C. elegans* (Stone et al., 2009). The second kind of unicellular tubes do not have junctions along the long axis of the tube-forming cell and are thus also called seamless or intracellular tubes (Figure 4.2 C). Such tubes are found in the terminal cells of the tracheal system, in the *C. elegans* digestive tract (Rasmussen et al., 2008) as well as in the vascular system (Wolff and Bar, 1972).

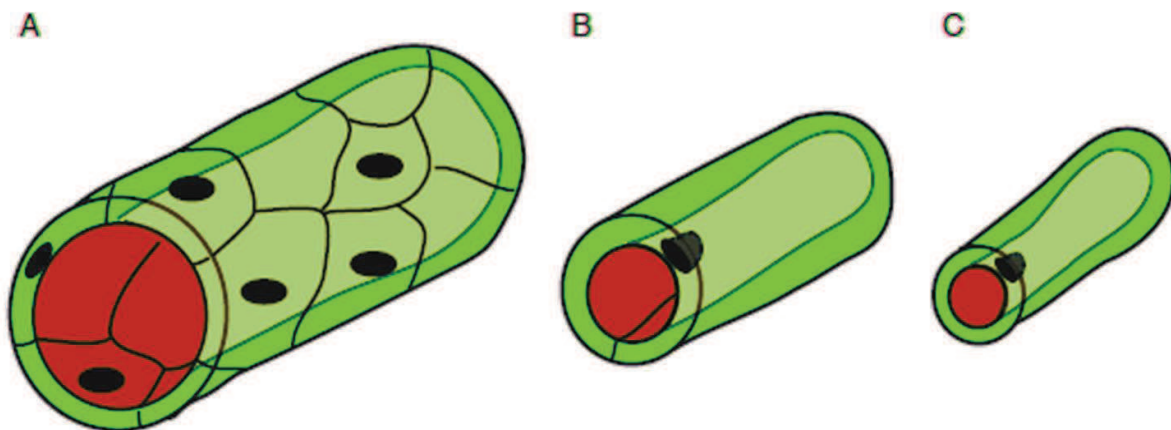


**Figure 4.2**

**Different tube architectures:** Three basic architectures of tubes have been described: (A) multicellular tubes: several epithelial cells organize around the circumference of the lumen. This results in a characteristic meshwork of junctions. (B) Unicellular tubes with autocellular junctions: the lumen is formed by a single cell sealed along the tube axis with an autocellular junction. (C) Seamless tubes: the lumen is within a cell without junctions along the tube resulting in an intracellular lumen (Baer et al., 2009).

### 4.1.3 Tube formation mechanisms

There are different mechanisms controlling the development of these tubes: An already polarized epithelial layer can undergo *wrapping* by first forming a groove along an axis where eventually the edges of the groove will seal and form a tube separated from the rest of the epithelial layer. This mechanism is found in neural tube development of various species (Figure 4.3 A;(Colas and Schoenwolf, 2001)). During *budding* a new tube grows from a preexisting epithelial tube. During this process, cells remain polarized and the lumen of the

growing tube is extended as the tube extends (Figure 4.3 B). This mechanism is used for many branching processes such as vascular, tracheal or lung branching morphogenesis (Adams and Alitalo, 2007; Metzger et al., 2008; Samakovlis et al., 1996a). The next two mechanisms do not involve a pre-polarized epithelium but aggregates or cords of cells. During *cavitation* a thick cord of cells forms a tube by eliminating cells inside the cord and polarizing the outer ones (Figure 4.3 C). During *cord hollowing* a rather thin cord of cells is transformed in an epithelial tube by polarizing all available cells (Figure 4.3 D). Examples are found in the vascular system (Jin et al., 2005; Strlic et al., 2009). *Cell hollowing* will create a lumen spanning through a single cell resulting in the above mentioned intracellular lumen (Figure 4.3 E). Such a lumen can be formed by the invagination and the fusion of apical membranes as seen in the fusion cells of the tracheal system of *Drosophila melanogaster* (Samakovlis et al., 1996a) or by the formation of large vacuoles as proposed for parts of the zebrafish vasculature (Kamei et al., 2006). A third possibility is the self-wrapping of a single cell resulting in an auto-cellular junction with subsequent cell self-fusion, thereby generating a seamless tube. Such a mechanism has been identified in the *C.elegans* digestive tract and requires specific fusogenic proteins (Figure 4.3 F; (Rasmussen et al., 2008)). *Budding, cord hollowing* and *cell hollowing* are the important mechanisms during vascular development.

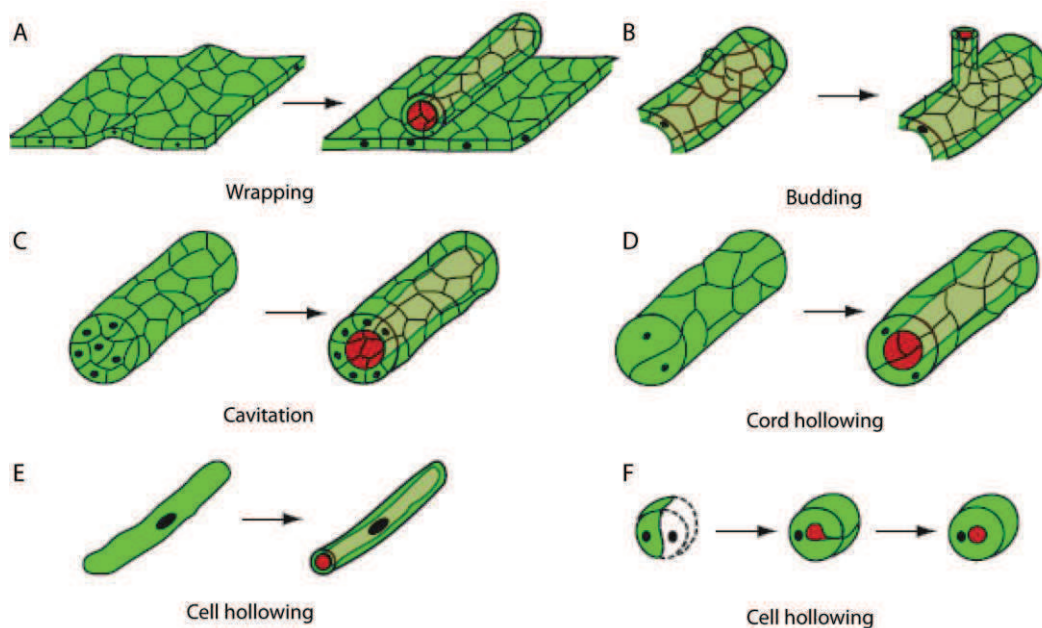


**Figure 4.3**

**Cellular mechanisms involved in lumen formation:** A number of mechanisms used to form biological tubes. (A) *Wrapping*: An epithelial sheet invaginates along the future tube axis until the edges meet and the tube separates from the sheet. (B) *Budding*: a new tube is formed from an existing tube maintaining polarity. (C) *Cavitation*: Cells in the middle of a cord of cells are eliminated. Concomitantly, the outer cells are polarized thereby forming a tube. (D) *Cord hollowing*: All cells in a cord of cells polarize and form a tube. (E) *Cell hollowing*: a lumen is formed in a single cell by the formation of vacuoles or by invagination of apical membrane. (F) A special variation of cell hollowing, is the wrapping of a single cell and subsequent cell-self fusion (Baer et al., 2009).



## 4.2 Vascular development

### 4.2.1 The vascular system and the zebrafish as a model system

In the vertebrate kingdom the vascular system ensures the supply of oxygen and nutrients as pure diffusion cannot fulfill this task in larger animals. Performing this task, it is one of the first organs to develop in vertebrate systems as it is not only important for the maintenance of other organs, but also for the proper development of these organs.

Before it can do so, the vascular system has to develop and form an extensive network of vessels and capillaries. The vascular system is built up by endothelial cells (EC), which have to undergo a number of activities such as cell migration, cell rearrangement, cell polarization, cell shape change and cell division to guarantee proper development and function. If all these cellular mechanisms are correctly coordinated, morphogenetic events such as vessel sprouting, fusion and lumen formation occur in a proper way.

During the last decades a number of molecular pathways have been shown to be essential for vascular development, the most prominent one being VEGF (vascular endothelial growth factor).

Different model systems have been used to study the vascular system such as mouse, chicken and cell culture systems. In more recent years, the zebrafish has proved to be an excellent model organism to study vascular development. Many aspects of vascular development and anatomy are conserved among vertebrates. For instance, early vascular anatomy in mice and zebrafish is similar including the dorsal aorta (DA), intersegmental vessels (ISVs) and the dorsal longitudinal anastomotic vessel (DLAV) (Figure 4.4). Due to its optical clarity and experimental accessibility, the zebrafish embryo is especially well suited for morphogenetic analysis using live imaging techniques. Endothelial specific transgenic lines such as the *fli1a:GFP* line and microangiography (the injection of a fluorescent dye into the circulation) have greatly contributed to our knowledge of vascular anatomy and development of the zebrafish (Isogai et al., 2001; Isogai et al., 2003).

Another advantage of the zebrafish when studying vascular development is the fact that the zebrafish embryo survives up to 5 days post fertilization (dpf) without a functional vascular system as enough oxygen is supplied by simple diffusion. This allows the analysis of cardiovascular mutants, which would not be possible in mice due to early lethality.

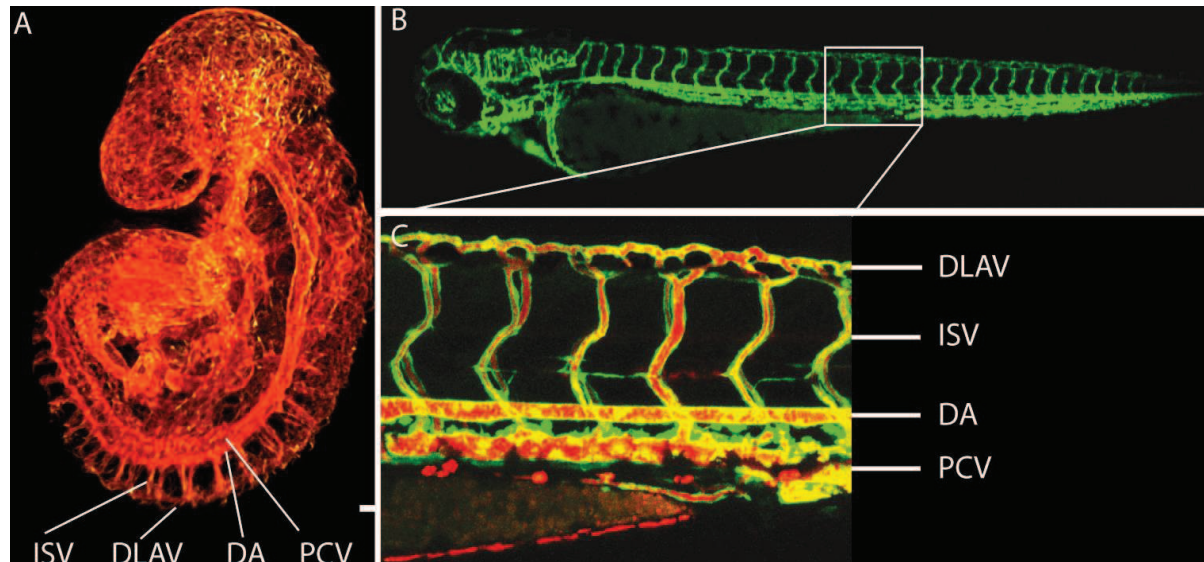


**Figure 4.4**

**Conserved vascular anatomy:** A number of vessels such as the dorsal aorta (DA), the intersegmental vessels (ISV) and the dorsal longitudinal vessel (DLAV) are conserved in the early embryo of mouse (A) and zebrafish (B and C) (Ellertsdottir et al., 2010; Walls et al., 2008).

## 4.2.2 Vasculogenesis

Vascular development is usually subdivided into two processes, where the initial formation of a primary network of vessels from endothelial precursor cells (EPC or angioblast) is termed vasculogenesis, and the subsequent formation of new blood vessels from this primary network, which leads to the formation of a fine network of capillaries, is called angiogenesis.

### 4.2.2.1 Origin and differentiation of endothelial cells

Vasculogenesis can be subdivided into three steps: first angioblasts are differentiated from the mesoderm; second, angioblasts migrate and assemble to form cord-like structures, and third, a lumen is formed creating an endothelial tube.

The development of the primary vessels is tightly linked with primitive hematopoiesis. Since a long time it has been suggested that endothelial cells and hematopoietic cells arise from a common progenitor called hemangioblast (Risau and Flamme, 1995). Fate mapping studies in zebrafish revealed that at least some endothelial cells and hematopoietic cells arise from common hemangioblasts (Vogeli et al., 2006; Warga et al., 2009).

In zebrafish, angioblasts differentiate from the lateral plate mesoderm. On the one hand angioblasts that originate from the anterior lateral plate mesoderm (ALPM) give rise to the cranial vasculature and, on the other hand, angioblasts that originate from the posterior

lateral plate mesoderm (PLPM) will form the main trunk vessels, the dorsal aorta and the cardinal vein (Jin et al., 2005; Proulx et al., 2010).

A set of factors such as Bmp, Fli1, an unknown factor encoded by the gene *cloche* and Scl are needed to differentiate the ventral mesodermal cells to angioblasts/hemangioblasts and later to endothelial cells (Gupta et al., 2006; Liao et al., 1998; Liao et al., 1997). Activation of Scl triggers genes such as *vegfr-2* (also known as *flk1*), the ets transcription *fli1* and *gata1*. Later cells acquire a unique combination of *scl/flk* expression, which segregates endothelial cells (*flk1<sup>+</sup>/scl<sup>+</sup>*) from hematopoietic cells (*flk1<sup>+</sup>/scl<sup>-</sup>*) (Gering et al., 1998).

Sonic hedgehog (Shh) is expressed in the zebrafish notochord and triggers transcription of *vegf* (vascular endothelial growth factor), the main growth factor acting on endothelial cells (Lawson et al., 2002). Interestingly, VEGF does not seem to be essential for the migration of angioblasts from the LPM to the midline but is required for the differentiation of angioblasts to arterial ECs (Jin et al., 2005). This is in contrast to mouse and *Xenopus* where VEGF is essential for the migration and formation of the primary vessels (Carmeliet et al., 1996; Cleaver and Krieg, 1998).

#### 4.2.2.2 Dorsal Aorta, Cardinal Vein formation and arterial venous differentiation

Angioblasts migrate in two waves, where the first wave starts to migrate at 14hpf and the second wave at 16hpf. The first wave aggregates at the midline between the endoderm and the notochord. These cells are not yet polarized and initially do not form junctions among each other. Starting at 17hpf these cells start to form adherens junctions and to polarize, eventually forming a patent vessel. During this process, endothelial cells change their cell shape from a cuboidal to an elongated shape. At 30hpf, when circulation is established, junctional proteins such as ZO-1 are present in the DA and in the posterior cardinal vein (PCV) (Jin et al., 2005).

Although it was initially thought that the PCV forms via the same mechanism using the second wave of angioblasts, new insight suggests that only one EC cord is formed at the midline, from which cells fated to be venous segregate and sprout ventrally to form the PCV. This so called selective cell sprouting mechanism is impaired if arterial-venous differentiation is defective (Herbert et al., 2009).

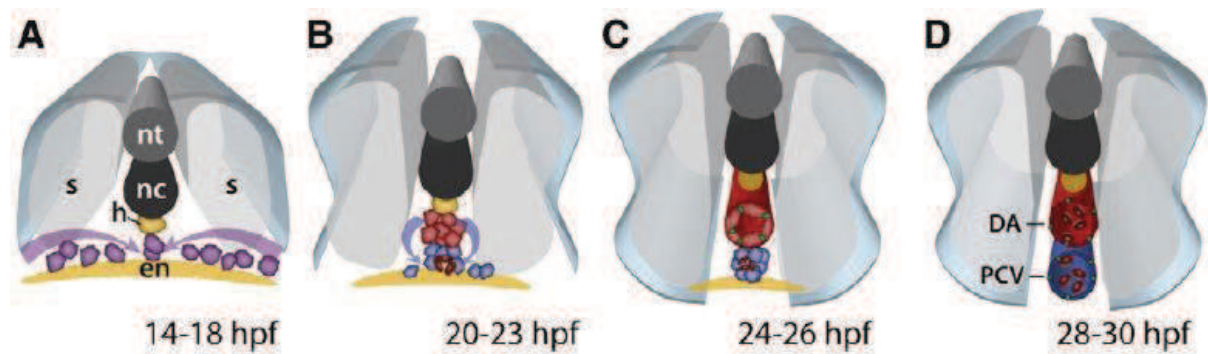


**Figure 4.5**

**Vasculogenesis in the zebrafish embryo:** (A) Endothelial cells differentiate from the lateral plate mesoderm and migrate to the midline just above the endoderm (en). (B) Cells aggregate into a cord at the midline. (C-D) From there venous fated cells segregate ventrally and engulf blood cells, thereby forming the posterior cardinal vein (PCV). The dorsal aorta (DA) forms by cord hollowing (Ellertsdottir et al., 2010). s: somite, nc: notochord, nt: neural tube.

Arterial and venous ECs have to fulfill different tasks and were initially thought to be defined by different directions of blood flow. However, recent evidence strongly suggests that the differences are genetically specified and determined before onset of blood circulation (Lawson and Weinstein, 2002a). One of the first evidence for molecular differences in arteries and veins came from a study in the mouse embryo. This study described the differential expression of the EphrinB2-EphB4 ligand receptor pair in arteries and vein. While the ligand EphrinB2 is only expressed in the arteries, the level of expression of the receptor EphB4 is much higher in the vein (Wang et al., 1998). Since the discovery of these first markers, a whole set of markers and pathways have been discovered, which ensures the identity of arteries or veins. Shh signaling from the notochord activates VEGF in the somites, which in turn activates Notch signaling in arteries due to their closer proximity to the VEGF signal (Lawson et al., 2002). Notch signaling activates EphrinB2 and, via Hey/Gridlock, suppresses EphB4 (Lawson et al., 2001; Zhong et al., 2001; Zhong et al., 2000). Venous fate was initially thought to be the ground state of ECs but recent studies discovered COUP-TFII as a transcription factor that represses Notch signaling and thereby actively inhibiting arterial differentiation (Swift and Weinstein, 2009; You et al., 2005).

In the case of selective cell sprouting described above, changing EphrinB2-EphB4 levels and their upstream regulators leads to segregation of all or none of the ECs to venous or arterial fate respectively (Herbert et al., 2009).

#### 4.2.2.3 Lumen formation during vasculogenesis

It is thought that the lumen is formed by a cord hollowing process. Not many factors are known to be essential for lumen formation of the zebrafish DA and PCV. EGFL7 has been shown to be required (Parker et al., 2004), but mechanistic insight is lacking. Recent studies

have revealed the molecular basis of lumen formation of the DA in the mouse embryo. Similar to the zebrafish, ECs form cords, which are subsequently lumenized. Initially ECs have junctions at multiple positions (sheet of junctions) along their cell-cell contact. In a second step proteins of the CD34-sialomucin family (CD34 and Podocalyxin (PDXL)) are recruited to the EC cell-cell contact demarking the future apical membrane. The antiadhesive extracellular domain of the CD34-sialomucin is important to separate the apposing apical membranes from each other. Ve-cadherin is essential for the recruitment of CD34 and PDXL to the apical membrane. Moesin, a member of the ERM protein family, is phosphorylated by PKC (protein kinase C) and recruits F-actin to the apical membrane. A VEGF driven activation of non muscular myosin II initiates EC shape changes and completes vascular lumen formation (Strilic et al., 2009).

A recent study in zebrafish implicates moesin1 in ISV lumen formation, vessels, which form via angiogenesis (see below). The dorsal aorta seems to be unaffected as injected dye spreads in the dorsal aorta but not in the ISVs. More molecular markers will be needed in the zebrafish to prove or disprove a similar mechanism for the lumen formation in the DA of the zebrafish embryo (Wang et al., 2010).

#### **4.2.2.4 More anterior vessels**

The trunk vessels of the zebrafish are the best characterized as the trunk is rather thin and easy to image. But vessels at different locations in the embryo may utilize different mechanism. Anterior to the zebrafish trunk, the DA splits in two bilateral vessels named lateral dorsal aorta (LDA) (Isogai et al., 2001). Recent work shows, that LDA development is dependent on the endoderm (Siekmann et al., 2009), whereas in the trunk the endoderm only delays the development of the DA (Jin et al., 2005). The endoderm is expressing the chemokine ligand CXCL12 and the ECs in the region of the LDA, but not ECs in the DA, express the receptor CXCR4. Mutants for *cxcr4* do not complete formation of the LDA and connection to the DA (Siekmann et al., 2009).

In the head region, the ALPM produces two so called organizing centers, the rostral (ROC) and the midbrain organizing center (MOC). Whereas the ROC will form the anterior part of the cranial vasculature, the MOC will form the vessels around the midbrain and hindbrain. In contrast to the angioblasts of the PLPM, these angioblasts do not migrate to the midline to form a single cord at the midline (except for cells of the MOC, which will give rise to endocardial cells), but rather stay as bilateral stripes to form the appropriate cranial vessels. Still, angioblasts of the ROC and MOC are rather motile and migrate in an angiogenic way to form the vessels. It's not clear yet at what time point these angioblasts become polarized endothelial cells and form endothelial tubes. Eventually, the vessels of the ROC and MOC will join completing the primary vascular system (Proulx et al., 2010).



### 4.2.3 Angiogenesis

After the primary vessels have formed via the process of vasculogenesis, new vessels form via angiogenesis, a process which involves several cellular activities such as cell migration, cell division, cell rearrangement, anastomosis and lumen formation.

Angiogenesis has gained particularly high attention since it was first described in the 1970 due to its relevance in pathological situations. Especially the fact that angiogenesis is essential for the growth of tumors and for metastasis in cancer pathologies (Ausprunk and Folkman, 1977; Folkman, 1971; Folkman, 1982; Proulx et al., 2010), let the field to explode.

Two model systems have emerged and showed to be particularly useful to study angiogenesis *in vivo*. One is the retinal vasculature of the mouse as its development occurs after birth, and is thus more accessible. The second one are the intersegmental/intersomitic vessels (ISVs) of the zebrafish due to its reproducible pattern and optical clarity of the fish, allowing extensive live imaging studies.

ISVs form a regular pattern in the zebrafish trunk, positioned at each somite boundary. The formation of ISVs has been described in detail by Isogai et.al. in 2003. In an initial step ISVs sprout bilaterally from the DA at each somite boundary at around 22 hpf (Figure 4.6 A,A'). There is an anterior to posterior delay of sprouting, with more anterior ISVs sprouting earlier. ISVs sprouts subsequently grow dorsally following the somite boundary up to the midline where they take a more direct path towards the dorsal side of the embryo. Once the ISVs reach the dorsal part of the neural tube, they stop growing dorsally and start to make projections in anterior and posterior direction, eventually meeting and connecting with their neighbouring ISVs at around 30 hpf (Figure 4.6 B,C,B',C'). These first loops consist of ISVs exclusively connected to the DA and are thus not suitable to build up circulation (Isogai et al., 2003). Therefore, connections to the PCV are established in a second step. New sprouts emerge from the PCV approximately at 36 hpf and grow dorsally (Figure 4.6 D,D'). The number of sprouts and the timing of sprouting is not as stereotyped as for the initial sprouting from the DA. The venous sprouts grow adjacent to existing ISVs, where they either connect to the ISV forming a venous ISV, or they contribute and form the parachordal vessel, a primordium for the lymphatic vessels (Hogan et al., 2009a; Yaniv et al., 2006) (Figure 4.6 E,E'). The distribution of arterial and venous ISVs is not regular except for the first 5 sets of ISVs. The distribution is likely a result of adaptation to hemodynamic forces in each individual embryo and thus changes from embryo to embryo (Isogai et al., 2003).

This process requires different steps, like sprout formation, vessel growth and guidance, fusion and lumen formation as well as vessel stabilization and regression. All of these steps need molecular control and a variety of factors to occur properly.

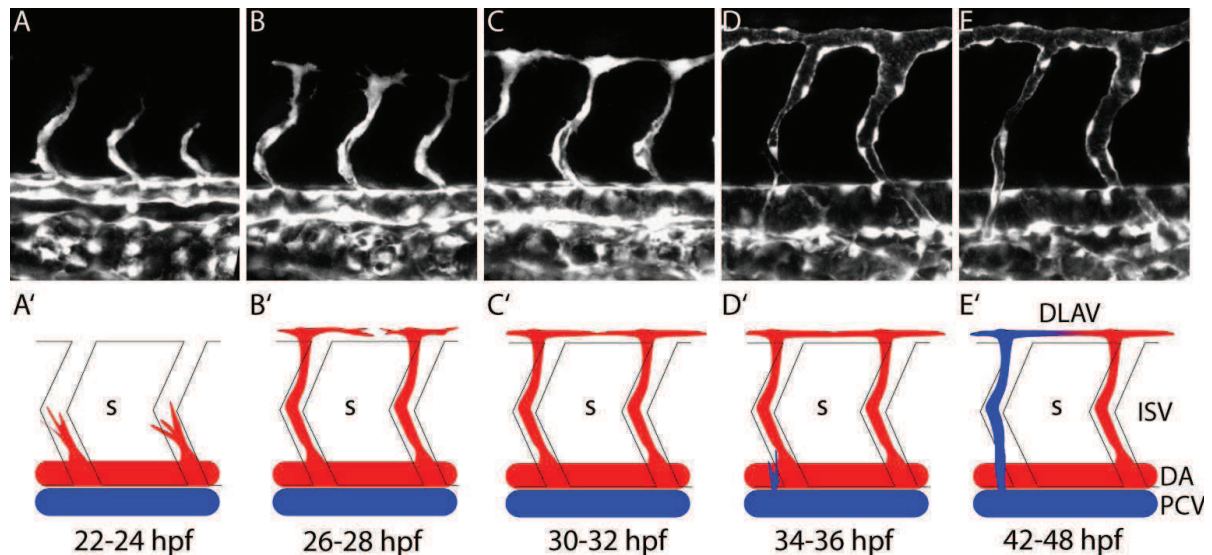


**Figure 4.6**

**Formation of intersegmental vessels (ISVs):** ISVs form at each somite (s) boundary and elongate towards dorsal following the somite boundaries (A,A'). Once they reach the dorsal side they form protrusions and filopodia in anterior and posterior directions (B,B'). Eventually ISVs anastomose forming the DLAV (C,C'). From 35 hpf onward sprouts from the PCV form (D,D'). Some of these sprouts eventually connect with existing arterial ISV turning them into venous ISVs forming circulatory loops in ISVs (E,E') (modified from Isogai et al., 2003).

#### 4.2.3.1 Sprout formation

When it comes to the formation of a new vessel, a leading cell is determined, usually referred as the tip cell, which guides vessel outgrowth along the correct path.

Even though some vessels such as ISVs may form during early development according to an inherent blueprint established by a genetic cascade of signaling, the vasculature has to react to needs of oxygen and nutrients in the surrounding tissue. Nature has selected for a clever system to react upon oxygen shortage by utilizing a  $O_2$  sensing system. This system consists of the transcription factors Hypoxia Inducible Factor  $\alpha$  1-3 (HIF $\alpha$  1-3) and the Prolyl Hydroxylase protein Domain (PHD1-3). PHDs are the  $O_2$  sensing proteins and during normoxia they use  $O_2$  to hydroxylate proline residues on the HIF-1 $\alpha$  protein. These residues are then recognized by the von Hippel Lindau (VHL) protein, which targets HIF-1 $\alpha$  to the proteasome for degradation. Under hypoxic conditions  $O_2$  levels are not high enough for hydroxylation of HIF1- $\alpha$  and HIF1- $\alpha$  can thus, together with HIF1- $\beta$ , a non regulatory subunit, activate downstream targets (Fraisl et al., 2009; Hanze et al., 2007). Importantly, one of the major target genes is *vegf* (Liu et al., 1995), important for many angiogenic behaviors of ECs and the formation of new vessels (see also Figure 4.7 A).

VEGF was initially discovered as Vp1 (vascular permeability factor 1) (Senger et al., 1983), and later cloned by Ferrara and colleagues in 1989 and termed VEGF (Leung et al., 1989).

VEGFs and their tyrosine kinase receptors (VEGFR) are likely the most important regulators of angiogenesis and vascular development. The family includes five ligands, VEGF-A (or just VEGF), VEGF-B, VEGF-C, VEGF-D and Placental Growth Factor (PLGF). All these ligands bind with different specificity to the three main receptors, VEGFR-1 (also called fms-like tyrosine kinase 1 (Flt1)), VEGFR-2 (also known as kinase insert domain receptor (KDR) in human, fetal liver kinase 1 (Flk1) in mouse or KDR-like (KDRI) in zebrafish) and VEGFR-3 (or Flt4). In addition Neuropilin 1 and 2 can act as co-receptors (Olsson et al., 2006). VEGF signaling via VEGFR-2 is responsible for activating angiogenic behavior in ECs. VEGFR-2 signals via different downstream pathways including the phospholipase C (PLC) $\gamma$ / protein kinase C (PKC)- MAP-kinase pathway and the phosphoinositide 3-kinase (PI3K)-Akt pathway, thereby regulating EC proliferation, migration, survival and permeability (Lohela et al., 2009). In contrast, VEGFR-1 has high affinity to the VEGFs but low tyrosine kinase activity and thus serves as a VEGF trap. Studies have shown that mice lacking the tyrosine kinase domain of VEGFR-1 are viable and show a normal vasculature, whereas knockout mice lacking the complete function of VEGFR-1 die early due to disorganized vessels and an excess of ECs (Fong et al., 1995; Hiratsuka et al., 2005). VEGF-C mostly signals through VEGFR-3 and is important for venous sprouting and for lymphangiogenesis but has also been implicated in potentiating VEGFR-2 signaling during angiogenesis (Covassin et al., 2006; Hogan et al., 2009b; Karkkainen et al., 2004; Tammela et al., 2008).

Correct VEGF levels are essential for proper angiogenesis as VEGF heterozygous mutant mice die during embryogenesis due to abnormal vascular development. In contrast, heterozygous mutants for the receptors VEGFR-1 and 2 are viable and show a normal vasculature (Carmeliet et al., 1996; Ferrara et al., 1996).

Studies in the mouse retinal system have shown that a gradient of VEGF is essential to specify a normal amount of tip cells. Changing the amount or the gradient of VEGF results in loss or gain of tip cell identity (Gerhardt et al., 2003). A recent study shows that tip cell selection is dependent on relative amounts of VEGFR-1 and VEGFR-2. In chimeric assays *in vitro* and *in vivo* using heterozygous cells for VEGFR-1 or 2, VEGFR-1 heterozygous cells show a higher probability to contribute to tip cells (VEGF signaling is higher due to lack of one copy of VEGFR-1), whereas VEGFR-2 heterozygous cells contribute more to stalk cells (Jakobsson et al., 2010). VEGF signaling activates Dll4, which activates Notch in neighboring cells. Notch signaling down-regulates VEGFR-2 and 3, but up-regulates VEGFR-1. This means that Notch signaling limits angiogenic behavior of cells next to tip cells. Thus cells sensing the highest amount of VEGF will become tip cells and via Notch instruct its neighboring cells to become stalk cells. Losing a single *dll4* allele or loss of Notch results in increased sprout formation and increased number of tip cells (Hellstrom et al., 2007; Lobov et al., 2007; Suchting et al., 2007; Tammela et al., 2008) (Figure 4.7 B).



Similar studies in zebrafish showed that upon suppressing the Notch pathway in *dll4* knockdown embryos or with chemical inhibitors, ISVs show excessive filopodia formation and at later stages increased vessel formation in the DLAV and other regions such as the gut vasculature (Leslie et al., 2007). In addition, down-regulation of the Notch pathway, results in increased EC number and proliferation (Leslie et al., 2007; Siekmann and Lawson, 2007).

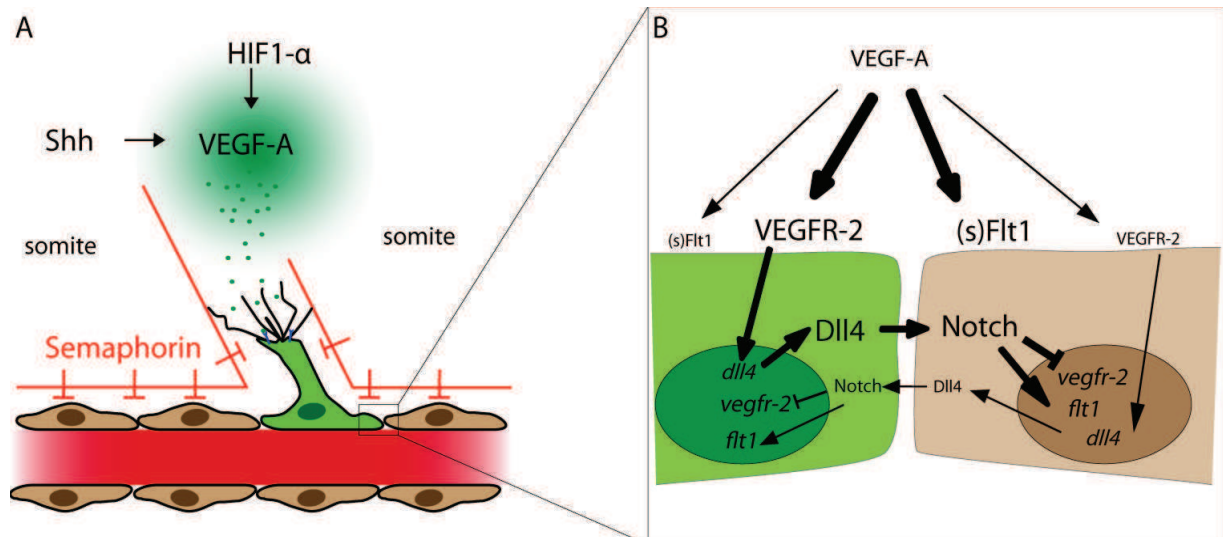


**Figure 4.7**

**Tip cell selection:** (A) VEGF-A via its receptor VEGFR-2 will activate ECs and form angiogenic sprouts. VEGF can be activated upon hypoxia by activation of HIF1- $\alpha$  or by other means such as Shh in the developing zebrafish embryo (Lawson). (B) Lateral inhibition through Notch signaling limits number of sprouts by selecting for tip and stalk cells. The tip cell sense a higher degree of VEGF signaling, which in turn will increase production of Dll4 and result in stronger Notch signaling in neighboring cells. Notch will inhibit transcription of *vegfr-2* and activate transcription of the VEGF trap *flt-1* and its soluble variant. In addition sprout formation in the zebrafish ISVs is also limited by Semaphorin-Plexin interaction from the somite(A) (Phng et al., 2009).

In the zebrafish trunk, sprout formation is restricted to the somite boundaries. This is achieved by PlexinD1 signaling, which accounts for the *out of bound (obd)* mutant phenotype in zebrafish. The receptor PlexinD1 is expressed in ECs whereas the ligand, Semaphorin3a, is expressed in somites. Upon ligand binding of Sema3a to the receptor PlexinD1, a repulsive signal is activated, inhibiting ECs to move in the somite region and thus restricting the sprout to the somite boundary as described in Isogai et al., 2003 (Childs et al., 2002; Torres-Vazquez et al., 2004) (Figure 4.7 B).

In addition, Plexin-Semaphorin signaling has an effect on the timing of the formation of a new sprouts during zebrafish ISV formation in addition to their role in vessel guidance. Where the absence of Plexin D1 results in precocious sprouting of ISVs (Childs et al., 2002; Torres-Vazquez et al., 2004), a new study investigating the role of Sema3E and PlexinB2 showed that morphants of either gene show delayed sprouting (Lamont et al., 2009).

Once a tip cell is determined it does not necessarily mean that it will stay a tip cell for the entire period of the formation of the vessel. Work in allantoic explants of the mouse shows that sprouting vessel can in fact change its leading cell (Perryn et al., 2008). A recent study shows similar results in the mouse retina and in zebrafish vessels and suggests a constant re-evaluation of the VEGF-VEGFR-Dll4-Notch-VEGFR signaling loop during shuffling of tip cells (Jakobsson et al., 2010).

#### 4.2.3.2 Vessel outgrowth and guidance.

Tip cells are thought to be the actively migrating cell of a growing vessel. In different model systems such as mouse retina and zebrafish as well as in cell culture experiments tip cells show extensive amounts of filopodia searching their environment (Gerhardt et al., 2003; Isogai et al., 2003; Ruhrberg et al., 2002). The tip cell migrates towards a source of growth factors, usually VEGF or members of the VEGF family, dragging along its stalk cells.

In an effort trying to find differences in gene expression between tip and stalk cells, microarray data were acquired, comparing wt mouse retinas to *dll4* heterozygous mouse retinas, in which most of the ECs have tip cell identity (Suchting et al., 2007). A set of factors were found to be enriched in tip cells including extracellular matrix (ECM) degrading but also forming factors as well as secreted factors (Del Toro et al., 2010).

Several Metalloproteinases are important to degrade ECM to allow the sprouts to invade the tissue. For instance, Mt1-mmp has been shown to be important for the degradation of collagen type IV and other ECM proteins in mouse explant culture and in vivo. Mt1-mmp is activated upon VEGF signaling and other stimulating factors whereas it is down-regulated by factors which promote vessel stabilization such as shear stress (van Hinsbergh and Koolwijk, 2008).

Important for a new sprout is that it does not immediately fall back on its parental vessel. This is controlled by VEGFR-1. As mentioned above, VEGFR-1 has high affinity to VEGF but in contrast to VEGFR-2 its kinase activity is low and it thus serves as a VEGF trap. In addition VEGFR-1 is present in two different isoforms, one being a transmembrane receptor and one being a secreted soluble version lacking the kinase and transmembrane domain and thus creating a VEGF sink around the expressing cell. Since VEGFR-1 is expressed at higher levels by stalk cells due to activation by Notch, a VEGF sink is produced behind the tip cell and so ensures that it does not fall back on the parental vessel (Chappell et al., 2009).

When the vasculature is growing, branches are elongating to reach distant places. This can involve several mechanisms. Cells can rearrange and change their shape to a more elongated form. This scenario is found during the development of the embryonic tracheal system of *Drosophila melanogaster*, where paired cells of branches undergo an intercalation mechanism to end up in a head-to-tail manner (Ribeiro et al., 2004). To what extent such a

mechanism is involved during angiogenesis is not clear and remains to be elucidated (see also results). A more prominent mechanism for branch elongation is cell division, which is found in most vertebrate tube formation models (Andrew and Ewald, 2010). Cell division is very prominent during angiogenesis, but interestingly, there seem to be different patterns of cell division in different model systems of different vessels. In an *ex vivo* explant culture using murine tissue, only endothelial tip cells which express Mt1-mmp do divide (Yana et al., 2007). In the mouse retina, tip cells do not divide but stalk cells undergo cell proliferation (Gerhardt et al., 2003). In zebrafish cell division occurs in tip and stalk cells in the developing ISVs (Blum et al., 2008). Cell division and cell migration are regulated by VEGF signaling and its two receptors VEGFR-1 and -2 (Ferrara et al., 2003). It remains to be elucidated how different sets of signaling result in these different patterns of cell division.

Zeng et. al. could show that the plane of cell division is oriented perpendicular to the vessel long axis in cell culture and in *in vivo* rat retinas, therefore increasing the length of a vessel rather than its diameter. In VEGFR-1 loss of function assays, this orientation was lost and random, indicating that VEGF via VEGFR-1 regulates orientation of cell division. The fact that the cell culture assay is flow-independent shows that shear stress induced by flow is not a main regulator of orientation of cell division (Zeng et al., 2007).

The zebrafish ISVs are an excellent model to study guidance of blood vessel morphogenesis, because ISVs have a reproducible pattern in the trunk and follow stereotyped pathways. ISVs form at each somite boundary and follow it up to the myoseptal midline; from thereon they leave the somite boundary and grow more directly to the dorsal side where they subsequently branch in anterior and posterior direction (Isogai et al., 2003). This pattern is established by guidance cues, notably the same guidance systems which guide neuronal axons to their correct position (Eichmann et al., 2005).

As mentioned above, Plexin-Semaphorin signaling is important to guide vessels between somites. In *obd* mutant fish, vessels grow into somites establishing a plexus of vessels in the trunk (Childs et al., 2002; Torres-Vazquez et al., 2004). Sema3E and Plexin D1 control vascular development and vessel guidance in mice and similarly guide ISVs in mice along their track (Gu et al., 2005; Zhang et al., 2009). A second system to guide axons and vessels is the Unc-Netrin family. Unc5b is expressed in zebrafish as well as in murine endothelial cells. Zebrafish knockdowns of *unc5b* and *netrin-1a* results in altered branching patterns and an increased number of filopodia. Especially the dorsal part of ISVs shows miss patterning. In a mouse retinal and hindbrain vasculature study Netrin-1-Unc5b signaling was shown to regulate the number of tip cell filopodia and branchpoint (Lu et al., 2004). In contrast to this study, another study proposes a proangiogenic role for Netrin-1 (Park et al., 2004). More recently Netrin-4 was shown to be up-regulated in VEGF activated endothelial cells and

thereby inhibiting angiogenesis by signaling via Neogenin and Unc5B (Lejmi et al., 2008). Thus, Netrins not only regulate guidance but also the migratory potential of ECs

When ISVs reach the dorsal part of the trunk, tip cells branch in anterior and posterior direction. A recent study showed that this branching of endothelial (tip) cells is dependent on local down-regulation of myosin II, at branchpoints. Further, a stiff ECM reduces ability of branching. Hence, Mmps are needed to reduce stiffness of the ECM and allow branching of ECs (Fischer et al., 2009).

#### 4.2.3.3 Vessel anastomosis

As soon as ISVs have branched rostrally and caudally at the roof of the neural tube, the branches elongate and subsequently connect with their adjacent ISVs (Isogai et al., 2003). So far, we lack insight into the process of vessel anastomosis. Based on antibody stainings and single cell live imaging, we propose that tip cells make initial contacts and subsequently increase their contacts by “crawling” over each other (Blum et al., 2008). This scenario recently gained support from experiments using stacks of electron microscopy images (Armer et al., 2009).

Fusion of tubes has best been described in the tracheal system of *Drosophila melanogaster*. The tracheal system develops from 20 metameres that undergo remodelling, branching and fusion (Samakovlis et al., 1996a). Some of these branches, the dorsal branches, grow dorsally and ultimately fuse with their contra-lateral dorsal branches. Interestingly, these branches are lead by two different tip cells. The terminal cell will ultimately produce a tree of fine tubules, whereas a special genetically determined fusion cell will carry out the fusion process (Samakovlis et al., 1996b). It has been demonstrated that fusion is initiated with a spot of adherens junctions (AJ) between the two fusion cells establishing a first contact. This spot is subsequently elaborated into a ring, which is accompanied by cell shape change of the fusion cell forming a donut-like structure (Samakovlis et al., 1996b; Tanaka-Matakatsu et al., 1996). The fusion cell forms a track of microtubules connecting the pre-existing and the novel apical membranes, presumably allowing invagination of these two juxtaposed apical membranes (Lee and Kolodziej, 2002). These two apical membranes eventually fuse opening a lumen at the fusion point. The initial formation of tight contacts of fusion cells is dependent upon *Drosophila* E-cadherin, the counterpart of vascular endothelial cadherin in ECs. *Drosophila* null mutants for E-cadherin fail to connect adjacent tracheal branches.

A recent study in zebrafish shows a role for Ve-cadherin in vessel fusion. In loss of function experiments knocking down Ve-cadherin, it was observed that ISVs have trouble to fuse and make only weak or no contact (Montero-Balaguer et al., 2009).

Interestingly, vessels still appear to make some contacts in *Ve-cadherin* morphants, indicating that redundant or additional factors could be important for contact formation during anastomosis. One important family of proteins could be the Nectin and Nectin-like proteins. Nectins are immunoglobulin-like transmembrane proteins which undergo homo- and heterophilic interactions among each other. Nectins are ubiquitously expressed and part of a multiprotein family suggesting a certain degree of redundancy. Nectins have been shown to be important for the formation of new adherens junctions by making initial contacts between cells, which trigger a signaling cascade and subsequently recruits Cadherins to the new junction site (Takai et al., 2008). Therefore they could play a major role in vessel contact formation and explain why ISVs in *ve-cadherin* morphants still connect partially.

A recent study suggests a role for macrophages during vessel fusion. Tip cells in the murine hindbrain vasculature associate with tissue macrophages and *pu.1* homozygous mutant mice lacking macrophages show a decreased number of intersections and branch points. In addition macrophages interact with tip cells during ISV fusion in zebrafish. Whether they play a mechanistic role during ISV anastomosis remains to be elucidated (Fantin et al., 2010).

#### 4.2.3.4 Lumen formation

When a new vessel is formed it has to be lumenized to allow blood flow. Lubarsky and Krasnow in 2003 proposed different mechanisms to form epithelial tubes, including blood vessels (Figure 4.3). From these, budding, cord hollowing and cell hollowing are presumably the most relevant mechanisms during vascular development (Adams and Alitalo, 2007). Whereas a variation of cord hollowing has been shown to be involved in vasculogenesis (Strilic et al., 2009), cell hollowing has received quite a bit of attention as a major process involved in lumen formation during angiogenesis. This comes mainly from studies in 2D and 3D cell culture. In cell culture, vacuoles form via a pinocytic mechanism in ECs and subsequently coalesce to form lumens in capillaries (Davis and Bayless, 2003). The formation of these pinocytic vacuoles is dependent on interaction of integrins with the ECM (Bayless et al., 2000; Davis and Camarillo, 1996). Furthermore, small GTPases like Cdc42 and Rac1 are required for cytoskeleton reorganization (Bayless and Davis, 2002).

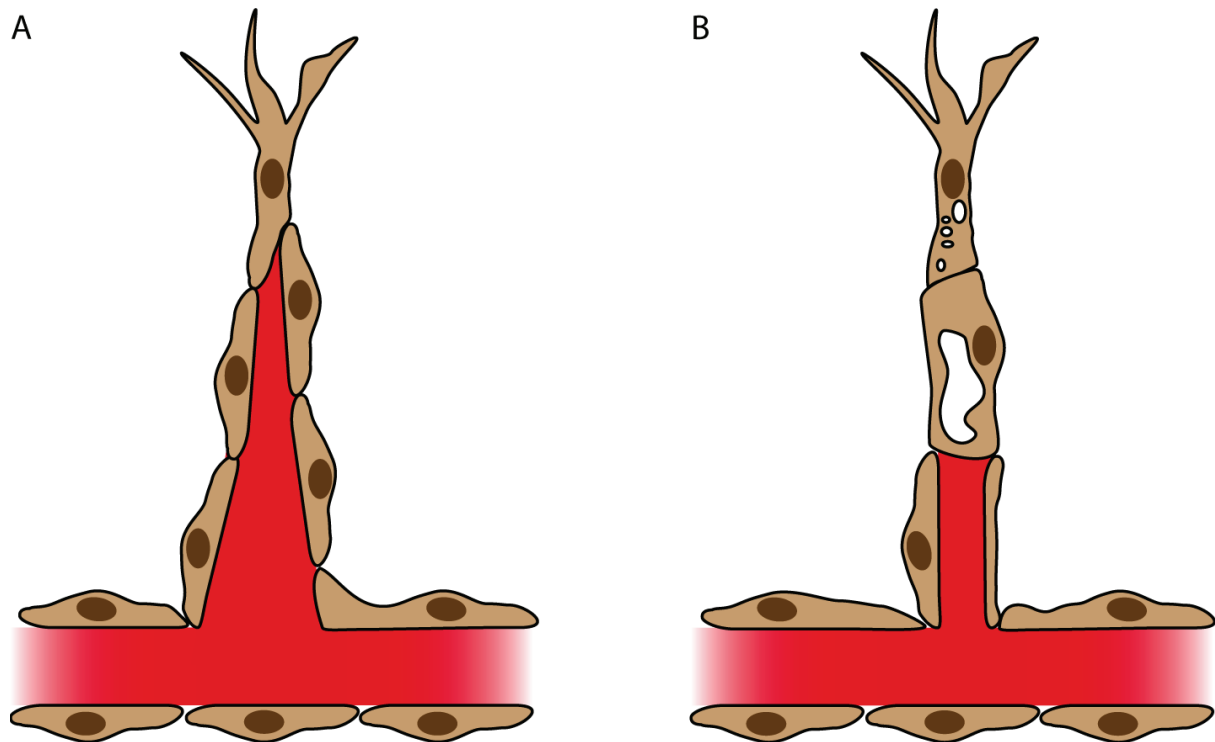


**Figure 4.8**

**Lumen formation in ISVs:** Two different ways how the lumen may form in ISVs. (A) The lumen may form by budding; a multicellular tube with an extracellular lumen would form concomitantly while the branch elongates (Blum et al., 2008). (B) Alternatively a row of single cells is lumenized by the fusion of large vacuoles with the growing lumen resulting in a seamless tube (Kamei et al., 2006). Possibly, both models are involved in lumen formation.

Indications for the presence of vacuoles *in vivo* have been observed in TEM thin sections of rat capillaries (Dyson et al., 1976). In zebrafish, the cellular architecture of ISV was described as single cells arranged in a head to tail fashion (Childs et al., 2002). More recent study proposed a model where vacuoles form in these single cells; the vacuoles of individual stalk cells fuse together and form an intracellular lumen in ISVs with cells arranged in a head to tail fashion (Kamei et al., 2006) (Figure 4.8 B). In contrast to this, we have shown that ISVs consist to a large extent of multicellular tubes with an extracellular lumen. We have also shown that ISVs extend as multicellular tubes and therefore possibly already have a prelumenal apical surface during outgrowth suggesting a budding mechanism for ISV lumen formation (Blum et al., 2008) (Figure 4.8 A). Moesin1 has recently been implicated in ISV lumen formation possibly suggesting a similar mechanism as proposed for the DA formation in mouse by Strilic et al. (Wang et al., 2010). Vacuoles could still play a role in increase the apical side of the extracellular lumen. Seamless tubes have been observed in capillaries of different tissues, like in the rat brain microvasculature (Bar et al., 1984). If and to what degree seamless tube are present in ISVs and how they are generated is one of the aims of this thesis.



#### 4.2.3.5 Vessel stabilization and integrity

During and after blood vessel formation, vessels have to maintain their integrity and regulate permeability. Integrity and permeability are regulated by cell-cell junctions between endothelial cells. A variety of different adherence junctions (AJ) and tight junctions (TJ) protein are present in endothelial cells (for a review see (Bazzoni and Dejana, 2004)). AJ and TJ have different functions. The main task of AJ is to form new cell-cell contact and maintain the integrity of the endothelium, whereas TJ regulate the passage of ions and molecules through the paracellular path. Both AJ and TJ utilize transmembrane protein, such as Cadherins (AJ) and Claudins (TJ), respectively, which undergo homophilic interactions to establish junctions along the lateral cell boarder. Endothelial cells express specific versions of Cadherins (vascular endothelial cadherin (Ve-cadherin)) and Claudins (Claudin-5). In addition a number of intracellular adapter proteins, such as  $\beta$ -catenin,  $\alpha$ -catenin or ZO-1 are important for the formation and maintenance of junctions as well as for signal transduction (Bazzoni and Dejana, 2004; Dejana et al., 2009).

Ve-cadherin has been shown to be essential for mouse development; *ve-cadherin* mutant mice die at midgestation. Although an initial vascular plexus forms in mutant mice, it fails to mature and remodel, which ultimately leads to endothelial apoptosis (Carmeliet et al., 1999). Ve-cadherin not only ensures cell-cell contact, it is also involved in downstream signalling and thereby controls cell behaviors such as migration or cell division. Ve-cadherin can form complexes with VEGFR-2 and does limit the internalization of VEGFR-2, thereby reducing signaling essential for cell proliferation and migration (Lampugnani et al., 2006). Ve-cadherin knock down experiments on quiescent vessels in an organotypic cell culture assay induces formation of protrusion and sprouting. Sprouting appears to be VEGF-A driven and dependent on Rac1 and is suppressed by Ve-cadherin downstream signaling in quiescent vessels (Abraham et al., 2009). Similar hyper sprouting phenotypes can be observed in Ve-cadherin knockdown experiments in the zebrafish embryo (Abraham et al., 2009; Montero-Balaguer et al., 2009). In contrast, a Ve-cadherin/VEGFR-2 complex together with  $\beta$ -catenin is important to inhibit apoptosis via PI3kinase and Akt signaling (Carmeliet et al., 1999). Two recent studies implicate micro RNA *miR-126* in the fine tuning of vascular integrity. *miR-126* post-transcriptionally down-regulates *spred1* and *pik3r2*, two negative regulator of PI3K, Akt (*pik3r2*) and MAP-kinase (*spred1*) (Fish et al., 2008; Wang et al., 2008). Thus Ve-cadherin seems to tightly regulate VEGF signaling, thereby allowing survival signals but down-regulating proliferative and migratory signals in a quiescent endothelium.

Junctions are not static structure but are very dynamic. While this seems to be obvious for a remodeling epithelium where junctions have to form and dissolve, this is also true for resting confluent layers of cells. Ve-cadherin shows a flow like movement from basal to apical (Kametani and Takeichi, 2007).

Not only the typical AJ and TJ proteins are required to maintain integrity and stabilize the vasculature but also proteins of the cerebral cavernous malformations (CCM) family and angiopoetins and their appropriate Tie receptors.

Cerebral cavernous malformations (CCM) are vascular lesions showing dilated, slow flow capillaries in the brain. They have sporadic form in 80% of the cases and a familial autosomal dominant form in 20% of the cases. Familial cases have been associated with three *ccm* genes; *krit1/ccm1*, *osm/ccm2* and *pdc10/ccm3*. Recently, the Heg1 receptor has been shown to be involved in a Heg1-Ccm signaling pathway regulating blood vessel integrity (see Kleaveland et al., 2009 in appendix; Dejana et al., 2009).

Tie receptors and their corresponding Angiopoetin (Ang) ligands represented the second EC specific Tyrosine kinase signaling system to be discovered in vascular development. Components are the two receptors Tie1 and Tie2 and several Ang and Ang-like ligands among which Ang1 and Ang2 are the best studied. The system is thought to be essential for vessel maturation and regulates vessel quiescence. Ang1 is predominantly expressed by mural cells and thus thought to be important for EC-mural cells interaction. In contrast, Ang2 is an antagonist of Tie2 and leads to vessel destabilization and allows new sprout formation in the presence of VEGF or vessel regression in the absence of VEGF (Augustin et al., 2009; Saharinen et al., 2010).

Blood vessels are surrounded and stabilized by mural cells. For larger caliber vessels these cells are called vascular smooth muscle cells, which form dense multiple layers around larger arteries and veins. Smaller diameter vessels and capillaries recruit pericytes, which form loose layers or are sometimes only present as solitary cells around capillaries (Gaengel et al., 2009).

#### **4.2.3.6 Vessel remodeling**

New vessels formed by vasculogenesis or sprouting angiogenesis will remodel and adapt to the local inputs. One of the most prominent remodeling processes is termed intussusceptive angiogenesis (IA). This process is characterized by the formation of an endothelial wall pillar in the vascular lumen, ultimately splitting a single tube into two (Figure 4.9). Once the pillar is formed it is fortified by pericytes and fibroblasts. While molecular control of IA is not well defined, hemodynamic forces and shear stress appears to be important (Makanya et al., 2009). An increase of blood pressure on the chicken chorioallantoic membrane (CAM) microvascular bed increases speed of IA pillar formation (Djonov et al., 2002). In contrast, the mouse yolk sac vascular plexus fails to remodel into a vascular tree when blood cells are trapped in acryl amide (Lucitti et al., 2007).



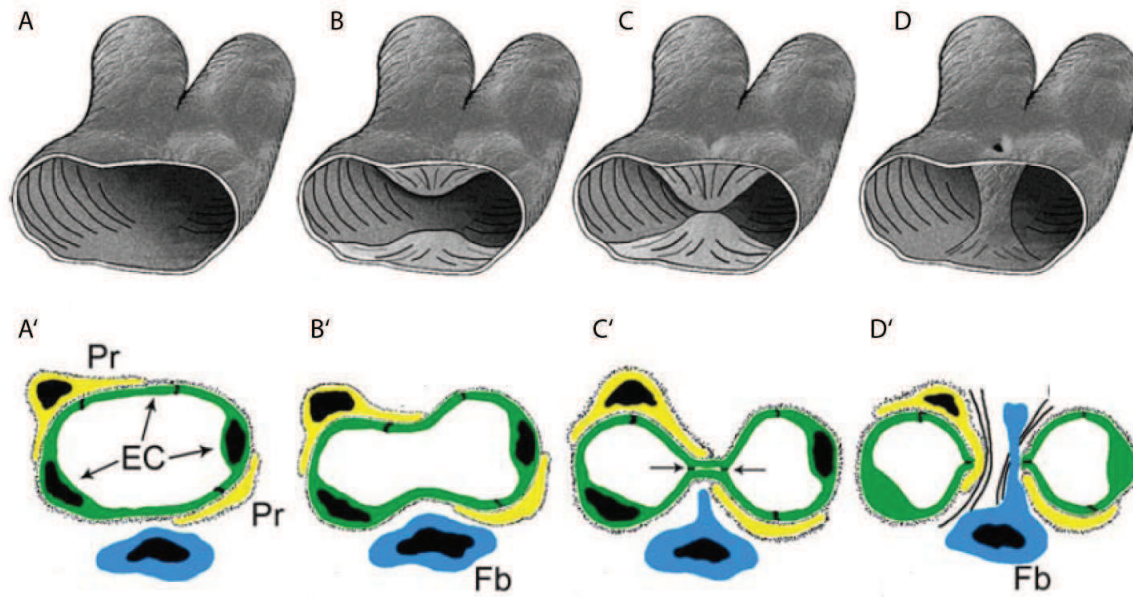


**Figure 4.9**

**Intussusceptive angiogenesis:** IA is characterized by the formation of pillars in endothelial tubes. The different steps are demonstrated in this Figure. The opposing walls of an endothelial protrude towards the inside of the tube (A,A',B,B'). Ultimately the two walls contact and form a pillar (C, C'). The exact cellular mechanism is not known, but presumably, EC rearrange to seal off the two tubes. The pillar is then reinforced by pericytes (Pr) and fibroblasts (Fb)(D,D') (Makanya et al., 2009).

Vascular pressure and shear stress plays an important role in vascular development, also in zebrafish. Already some time ago, it has been shown that the DLAV fails to remodel in *silent heart* morphant embryos, where heart beat is not present (Isogai et al., 2003). More recently, it was found that also the aortic arches (AA) require flow to correctly interconnect (Nicoli et al., 2010). Aortic arches connect to the LDA after onset of circulation (Isogai et al., 2001). Using different drugs, which stop heart beat, Nicoli et al. showed that the connection to the LDA fails to form. Interestingly, in contrast to the mouse yolk sack, contribution of blood cells is not necessary as the connection forms in *gata1* morphant embryos, which lack blood cells. Hence the process is dependent on shear stress effects from plasma flow. Genetic analysis revealed that flow is required to activate *klf2* (krüppel-like factor), a sensor of shear stress, which in turn allows transcription of the micro RNA *miR-126*. This micro RNA is a negative regulator of *spred1*, which itself is a negative regulator of the VEGF signaling pathway (Nicoli et al., 2010). Thus VEGF is required for the vessel formation and flow is required to allow VEGF signaling.

### 4.3 Aim of this thesis

The vascular system is a vital organ for the function of a vertebrate animal. Especially angiogenesis, the formation of new vessels from pre-existing ones, has attracted much attention also due to its importance in cancer pathology. During the past decades, a number of molecular pathways controlling the development of the vascular system have been identified (Adams and Alitalo, 2007; Carmeliet, 2005; Coultas et al., 2005). However, tube architecture and cellular mechanism driving morphogenesis of the vascular system are ill characterized.

The zebrafish embryo is an ideal model system to study morphogenetic mechanisms *in vivo* during development. It is optically, it has a fast development and a number of transgenic lines and transgenic techniques are available (Lawson and Weinstein, 2002b). In recent years, the zebrafish ISVs have served as a paradigm to study angiogenesis *in vivo*.

Our aim was to use similar approaches as were used to understand morphogenesis of the tracheal system in *Drosophila melanogaster* (Ribeiro et al., 2004). We wanted to label EC junctions to follow individual cells in the context of angiogenesis. Initially using Ab stainings, and ultimately with transgenic lines expressing fluorescently tagged junctional proteins to monitor cellular mechanisms during angiogenesis.

The main focus was to understand cellular mechanisms during anastomosis, the formation of new connections between blood vessels. Even though anastomosis is an essential step to form a functional vascular network, molecular and cellular mechanisms driving anastomosis remain completely obscure.

## **5 Materials and Methods**

## 5.1 Molecular biology protocols

### 5.1.1 Standard protocol

#### 5.1.1.1 Restriction enzyme digestion

DNA	1-2 µg
Restriction buffer	5 µl
Restriction enzyme(s)	1 µl of each (Roche or NEB)
Q-H <sub>2</sub> O	up to 50 µl

Reagents were mixed in a 1.5 ml Eppendorf tube and placed on a 37°C warm heat block for 1 – 2 hours. Double digest were performed in the buffer according to the list of NEB or/and Roche.

#### 5.1.1.2 Dephosphorylation with Alkaline Phosphatase

Dephosphorylation of the vector was performed to avoid self ligation. Dephosphorylation was performed immediately after restriction enzyme digestion. To the 50 µl restriction mix 5.5 µl of a 10 x phosphatase buffer and 0.5 µl of Shrimp Alkaline Phosphatase (SAP, Roche) was added. Reaction was put back onto the 37°C heat block for half an hour.

#### 5.1.1.3 PCR mix

For all PCR done in this work the following mix was done:

Template DNA	100-200 ng
Primers (10µM)	1 µl of each (ordered by Sigma)
DNA polymerase buffer 10x	5 µl
DNA polymerase	0.5 µl (Taq (NEB), Pfu (Sigma), Phusion (Finnzyme))
dNTPs (2.5 mM)	5 µl
Q-H <sub>2</sub> O	up to 50 µl

#### 5.1.1.4 Agarose Gel

Agarose (Eurogentec or Sigma) gels were poured by mixing 0.5 g of agarose with 50 ml 1xTAE into an Erlenmeyer flask. Agarose was dissolved by heating it in the microwave until it boiled. Then it was stirred and 5 µl of ethidium bromide was added. After, it was poured into a gel chamber and let polymerize with a desired comb. After polymerization the comb was removed and the gel was put in the running chamber (Amersham Bioscience) in 1xTAE. Gels were loaded with marker DNA (1Kb (+) Ladder Invitrogen) and DNA fragments with loading buffer. Gels were run at 100 mV (Biowerk).

#### 5.1.1.5 Gel extraction

Gels were analyzed under an UV lamp. Desired bands were cut out and put into a 2 ml Eppendorf tube. The extraction was made following the QIAGEN or Sigma Gel Extraction protocol.

#### 5.1.1.6 Ligation

Vector	50-100 ng
Insert	150-300 ng (at least 3 times amount of vector DNA)
T4 DNA Ligase buffer 10x (NEB)	1 $\mu$ l
T4 DNA Ligase	1 $\mu$ l
Q-H <sub>2</sub> O	up to 10 $\mu$ l

For easy ligations (small insert, vector 3-5 kb) reaction took place at room temperature for about 20 min. For difficult ligations (insert bigger than vector, large vector >10kb, other issues) reaction took place at 16°C over night.

#### 5.1.1.7 Transformation

Electrocompetent *E. coli* bacteria were used for transformation. The whole procedure was performed on ice. Frozen *E. coli* (50  $\mu$ l in Eppendorf tubes) from the -70°C freezer were thawed on ice. 1  $\mu$ l of the DNA ligation was added and mixed. Then the bacteria were transferred to a 1 mm electroporation cuvette (Bio Rad). The bacteria were electroporated (Bio Rad 1.8 mV, 200 ohm, 25  $\mu$ F) and then transferred with 0.5 ml LB medium to a 2 ml Eppendorf tube. Bacteria were grown at 37°C on a shaker or rotator for 1 hour and then plated on an agar plate with the appropriate antibiotic. Colonies were grown over night in the 37°C breeding room.

#### 5.1.1.8 Miniprep

Clones were picked from the agar plate and grown in 2 ml LB medium with the appropriate antibiotic on a shaker at 37°C over night. Then minipreps were performed following the SIGMA GenElute™ Plasmid Miniprep Kit.

#### 5.1.1.9 Midiprep

10  $\mu$ l of a positive miniprep culture or a clone from an agar plate was put into 30 ml LB medium with antibiotic. Culture was grown over night and then centrifuged for 15 min in the Heraeus centrifuge at 4°C. Then the QIAGEN or the Sigma Plasmid Midi Kit was followed. Purity and amount were measured with a spectrometer.

### 5.1.2 Plasmids

To produce a plasmid containing an EGFP-NLS sequence downstream of the *flk1* promoter, EGFP-NLS cDNA was cloned from the pStinger vector (Barolo et al., 2000) into pBSII-SK with BamHI and SpeI. From there, EGFP-NLS was cloned into a modified pG1 vector with EcoRI and SacII (details available upon request). The *flk1* promoter was cloned from the pCRII-TOPO vector containing the *flk1* promoter into the modified pG1 (Henry Belting) containing the EGFP-NLS sequence with Sall and EcoRI.

To allow easy cloning of cDNAs under the control of the *flk1* promoter, a multiple cloning site and a SV40-polyA tail was cloned downstream of the *flk1* promoter. The SV40 polyadenylation signal sequence was amplified by PCR using the following primers, one containing the MCS (EcoRI, KpnI, XhoI, EcoRV, BamHI, SacII and NotI): forward (containing MCS):

5'ACTGAGAATTCGGTACCCTCGAGGATATCGGATCCCCGCGGGCGGCCGCGATCATAA TCAGCCATAC-3', rev: 5'-CTAGTGC GCGCGTTAAGATA CATTGATGA-G-3'. The PCR fragment was then cloned into the pG1 *flk1*:EGFP-NLS vector using EcoRI and BssHII giving rise to the pG1 *flk1*:MCS-SV40 vector.

The mCherry coding sequence was cloned from pRSET-B mCherry vector (Tsien lab) into pCRII-TOPO vector containing the *flk1* promoter with BamHI and EcoRI. This vector was used to clone mCherry into the pG1 *flk1*:MCS-SV40 vector using BamHI and NotI (Lukas Herwig). The *fli1*:GFF and the UAS:EGFP-hZO1 constructs were cloned by Lukas Herwig in the lab.

## 5.2 Fish protocols

### 5.2.1 Maintenance and strain

Zebrafish were maintained and bred using standard protocols (Westerfield, 2000). The following zebrafish strains were used:

#### Wildtypes

AB/EK (W. Driever, Freiburg)

AB/TL (W. Driever, Freiburg)

#### Transgenic

*fli1*:EGFP (Lawson and Weinstein, 2002b)

*flk1*:EGFP (Jin et al., 2005)

*flk1:EGFP-NLS* (Blum et al., 2008)

*fli1:GFF* (Lukas Herwig); *UAS:Kaede* (ZIRC)

*fli1:GFF* (Lukas Herwig); *UAS:RFP* (Asakawa et al., 2008)

*UAS:EGFP-hZO1* (Lukas Herwig)

## 5.2.2 DNA and morpholino injecting

Capillaries were pulled to produce thin glass needles (Sutter instruments). Injection plates were made by pouring 1% agarose into a petridish and putting a mold with rills on the agarose. The mold was removed after polymerization of the agarose. The plate were stored at 4°C and covered with eggwater (0.3g seasalt in 1l ddH<sub>2</sub>O).

Freshly laid eggs (1-4 cells for morpholino, 1-2 cells for DNA) were gently pressed into the rills of the injection plate. Needles were filled with the DNA solution using Eppendorf Microloader. Needles were mounted on the Eppendorf FemtoJet injector or hand injector. The tips of the needles were broken with a forceps to allow outflow. Small drops (2-3 nl) were injected trying to hit the cells.

## 5.2.3 Generation of *flk1:EGFP-NLS* transgenic fish line

Approximately 200 embryos (AB/EK strain) were injected at one cell stage. Embryos were screened for transient GFP expression at 24 hpf. 24 embryos showed strong transient expression in the developing vasculature and were raised separately. Founders were crossed and screened for germ line transmission. From 7 pairs, we recovered two transgenic carriers which displayed different levels of EGFP expression. The strongest expressing carrier was propagated to establish the *flk1:EGFP-NLS* line.

## 5.3 Immunofluorescence and Live imaging

### 5.3.1 Ab stainings

To inhibit pigmentation, PTU (propylthiouracil) was used. Egg water of 24 hpf old embryos was exchanged with PTU egg water. PTU egg water was produced by adding 10 ml of a 40x PTU stock solution to 390 ml of egg water.

Embryos from 22–48 hpf were fixed in 4% paraformaldehyde for 2 h at room temperature. Embryos were then washed 4×5 min in PBST (PBS+0.1% Tween20) and once in PBSTX (PBS+0.1% Tween20+0.1% Triton ×100). Embryos were then blocked in PBSTX+10%

BSA+1% NGS for 2 h. Embryos were incubated with primary antibodies (in PBSTX+1% BSA+0.1% NGS) overnight at 4 °C. Embryos were then washed 6×1 h in PBSTX+1% BSA+0.1% NGS and then incubated with the secondary antibody (in PBSTX+1% BSA+0.1% NGS) overnight at 4 °C. Embryos were finally washed several times in PBST. All steps were performed at RT except for antibody incubations. The following antibodies were used: mouse anti human ZO-1, 1:200 (Zymed); rabbit anti-zf-CDH5 (Henry Belting), 1:1000; Alexa-568 goat anti-rabbit IgG, 1:1000; Alexa- 568 goat anti-mouse IgG, 1:1000; Alexa-633 goat anti-mouse IgG, 1:1000 (All secondary antibodies were purchased from Invitrogen.).

#### **5.3.1.1 Mounting and confocal microscopy of Ab stained embryos**

The head and yolk bulb were severed from the trunk with a razorblade and the trunk was mounted in Vectashield. Images were taken with a Leica SP1 confocal microscope. For ZO-1 immunofluorescence, confocal stack sizes are 100–200 optical sections per stack at a step size of 0.1221  $\mu\text{m}$  (as recommended for the 100× lens). For CDH5 staining the step size was increased to 0.2442  $\mu\text{m}$  (50–100 sections) due to a weaker signal and faster bleaching.

#### **5.3.2 Live imaging (Leica Sp1 confocal microscope)**

Embryos were embedded in a drop of 0.7% low melting agarose (Sigma) containing 0.01% tricaine (pH 7.5) on a cover slip. This cover slip was put up side down on an aluminum depression slide containing egg water with 0.01% tricaine (brand) and. Temperature was kept at approximately 28.5 °C. Stacks were taken with a Leica Sp1 confocal microscope (40x lens) every 8 min with a slice number between 30 and 50 having a space of 1.5–2.0  $\mu\text{m}$ . Movies were processed using Imaris (Bitplane) and ImageJ.

#### **5.3.3 Single cell labeling using Kaede**

2dpf old *fli1:GFF; UAS:Kaede* transgenic embryos were anaesthetized with tricaine and mounted in 0.7% low melting agarose. Using the confocal software, a region of interest was drawn around EC nuclei. EC nuclei were easily discernible in 2 dpf ISVs with inflated lumen due to much higher amount of Kaede in the nucleus compared to the very thin cytoplasm of ECs (see also Figure 6.1). This region of interest was then illuminated for 20 seconds using 100% UV laser power. Subsequently high resolution x,y,z stacks were acquired with a 63x glycerol immersion lens using the suggested slice thickness. Slice numbers ranged from 80 to 200 slices. Images were analyzed using Imaris software (Bitplane).



### 5.3.4 Live imaging with *fli1:GFP*; *UAS:EGFP-hZO1*; *UAS:RFP* embryos (Leica Sp5)

First triple transgenic embryos were selected using a Leica MZ FLIII fluorescent stereomicroscope. Embryos were selected for RFP ensuring the presence of the *fli1:GFP* and *UAS:RFP* and for the heart marker *cmhc2:EGFP* (green heart) present on the *UAS:EGFP-hZO1* transgenic line. EGFP-hZO1 was too faint to detect under the fluorescent stereomicroscope. The selected embryos were anaesthetized using tricaine and mounted in 35 mm special petri dishes with a 0.17mm coverslip glass on the bottom (MatTek), using 0.7% low melting agarose (sigma) with 0.01% tricaine and 0.003% PTU. Mounted embryos were then analyzed for good expression (due to mosaic of EGFP-hZO1) under a widefield Leica DM6000 fluorescent microscope.

Embryos with suitable expression were then imaged overnight on the Leica Sp5 using a 63x glycerol immersion lens with a numerical aperture of 1.2 with additional zoom of 1-1.3x depending on the situation. All movies have an initial frame size of 512x512 pixels. Stacks were ranging from 50-80 slices always keeping a slice thickness of 1  $\mu\text{m}$ . For all movies on the Sp5 (all movies in chapter II and II), timepoints were 5 minutes apart except if noted differently.

#### 5.3.4.1 QD-injection

705 nm QD (Invitrogen) were injected directly in the sinus venosus of mounted embryos at a concentration of 1:2. Special manufactured glass needles with tip opening of 10  $\mu\text{m}$  and beveled tip were utilized to reduce damage to the embryo.

## 6 Results

## ***Results preface***

The result section is divided in three chapters:

**Chapter I** covers our paper published in 2008: “complex cell rearrangements during intersegmental vessel sprouting and vessel fusion in the zebrafish embryo”

**Chapter II** quantifies different tube architectures in the ISV and the DLAV

**Chapter III** describes cellular mechanisms we found during ISV formation and anastomosis.

As some of the fluorescent signals were weak and are difficult to see on printed paper, all Figures of Chapter II and III can be found as high resolution Tiff files on the enclosed DVD. In addition all movies can be found as uncompressed avi files. The Quicktime player appears to show a better quality compared to Windows media player. Windows media player also shows some compatibility issues on certain pc.

Additional results from collaborations can be found in the appendix as published papers.

## **6.1 Chapter I: Blum et al., 2008**

Previous work on cellular architecture of ISVs in the zebrafish embryo has proposed that ISVs consist of three types of cells lined up behind each other. A T-shaped cell located in the DLAV, an inverted T-shaped cell in DA and a cell connecting these two cell (Childs et al., 2002). More recently it was proposed that these cells form an intracellular lumen (Kamei et al., 2006). This cellular architecture suggested a junctional pattern, which would only show loops at the interface between cells. To test this, we used Ab stainings against junctional proteins combined with single cell labeling. We also generated a new transgenic line expressing a nuclear localized version of EGFP under the control of the endothelial specific promoter *flk1*. This line allowed us to follow some of the dynamics during ISV development.

My contribution to this work was: I made all Figures except for Figure 2A-F. I generated the transgenic line *flk1:EGFP-NLS*. The *flk1:mCherry* plasmid was cloned by Lukas Herwig and Florian Lüders in the lab and the Ve-cadherin (CDH5) Ab was generated by Henry Belting in the lab.

# Complex cell rearrangements during intersegmental vessel sprouting and vessel fusion in the zebrafish embryo

Yannick Blum<sup>1</sup>, Heinz-Georg Belting<sup>\*,1</sup>, Elin Ellertsdottir, Lukas Herwig,  
Florian Lüders, Markus Affolter<sup>\*</sup>

*Biozentrum der Universität Basel, Klingelbergstrasse 70, CH-4056 Basel, Switzerland*

Received for publication 2 October 2007; revised 17 December 2007; accepted 21 January 2008

Available online 13 February 2008

## Abstract

The formation of intersegmental blood vessels (ISVs) in the zebrafish embryo serves as a paradigm to study angiogenesis *in vivo*. ISV formation is thought to occur in discrete steps. First, endothelial cells of the dorsal aorta migrate out and align along the dorsoventral axis. The dorsal-most cell, also called tip cell, then joins with its anterior and posterior neighbours, thus establishing a simple vascular network. The vascular lumen is then established via formation of vacuoles, which eventually fuse with those of adjacent endothelial cells to generate a seamless tube with an intracellular lumen. To investigate the cellular architecture and the development of ISVs in detail, we have analysed the arrangement of endothelial cell junctions and have performed single cell live imaging. In contrast to previous reports, we find that endothelial cells are not arranged in a linear head-to-tail configuration but overlap extensively and form a multicellular tube, which contains an extracellular lumen. Our studies demonstrate that a number of cellular behaviours, such as cell divisions, cell rearrangements and dynamic alterations in cell–cell contacts, have to be considered when studying the morphological and molecular processes involved in ISV and endothelial lumen formation *in vivo*.

© 2008 Elsevier Inc. All rights reserved.

**Keywords:** Angiogenesis; ISV; Vessel fusion; VE-cadherin; Adherens junctions; Transgenic; ZO-1; Zebrafish

## Introduction

Branched tubular organs are widely used to transport and distribute liquids, nutrients or gas within multicellular animals. In many cases, ramified tubular organs arise from pre-existing epithelial structures via branching morphogenesis. Cell migration and cell division are key processes underlying branch formation. In addition, cell rearrangement and the control of cell shape play important roles in shaping the outgrowing branches.

In invertebrates, one of the best characterized organs formed by branching morphogenesis is the tracheal system of *Drosophila melanogaster*. In recent years, a large number of mutations affecting the branching process has been identified and characterized. Using forward and reverse genetic as well as

4D-live imaging approaches at cellular resolution, the corresponding genes were found to control directed cell migration, cell rearrangement, branch-specification, tube size regulation and branch fusion. A large number of key molecules has been identified, including chemotactic ligands, their respective receptors, transcriptional regulators, junctional components and luminal proteins, which either act at the top or at the bottom of the regulatory network that controls the branching process (reviewed in Affolter et al., 2003; Ghabrial and Krasnow, 2006; Uv et al., 2003).

In vertebrates, the molecular pathways controlling the development of the vasculature have attracted much attention in the past decade (Adams and Alitalo, 2007; Carmeliet, 2005; Coultas et al., 2005; Lawson and Weinstein, 2002a; Ny et al., 2006). The vascular anatomy of the developing trunk is both reproducible from animal to animal (Isogai et al., 2001) and conserved in the vertebrate body plan with some species-specific variation. The first blood vessels that form in the embryo are the large midline artery and vein, which arise

\* Corresponding authors. Fax: +41 61 2672078.

E-mail addresses: [heinz-georg.belting@unibas.ch](mailto:heinz-georg.belting@unibas.ch) (H.-G. Belting), [markus.affolter@unibas.ch](mailto:markus.affolter@unibas.ch) (M. Affolter).

<sup>1</sup> These authors contributed equally to this study.

through vasculogenesis, a process involving the migration, differentiation and assembly of angioblasts. After the establishment of the major axial blood vessels, smaller vessels such as the trunk intersegmental vessels (ISV) are formed through sprouting angiogenesis, which involves the migration of endothelial cells from the existing large vessels. The processes by which these sprouts develop appear similar to those involved in branching morphogenesis of other tissues and include a remodelling of pre-existing epithelial structures. However, the temporal and spatial coordination of events such as cell migration, cell rearrangement, cell division or lumen formation, which eventually lead to the establishment of correctly interconnected vascular tubes of distinct size and shape, remains ill characterized (Adams and Alitalo, 2007).

The genetic amenability, the experimental accessibility and the optical clarity make the zebrafish embryo an excellent model system for deciphering the cellular mechanisms underlying angiogenesis (Beis and Stainier, 2006; Lawson and Weinstein, 2002b). Because of their metameric arrangement and relative anatomical simplicity ISVs are ideally suited to study the cues and mechanisms leading to the ordered formation of new blood vessels. Single cell labelling experiments have shown that the ISVs consist of three types of cells: (1) a ventral cell embedded in the dorsal aorta carrying a sprout oriented towards dorsal, (2) a dorsal T-shaped cell in the dorsal longitudinal anastomotic vessel (DLAV) and (3) an elongated cell linking these two (Childs et al., 2002). Because of the

stereotypic location and behaviour of these cells, it was suggested that ISVs are made up by three cells that originate from the dorsal aorta and migrate between somites to their final position in the ISV and the DLAV (Childs et al., 2002) (Fig. 1A). By live imaging of transgenic zebrafish embryos, Weinstein and colleagues have shown that the ISVs indeed form via angiogenesis, and that cells migrate out of the dorsal aorta to form, in a first phase, the DLAV and its connections to the dorsal aorta (Isogai et al., 2003; Lawson and Weinstein, 2002b). More recently, elegant live imaging studies revealed that the lumen in the ISVs is built in vivo via the formation of endothelial vacuoles that undergo intracellular and intercellular fusion to generate a patent lumen (Kamei et al., 2006). ISV formation in the early zebrafish embryo is thus characterized by cell migration to generate a stereotyped cell arrangement, followed by a hollowing process of single cells and subsequent lumen connection, resulting in an interconnected luminal pathway from the dorsal aorta to the DLAV. Recent studies have shown that endothelial cells also divide as they migrate out of the dorsal aorta and form the ISVs (Leslie et al., 2007; Siekmann and Lawson, 2007), adding another cellular process to ISV formation.

To characterize the cellular architecture of the developing ISVs in the zebrafish in more detail, and to better define the cellular events that contribute to ISV formation, we have used single cell imaging in vivo combined with the analysis of the distribution of proteins at the endothelial adherens junctions

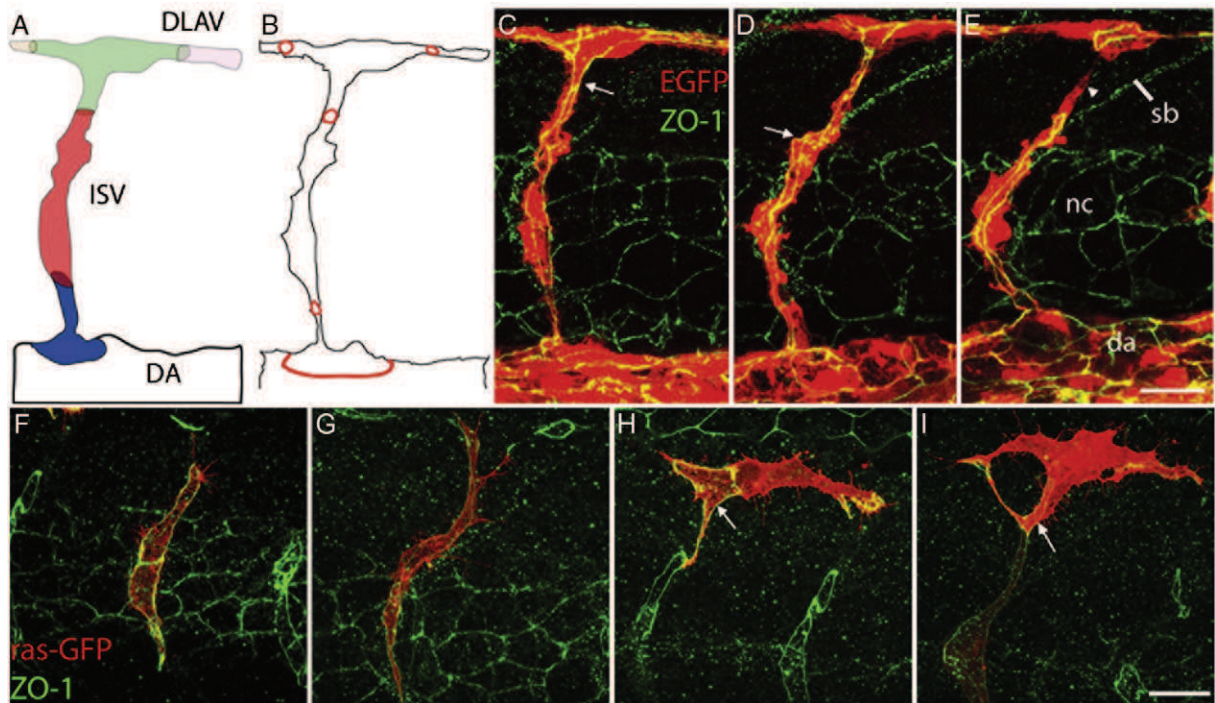


Fig. 1. Complex distribution of junctional proteins in ISV. (A) Cellular model of ISVs according to Childs et al. (2002). (B) Putative distribution of cell junctions (red rings) in an ISV in which endothelial cells are arranged in a head-to-tail fashion forming a seamless tube. (C–E) Confocal projection of 36 hpf *fli1:EGFP* (red) embryos labeled with an anti-ZO-1 antibody (green). ZO-1 protein is mostly detected as two “stripes” (arrows in panels C and D) along the stalk of the ISV, and also in parts of the DLAV. Sometimes, ZO-1 is absent from short regions of the ISVs, including the DLAV (E, arrowheads). (F–I) ZO-1 outlines single cells. 30 hpf wild-type fish injected with *fli1:RAS-GFP* (red) plasmid and labeled with anti ZO-1 antibodies (green). (F and G) Putative single stalk cells are entirely lined by ZO-1. (H and I) Putative tip cells show ring-like ZO-1 pattern at their base, where they make contact with stalk cells (arrows). Abbreviations: da: dorsal aorta, nc: notochord, sb: somite boundary. Scalebars: 20 μm.



(AJs) and tight junctions (TJs). Our studies show that the architecture of the ISV is significantly different from what has been proposed previously. Furthermore, we suggest that a number of additional cellular activities have to be taken into consideration when studying the molecular processes involved in ISV sprouting angiogenesis in the zebrafish embryo.

## Materials and methods

### *Fish maintenance and stocks*

Zebrafish were maintained at standard conditions (Westerfield, 2000). Embryos were staged by hours post-fertilization (hpf) at 28.5 °C (Kimmel et al., 1995). Embryos derived from wild-type fish (AB/EK), TG(*flk1:EGFP*)<sup>1</sup> (Lawson and Weinstein, 2002b), TG(*flk1:EGFP*)<sup>S843</sup> (Jin et al., 2005) and TG(*flk1:EGFP-NLS*) (this study) were used.

### *Generation of TG(*flk1:EGFP-NLS*) transgenic fish line*

Approximately 200 embryos (AB/EK strain) were injected at one cell stage. Embryos were screened for transient GFP expression at 24 hpf. 24 embryos showed strong transient expression in the developing vasculature and were raised separately. Founders were crossed and screened for germ line transmission. From 7 pairs, we recovered two transgenic carriers which displayed different levels of EGFP expression. The strongest expressing carrier was propagated to establish the TG(*flk1:EGFP-NLS*) line.

### *Live imaging*

Embryos were embedded in a drop of 0.7% low melting agarose containing 0.01% tricaine (pH 7.5) on a cover slip. This cover slip was put up side down on an aluminum depression slide containing egg water with 0.01% tricaine. Temperature was kept at approximately 28.5 °C. Stacks were taken with a Leica Sp1 confocal microscope every 8 min with a slice number between 30 and 50 having a space of 1.5–2.0 μm. Movies were processed using Imaris (Bitplane) and ImageJ.

### *Generation of anti-CDH5 antibodies*

A cDNA fragment encoding a polypeptide comprising the extracellular domain of zebrafish CDH5 (Ala<sup>22</sup> to Lys<sup>464</sup>) was cloned into pET22b and expressed in *E. coli* using the T7 expression system. The protein was purified on Ni-charged IMAC resin (BioRad) under denaturing conditions. Antiserum was raised in a rabbit by Eurogentec (Seraing, Belgium) using standard immunization procedures. Prior to use, the anti-CDH5 antiserum was diluted 1:1000 in blocking solution (PBS, 1% BSA, 5% normal goat serum, 0.2% TritonX-100) and incubated with fixed zebrafish embryos (10 embryos/ml) to reduce non-specific activity.

### *Immunofluorescence*

Embryos from 22–36 hpf were fixed in 4% paraformaldehyde for 2 h at room temperature. Embryos were then washed 4 × 5 min in PBST (PBS+0.1% Tween20) and once in PBSTX (PBS+0.1% Tween20+0.1% Triton ×100). Embryos were then blocked in PBSTX+10% BSA+1% NGS for 2 h. Embryos were incubated with primary antibodies (in PBSTX+1% BSA+0.1% NGS) overnight at 4 °C. Embryos were then washed 6 × 1 h in PBSTX+1% BSA+0.1% NGS and then incubated with the secondary antibody (in PBSTX+1% BSA+0.1% NGS) overnight at 4 °C. Embryos were finally washed several times in PBST. All steps were performed at RT except for antibody incubations. The following antibodies were used: mouse anti human ZO-1, 1:200 (Zymed); rabbit anti-zf-CDH5, 1:1000; Alexa-568 goat anti-rabbit IgG, 1:1000; Alexa-568 goat anti-mouse IgG, 1:1000; Alexa-633 goat anti-mouse IgG, 1:1000. (All secondary antibodies were purchased from Invitrogen.) The head and yolk bulb were severed from the trunk with a razorblade and the trunk was mounted in

Vectashield. Images were taken with a Leica SP1 confocal microscope. For ZO-1 immunofluorescence, confocal stack sizes are 100–200 optical sections per stack at a step size of 0.1221 μm (as recommended for the 100× objective). For CDH5 staining the step size was increased to 0.2442 μm (50–100 sections) due to a weaker signal and faster bleaching.

### *Plasmids*

To produce a plasmid containing an EGFP-NLS sequence downstream of the *flk1* promoter, EGFP-NLS cDNA was cloned from the pStinger vector (Barolo et al., 2000) into pBSII-SK with *Bam*HI and *Spe*I. From there, EGFP-NLS was cloned into a modified pG1 vector with *Eco*RI and *Sac*II (details available upon request). The *flk1* promoter was cloned from the pCRII-TOPO vector containing the *flk1* promoter into the modified pG1 containing the EGFP-NLS sequence with *Sal*I and *Eco*RI.

To allow easy cloning of cDNAs under the control of the *flk1* promoter, a multiple cloning site and a SV40-polyA tail was cloned downstream of the *flk1* promoter. The SV40 polyadenylation signal sequence was amplified by PCR using the following primers, one containing the MCS (*Eco*RI, *Kpn*I, *Xho*I, *Eco*RV, *Bam*HI, *Sac*II and *Not*I): forward (containing MCS): 5'-ACTGAGAATTCGGTACCCCTCGAGGATATCGGATCCCCGCGGGCGGCCGCGATCATAATCAGCCATAC-3', rev: 5'-CTAGTGC GCGCTTAAGATACATTGATGA-G-3'. The PCR fragment was then cloned into the pG1 *flk1:EGFP-NLS* vector using *Eco*RI and *Bss*HIII giving rise to the pG1 *flk1:MCS-SV40* vector.

The mCherry coding sequence was cloned from pRSET-B mCherry vector (Tsien lab) into pCRII-TOPO vector containing the *flk1* promoter with *Bam*HI and *Eco*RI. This vector was used to clone mCherry into the pG1 *flk1:MCS-SV40* vector using *Bam*HI and *Not*I.

## Results

### *Complex junctional organization of ISVs*

It has previously been shown that the ISVs in the early zebrafish embryo consist of three types of endothelial cells (Childs et al., 2002; Fig. 1A). Based on their stereotypic location it has been assumed that these cells line up in a head-to-tail fashion with no or very little overlap along the dorsoventral extent of the ISV. Recently, this view has gained support by live imaging studies suggesting that the lumen of ISVs is formed via the formation and fusion of intracellular vacuoles that will fuse with those of neighbouring endothelial cells to generate a seamless tube with an intracellular lumen (Kamei et al., 2006).

To examine the cellular architecture of ISVs in more detail, we visualized the junctional complexes between individual endothelial cells using an antibody directed against human Zona Occludens 1 (ZO-1) (see Materials and methods). Tight junctions and adherens junctions form between cells at the apical side of an epithelium and are excellent indicators for cellular contacts within epithelial tissues. Moreover, junctional patterns between epithelial cells have been used to determine the cellular architecture of tubular structures (Lubarsky and Krasnow, 2003; Ribeiro et al., 2004). For instance, a seamless tube in which the cells are arranged serially would most likely result in a junctional “ring” pattern as illustrated in Fig. 1B.

Because the anti-ZO-1 antibody labels cell junctions in many epithelial tissues in zebrafish embryos, including notochord and spinal cord, we performed our analysis on transgenic TG(*flk1:EGFP*) embryos to independently visualize the developing trunk vasculature (Lawson and Weinstein, 2002b). To ensure reproducible observations we focused our study on the ISVs

located in the posterior region of the yolk extension. We first analysed embryos after 1.5 days of development, when ISVs have formed in much of the trunk region and their lumen is about to become patent (Isogai et al., 2001). At this stage we observed a complex pattern of ZO-1 (Figs. 1C–E). Whereas the dorsal aorta showed a mesh-like distribution of ZO-1, which is typical for multicellular tubes (Lubarsky and Krasnow, 2003), in most ISVs, the medial region was lined by two “stripes” of ZO-1 along the tube axis. On the dorsal side, we also observed two or more lines of ZO-1 staining in the DLAV. Owing to the heterogeneity of ISVs at this stage, ZO-1 distribution was slightly variable between individual ISVs within a single embryo. For example, sometimes no ZO-1 staining was seen in short regions along the tube extension (arrowhead in Fig. 1E) most likely reflecting the dynamic behaviour of endothelial cells during angiogenic remodelling. Thus, the ZO-1 pattern we observe in ISVs is contrasting the pattern that would have been predicted from the current models of ISV architecture and is most readily explained if two endothelial cells make up the tube in most regions of the ISV.

To unambiguously link individual endothelial cells within developing ISVs to the complex pattern of ZO-1, we examined the distribution of ZO-1 in embryos that had been injected with a plasmid encoding a membrane-bound form of GFP (RAS-GFP) under the control of the *flk1* promoter (Jin et al., 2005). Because injected DNA is mosaically transmitted in the zebrafish embryo, it is possible to label single endothelial cells with this technique. When examining single, RAS-GFP positive stalk cells, we found that the circumference of stalk cells was entirely lined by ZO-1 protein, suggesting that they indeed contacted another cell(s) over their entire extent along the tube axis (Figs. 1F, G). RAS-GFP labelled tip cells showed a circular staining of ZO-1 at their ventral base, where they contacted the stalk cells (Figs. 1H, I). At the tip of their anteroposterior extensions, where these cells contacted each other, ZO-1 staining was also prominent, presumably as a result of novel cell–cell contacts established between adjacent ISVs. Taken together, our immunofluorescence and single cell studies demonstrate that the ISVs are made up by endothelial cells sharing extensive cell–cell contacts with neighbouring endothelial cells, rather than by cells that are arranged in a head-to-tail fashion.

#### *Endothelial cells appear paired in ISVs*

While the distribution of cell junctions indicates a complex pattern of spatial relationships between endothelial cells, it does not reveal directly the cellular architecture of ISVs. We therefore generated a plasmid encoding a cytoplasmic mCherry protein under the control of the *flk1* enhancer. We injected this plasmid into *fli1:EGFP* transgenic embryos to differentially label a single (or a subset of) cells within an ISV. As expected, we found mCherry labelled either dorsal cells of the DLAV, basal cells contacting the aorta, or, most frequently, medial cells linking these two (Figs. 2A–D; the green and red colours of the fluorescent proteins were inverted to obtain better contrast). However, in most of the medial cells analysed (12/15), we found that mCherry-labelled cells did not appear to extend over

the entire circumference of the tube, but aligned with one or more only EGFP positive cell(s) along the tube axis (see arrows in Figs. 2B–D). We analysed the Z-stacks of such double-labelled vessels and discovered that two cell bodies were surrounding the luminal space, one mCherry/EGFP double-labelled endothelial cell and an EGFP-positive, mCherry negative cell (Figs. 2D–F). To confirm this observation, we re-examined the distribution of ZO-1 in cross sections of ISVs and detected ZO-1 protein between adjacent cells in close proximity to the lumen (Figs. 2G, H). The number of cells surrounding the lumen of the ISV does not appear to be fixed. At different proximodistal levels within a single ISV we were able to find either 2 or 3 junctional complexes in a cross section (Figs. 2G, H) corresponding to 2 or 3 endothelial cells enclosing the vascular lumen, respectively.

In summary, these findings show that the three types of cells that have previously been described as the building blocks of the ISV are not arranged in a simple head-to-tail fashion. Instead, they align over extended regions with neighbouring cells resulting in tubes that consist of two or more cells surrounding the luminal circumference, thus forming a multicellular tube.

#### *Dynamic behaviour of junctional proteins during ISV sprouting*

Because ZO-1 is not only present in junctional complexes of endothelial cells but also in the epidermis, the neural tube and other tissues, we wanted to use an endothelial-specific junctional marker to confirm our findings. Therefore, we raised antibodies against zebrafish VE-Cadherin (CDH5), which is expressed exclusively in the developing vasculature (Larson et al., 2004). We analyzed the distribution of the CDH5 protein by immunofluorescence and found that it was limited to the vasculature (Fig. 3A); no CDH5 was seen in the notochord or in the neural tube. The antiserum appeared to recognize a different cadherin in the pronephric duct (data not shown). Staining in the pronephric duct persisted upon morpholino inhibition of *cdh5*, while the staining in the endothelial cells disappeared (H.B. and M.A.; unpublished results). Immunofluorescent colabelling of ZO-1 and CDH5 proteins in *fli1:EGFP* embryos demonstrated that the two proteins co-localized in the developing vasculature, both in the dorsal aorta and in the caudal veins (not shown), as well as in ISVs (Fig. 3). In the developing ISVs, the distribution ZO-1 and CDH5 was indistinguishable, suggesting that they both label junctional complexes of endothelial cells during the sprouting process.

To obtain a better idea of how endothelial cells connect to each other during ISV formation, we analysed the distribution of ZO-1 (Figs. 4A–D) and CDH5 (Figs. 4E–H) at different stages of ISV development (from 22 hpf to 36 hpf). A differential distribution of cell junctions in ISVs was already apparent at the onset of angiogenic sprouting (Figs. 4A, E). While cells within the dorsal aorta were labelled around their entire circumference, both proteins were absent from the dorsal most part of the leading cell as it appears to migrate out of the dorsal aorta. At this stage cell junctions appear to be restricted to the base of the leading cell, which is in contact with trailing endothelial cells.



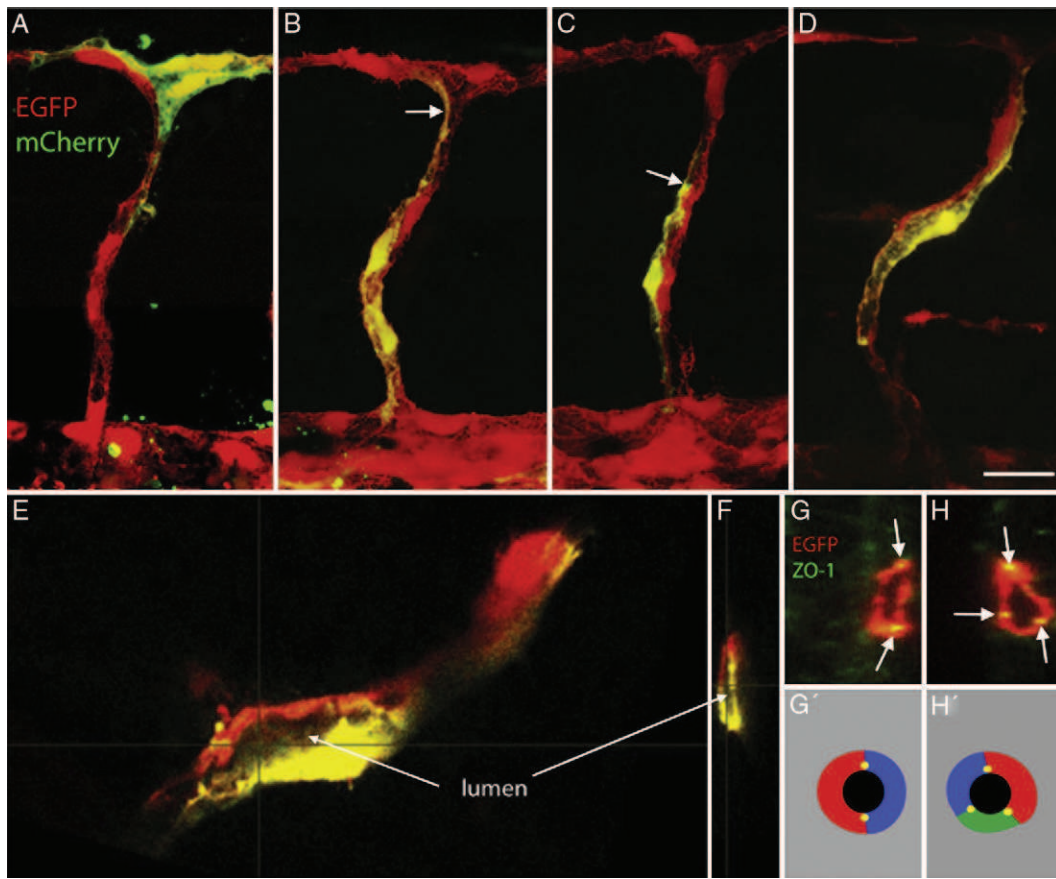


Fig. 2. Endothelial cells are paired in the ISV. (A–D) Confocal projection of single cells expressing mCherry under control of the *flkl* promoter (shown in green for better contrast) in *fli1:EGFP* transgenic embryos (red) in ISVs at 36 hpf (A–C) and 48 hpf (D) of development. (B) T-shaped cell embedded in the DLAV; (C, D) extended stalk cells. In all cases, mCherry-expressing cells appear to make up only part of the circumference of the tube (arrows), and appear paired or aligned with cells expressing EGFP only. (E) Single section (X–Y plane) of the cell shown in panel D. (F) Single cross section (Y–Z plane) of the ISV showing the lumen and the surrounding cells. (G, H) Single cross sections of ISVs at 48 hpf showing ZO-1 staining (arrows) between cells surrounding the lumen (2 cells in panel G, 3 cells in panel H). (G', H') Schematic representation of the cellular arrangement shown in panels G and H. Scalebars: 20  $\mu$ m.

Slightly later (Figs. 4E, F), when more cells have left the aorta, the junctional pattern becomes more complex. While the dorsal part of the tip cell was largely devoid of ZO-1 and CDH5, we saw extensive junctions between the tip cell and the following

cells, as well as among the latter. At 30 hpf, we already detected the predominant distribution pattern of CDH5 and ZO-1, namely the occurrence of two parallel lines extending along the tube axis (arrowheads in Figs. 4C, G).

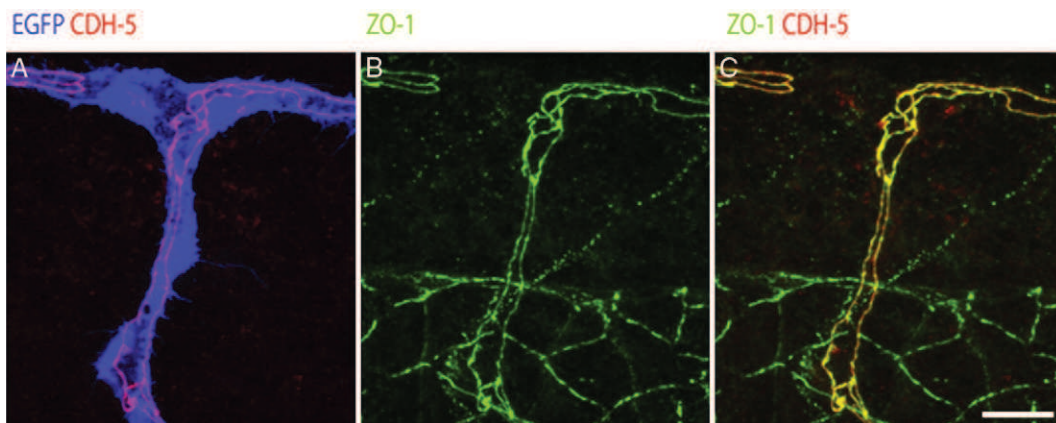


Fig. 3. CDH5 colocalizes with ZO-1 in endothelial cells. (A–C) Confocal projections of 36 hpf *fli1:EGFP* (blue) transgenic embryos labelled with anti CDH5 (red) and anti ZO-1 (green) antibodies. (A) CDH5 and the GFP show that CDH5 labels exclusively junctions of endothelial cells. (B) ZO-1 labels endothelial cells as well as cells in the notochord and the neural tube. (C) CDH5 and ZO-1 show co-localization (yellow) of the two junctional proteins in endothelial cells. Scalebars: 20  $\mu$ m.

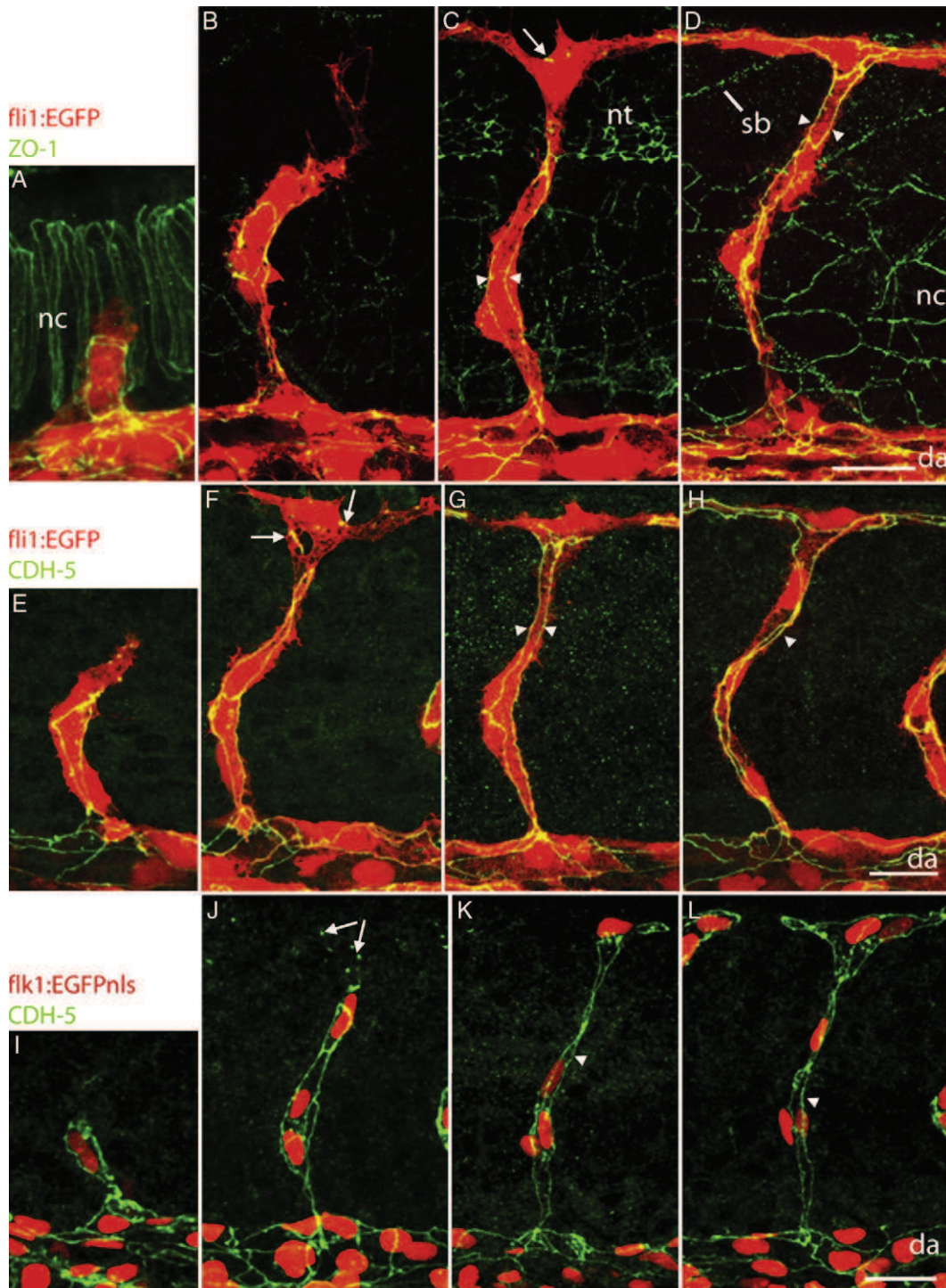


Fig. 4. Dynamic expression of junctional proteins during ISV formation. Confocal projections of *fli1:EGFP* embryos labelled with anti-ZO-1 (A–D) or CDH5 (E–H) antibodies and of *flk1:EGFPnls* embryos labelled with CDH5 (I–L) antibody at different developmental stages. (A, E, I) 22–24 hpf, (B, F, J) 26–28 hpf, (C, G, K) 30 hpf, (D, H, L) 36 hpf. Already at early stages (A, E) both proteins are localized along the stalk of the ISVs, presumably between putative tip cells on the one hand, and between stalk cells on the other hand. Spots and lines (arrows in panels C, F and J) of ZO-1 and CDH5 are visible when tip cells start to extend in anterior and posterior direction to eventually form the DLAV. Arrowheads point to parallel junctions running along the axis of the ISV. Abbreviations: see Fig. 1, nt: neural tube. Scalebars: 20  $\mu$ m.

To visualize junctions relative to the localization of cell nuclei, we examined the distribution of CDH5 (Figs. 4I–L) and ZO-1 (data not shown) in embryos carrying a *flk1:EGFP-NLS* transgene which labels the nucleus of endothelial cells (see below and Materials and methods). As in the previous

experiments, we found that the leading cell remains in close contact with the trailing cell(s) during EC sprouting. During sprouting, cell junctions of the leading cell were largely restricted to its proximal portion (Figs. 4I, J), while distal junctions were formed during establishment of the DLAV (Figs.



4K, L). Moreover, in the basal part of the ISV nuclei can be found in direct apposition to each other (Figs. 4K, L), thus further illustrating that the parallel lines of junctional complexes represent cell contacts between paired endothelial cells.

#### Complex cell rearrangements during vessel fusion in the DLAV

During formation of the DLAV the distribution of CDH5 and ZO-1 in the tip cell is highly dynamic. When the tip cells have reached the dorsal side of the embryo, they start to extend cellular processes in anterior and posterior direction. At this stage, before they make contact with their neighbouring endothelial cells, spots and lines of ZO-1 and CDH5 protein became evident (arrows in Figs. 4F, J). As soon as two tip cells

of adjacent sprouts contacted each other, a prominent localization of ZO-1 (Fig. 5A) and CDH5 (data not shown) was apparent at the contact site. During further development, this contact point expanded (Figs. 5B, C) and eventually appeared as an extended oval along the axis of the DLAV. Thereafter, the pattern became more complex with time (see Figs. 1 and 4), suggesting extensive cell rearrangements (see below).

To investigate the behaviour of endothelial cells during DLAV formation in more detail, we performed time-lapse analyses. By injecting *flkl:mCherry* plasmid into transgenic *flkl:EGFP* embryos we were able to observe the interaction between differentially labelled tip cells from adjacent segments. We found that tip cells from neighbouring ISVs “crawl” over each other after having made contact (Fig. 5D; supplementary

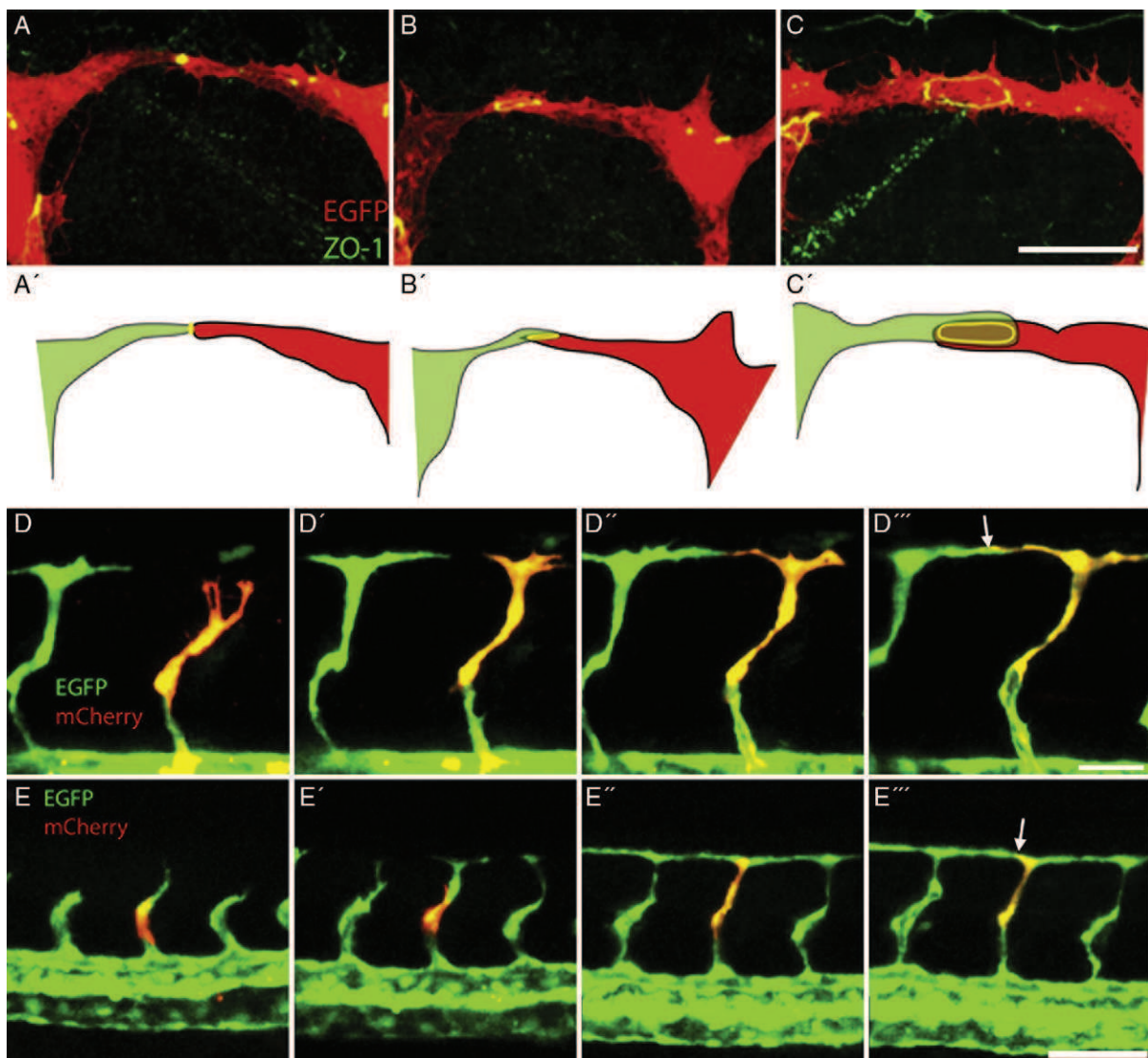


Fig. 5. Endothelial cell behaviour during formation of the DLAV. The figure depicts different ISVs within a single embryo. (A–C) ZO-1 pattern during vessel fusion. Confocal projections of 30 hpf *flkl:EGFP* fish (red) labeled with anti ZO-1 (green). (A) ZO-1 accumulates at the contact site of two putative tip cells, which then crawl over each other resulting in a small (B) oval-shaped ZO-1 pattern, which eventually expands to an extended oval (C). (A'–C') Schematic representation of the ZO-1 pattern shown in panels A–C. (D, E) Picture series of supplementary movies 1 and 2 showing dynamic cell behaviour during ISV formation. Movie (D) shows a tip cell expressing mCherry in a *flkl:EGFP* embryo. Within 5 h, the tip cell migrates dorsally and expands in anterior and posterior direction to fuse and form the DLAV. After first contact (D'') tip cells “crawl” over each other to some extent (arrow in panel D'''). Movie (E) shows a single stalk cell migrating dorsally to contribute to the DLAV (arrow in panel E'''). Scalebars: (A–C) 20 µm; (D–D''') 50 µm; (E–E''') 100 µm.

movie 1). This behaviour is consistent with the localization ZO-1 upon tip cell contact (see above). When we followed individually labelled stalk cells, we found that these cells moved dorsally and ultimately contributed to parts of the DLAV (Fig. 5E; supplementary movie 2). Clearly, the movement of stalk cells into the DLAV must be accompanied by the reorganization of cell–cell contacts, and account in part for the complexity of the junctional pattern within the DLAV, such as seen in Figs. 1 and 2.

#### *Sprouting of ISVs is accompanied by extensive cell divisions*

Our studies using single cell labelling and localization of cell junction components have shown that throughout the ISV, several cells appear to make up the apical surface of the luminal circumference. This is particularly surprising in the DLAV, which is thought to arise by the fusion of tip cells from adjacent ISVs and the formation of an intracellular lumen (Kamei et al., 2006). While cellular rearrangements and cell migration play a crucial role in this process (see above), it is also clear that additional cells have to be generated in order to contribute to the DLAV. Tip cells could divide either shortly before or after the fusion with the adjacent metamer. It has indeed been shown that tip cells do divide, but they appear to do so during the dorsal migration, before single tip cells contact each other (Leslie et al., 2007; Siekmann and Lawson, 2007).

To monitor such cell divisions, we generated a transgenic fish line expressing a nuclear localized GFP under the control of the *flk1* promoter (*flk1*:EGFP-NLS). These fish allowed us to analyze the number of nuclei in different ISVs and to monitor

the behaviour of the nuclei during ISV formation. The GFP protein expressed in these transgenic lines translocates from the nucleus into the cytoplasm shortly before cell division, and then re-enters the daughter nuclei after nuclear division. This property makes it possible to study cell behaviour also, because the outline of the cells that are going to divide can be visualized shortly before cell division (see arrow in Fig. 6A). Shortly after the establishment of the DLAV (36 hpf), we determined the number of cells per ISV by counting the nuclei located within the ISVs. We found that ISVs contained between 3 and 7 nuclei. The majority of ISVs, however, contained 4 or 5 nuclei (43 out of 55). When we observed the endothelial cell nuclei during ISV formation in vivo, we found that in all segments, nuclei divided as they were migrating towards the dorsal side, similar to what has been recently reported (Leslie et al., 2007; Siekmann and Lawson, 2007) (see movie 3; Fig. 6). However, and consistent with the variations in ZO-1 or CDH5 distribution in different ISVs, we found considerable variability in the “nuclear behaviour” of different ISVs. In most cases, three cells (as visualized by three nuclei) migrated out of the dorsal aorta. Divisions were often observed in the dorsal most nuclei (representing the leading cell of the outgrowing branch), arguing that tip cells divide as they migrate out. In many branches, we observed that the stalk cells also divided, before the tip cell of the same ISV did so (Fig. 6; supplementary movies 3 and 4). We also observed that nuclei arising in a given ISV could end up in the stalk of an adjacent ISV (supplementary movie 5). Based on the analysis of five different time-lapse movies, two to three cells migrated out of the dorsal aorta, and, in most cases, two of them underwent another round of cell division (one tip cell and one stalk cell),

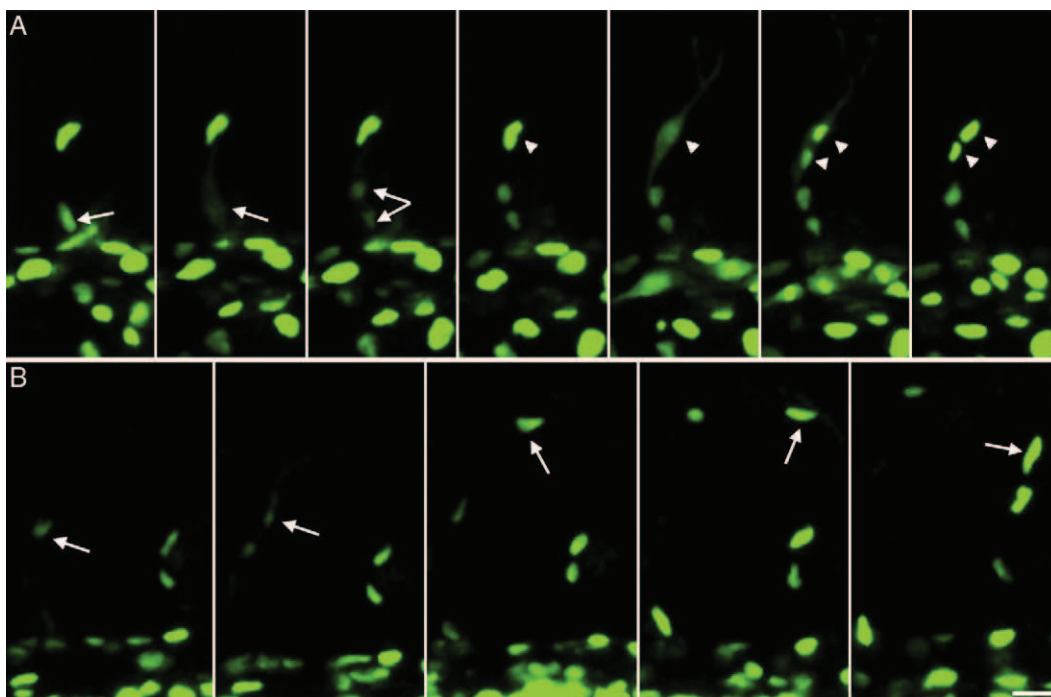


Fig. 6. Non-stereotyped behaviour of nuclei in ISVs. Picture series taken from supplementary movies 3 (A) and 4 (B) showing sprouting ISV in *flk1*:EGFP-NLS embryos. (A) A stalk cell (arrow) divides prior to the tip cell (arrowhead). Outline of the cell can be visualized during cell division. (B) A tip cell nucleus ends up in an adjacent ISV (arrows are following the nuclei). Scalebars: 20  $\mu$ m.

eventually giving rise to the 4 or 5 endothelial cells present in the majority of ISVs. Thus, the process of ISV formation is accompanied by cell migration and cell division, but these processes do not appear to be stereotyped and we observed a high degree of variation, suggesting that they are not under strict genetic control.

## Discussion

### *A model for the cellular architecture of ISVs in the trunk region in the zebrafish embryo*

The formation of the ISV in the trunk of the zebrafish embryo serves as a paradigm to study how endothelial tubes form in an *in vivo* model system. To better characterize the cellular architecture of ISVs, we have studied the organization of their intercellular junctions. For this purpose, we generated antibodies against the CDH5 protein, an endothelial-specific VE-type cadherin in the zebrafish. Furthermore, we have used two-colour, single cell imaging to differentially label endothelial cells within a given ISV. Together, these approaches have allowed us to define the spatial relationships between neighbouring endothelial cells. Based on our findings, we propose that the architecture of the ISV is different from what has been suggested previously. Instead of being arrayed in a serial fashion, we demonstrate that in most regions, endothelial cells are paired along the axis of the ISVs. In this modified cellular model of ISVs, the luminal space appears to be in-between endothelial cells. The ISV thus qualifies as a multicellular tube containing an “extracellular” lumen (Lubarsky and Krasnow, 2003). This model has considerable implications on several aspects of ISV formation, such as cell behaviour and lumen formation.

### *How is the lumen formed in the ISVs?*

Lumen formation in ISVs has previously been studied using two-photon confocal time-lapse imaging (Kamei et al., 2006). This study provided strong support for a model in which the vascular lumen is formed *de novo* by formation and intracellular and intercellular fusion of endothelial vacuoles. Vessels formed in this fashion consist of a “seamless” tube containing an intracellular lumen. This interpretation was based on a previous model proposing that ISVs consist of three cells arranged in a linear fashion (Childs et al., 2002). However, based on our analyses, we conclude that endothelial cells in the ISV share cell junctions over the entire vessel length. This strongly argues that the luminal space is in-between adjacent cells, and therefore “extracellular”, and not contained within the cytoplasm of single cells (“intracellular”). It appears likely that the lumen of ISV is formed in such a way that intracellularly generated vacuoles are exported through exocytosis into a common intercellular space bounded by at least two endothelial cells that are joined together by junctional contacts. This process eventually leads to the formation of a common intercellular luminal space as suggested by Kamei et al. (2006) for larger calibre vessels. It may be advantageous for ISVs to be made up

by a multicellular tube; it is difficult to imagine how tubes made of chains of cells with an intracellular lumen would ramify later during development through sprouting angiogenesis. In the *Drosophila* embryo, terminal cells of the trachea do form an extensive intracellular luminal network, these terminal cells do not divide anymore during later stages of development (Samakovlis et al., 1996).

### *Dynamic tip cell rearrangements during vessel fusion*

The dynamic cell behaviour during ISV formation in the zebrafish embryo is exemplified by the behaviour of the tip cells during the process of vessel fusion. During dorsal migration of the tip cells, “dot-like” and short “line-like” ZO-1 and CDH5-containing structures are already visible in these cells. Immediately upon the first contact between tip cells from adjacent ISVs, ZO-1 and CDH5 localize to the contact point. This is reminiscent of the initial steps in branch fusion in the developing tracheal system in the *Drosophila* embryo, where filopodial contacts of specialized fusion cells from adjacent metameres result in the immediate localization of DE-cadherin to the contact site (Samakovlis et al., 1996; Tanaka-Matakatsu et al., 1996). In the absence of DE-cadherin, branch fusion does not occur in the tracheal system (Uemura et al., 1996). However, the branch fusion process in the tracheal system appears to be rather different after this initial step when compared to the fusion of the ISVs in the zebrafish. In the tracheal system, the highly specialized fusion cells ultimately develop into so-called doughnut cells, which are made up of

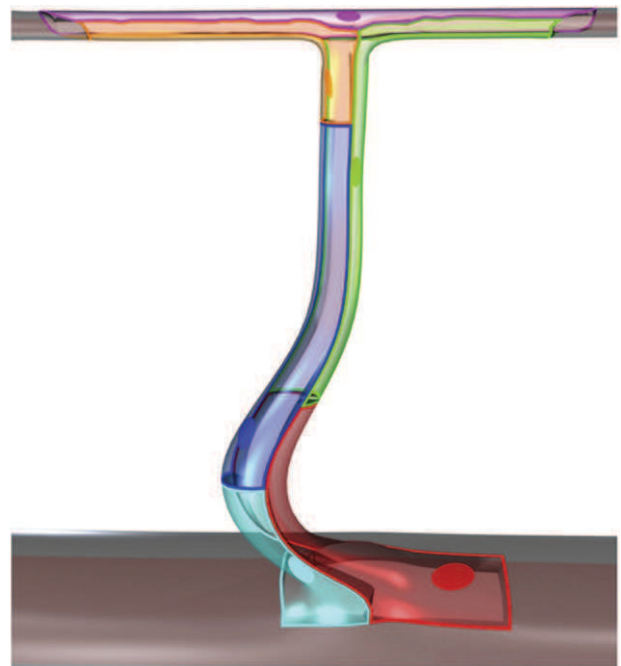


Fig. 7. Putative cellular architecture of ISVs in the zebrafish trunk. According to our model ISVs are multicellular tubes consisting of 4–6 cells per vessel. These cells are arranged in such a way that they overlap in a staggered fashion in the ISV as well as the DLAV. This arrangement allows extensive cell–cell contacts (coloured lines), which correspond to a complex pattern of intercellular junctions.



two apical sides and a seamless lumen in-between (Uv et al., 2003). Fusion points within the mature tracheal system can thus easily be identified using markers for adherens junctions. In the ISVs of the zebrafish embryos, it appears that endothelial tip cells first contact each other and establish a CDH5-containing interface. However, and in contrast to the *Drosophila* tracheal system, this interface is then enlarged such that adjacent tip cells make more and more extensive contact until they are paired over much of their extent (see model in Fig. 7). In addition, stalk cells move up to the DLAV and increase their contact surface with tip cells. In general, it appears that adjacent endothelial cell maximize their contact surfaces. It is possible that they do so because the intracellular vacuoles preferentially fuse with pre-existing apical membrane patches, resulting in their extension and the generation of a larger and larger surface surrounding the luminal space.

Our analysis of a transgenic line expressing a nuclear version of GFP also showed that both tip and stalk cells divide as they migrate during the process of ISV formation. It has been previously argued that the division of the tip cell is a unique feature of this particular cell imposed to it via the Dll/Notch and the Vegfr signalling pathways (Leslie et al., 2007). Our results do not favour the simplest version of such a model, and suggest that tip and stalk cells are more similar in their behaviour than anticipated: both can and do eventually divide as they migrate, and do so rather independently and not in a well established choreography. It will be important to study how lumen formation proceeds in such a dynamic cellular environment, in which cells even divide during the process of lumen formation.

Endothelial cells rearrange extensively as the ISVs form and eventually fuse. They migrate out of the dorsal aorta, divide as they migrate, and can even migrate into neighbouring ISV sprouts. We also find a lot of variation between individual ISV in respect to junctional organization and cell number, suggesting that cell behaviour during ISV formation is very plastic and cannot be easily stereotyped. To accurately describe these cell rearrangements, the formation of intercellular junctional complexes has to be imaged at high-resolution in live transgenic zebrafish embryos at the single cell level, similar to what has been done during tracheal development in the *Drosophila* embryo (Neumann and Affolter, 2006; Ribeiro et al., 2004). In addition, the formation and fusion of vacuoles and the formation of cell–cell contacts have to be imaged in parallel in the same live embryos, to find out whether there is coordination between the two processes, such that lumen formation eventually leads to the proper assembly of continuous vascular tubes.

## Acknowledgments

We thank Brant Weinstein for TG(*flil*:EGFP)<sup>y1</sup> and Didier Stainier for TG(*flkl*:EGFP)<sup>S843</sup> fish lines, Jon D. Larson for *cdh5* cDNA, Dimitris Beis for *flkl* promoter DNA, Alexander Weiss for help with illustrations, Markus Dürrenberger for help with confocal microscopy, Emmanuel Caussinus for help with image analysis and Kumutini Kalendra for fish care. This work

has been supported by the Kantons Basel-Stadt and Basel-Land, the Swiss National Science Foundation, KTI, and by a Network of Excellence grant “Cells into Organs” from the FP6 of the European Community.

## Appendix A. Supplementary data

Supplementary data associated with this article can be found, in the online version, at doi:10.1016/j.ydbio.2008.01.038.

## References

- Adams, R.H., Alitalo, K., 2007. Molecular regulation of angiogenesis and lymphangiogenesis. *Nat. Rev., Mol. Cell Biol.* 8, 464–478.
- Affolter, M., Bellusci, S., Itoh, N., Shilo, B., Thiery, J.P., Werb, Z., 2003. Tube or not tube: remodeling epithelial tissues by branching morphogenesis. *Dev. Cell* 4, 11–18.
- Barolo, S., Carver, L.A., Posakony, J.W., 2000. GFP and beta-galactosidase transformation vectors for promoter/enhancer analysis in *Drosophila*. *Biotechniques* 29, 726, 728, 730, 732.
- Beis, D., Stainier, D.Y., 2006. In vivo cell biology: following the zebrafish trend. *Trends Cell Biol.* 16, 105–112.
- Carmeliet, P., 2005. Angiogenesis in life, disease and medicine. *Nature* 438, 932–936.
- Childs, S., Chen, J.N., Garrity, D.M., Fishman, M.C., 2002. Patterning of angiogenesis in the zebrafish embryo. *Development* 129, 973–982.
- Coultas, L., Chawengsaksophak, K., Rossant, J., 2005. Endothelial cells and VEGF in vascular development. *Nature* 438, 937–945.
- Ghabrial, A.S., Krasnow, M.A., 2006. Social interactions among epithelial cells during tracheal branching morphogenesis. *Nature* 441, 746–749.
- Isogai, S., Horiguchi, M., Weinstein, B.M., 2001. The vascular anatomy of the developing zebrafish: an atlas of embryonic and early larval development. *Dev. Biol.* 230, 278–301.
- Isogai, S., Lawson, N.D., Torrealday, S., Horiguchi, M., Weinstein, B.M., 2003. Angiogenic network formation in the developing vertebrate trunk. *Development* 130, 5281–5290.
- Jin, S.W., Beis, D., Mitchell, T., Chen, J.N., Stainier, D.Y., 2005. Cellular and molecular analyses of vascular tube and lumen formation in zebrafish. *Development* 132, 5199–5209.
- Kamei, M., Saunders, W.B., Bayless, K.J., Dye, L., Davis, G.E., Weinstein, B.M., 2006. Endothelial tubes assemble from intracellular vacuoles in vivo. *Nature* 442, 453–456.
- Kimmel, C.B., Ballard, W.W., Kimmel, S.R., Ullmann, B., Schilling, T.F., 1995. Stages of embryonic development of the zebrafish. *Dev. Dyn.* 203, 253–310.
- Larson, J.D., Wadman, S.A., Chen, E., Kerley, L., Clark, K.J., Eide, M., Lippert, S., Nasevicius, A., Ekker, S.C., Hackett, P.B., Essner, J.J., 2004. Expression of VE-cadherin in zebrafish embryos: a new tool to evaluate vascular development. *Dev. Dyn.* 231, 204–213.
- Lawson, N.D., Weinstein, B.M., 2002a. Arteries and veins: making a difference with zebrafish. *Nat. Rev., Genet.* 3, 674–682.
- Lawson, N.D., Weinstein, B.M., 2002b. In vivo imaging of embryonic vascular development using transgenic zebrafish. *Dev. Biol.* 248, 307–318.
- Leslie, J.D., Ariza-McNaughton, L., Bermange, A.L., McAdow, R., Johnson, S.L., Lewis, J., 2007. Endothelial signalling by the Notch ligand Delta-like 4 restricts angiogenesis. *Development* 134, 839–844.
- Lubarsky, B., Krasnow, M.A., 2003. Tube morphogenesis: making and shaping biological tubes. *Cell* 112, 19–28.
- Neumann, M., Affolter, M., 2006. Remodelling epithelial tubes through cell rearrangements: from cells to molecules. *EMBO Rep.* 7, 36–40.
- Ny, A., Autiero, M., Carmeliet, P., 2006. Zebrafish and *Xenopus* tadpoles: small animal models to study angiogenesis and lymphangiogenesis. *Exp. Cell Res.* 312, 684–693.
- Ribeiro, C., Neumann, M., Affolter, M., 2004. Genetic control of cell intercalation during tracheal morphogenesis in *Drosophila*. *Curr. Biol.* 14, 2197–2207.

- Samakovlis, C., Manning, G., Steneberg, P., Hacohen, N., Cantera, R., Krasnow, M.A., 1996. Genetic control of epithelial tube fusion during *Drosophila* tracheal development. *Development* 122, 3531–3536.
- Siekman, A.F., Lawson, N.D., 2007. Notch signalling limits angiogenic cell behaviour in developing zebrafish arteries. *Nature* 445, 781–784.
- Tanaka-Matakatsu, M., Uemura, T., Oda, H., Takeichi, M., Hayashi, S., 1996. Cadherin-mediated cell adhesion and cell motility in *Drosophila* trachea regulated by the transcription factor Escargot. *Development* 122, 3697–3705.
- Uemura, T., Oda, H., Kraut, R., Hayashi, S., Kotaoka, Y., Takeichi, M., 1996. Zygotic *Drosophila* E-cadherin expression is required for processes of dynamic epithelial cell rearrangement in the *Drosophila* embryo. *Genes Dev.* 10, 659–671.
- Uv, A., Cantera, R., Samakovlis, C., 2003. *Drosophila* tracheal morphogenesis: intricate cellular solutions to basic plumbing problems. *Trends Cell Biol.* 13, 301–309.
- Westerfield, M., 2000. *The zebrafish book. A guide for the laboratory use of zebrafish (Danio rerio)*, fourth ed. Univ. of Oregon Press, Eugene.



## 6.2 Chapter II: Distribution of different tube architecture in ISVs and the DLAV

We have previously shown that ISVs are to a large extent multicellular tubes; however, we didn't exclude that parts of the ISVs have a different tube architecture, such as unicellular tubes with autocellular junctions or tubes with an intracellular lumen as proposed by Kamei et al.. We do see lack/gaps of ZO1/CDH5 expression in ISV in stainings at 36 and also at 48 hpf suggesting the presence of intracellular lumens. But, as this tissue is fixed and a potential lumen would mostly collapse in fixed tissue, we cannot discriminate between a collapsed lumen and a non-lumenized vessel.

To clearly discriminate between these two possibilities we used live embryos at 2dpf, where the lumen is clearly inflated seen by the darker spaces in the middle of the tube or by cross-sections (see Figure 6.1). We used the photo-convertible protein Kaede to label individual cells in the ISV and the DLAV. We expressed Kaede with the Gal4/UAS system using a *fli1a:GFF* transgenic driver line, which was established by Lukas Herwig in the lab, and a *UAS:Kaede* responder line (ZIRC). Kaede can be easily converted from green to red using an UV laser (405 nm). To label single cells, we illuminated a region of interest, which encompassed a cell nucleus, for 20 seconds with 100% UV laser power. The turnover of the converted Kaede between cytoplasm and nucleus appeared to be very fast, as immediately after photo conversion of the cell nucleus the cytoplasm turned red as well, clearly discerning borders between 2 cells (see Figure 6.1 and movie 1-4).

As previously shown with transient expression (Figure 2 in Blum et al., 2008), we found labeled cells, which were paired with one or more unlabeled cells (Figure 6.1 A, A' movie 1 (x,y slices) and 4 (y,z slices)). But we also found cells where the whole circumference of the lumen was encompassed by one single red labeled cell (Figure 6.1 B, B'). To ensure that the lumen was entirely engulfed by this individual cell we made movies through x,y slices and y,z slices of what we thought represented single cells around the lumen (movie 3 and 4). The x,y slices movie clearly showed the border between the red cell and the green cells, where the green cells in none of the x,y slice spans over the whole vessel/cell length. Going through the y,z slices, we found that in a set of slices only the red labeled cell was surrounding the lumen. In this assay we were not able to discriminate between a cell with autocellular junction and a cell with an intracellular lumen. But as we only very rarely saw stretches of autocellular junctions in stainings, our finding suggested that these cells have an intracellular lumen.

In another assay, we injected fluorescent high molecular weight dextran, and fixed embryos at 2 dpf. The dextran got fixed and stayed partially in the luminal spaces. We found stretches

where dextran was present, suggesting a lumen, but no junctions were visible, strongly suggesting an intracellular lumen (see arrows in Figure 6.2).

Having obtained good evidence that intracellular lumens are present, we wanted to get a rough idea of the quantitative distribution of these different kinds of tubes

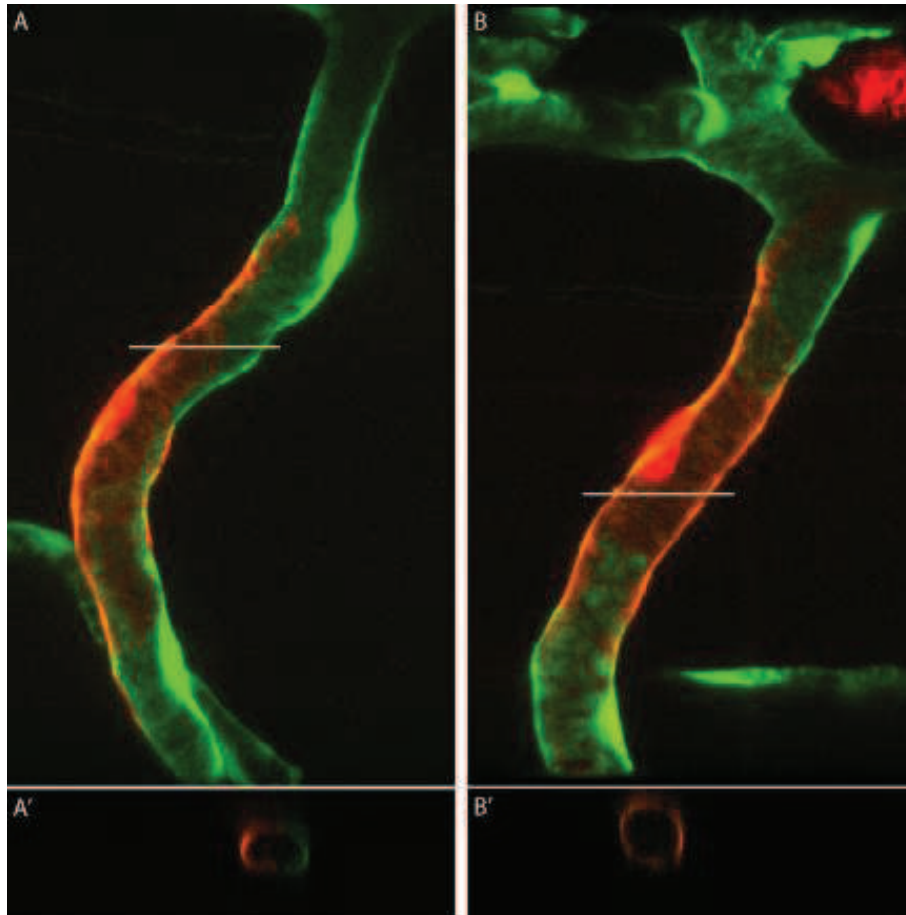


Figure 6.1

**Tube variation in ISVs at 2 dpf:** Kaede converted single cells (red). (A) shows a cell in a multicellular context, (B) shows a unicellular tube with. Representative cross-sections at the level of the white bars are shown in A' and B' (see also movies of slice through x,y (movie 1 for A and movie 3 for B) and y,z slices (movie2 for A and movie 4 for B)) .

We decided to quantify separately the ISV stalk and the DLAV and used two approaches to quantify the amount of seamless tubes. On the one hand we randomly labeled single cells in transgenic *fli1a:GFF; UAS:Kaede* embryos and on the other hand we used antibody stainings and measured the extent of vessel length without junctions compared to the entire vessel length, giving an idea of the percentage of intracellular lumen in ISV and DLAV (see Figure 6.3 A for an example). ISVs were measured from the DA to the DLAV and DLAV sections were measured from ISV to ISV. All quantifications were made in an area of 5-6 ISVs anterior to the end of the yolk extension.

### ISV stalk

In 36 labeled cells, 9 had stretches of intracellular lumen (or autocellular junctions). When we looked at the distribution of junctions within the stalk, we found that within a total length of 44

measured ISVs, 88% of the total length showed a multicellular pattern of junctions. 50 % of

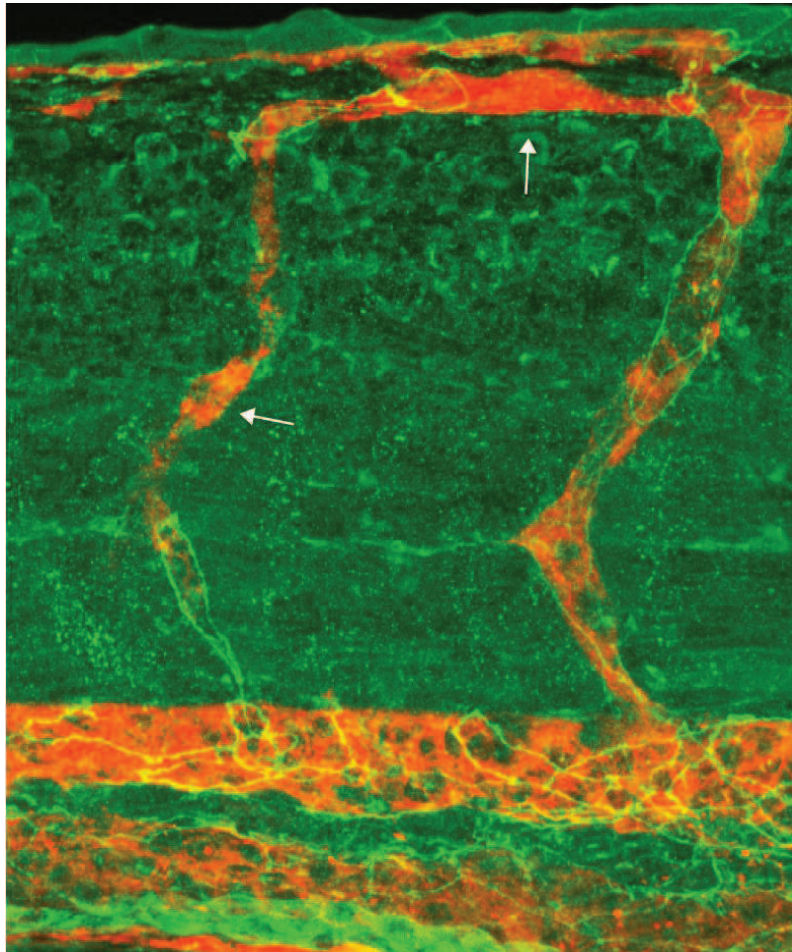


**Figure 6.2**

**Dextran injection revealed intracellular lumen:** 2dpf dextran (red) injected embryos showed a filled lumen in regions where VE-cadherin was not present (arrows).

the ISVs were entirely multicellular from the DA/PCV up to the DLAV. In the other 50%, we found 1-2 gaps per vessel, meaning one or two cells per vessel with intracellular lumen. The length of intracellular stretches varied from 5 to 45 microns at an average ISV length of 130 microns (see Figure 6.3).

### **DLAV**

When considering the DLAV, the story looked quite different. In the DLAV, 16 from 24 cells had an intracellular lumen, thus 66 percent of the cells compared to 25% in the stalk. Compared to the stalk, an intracellular lumen is the predominant form of lumen in the DLAV at least at 2 dpf. This was also confirmed with staining where only 63 % of the DLAV showed a multicellular pattern of junctions, but more importantly only 7 out of 36 measured DLAV sections (from ISV to ISV) were entirely multicellular. 14 sections had one gap and 15 showed two gaps, which varied in length from 8 to 47 microns at an average DLAV section length of 75 microns. We also observed more autocellular junctions in the DLAV (see Figure 6.3 B-D).

Taken together, the majority of the ISV stalk consists of multicellular tubes with an extracellular lumen, whereas the DLAV has more intracellular lumen and thus suggests a different mechanism for lumen formation.

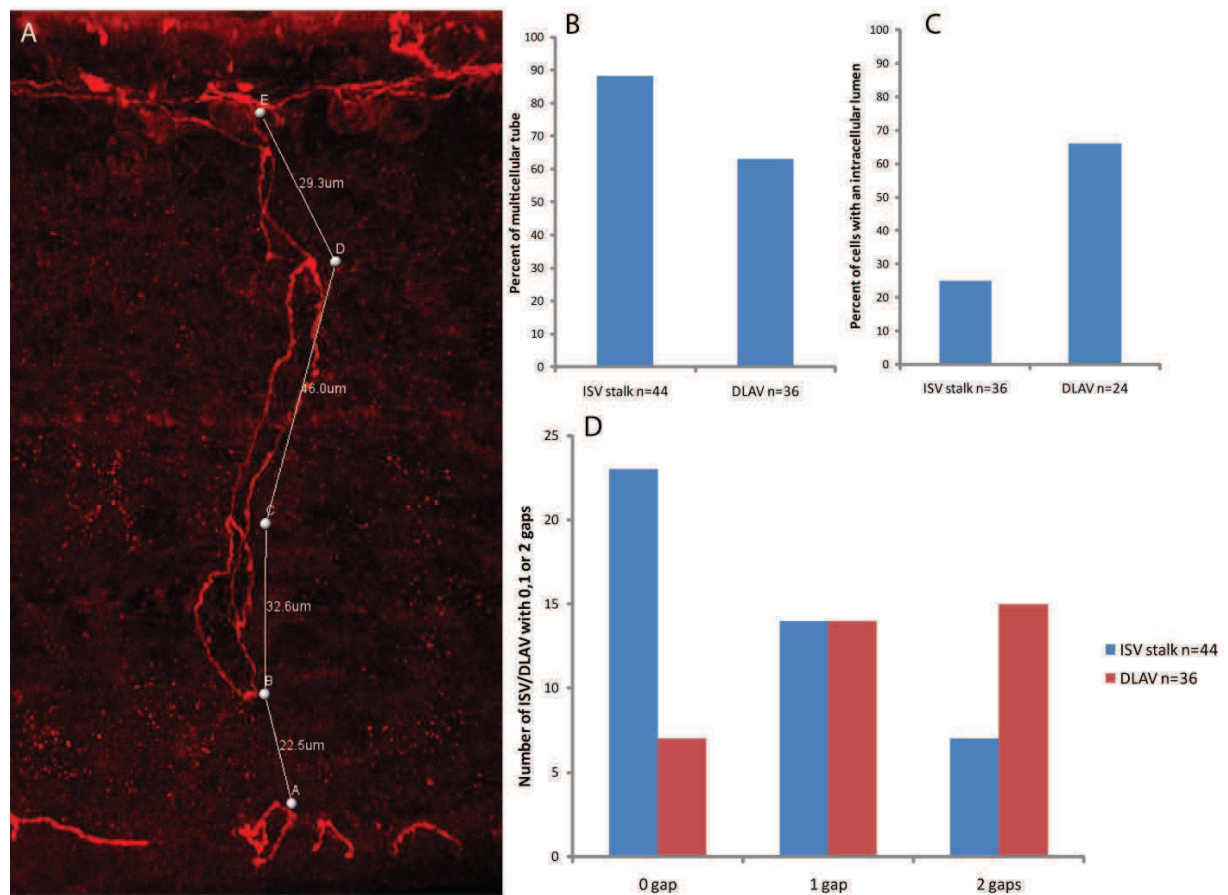


**Figure 6.3**

**ISV stalk and DLAV have different distribution of tube architecture at 2 dpf:** (A) shows an example of quantification of junctions. The measurement points A-E is the total length of the ISV stalk and A-B the length of intracellular lumen as 1 gap. (B) shows percentage of multicellular tube in ISV and DLAV. (C) shows percentage of cells showing an intracellular lumen using Kaede conversion. (D) shows number of ISVs/DLAV, which have 0,1 or 2 gaps.



## 6.3 Chapter III: Cellular mechanisms during ISV formation and anastomosis

Using antibody staining and single cell labeling we have shown that ISVs have for a high percentage of their extent a different architecture than formerly proposed in Kamei et al., 2006. The stalk appeared to consist predominantly of multicellular tubes suggesting a budding mechanism for lumen formation. The DLAV, in contrast, had a high portion of seamless tubes with intracellular lumen, suggesting a cell hollowing mechanism for lumen formation. Interestingly, the DLAV is the location where anastomosis of ISVs takes place and this might explain the degree of seamless tubes.

### 6.3.1 Cellular mechanisms during anastomosis

Cellular mechanisms during anastomosis have remained ill described despite the importance of anastomosis to form a proper and functional vascular system. ISVs have been shown to anastomose at around 28-30 hpf (Isogai et al., 2003). Before anastomosis, tip cells of ISVs extend filopodia and protrusions in anterior and posterior direction exploring their environment (see arrow in Figure 6.4 A). Protrusions from adjacent tip cells eventually contact each other forming a stable bridge between two stalks (Figure 6.4 B). The lumen extends from the stalk (arrow in Figure 6.4 C) and eventually reaches the DLAV, thus completing anastomosis (Figure 6.4 D, movie 5).

We have characterized a few aspects of anastomosis of ISVs using antibody staining against ZO-1 and Ve-cadherin in fixed embryos (Blum et al., 2008). At 30 hpf, we found different patterns including dots, small loops and larger loops in the DLAV at presumptive locations of anastomosis. In addition, tip cells appeared to crawl over each other during anastomosis suggesting a mechanism, whereby the interface between two tip cells is increased (see Figure 5A-C and D-D'' as well as suppl. movie 1 in Blum et al., 2008). Unfortunately, we lack either time (fixed embryos) or cellular resolution in these experiments making it impossible to prove the proposed model and to evaluate further steps during anastomosis.

To circumvent these limitations, the idea was to use similar methods, which were used earlier in the lab to study the tracheal system of *Drosophila melanogaster*. The use of transgenic flies expressing an  $\alpha$ -cateninGFP localizing to the junctions of tracheal epithelial cells, has unambiguously revealed the cellular mechanism during branch elongation (Ribeiro et al., 2004).

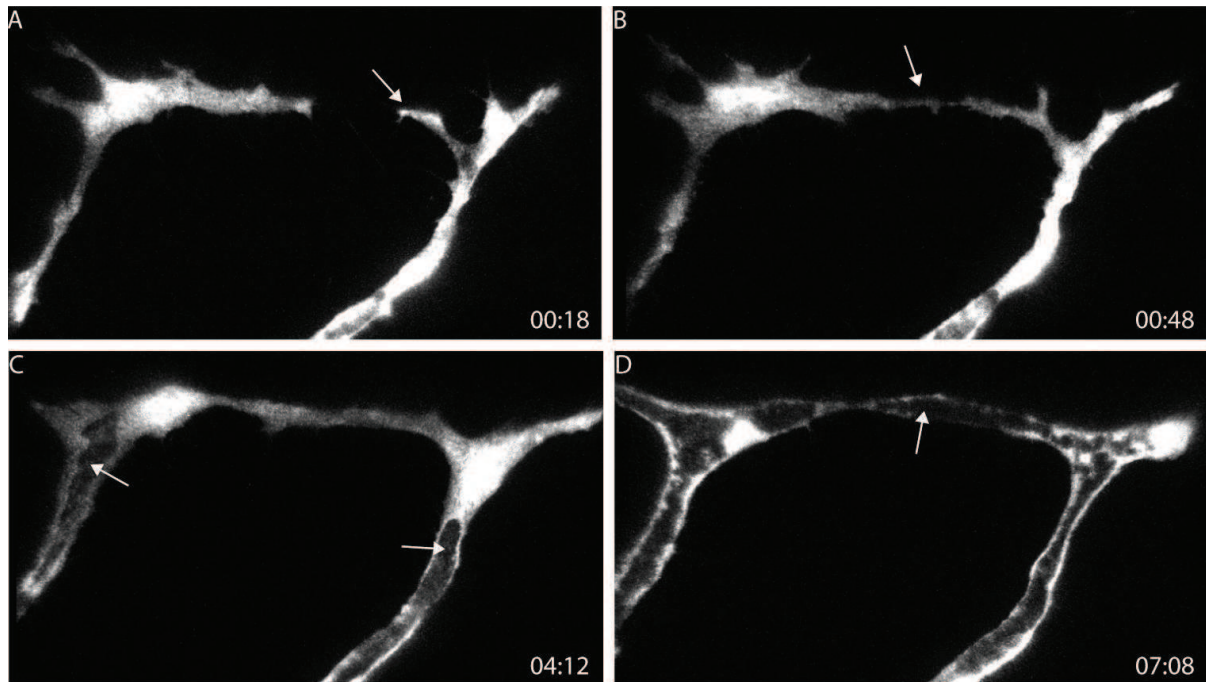


**Figure 6.4**

**Anastomosis of ISVs in *flk1:EGFP* zebrafish embryos:** Series of pictures taken from movie 5. High resolution movie (63x lens, 2x zoom, 2 minutes between timepoints) shows steps during DLAV formation. Tip cells reaching the dorsal part of the embryo showed protrusion and filopodia in anterior and posterior direction (A, arrow). Tip cells made an initial contact forming the DLAV (B). The lumen opened from the stalk and proceeded through the DLAV (arrow in C and D).

In an effort to establish the UAS-Gal4 system for the vascular system in the zebrafish, Lukas Herwig in the lab established the above mentioned *fli1:GFF* driver line (GFF is a variation of Gal4 less toxic to the zebrafish (Asakawa et al., 2008)) and a UAS responder line controlling a N-terminally EGFP tagged version of human ZO-1 (Riesen et al., 2002). A *UAS:RFP* responder line (Asakawa et al., 2008) was used for cytoplasmic labeling of endothelial cells. While the GFF protein was expressed in all endothelial cells and some ectopic locations such as muscles as visualized by RFP expression (see below), expression of the EGFP-hZO1 fusion protein was only seen in a mosaic fashion when the two constructs were brought together upon crossing the driver and the responder lines. Although such mosaic expression makes it more difficult to identify embryos with tip cells expressing EGFP-hZO1 at the right stage (before anastomosis, during ISV sprouting), the mosaics' can be used to unambiguously identify which one of two contacting tip cells expresses the fusion protein and, accordingly, from which tip cell the labeled junctional complexes arise.

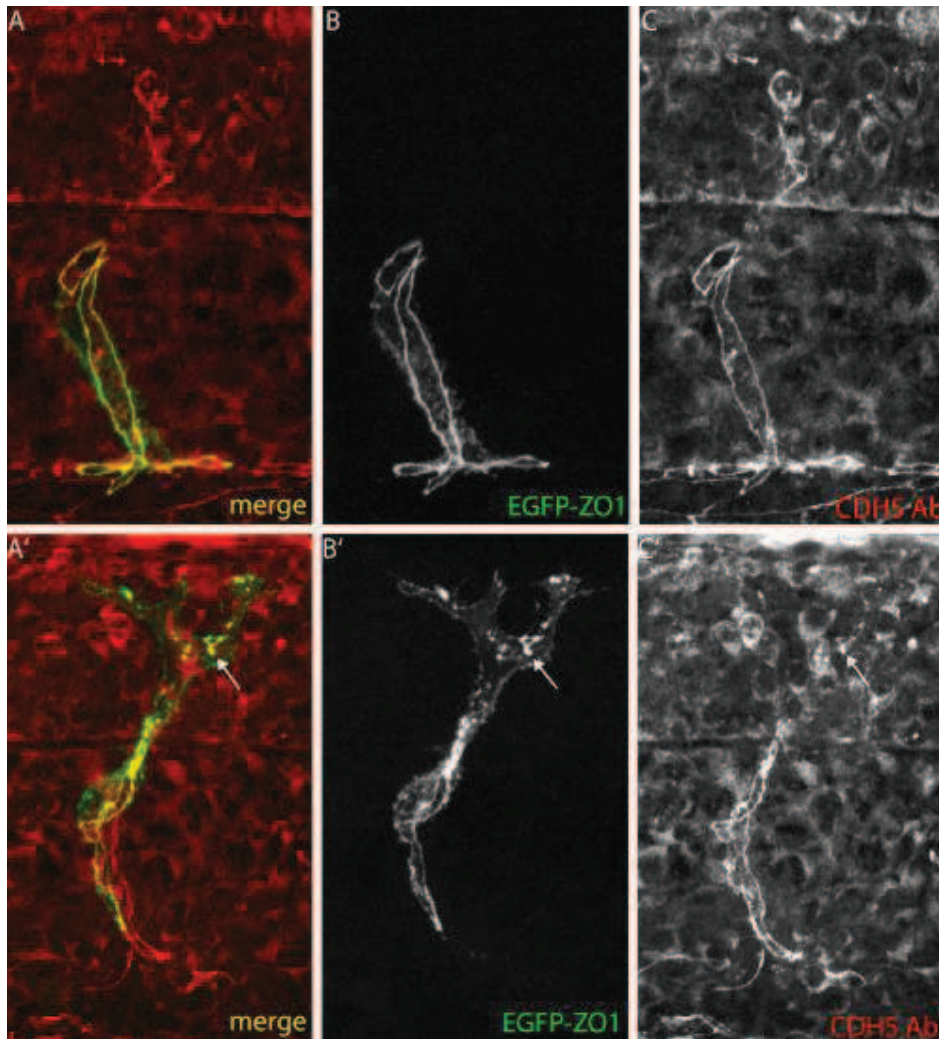


**Figure 6.5**

**EGFP-hZO1 co-localizes with endogenous VE-Cadherin:** A-C show a stalk cell and A'-C' show a tip cell, where even dots do co-localize (arrow).

We first verified whether the expression of EGFP-hZO1 co-localized with endogenous AJ complexes. In wild type embryos, endogenous ZO1 and VE-cadherin staining overlapped (see Figure 3 in Blum et al., 2008). We therefore stained double transgenic *fli1:GFF, UAS:EGFP-hZO1* embryos with Ve-cadherin antibodies. In a stalk cell EGFP-hZO1 recapitulated and co-localized with the Ve-cadherin Ab staining. EGFP-hZO1 did show some cytoplasmic labelling but clearly enriched at junctions (Figure 6.5 A-C). Quite remarkably, EGFP-hZO1 was apparent in a number of dots and short lines in proximal regions of tip cells. Even these dots did co-localize with endogenous Ve-cadherin (see arrow in Figure 6.5 A'-C') and such patterns were also found for endogenous ZO1 (see Figure 4 C and F in Blum et al., 2008). Thus, EGFP-hZO1 faithfully reflected the distribution of endogenous Ve-cadherin and ZO1 containing cell junction complexes in live embryos and therefore allows us to follow individual cells and their behavior by monitoring their AJ in vivo using high resolution 4D confocal microscopy.



In the following set of movies we used triple transgenic embryos (all movies have the same colour code: *fli1:GFP*; *UAS:RFP*(red); *UAS:EGFP-hZO1*(green); if present, QD(blue)) to follow the formation of tip cell contacts and the elaboration of these contacts during the process of ISV anastomosis and lumen formation in the DLAV. While cell contacts were monitored by the EGFP-hZO1, lumen inflation was observed using the cytoplasmic RFP, which upon lumen inflation got pushed to the side of the vessel resulting in a fainter RFP signal in the middle of the vessel (see also arrows in Figure 6.4 C and D as well as movie 5). Alternatively quantum dots (QD) were injected in the sinus venosus, which are carried by the blood plasma throughout the vasculature, unambiguously labeling open lumens with a connection to the DA. Observing only the RFP channels in such movies confirmed that these fainter, almost black areas in vessels were indeed inflated lumens as they were filled with QD (Figure 6.6 and movie 6 A,B,C).

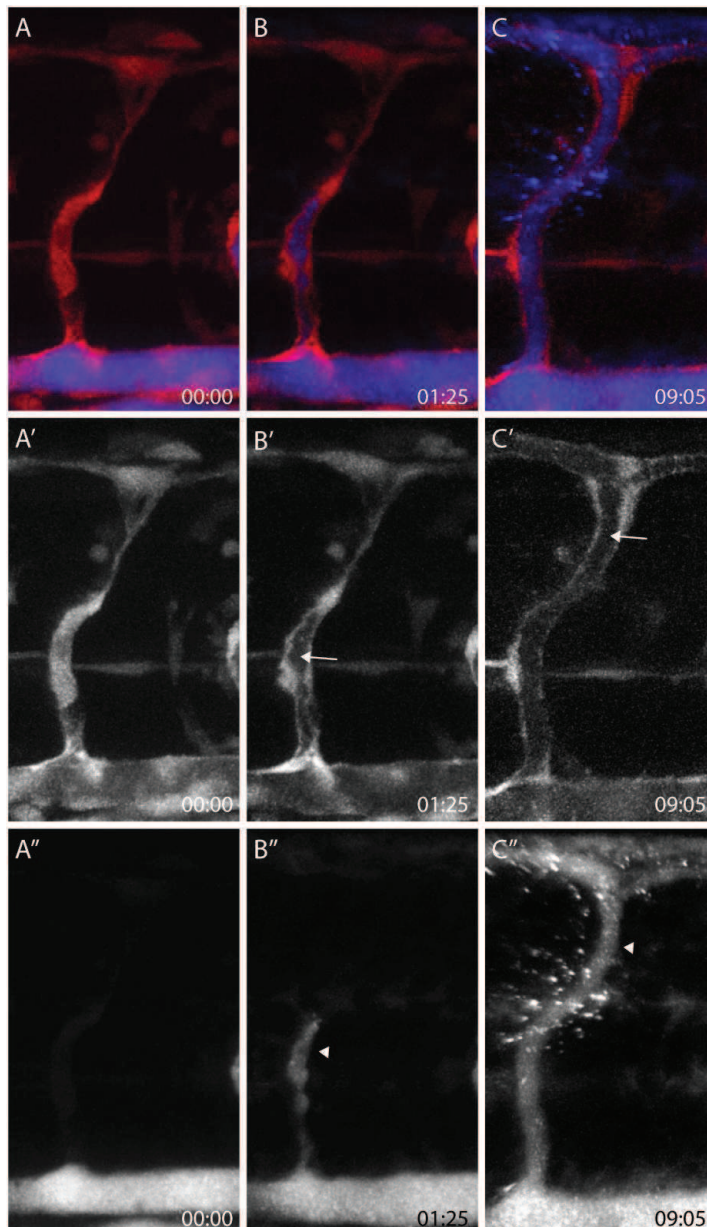


**Figure 6.6**

**Fainter areas in ISVs correlate with lumen formation:** QD injected in the sinus venosus spread in the circulation demarking open lumens. Initially, QD were restricted to the DA and ISV did not show fainter areas (A,A',A''). Later the lumen filled from the DA and first smaller fainter areas were visible and later, as the lumen extended, these areas became larger (arrows in B' and C'). These areas were concomitantly filled with QD (arrowhead in B'' and C''). A-C shows the merge of both channels (see movie 6 A,B,C).

### 6.3.1.1 Initial contact formation

The first aspect of anastomosis we analysed was the formation of the initial contacts between two contacting tip cells and how such contacts refined. To our delight, already the very first movie we did with the *UAS:EGFP-hZO1* line showed a tip cell which already had made contact to its neighbor, visible by a spot of EGFP-hZO1 (see arrow in Figure 6.7A). This spot was then elaborated into a small loop which subsequently became larger (see arrow in Figure 6.7B and then C, movie 7), confirming our suggested model for initial contact of tip cells. We found this mechanism in virtually all movies we analyzed. Thus, after a tip cell has formed its initial contacts (from then on called fusion cell) with the adjacent tip cells, these cells have contacts with at least three if not more cells. The two new contacts with the neighboring fusion cells as well as one or more cells of the ISV stalk (depending on the architecture of the stalk, multicellular or head to tail organization) the tip cell was dragging along during outgrow. Interestingly, these fusion cells also presumably have three independent apical membranes, one at the connection with the stalk cells and one each at the fusion points encompassed by the newly formed AJ loops.



**Figure 6.7**

**Initial contact formation during anastomosis:** An initial contact spot of EGFP-hZO1 ( arrow in A) was elaborated into a small (arrow in B) and subsequently into a larger loop (arrow in C), thereby stabilizing the fusion cell contact (see movie 7).

### 6.3.1.2 Intracellular lumen formation

After contacts between ISVs have been established we wanted to follow how the lumen opens in the newly formed DLAV. In other words: how are the three separated apical membranes of a fusion cell brought together to form a continuous lumen through the DLAV?

Movie 8 revealed one possible mechanism of lumen formation. A fusion cell, which just made contact with its neighbors was seen as spots of EGFP-hZO1, which then further elaborated to loops as described above. Due to the mosaics' of EGFP-hZO1 only the fusion cell and one or two stalk cells were labeled; the stalk appeared to be of multicellular nature showing the reminiscent junctional pattern of lines along the ISV stalk (arrowhead in Figure 6.8B). The lumen (dark space) was open (inflated) in the multicellular part of the stalk (waved arrow in Figure 6.8B) and then invaginated into the fusion cell and eventually reached one of

the two loops at the contact points (follow arrow in Figure 6.8C-E and see movie 8). When the lumen reached the junctional loop at the contact point, the loop was immediately lumenized (one time point difference, 5') and the lumen proceeded in the unlabeled adjacent fusion cell (arrow Figure 6.8F and G). Note that before doing so, the lumen transiently collapsed (even in the stalk) and subsequently reopened (see movie 8 between 3:00 and 5:20). Later, a red blood cell (occasionally labeled with RFP) squeezed through the vessel (see arrowhead in Figure 6.8G-J and movie y, note: timepoints are 5' apart, thus the red blood cell is rather slow even though in the movie it passes relatively fast). Thus, a seamless tube with an intracellular lumen was generated in this fusion cell (no junctions were identified in the DLAV except for the loop at the fusion point). To unambiguously prove that such invaginating lumens into fusion cells were connected to the lumen of the DA, a similar movie with QD injected embryos was acquired (movie 9A and B, Figure 6.9). In movie 9A, QD complemented with the dark areas and filled the invagination into the fusion cell, better seen in the separate channel of the QD (arrows in Figure 6.9B and C and arrowheads in Figure 6.9B' and C'). Remarkably, the QD also leaved the vessel when the lumen collapsed and immediately reappeared when the lumen reopened (see movies 9A and B). In our set of 15 movies analyzed we found that the fusion cell hollowing process as just described occurred in 12 movies. Thus, this mechanism is a very common way to generate a lumen in the DLAV.



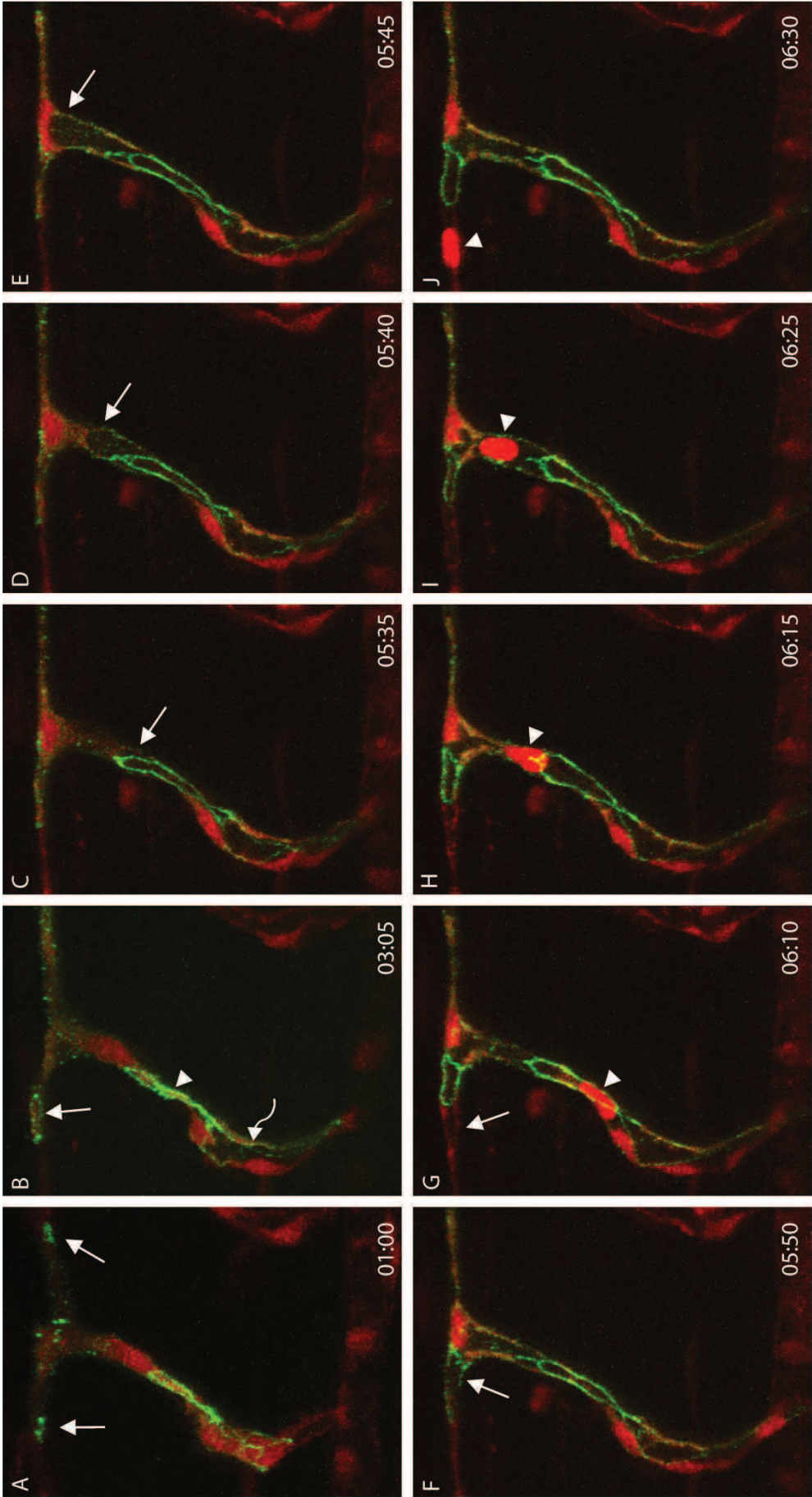


**Figure 6.8**  
**Intracellular lumen formation:** Picture series of movie 8. A tip cells formed initial contacts, which subsequently formed loops (arrow in A and B). The stalk showed a multicellular organization (two lines of EGFP-hZO1, arrowhead in B) and the lumen had opened in those region (waved arrow in B). From (C) on the lumen invaginated into the fusion cell (follow arrow from C to E) and finally reached the left loop of EGFP-hZO1, which was subsequently inflated (arrow at F). The lumen then continued to extend in the not labeled fusion cell on the left (arrow at G). Right after, a red blood cell passed the newly formed intracellular lumen (follow arrowhead from G to J). From timepoint 3:05 to 5:35 the lumen opened, then collapsed and subsequently reopened (see in movie 8).

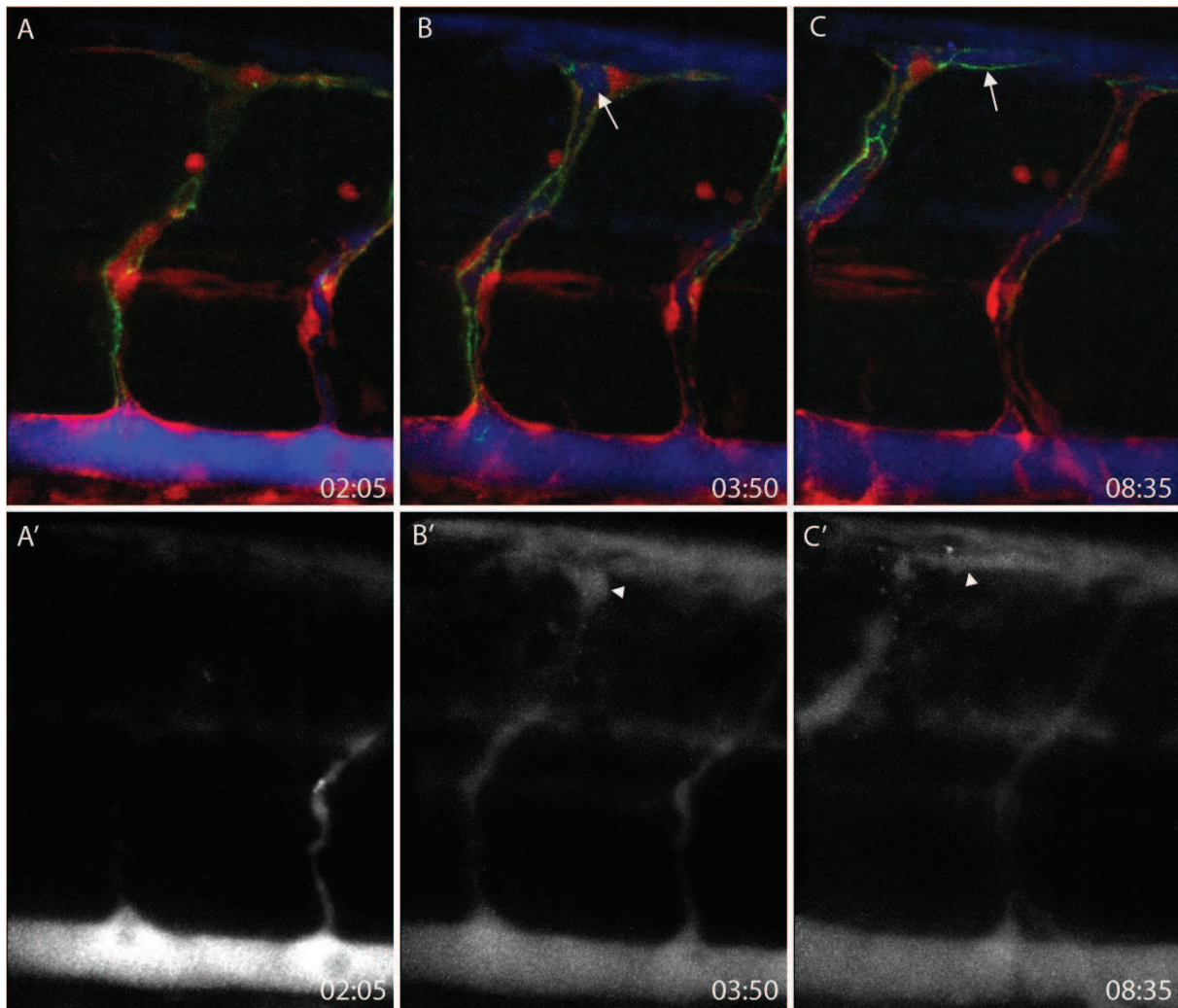


**Figure 6.9**

**QD injections confirms intracellular lumen formation:** Series of pictures of movie 9A and B. As in Figure 6.8 the lumen invaginated and reached one of the fusion points. Doing so, the lumen was permanently filled with QD (arrow and arrowhead in B and B') and QD filled the loop at the contact point as soon as the lumen reached it (arrow and arrowhead in C and C').

### 6.3.1.3 Extracellular lumen formation

We also found a different mechanism involved in the lumen formation process in the DLAV. Movie 10 showed again a fusion cell right after it made contact. Interestingly the fusion cell only had contact with one cell from its stalk seen as a loop (arrow in Figure 6.10A, see below Figure 6.15 for mechanism). This loop and the loop at the fusion point to the right subsequently increased in size. This means that the contact of the fusion cell with its stalk cell and the neighboring fusion cell increased, meaning that these two putative apical membranes of the fusion cell enlarged. So far there was no lumen apparent. Eventually, these two loops joined together (arrow Figure 6.10C). In other words; the two apical membranes of the fusion cell joined and concomitantly the stalk cell and the other fusion cell to the right contacted and made new junctions together (see also Figure 7.3 in discussion). At the same moment we observed that the lumen opened up. When the two loops contacted



each other, there appeared to be an increase of EGFP-hZO1 possibly accounting for the new contact between the stalk cell and the other fusion cell.

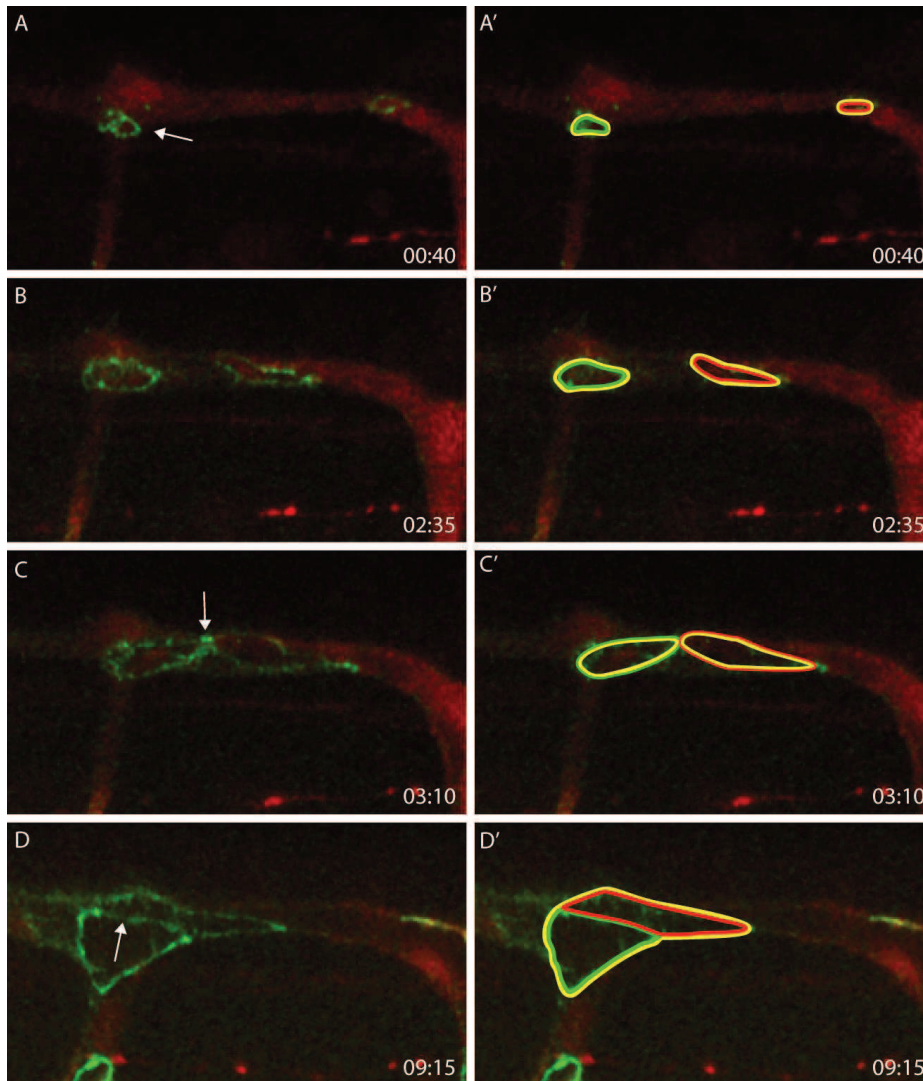


**Figure 6.10**

**Extracellular lumen formation:** Series of pictures of movie 10. A fusion cell formed a junctional loop with an adjacent fusion cell (on the right) and with a stalk cell (arrow in A). These loops extended and eventually met (B,C). A'-D' show contribution of junctions of the different cells (yellow: fusion cell, green: stalk cell, red: fusion cell on the right). Thus, the stalk cell and the adjacent fusion cell met and formed a new contact/ junctions (arrow in D, green/red line in D').

The new contact between these two cells was then presumably enlarged, seen as a line between the now single loop of junctions of the fusion cell (see arrow in Figure 6.10D, and movie 10, and see the marked contribution of junctions of the different cells in Figure 6.10A'-D', colour code is: fusion cell: yellow, stalk cell: green, other fusion cell on the right: red; the yellow line in D' shows the single loop of junctions of the fusion cell). This mechanism, which involves cell rearrangements, resulted in the incorporation of the fusion cell as a part of a multicellular tube, and is thus fundamentally different from the first mechanism described above. Such a mode of lumen formation has previously been described during notochord

formation in *Ciona intestinalis* (Dong et al., 2009). We found this mechanism to be less prominent than the fusion cell hollowing process, as we only observed it 7 times.

#### 6.3.1.4 Blood pressure is not important for initial contact formation and extracellular lumen formation but might be important for intracellular lumen formation

We found ISVs where the lumen did not form from the DA into the ISV stalk but from the DLAV. In such movies we observed that the lumen formed from the DA into an ISV and DLAV, and from there expanded into an adjacent ISV stalk (Figure 6.11). EGFP-hZO1 showed that the same invaginating mechanism required for intracellular lumen formation, was involved in this situation, suggesting that this mechanism is depend on luminal pressure. (follow arrows in Figure 6.11 and see movie 11, movie from Lukas Herwig).

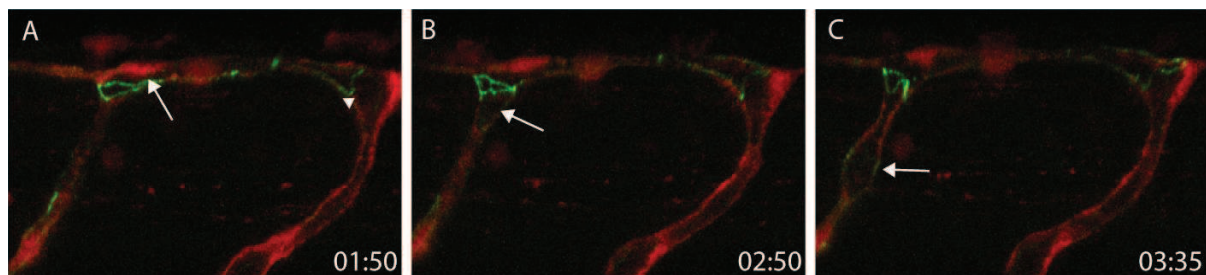


**Figure 6.11**

**Luminal pressure might be important for lumen formation:** Series of pictures from movie 11. The lumen opens from the right ISV (arrowhead) over the DLAV into the stalk of the left ISV (follow arrow in A-C).

Thus, luminal pressure might play a key role in extending apical membranes through a fusion cells. In *silent heart (sih)* mutants (or in *sih* MO injected embryos), the heart fails to contract and blood pressure fails to be established. Unfortunately, lumen formation could not be monitored in such embryos, since the lumen in ISVs did not open (inflate). However, we found that tip cell contacts as well as enlargement of contact points into larger loops did occur in *sih* MO-injected embryos (arrow in Figure 6.12A, movie 12). We also observed the second mechanism described above, where cell rearrangements lead to a multicellular tube. (arrows in Figure 6.12B and C).

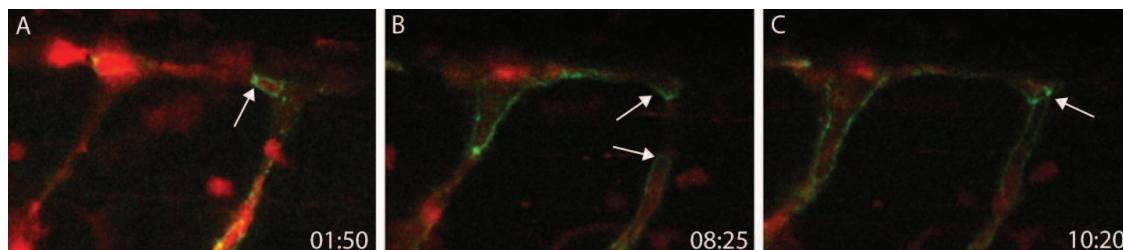


**Figure 6.12**

**Junctional remodelling is not dependent on circulation:** Series of pictures from movie 12. Fusion spots are still elaborated into loops in *sih* morphant embryos (arrow in A) and the extracellular lumen formation mechanism is functional as well (arrows in B and C)



These results demonstrate that the initial steps in the fusion process do not require blood pressure, and that one of the two mechanisms of lumen formation is still functional. To investigate whether apical membrane extension through fusion cells occurs in the absence of blood pressure will require monitoring fluorescent apical markers.

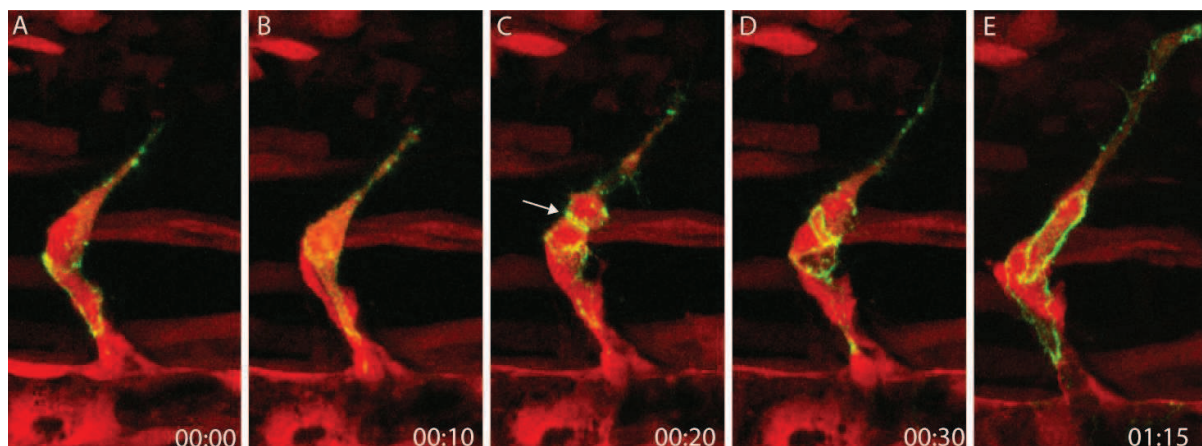
### 6.3.2 Other mechanisms observed during ISV formation

#### 6.3.2.1 EGFP-hZO1 during cell division

Initially we were focussing on the leading tip cells describing the fusion event and the subsequent lumen formation process in the DLAV. These observations led to two different mechanisms described above, forming either an intracellular lumen as a result of cell hollowing or an extracellular lumen as a result of cell rearrangements. These two different mechanisms show that endothelial cells within the vascular system can use different ways to form a patent lumenized vascular system, mostly likely depending on their internal and external inputs such as signaling and blood pressure.

Looking at the movies in detail, we found other interesting activities during ISV formation. ISV sprouting is, as shown in Blum et al., accompanied by extensive cell division. Most of the cells that migrate out of the aorta divide at least once. One interesting question is to understand how the junctions behave during cell division. In a regular sheet epithelium, when a cell divides, junctions are formed at the cleavage plane starting from the already existing junctions of the dividing cell (Kim and Raphael, 2007). We observed different situations of cell division of endothelial cells during ISV formation.

During all cell divisions we observed that EGFP-hZO1 partially delocalized, which resulted in a more or less evenly green cell. EGFP-hZO1 localized back to the junction during cytokinesis, thus right after cell division. It's not clear whether the junctions indeed disintegrate to such a degree or whether this is a property of ZO1/EGFP-hZO1. A transgene with Ve-cadherin or another transmembrane junctional protein might reveal to what degree the junction dissolve during cell division (Figure 6.13B and movie 13 ).

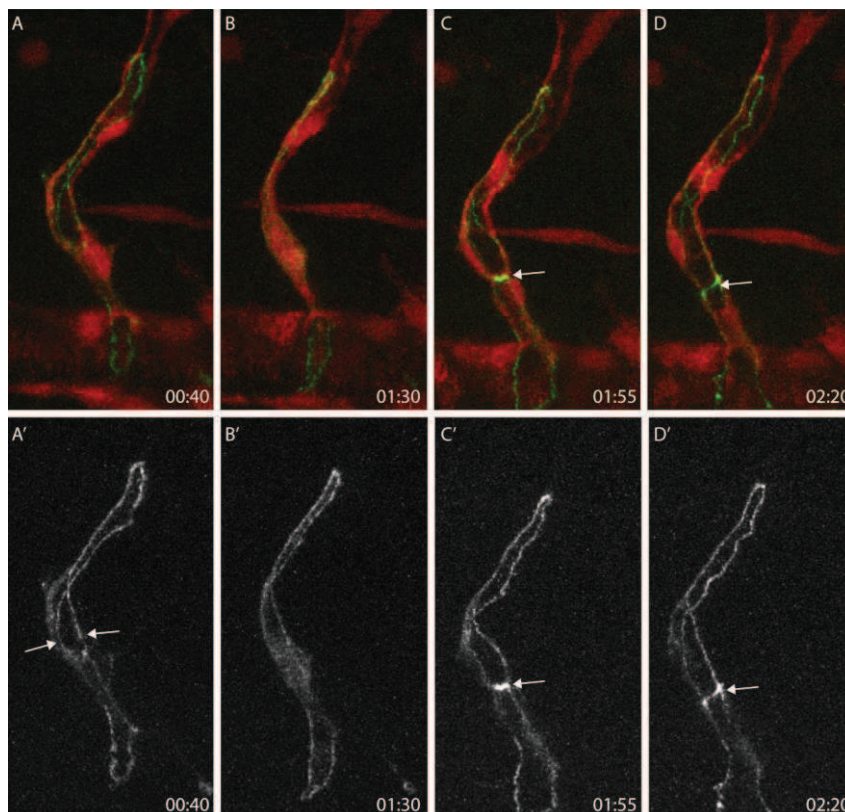


**Figure 6.13**

**Tip cell division:** Series of pictures from movie 13. A tip cell divided and formed an isolated new small loop of EGFP-hZO1 between the two daughter cells after division (arrow in C). The loop then contacted the other junctions and enlarged as the sprout grew (D and E). EGFP-hZO1 delocalized at the onset of cell division (B).

We found that tip cells in a sprouting ISV (app. 24 hpf), right after cell division, formed a new loop of ZO1 between the two daughter cells. This new loop did not have any connections to the junctions the initial tip cell had with the stalk cells (arrow in Figure 6.13C). Thus, presumably a new apical interface was established between the two daughter cells, somewhat similar to a fusion point. Afterwards, this loop met up with the other junctions and underwent cell rearrangements in a way as described above (Figure 6.13D and E, movie 13).

We also found a stalk cell dividing, which was part of a multicellular tube and had junctions with other cells, which resulted in two parallel lines of EGFP-hZO1 usually seen for such tube architecture (arrows in Figure 6.14A and A'). Upon division, a new line of EGFP-hZO1 formed between the two daughter cells. This line was connected with the two parallel lines, thus forming a bridge between the two lines (arrow in Figure 6.14C,C' and D,D', movie 14A and 14B). This is the way how one would expect cell division in an epithelial sheet (Kim and Raphael, 2007). Interestingly at the beginning of cell division the lumen appeared to be inflated, but shortly collapsed during the cell division and re-inflated again after cell division (Figure 6.14B and B', timepoint 1:30). This behaviour might depend on the maturity of the vessel.

**Figure 6.14**

**Cell division in a multicellular tube:** Series of pictures from movie 14. A cell in a multicellular tube (two lines in Figure A'(arrows)) divided (B) and formed a new junction between the two daughter cells. This junction was connected to the two parallel lines (arrows in C,C',D,D'). The lumen collapsed during cell division (B).



In early ISVs (29 hpf) we also found stalk cells, which were not in a multicellular context and thus aligned in a head-to-tail fashion for instance with the tip/fusion cell and other stalk cells (see Figure 6.10A and 6.15D). Interestingly, movie 15A and B also showed us how this organization came about. Prior to cell division of this stalk cell we saw an interesting behavior of this cell. This cell underwent the reverse mechanism of extracellular lumen formation described above (see Figure 6.15A-D, movie 15A and 15B).

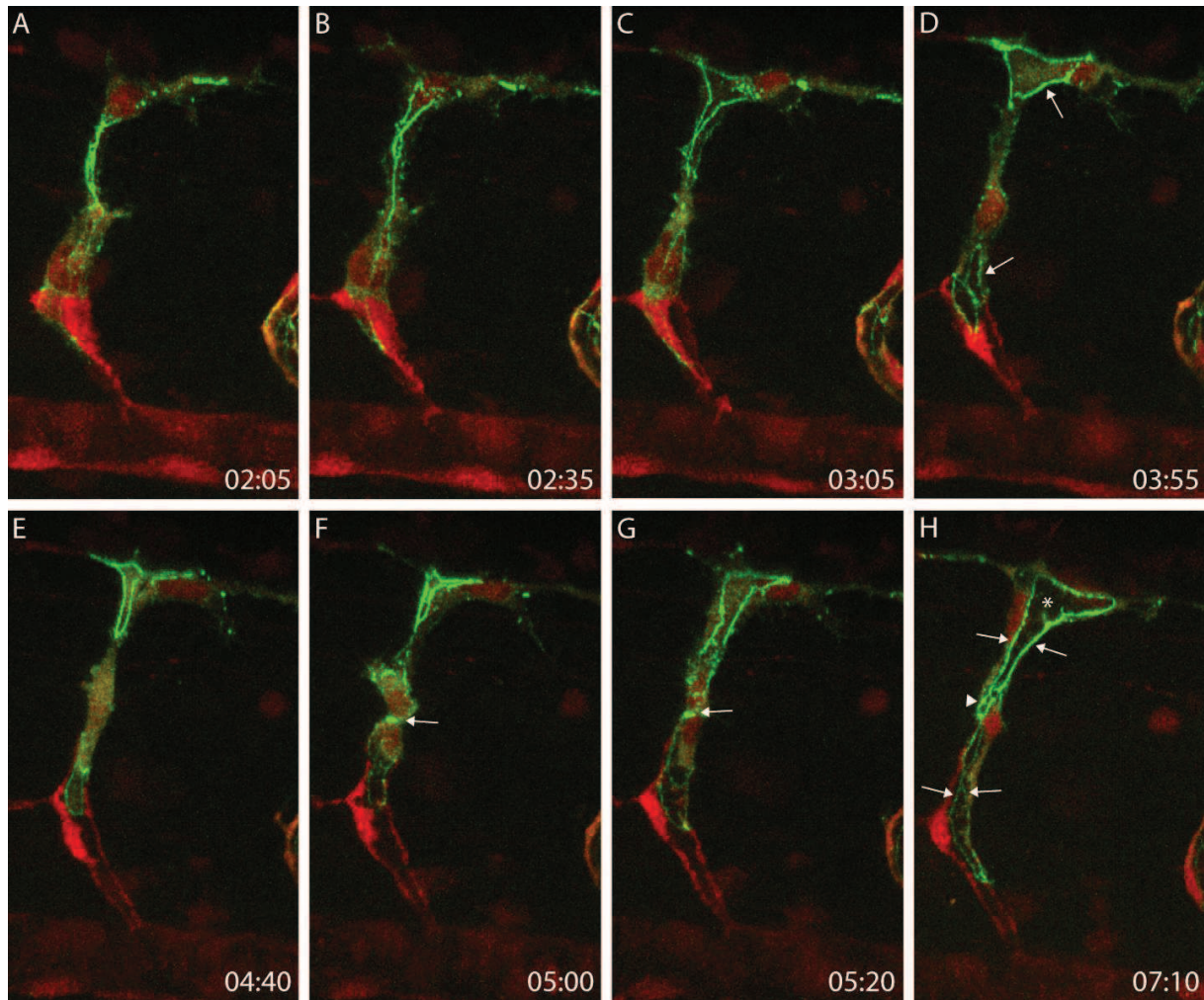


**Figure 6.15**

**Cell division is compatible with cell rearrangements:** Series of pictures from movie 15A. In the first part, a stalk cell went from a multicellular to a head-to-tail arrangement forming a loop with the fusion cell and another with underlying stalk cells (A-D, arrows in D show the two loops). Subsequently the stalk cell divided, formed a junctional interface between the two daughter cells (arrow in F,G) and concomitantly the underlying stalk cell and the fusion cell formed a new contact. The end result were parallel lines from dorsal to ventral (arrows in H) and a loop at the location of cell division (arrowhead in H). At the same time the lumen opened (asterisk in H).

In this scenario the stalk cell, which at the onset of the movie was arranged in a multicellular tube (EGFP-hZO1 expression along the vessel in Figure 6.15A and B, hard to see in the pictures, follow junction in movie 15A and movie 15B, which only shows the EGFP-hZO1), underwent rearrangements to end up in a head to tail manner, showing one loop with the fusion cell and one with underlying stalk cells (arrows in Figure 6.15D, the loop at the bottom

arrow looks like two loops but 3D analysis reveals that it is one (not shown)). This cell subsequently divided and first EGFP-hZO1 formed a spot between the two daughter cells (arrow in 6.15F and G), after EGFP-hZO1 localized back seen as dots and small stretches aggregating together, (see Figure 6.15G). At the end EGFP-hZO1 showed two lines from dorsal to ventral and a small loop at the location of cell division (arrows in Figure 6.15H show parallel lines, arrowhead shows the loop). Thus, while the stalk cell divided and formed new junctions between the new daughter cells, the fusion cell on top and a stalk cell on the bottom presumably made contact. This means that during cell division the stalk cell had undergone the cell rearrangement mechanism described in Figure 6.10. So presumably the loop demarks junctions of the two daughter cells and junctions of the fusion cell on top and the stalk cell on the bottom (following movie 15A and 15B makes it easier to figure out the mentioned loop). The lumen opened right after this process was completed (asterix in Figure 6.15H).

### 6.3.2.2 Endothelial cells undergo intercalation and cell self fusion

In the *Drosophila melanogaster* tracheal system, cells of the dorsal branches undergo intercalation going from a paired to a head-to-tail arrangement, where the individual cells form autocellular junctions revealed as one line connecting to two little rings at each end of a cell. To accomplish this, cells reach around the lumen, where they form an initial autocellular junction. From this point the cells zip up extending its autocellular junction and the junction with the formerly pairing cells is reduced to a little ring (Ribeiro et al., 2004). We were interested whether we would see a similar behavior with endothelial cells.

We indeed saw intercalation events in ISVs (see Figure 6.16, Figure 6.17 and the corresponding movies; movie 16A, 16B and 17). Initially two parallel lines of EGFP-hZO1 and a short line connecting these two parallel lines were visible in the ISV stalks (arrowheads show the parallel lines in Figure 6.16A and A' and Figure 6.17A; arrow shows the connecting line in Figure 6.16A, A' and 6.17A, the line is not really visible in Figure 6.16 but clear in Figure 6.17). The two parallel lines of EGFP-hZO1 met into one point where the line of EGFP-hZO1 was connecting these two lines, in other words, where two cells contacted (arrow in Figure 6.17B, in 6.16B and B'). This is the reaching around the lumen of the intercalating cell forming the initial auto-cellular junction. From this point, intercalation went on, resulting in a single line of EGFP-ZO1 (Figure 6.16C,C',D,D' and Figure 6.17C and D). Most strikingly this line eventually dissolved, leaving a cell arranged in a head-to-tail manner (Figure 6.16E,E',F,F' and 6.17E and F). We observed slightly different variations of this cellular mechanism during ISV formation.



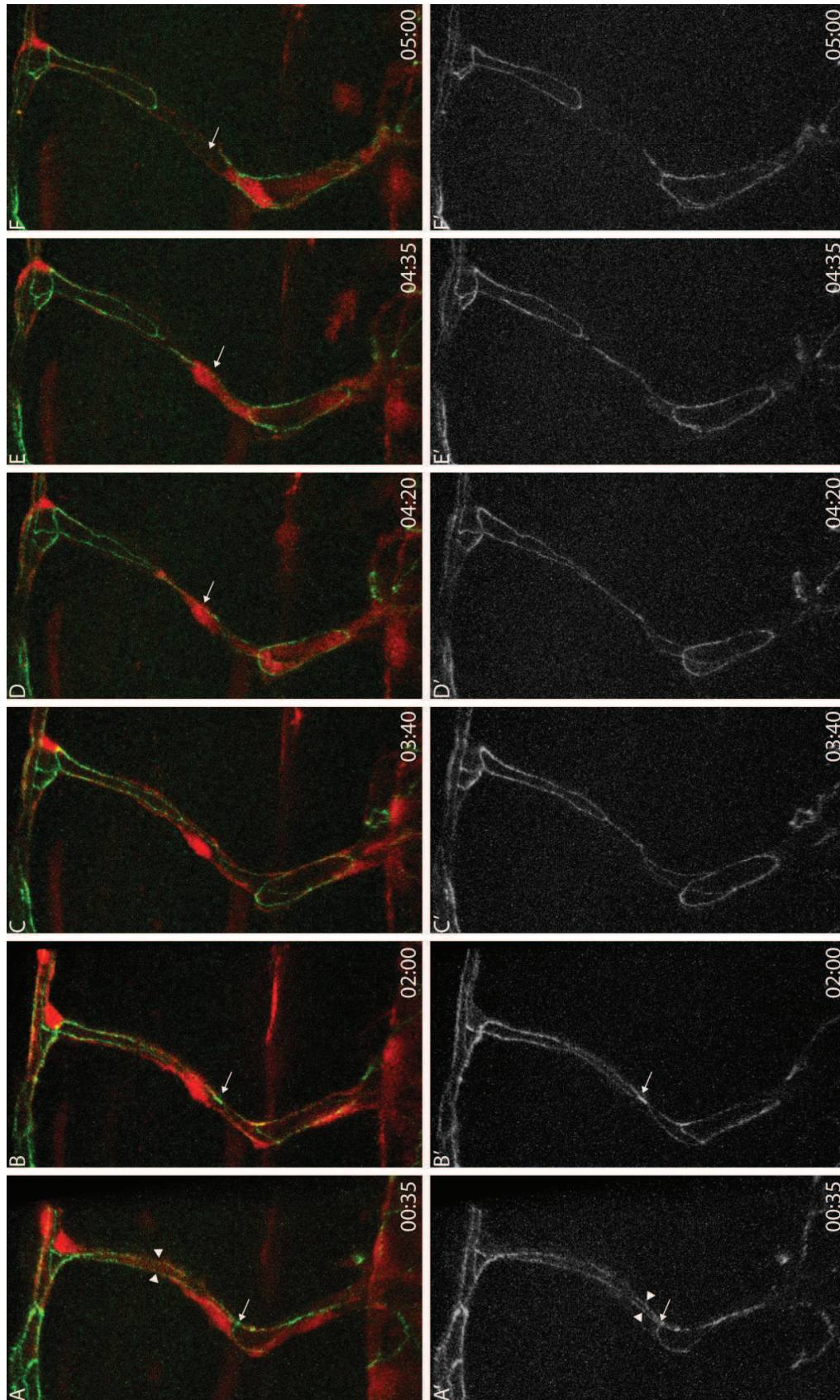


**Figure 6.16**

**Intercalation and cell self fusion I:** Series of pictures from movie 16A and B. A cell in a multicellular tube (two lines, see arrowhead in A,A') underwent intercalation. The cell reached around the lumen (arrow in A,A',B',B') in one point. Intercalation started and went on as one line extending (C,C',D,D'). This line subsequently dissolved leaving a cell in a head-to-tail arrangement (E,E',F,F'). The lumen collapsed at the end of intercalation and the lumen had to be reopened after (arrows in D,E,F).

In movie 16A the lumen collapsed (no “dark” areas in the vessel) at the end of intercalation event when the junction dissolved (arrows in Figure 6.16D and E). Then this cell appeared to



undergo an intracellular lumen formation process as described above (arrow in Figure 6.16F).

In movie 17, a movie where we used QD to mark the lumen, the lumen opened after initiation of intercalation and clearly remained open when the junction dissolved (Figure 6.17C-F).

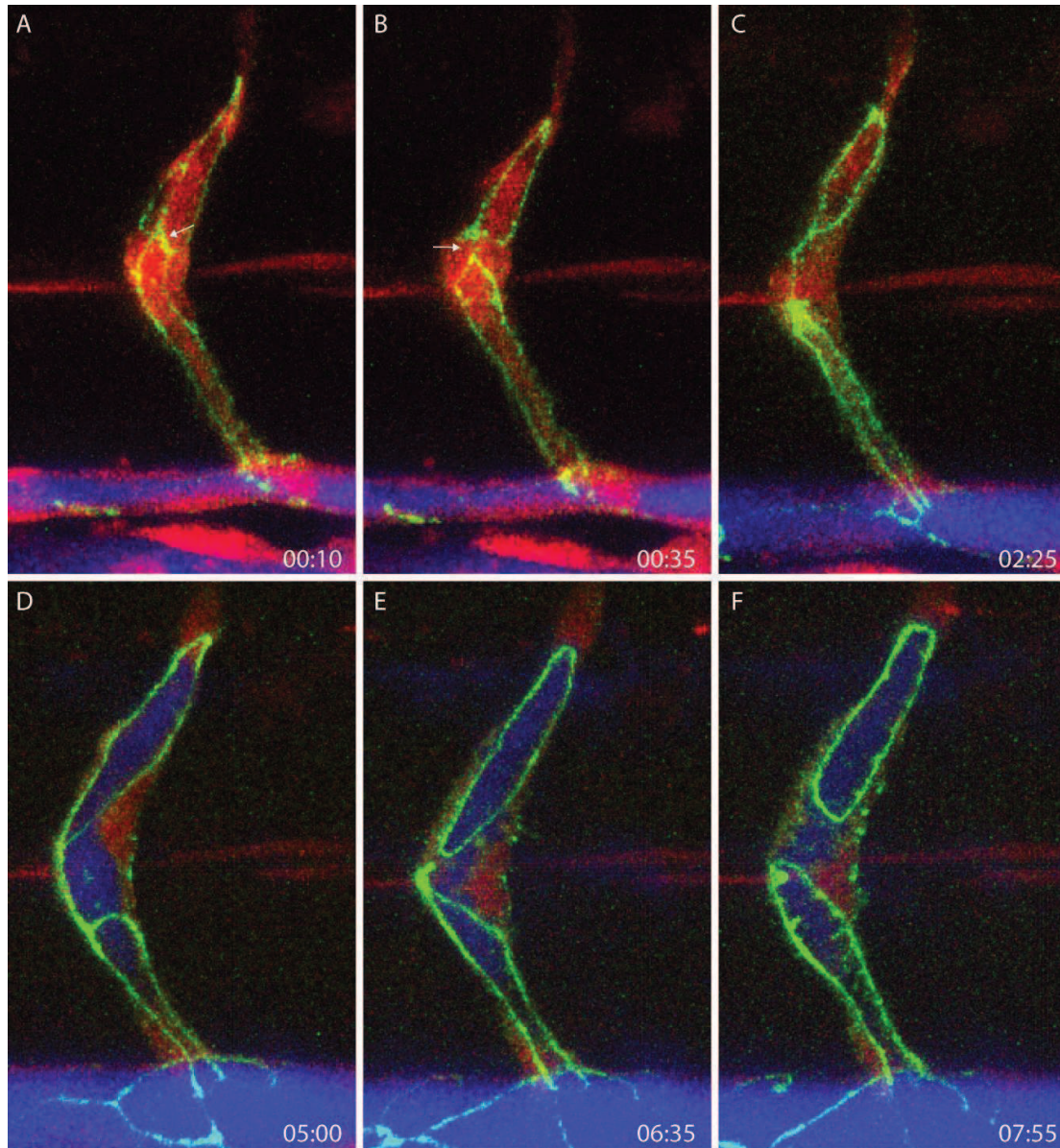


**Figure 6.17**

**Intercalation and cell self fusion II:** Series of pictures from movie 17. Similar situation as in Figure 6.16. Two parallel lines of EGPF-hZO1 merged into one (arrows in A,B). this line extended and eventually dissolved (B-E). In contrast to Figure 6.16 the lumen did not collapse when the line dissolved seen by injected QD (D-F).

Taken together our results show that ECs are very plastic and can use a variety of cellular mechanisms to form functional lumenized blood vessels.

# 7 Discussion

## 7.1 Different tube architectures in ISVs

Biological tubes can have three different tube architectures: multicellular, unicellular with autocellular junctions, and seamless (Baer et al., 2009; Lubarsky and Krasnow, 2003). Endothelial tubes consist of multicellular and seamless tubes. Capillary beds of mouse retinas show a dense network of junctions when stained with a junctional marker such as Claudin 5 suggesting multicellular tubes (Phng et al., 2009). However, seamless tubes have been found in a number of tissues and are known to exist since 1964 (Bar et al., 1984; Wolff, 1964). The architecture of zebrafish ISV has been described as a linear arrangement of single ECs forming seamless tubes (Childs et al., 2002; Kamei et al., 2006).

In this study we performed single cell labeling using transgenic lines expressing the photo-convertible protein Kaede, combined with stainings of junctions to quantify the distribution of multicellular and seamless tubes in ISVs. We have shown that the ISV stalks are mostly multicellular tubes. 88% of the extend of ISV stalks show a multicellular pattern of junctions and 75% of ECs pair over their whole extend with one or more cells. In contrast, the DLAV shows an almost opposite distribution, with 66% of the cells having at least some stretches of seamless tube at 2 dpf (Figure 6.3). Even though Kaede converted cells, which entirely surround the lumen, could also be cells with an autocellular junctions, the fact that we only very rarely see autocellular stretches in staining makes this possibility unlikely. Possibly, unicellular tubes with autocellular junctions are only a transient morphology and are subsequently transformed into seamless tubes as seen in Figure 6.16 and 6.17 and the corresponding movies.

Remarkably, our data correlates nicely with a study from 1984, where several capillary beds (mostly rat but also human capillary beds) were analyzed for their content of seamless ECs (Bar et al., 1984). This study used silver impregnation of endothelial cell junctions as well as electron microscopy to reveal seamless ECs. Depending on the capillary bed they find 30% - 50% of seamless endothelial cells. These seamless ECs are preferentially found at branching point and thus their abundance increases with number of branching point (Bar et al., 1984). Indeed also we also find more seamless ECs in the DLAV, which are the only branching points of ISV due to guidance cues restricting outgrow to the somite boundary. Most likely, branch numbers correlate with fusion points (Fantin et al., 2010) and thus seamless ECs correlate with fusion points. This makes sense, since regardless of whether the vessel stalk forms using a multicellular budding mechanism or another mechanism, the tip/fusion cell will have at least one protrusion of its cell body, which will have to be lumenized during anastomosis (see Figure 3A in Blum et al., 2008 and Figure 6.7). And, our study shows that one way to generate a lumen in these parts of the cell body of a fusion cell is by an invaginating mechanism forming a seamless section in the fusion cell (see Figure 6.8 and 6.9 and movie 8, 9A and B). It would be interesting to see whether *obd* mutant

embryos, which show a plexus like organization in the trunk due to their inability to restrict ISVs to the somite boundaries (Childs et al., 2002; Torres-Vazquez et al., 2004), have a higher degree of seamless tubes.

Seamless endothelial tubes are not found in all capillary beds (Bar et al., 1984). For instance seamless ECs are found in the fenestrated (round transcellular holes found in fenestrated and discontinuous (sinusoidal) endothelium with a diameter ranging from 60-170nm) capillaries of the renal glomeruli with up to 50% contribution but have not been found in sinusoidal vasculature of the liver, spleen or bone marrow (Bar et al., 1984). It is not clear whether slight differences in gene expression between these capillary networks account for these differences (Lalor et al., 2006; Satchell and Braet, 2009). Alternatively, different mechanical properties such as pressure could account for these differences. Seamless tubes are also not found in larger capillaries like arterioles and venules (Bar et al., 1984) indicating that seamless tubes most likely have a size limit.

Taken together, our study reports similar cellular morphologies as found in many mammalian, including human, capillary beds, and therefore substantiate the relevance of zebrafish ISVs as a model to study formation of capillary beds.

## 7.2 Cellular mechanisms during sprouting angiogenesis and anastomosis

### 7.2.1 Some considerations on using *fli1:GFP*; *UAS:EGFP-hZO1* transgenic fish

The *UAS:EGFP-hZO1* transgenic fish line, in combination with the *fli1:GFP* transgenic line represented an invaluable tool in unraveling the cellular mechanisms during ISV outgrow and anastomosis. Nonetheless, working with these transgenic embryos has some drawbacks and a few issues have to be considered in order to avoid misinterpretation of data.

EGFP-hZO1 expression is highly mosaic, meaning that even though the transgene is present (seen by the expression of *cmhc2:EGFP*, see materials and methods), expression in ECs can go from no expression at all to almost even expression throughout the endothelium. Mosaics' can help to make it easier to understand junctional remodeling and prove behavior of single cells but can also lead to misinterpretation especially when suggesting intracellular lumen formation due to the presence of non-expressing cells in the region analyzed. Fortunately, the *UAS:RFP* transgenic line is expressed throughout the endothelium and helps to spot potential non-expressing cells (for EGFP-hZO1). In addition, only junctions formed between two unlabeled cells will remain unlabeled. Figure 7.1 shows such an example: there are two EGFP-hZO1 labeled cells, the fusion cell on the dorsal side and a stalk cell on the ventral left part of the ISV (see arrows in Figure 7.1). The lumen is open and



one could conclude that there is an intracellular lumen between the two labeled cells as there are no junctions between the fusion cell and the stalk cell. But the RFP channels reveals the presence of two more unlabeled cells in the ISV (arrowhead), which potentially have junctions together since they are located in close proximity to each other. Therefore, we might oversee some junctions and a clear statement about the tube architecture in this region cannot be made.

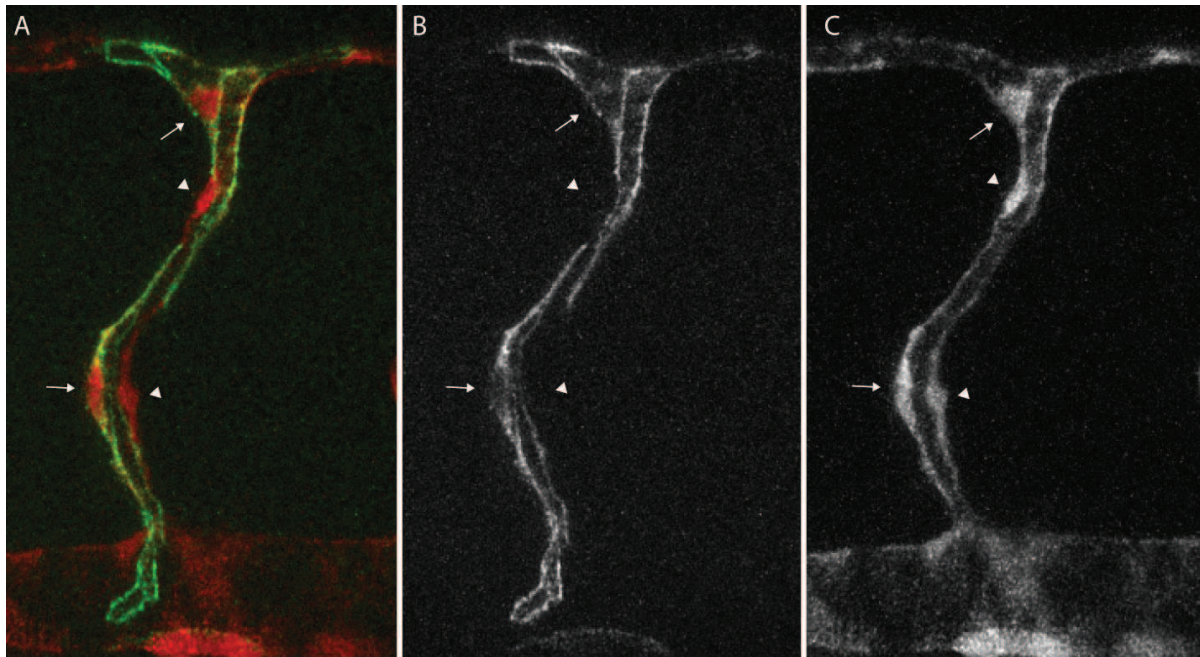


**Figure 7.1**

**Avoiding misinterpretation:** Pictures demonstrate mosaic property of the *UAS:EGFP-hZO1* transgenic line. (A) shows the overlay of (B) (EGFP-hZO1) and (C) (RFP). Two cells express EGFP-hZO1 (arrows) and two other cells do not express EGFP-hZO1 (arrowheads). The two non-expressing cells could have contacts together. Thus, we might not see all the relevant junctions in this ISV to faithfully interpret vessel architecture and cellular mechanisms.

Moreover, levels of expression differ and can change during ongoing time-lapse imaging. Especially cells with high expression also show some non-junctionally localized EGFP-hZO1 in the cytoplasm (not in the nucleus). Due to the thin morphology of ECs, this cytoplasmic labeling can look similar to junctions in the region around the nucleus and when the lumen is open. All the movies were thoroughly analyzed with regard of these potential artifacts to avoid misinterpretations.

### 7.2.2 Contact formation

Anastomosis starts with the formation of an initial contact between two tip cells. ISVs form these contacts around 30 hpf after they reached the dorsal roof of the neural tube and extend



protrusions and filopodia in anterior and posterior direction to find the neighboring ISV (Isogai et al. 2003; Figure 3 D (Blum et al., 2008) and Figure 6.4). We have shown, using antibody stainings with junctional markers and live imaging using EGFP-hZO1, that upon contact, new junctions are localized to the contact spot. This spot is then elaborated into a small loop, which subsequently increases in size (Figure 3 A,B,C (Blum et al., 2008) and Figure 6.7). Spots and stretches of junctions are seen before contact formation in the tip cell (Figure 2 (Blum et al., 2008) and 6.5) but observing these spots in live imaging shows that they will not necessarily transform into contact spots. Because of the 5 minutes spacing between time points we may lack some information, and the relevance of these spots during contact formation is not clear. Taken together, the results propose a model, in which the two tip cells contact and then form a de novo apical membrane when extending their contact (see Figure 3 A',B',C' (Blum et al., 2008)).

This contact formation preceding ISV anastomosis appears to be very similar to contact formation during tracheal branch fusion in *Drosophila melanogaster*. Concomitantly with branch fusion in the trachea, DE-cadherin is localized to the contact spot and elaborates into a ring (Tanaka-Matakatsu et al., 1996). Branch fusion does not occur in the absence of DE-cadherin (Uemura et al., 1996). Ve-cadherin knockdown experiments in zebrafish show a somewhat weaker phenotype; contacts in ISVs are partially formed but may dissociate and reform again (Montero-Balaguer et al., 2009). Whether this is an artifact of incomplete knockdown or additional or redundant players are involved is unclear.

Apical membrane formation is an essential mechanism of cells during tube formation mechanism. 3D culture of MDCK (Madin-Darby canine kidney) cells represents an excellent model system to investigate molecular pathways during epithelial polarization and lumen formation. Individual MDCK cells assemble and form a polarized monolayer of cells with a central lumen called cysts (Bryant and Mostov, 2008). Recently, new insight revealed molecular mechanisms during early polarization of these cysts. Using different markers of apical membrane and of the exocyst complex, Bryant et al. have shown that polarization requires two critical steps (Bryant et al., 2010). In an initial step, Podocalyxin is transported in vesicles using the exocyst complex to the so-called apical membrane initiation site (AMIS). Occludin, a tight junction protein marking the border between cells of the early cyst is initially localized at the AMIS. Localization of Podocalyxin to the AMIS results in the formation of the pre-apical patch (PAP). The PAP is apical membrane without a visible lumen in the cyst. Later the lumen is filled with the help of ion pumps (Bryant et al., 2010). It will be interesting to see whether ECs use a similar mechanism of polarization during anastomosis. Presumably, the initial spot of junction can be used as AMIS to drive apical membrane formation. New transgenic lines expressing various marker proteins will hopefully shed light on polarization mechanisms during anastomosis.

Macrophages associate with tip cells and potentially play a role in helping tip cells to contact other tip cells before anastomosis. Branch points are reduced in mice lacking macrophages. Macrophages do associate with tip cells in zebrafish as well but their functional role remains obscure (Fantin et al., 2010).

### 7.2.3 Lumen formation

Lumen formation in ISV starts at 27-29 hpf from the DA and forms in a stepwise manner towards the DLAV (Kamei et al., 2006). One possible reason why the lumen only starts to form when ISVs have already reached the dorsal side is that heart contraction starts between 24 and 26 hpf (Isogai et al., 2001). As ISVs start budding around 22 hpf (Isogai et al., 2003), there is potentially no pressure to open up the lumen and make it visible in transgenic lines such as *flk1:EGFP* or *fli1:GFF; UAS:RFP*. Also in *sih* morphant embryos the lumen is to a large extent not apparent (Figure 6.12 and movie 12, (Montero-Balaguer et al., 2009). Therefore, we have to discriminate between an open inflated lumen (seen as darker areas in *flk1:EGFP* or by filling with QD) and a pre-lumen or collapsed lumen. ECs are polarized cells where apical and basal membranes are separated by junctions. Therefore apical membranes can be assumed at areas, which are encompassed by junctions. Thus, a pre-lumen can be considered as apical membrane of one or more ECs sticking to each other. These pre-lumen open up very fast to a lumen (usually from one to the next time point) indicating that pressure might be enough to separate the apical membranes in ISVs (seen in several movies, for instance movie 8 and 9A). This may also explain the stepwise opening of the lumen in ISVs described by Kamei et al., 2006. Interestingly a recent study suggests a mechanism using repulsive electrostatic forces to open a pre-lumen. Negatively charged proteins on the apical membrane, such as Podocalyxin, are essential to separate the apical membranes from each other in the mouse DA and in cell culture assays (Strilic et al., 2010). It is not clear how relevant such a mechanism is in ISV lumen formation as *sih* morphants show very limited lumen (Figure 6.12 and movie 12). Possibly the apical membrane is not mature enough and such a mechanism would occur later.

#### 7.2.3.1 Intracellular lumen formation

Using the *fli1:GFF* and the *UAS:EGFP-hZO1* transgenic line, we have shown that ECs can use different mechanisms to form a patent lumen in the DLAV.

We see the lumen invaginating into the fusion cell towards one (possibly also both) of the fusion points. Upon reaching the fusion point, the lumen breaks through and continues its way in adjacent cells (Figure 6.8 and 6.9). The invagination of the lumen suggests invagination of apical membrane into the fusion cell. This apical membrane grows until it

reaches the apical membrane of the pre-lumen at the fusion point. Here the two apical membranes of the fusion cell will have to fuse and form a continuous apical membrane. This continuous apical membrane will engulf the newly formed intracellular lumen of the fusion cell (see Figure 6.8, 6.9 and Figure 7.2 for a representative model).

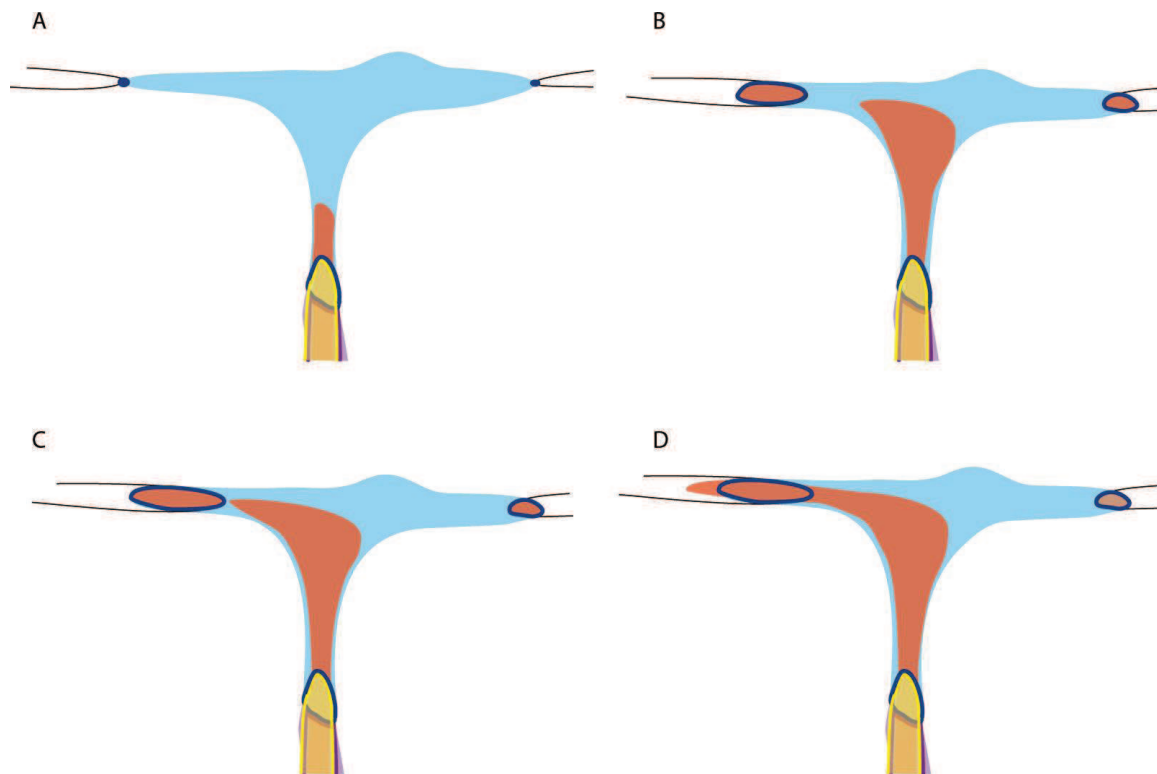


**Figure 7.2**

**Schematic representation of intracellular lumen formation:** (A and B) A fusion cell (blue) has made contact adjacent fusion cells (white) and formed junctional loops and apical membrane with a pre-lumen (red) (in B). (B) The lumen (red) is invaginating from the stalk into the fusion cell. (C) The lumen eventually reaches the pre-lumen. This means that two separate apical membranes of the fusion cell meet and eventually fuse to open the pre-lumen to a lumen which then continues to form in the DLAV (D) (see Figure 6.8 and 6.9 and movie 8 and 9A).

Fusion cells of the *Drosophila melanogaster* tracheal system invaginate their apical membrane along F-actin tracks to eventually fuse and establish an intracellular lumen in the fusion cell. In contrast to the vascular system, fusion cells in the tracheal system are thin and donut-shaped. The extent of apical membrane invagination is short (Kakihara et al., 2008; Lee and Kolodziej, 2002). In *Drosophila*, this process is genetically controlled and a number of genes are specifically expressed in fusion cells (Kakihara et al., 2008; Tanaka-Matakatsu et al., 1996). DE-cadherin recruits the plakin Short stop, which will allow the formation of F-actin tracks connecting the two apical membranes (Lee and Kolodziej, 2002). These tracks are supposed to facilitate vesicle fusion with the apical membrane and thus drive membrane invagination. Membrane fusion is thought to require the small GTPase Arf-like 3 to correctly localize exocyst complex and vesicle to the apical membrane (Kakihara et al., 2008).

In a previous study, large vacuoles have been associated with intracellular lumen formation in zebrafish ISVs (Kamei et al., 2006). However, we did not observe such extensive vacuoles during the process of apical membrane invagination. But, it is clear that new apical membrane has to be generated at the site of invagination. Whether vesicles or smaller vacuoles (as suggested by the work of Wang et al. in 2010) are involved will need to be investigated with additional transgenic lines specifically marking such compartments. Such markers could be components of the exocyst pathway as well as apical membrane marker such as Podocalyxin. Generating such transgenic lines is part of ongoing work in the lab.

We suggest that luminal pressure plays a role in lumen formation and apical membrane invagination. Our results show that the lumen can open in one ISV, making its way through the DLAV, and then from the DLAV, invaginate into a stalk cell in the adjacent ISV (Figure 6.11 and movie 11). Further, invagination of the lumen always progresses up to the loop at the contact point in Figure 6.8 and 6.9 before an apparent breakthrough occurs. Invagination of apical membrane without luminal pressure would suggest the formation of a not visible pre-lumen from invagination of apical membrane from contact points (for instance from the contact points in Figure 6.8 and 6.9). As soon as the lumen (visible) invaginating from the stalk into the fusion cell would reach this pre-lumen, we would expect a sudden inflation of the pre-lumen before the lumen reaches the loop at the contact point. We have not observed such situations but cannot excluded them as our ability to obtain quantitative data is limited for the moment (due to the mosaics' of *UAS:EGFP-hZO1* line). However, our results so far propose that apical membrane invagination can only occur where pressure is applied on the membrane. To unambiguously prove this point, we will have to show that apical membrane does not invaginate into fusion cells in *sih* morphant embryos. The lack of an apical marker makes this analysis impossible to date as *sih* morphant do not show a lumen and a possible pre-lumen is not visible in the RFP channel.

### 7.2.3.2 Extracellular lumen formation

We have also uncovered a different mechanism involved in lumen formation during DLAV anastomosis (Figure 6.10 and movie 10). The model in Figure 7.3 highlights the different steps during this mechanism. A fusion cell (blue) contacts a stalk cell (purple) and an adjacent fusion cell (yellow). The contribution of junctions of each cells are marked as blue, red and yellow lines. For instance, junctions between the purple and the blue cell are marked as a loop of blue and red. In addition, longitudinal sections along the black line are shown in A' to D' where orange lines mark apical membranes. The yellow and the purple cells slide over the blue cell, thereby increasing their contact with the blue cell resulting in larger loops (Figure 7.3 A-B). Concomitantly, the apical membranes of the blue cell are extended (Figure 7.3 A'-B'). Once the yellow and the purple cell meet, the two apical membranes of the blue

cell will meet and connect (Figure 7.3 C and C'). There might be a moment when the blue cell makes contact with the yellow and the purple cell, and in addition, the purple cell makes contact with the yellow cell (Figure 7.3 C'). This might explain the short increase in EGFP-hZO1 fluorescence when the two loops contact (Figure 6.10C). From there on, presumably, the junctions of the blue cell with the yellow and the purple cell at the new contact point between the yellow and purple cell retract and possibly dissolve, which merges the two apical membranes of the blue cell (Figure 7.3 D'). The contact between the yellow and the green cell is increased seen as the yellow and purple line (Figure 7.3 D).

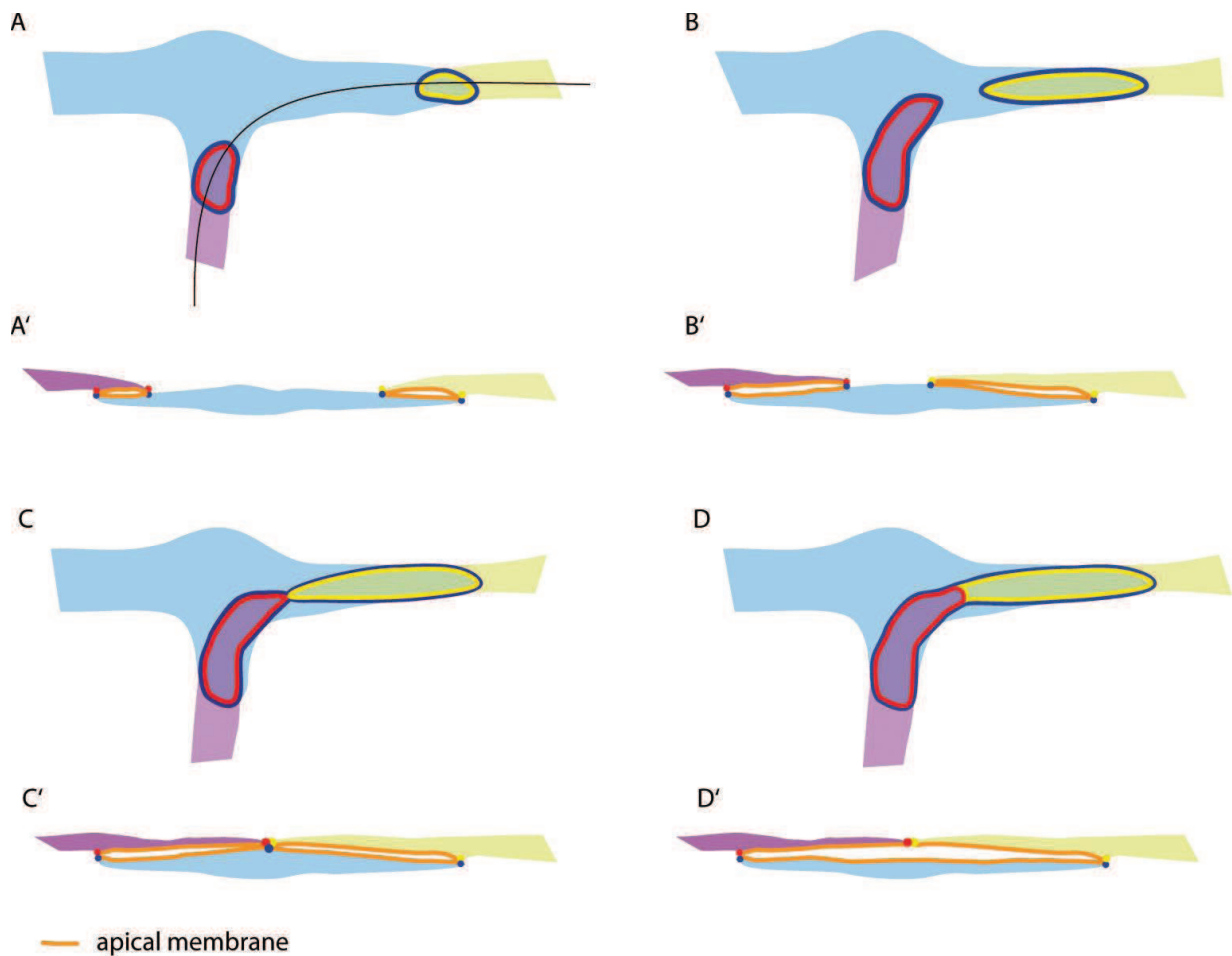


**Figure 7.3:**

**Schematic representation of extracellular lumen formation:** A'-D' shows longitudinal sections following the black line in (A). Junctions between cells are marked as double lines with the colors of the appropriate cells and as spots in the longitudinal sections. Apical membrane is marked as orange line in longitudinal sections. A fusion cell (blue) has formed a pre-lumen with a stalk cell (purple) and an adjacent fusion cell (yellow) (see also Figure 6.10 and movie 10) (A and A'). The stalk cell and the adjacent fusion cell extend their contacts with the fusion cell. The pre-lumens are increased and the two apical membranes of the fusion cell are brought closer together (B and B'). Eventually the stalk cell and the adjacent fusion cell meet. At this point the fusion cell might still have junctions with its two partner and in addition the stalk cell and the adjacent fusion cell already have made junctions (see C'). Ultimately the fusion cell will retract its junctions at this point joining its two apical membranes to a single one. Concomitantly the stalk cell and the adjacent fusion cell elaborate their new junction (D and D') (see Figure 6.10 and movie10).



The notochord of *Ciona intestinalis* uses a similar mechanism during development to form a multi-cellular tube. Notochord cells are initially arranged as non polarized serial row of round columnar cells. Cells then polarize forming an extracellular lumen at each cell-cell interface resulting in cells having to apical membranes similar to a fusion cell after contact formation. Cells then lose their radial symmetry, elongate on one side of the circumference and narrow down on the opposite side. Adjacent cells undergo complementary cell shape changes, thereby tilting the lumens and bringing the two apical sides of individual cells closer together. These cell shape changes are thought to come about by active crawling movements of the cells. Then the individual lumens join, resulting in a continuous lumen surrounded by a multi-cellular tube. This process is characterized by the joining of the two apical membranes of cells and new contacts between cells (for detailed information see (Dong et al., 2009). Molecules controlling this cellular mechanism remain mostly obscure in notochord development of *Ciona intestinalis*. Actin inhibitor and morpholino knockdown of *Ciona* ERM, an actin modulator, leads to failure of convergence of the lumens suggesting that crawling relies on active movements of the cells (Dong et al., 2009; Hotta et al., 2007).

#### **7.2.4 Cell division during vascular development**

We have shown that cells undergo extensive cell divisions during ISV formation (Blum et al., 2008). We further analyzed the behavior of junctions during cell division and found different ways of junction remodeling during and after cell division (Figure 6.13-6.15, movie 13-15).

Tip cells migrating towards the dorsal side can divide in such a way that a new junctional spot is established between the two emerging daughter cells. This spot is then elaborated into a junctional loop, very similar to what has been observed during contact formation between ISVs during DLAV formation (Figure 6.13, movie 13 and Figure 7.4 for a model). This is a rather new concept of cell division, but cells in the developing neural tube of the zebrafish have been shown to polarize during cell division resulting in mirror-image daughter cells with regard to apicobasal polarity (Tawk et al., 2007). Most of the cells executing this process during neural tube development will lose contact and will not form junctions with their daughter cell but rather move to the opposite side of the circumference of the neural tube with regard to their daughter cell (Tawk et al., 2007). In the case of a tip cell in the vascular system, the daughter cells have to keep contacts to avoid detaching from each other.

Stalks cells, which are part of an ISV organized as a multicellular tube, form a new junction between the daughter cells upon division, thus keeping the integrity of the multicellular tube (Figure 6.14, movie 14 and see Figure 7.5 for a model). Different studies have shown that epithelial cells keep their integrity during cell division. Junctions of a dividing cell are brought closer together at the plane of division during cytokinesis and subsequently a new junction is

formed between the two daughter cells when cytokinesis is completed (Gibson et al., 2006; Kim and Raphael, 2007), see also movie 14A and B and Figure 6.14 C).

EGFP-hZO1 appears to delocalize from the junctions to some extent during cell division (Figure 6.13B). However, ZO1 has been shown to remain at junctions of epithelial cells during cell division (Baker and Garrod, 1993; Kim and Raphael, 2007). Thus, it is not clear whether this is a property of ECs or a property of the transgene we use in our studies.

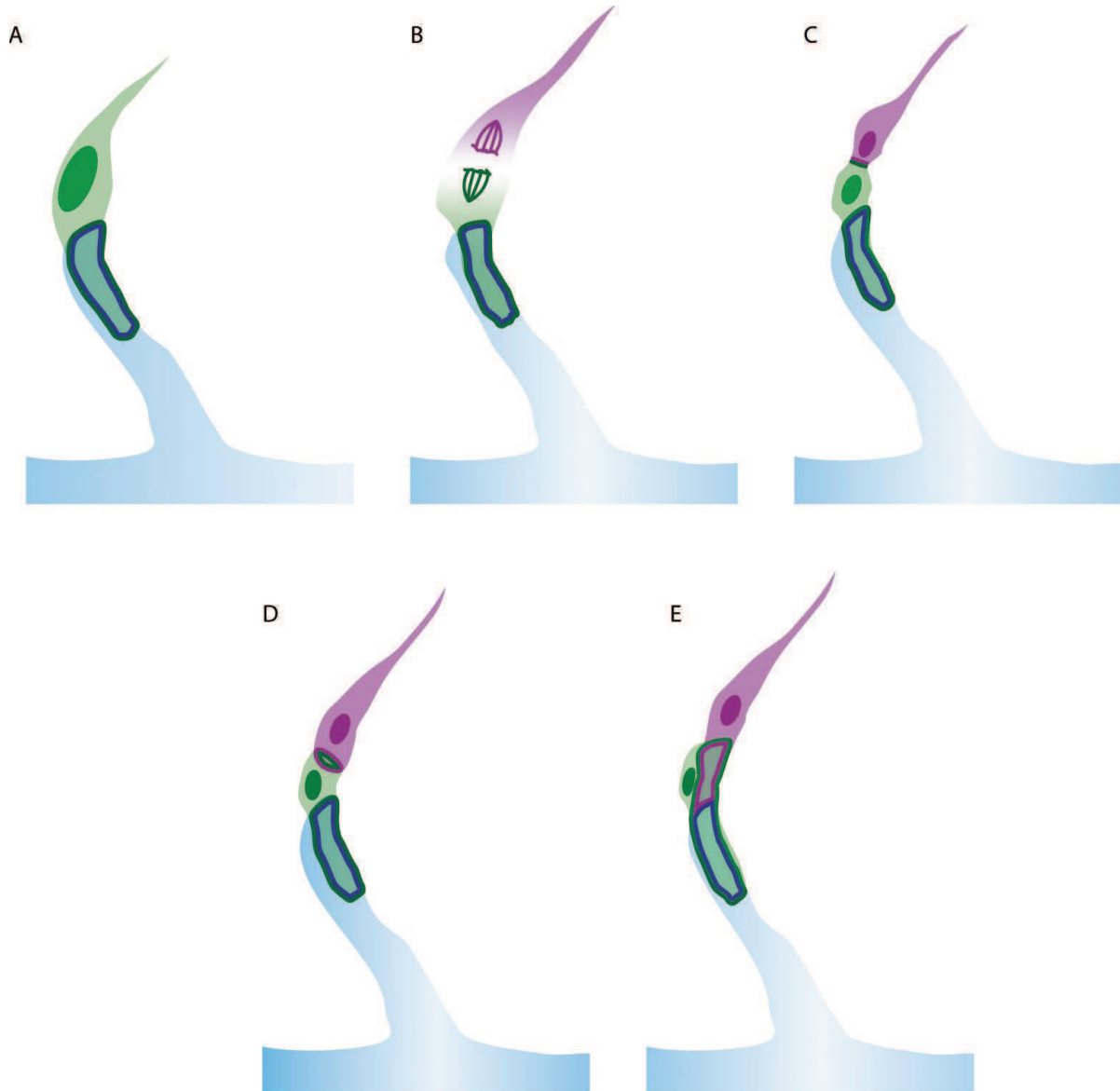


**Figure 7.4**

**Schematic representation of Figure 6.13:** Junctions between cells are marked as double lines with appropriate colors. A tip cell (green) has junctions with the stalk, which not defined in terms of cellular organization and junctions. The tip cell divides and new junctions are formed between the two daughter cells (green and purple) (B and C). These new junctions are then elaborated into a loop, which suggests apical membrane and a pre-lumen between the two daughter cells (D). The cells subsequently rearrange using the extracellular lumen formation mechanism described above in Figure 7.3 (E).

Most interestingly, we observed that cell division can occur concomitantly with cell rearrangements (see Figure 6.15, movie 15A and B, Figure 7.6 shows a model). This shows that ECs have a high degree of plasticity, at least during early steps of vessel formation.

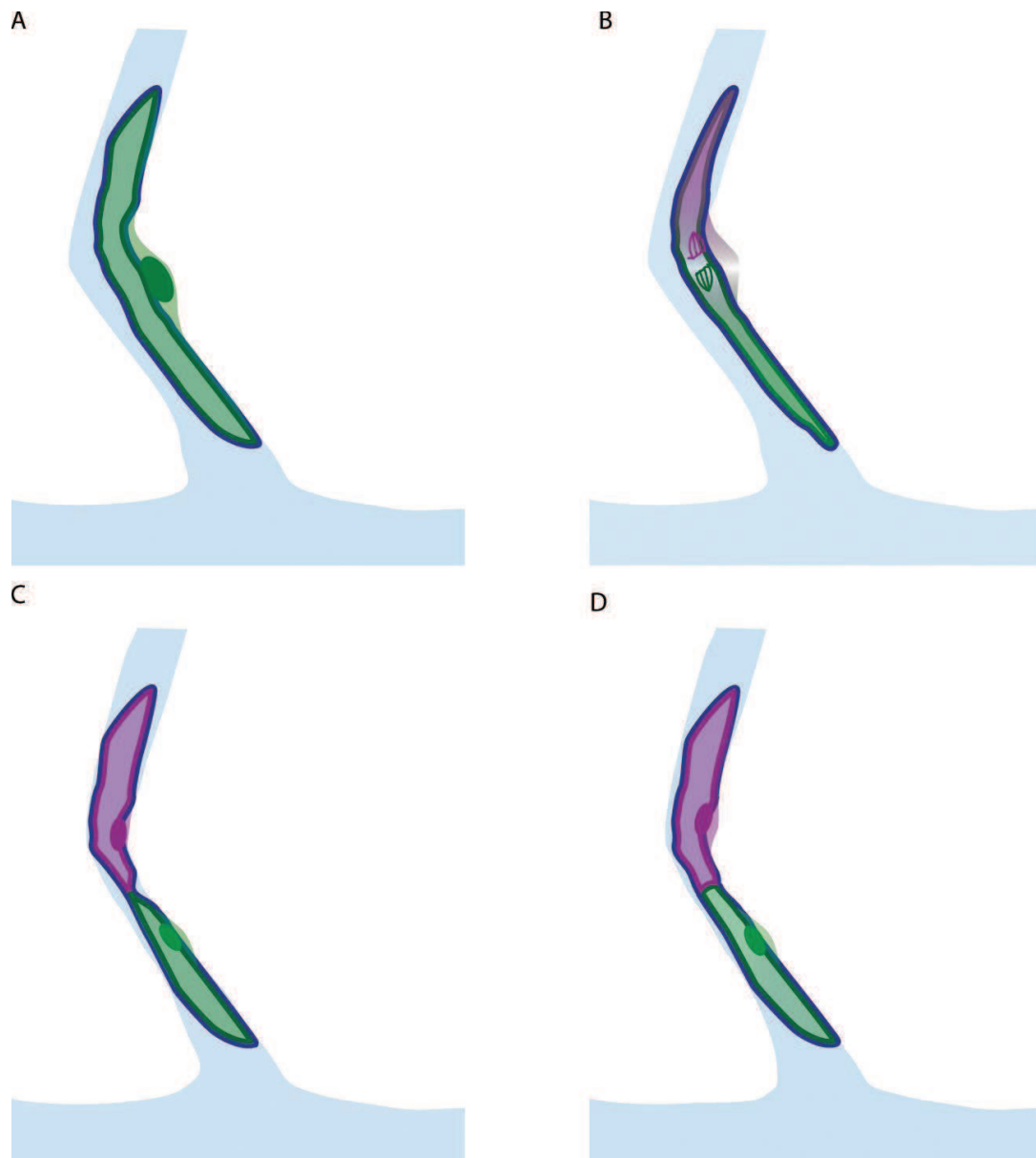


**Figure 7.5**

**Schematic representation of Figure 6.14:** Junctions between cells are marked as double lines with appropriate colors. A stalk cell (green) has junctions over its whole circumference and is thereby forming a multi-cellular tube with other stalk cells (blue, no specification of exact arrangement) (A). The stalk cell (green) divides (B). During cytokinesis the junctions are brought together at the plane of cell division (C) and new junctions are formed between the two daughter cells (green and purple) upon completion of cytokinesis (D). This junction is seen as a “Bridge” of junctions between the former junctions of the mother stalk cell (green in A) and the rest of the stalk cell/cells (blue).

ECs appear to partially retain their shape during cell division. This is seen during cell division using the *flk1:EGFP-NLS* transgenic line. Upon division of a tip cell in an ISV sprout, EGFP-NLS loses nuclear localization and is seen in the protrusions of the tip cell, demarking the elongated shape during cell division. EGFP-NLS localizes back to the nucleus after cell

division (Figure 6 in Blum et al., 2008). In contrast, epithelial cells round up during cell division (Gibson et al., 2006).

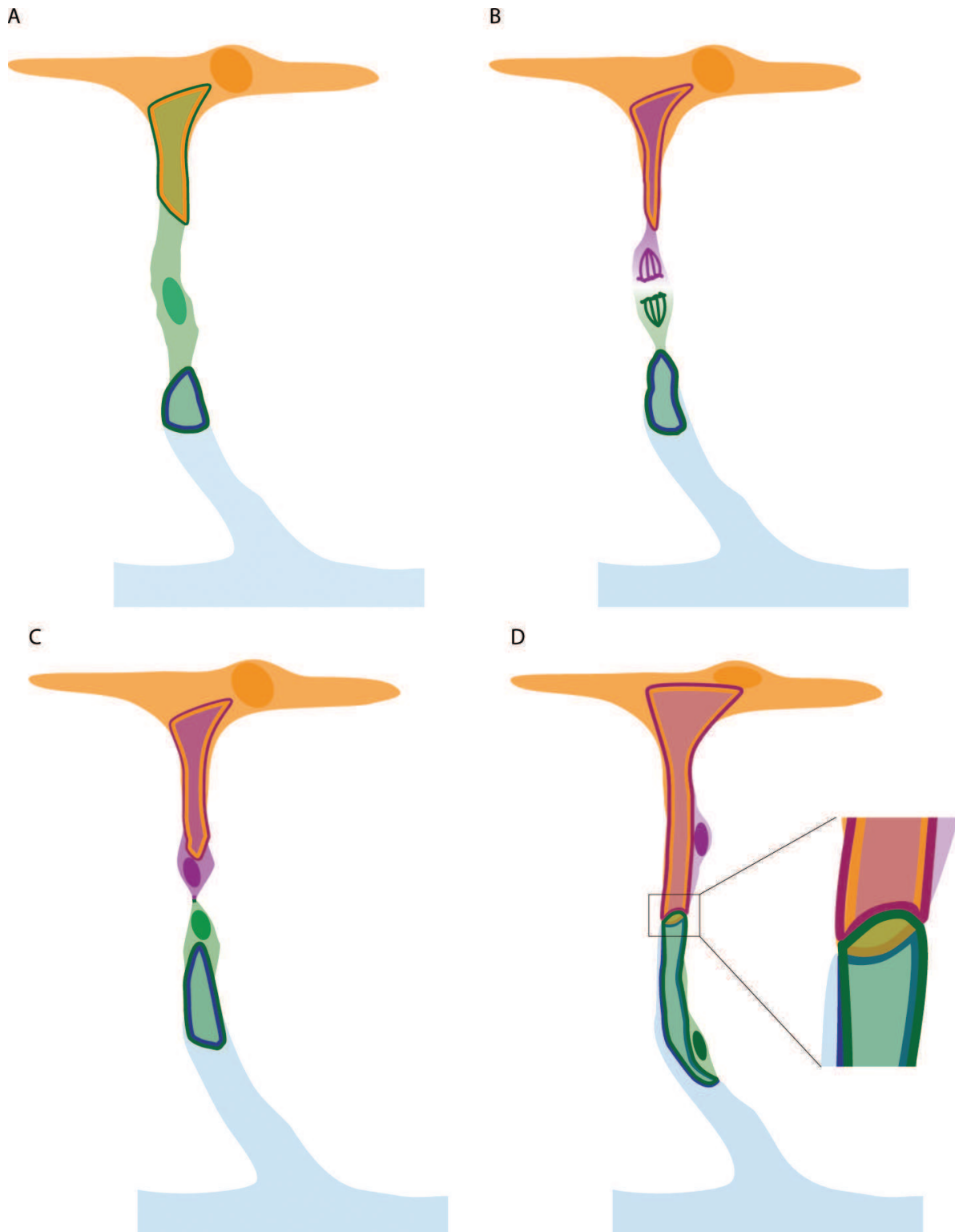


**Figure 7.6**

**Schematic representation of Figure 6.15:** Junctions between cells are marked as double lines with appropriate colors. A stalk cell (green) is arranged in a head-to-tail fashion with a fusion cell (orange) and the stalk (blue, no specification of exact arrangement) (A). The stalk cell divides (B) and during cytokinesis a new junction forms between the two daughter cells. Concomitantly the fusion cell and



the stalk (blue) have extended their contact with the dividing cell thereby coming closer to each other (C). The exact mechanism during the next steps remains obscure in Figure 6.15 and movie 15. It is not clear whether the fusion cell and the stalk first make new contact or whether the two daughter cells first form loop as in Figure 6.10 and 7.3 and the cell rearrange afterwards. However, the end result are parallel lines of junctions going from dorsal to ventral and loop of junctions at the plane of cell division, which is connected with the parallel lines (D). The parallel lines are formed from the contact of the fusion cell (orange) and the purple daughter cell, and from the stalk (blue) and the green daughter cell. The loop is formed from contacts of the two daughter cells (green and purple) and from contacts of the fusion cell (orange) and the stalk (blue)(seen as blow up in D).

### 7.2.5 Intercalation and cell self fusion

We only found very few auto-cellular junctions in Ab stainings. Thus, we didn't really expect to see intercalation events during ISV development. Live-imaging revealed that intercalation does occur during ISV formation. Cells do reach around the lumen and make auto-cellular junctions. These auto-cellular junctions then extend using a similar zipping mechanism as shown in the *Drosophila* tracheal system (Figure 6.16, 6.17 and movie 16A, B and 17, Ribeiro et al., 2004). In the tracheal system apically secreted zona pellucida proteins such as Dumpy and Piopio are required to avoid the complete intercalation of tracheal cells. In mutants for these genes, cells fail to stop intercalation and separate from the epithelium (Jazwinska et al., 2003). One could have thought that luminal pressure would play a similar role in the vascular system, but as the lumen collapses in one case (Figure 6.16D and E), this seems not to be the case. In the tracheal system, intercalation is driven by forces and tension, which are generated by the tip cell migration during branch outgrowth (Caussinus et al., 2008). However, all intercalations we observe in ISVs occur after anastomosis and thus a major pulling force from the tip/fusion cell is unlikely. Rather, local changes of tension in cells, which potentially lead to retraction of cell extensions, might be the driving force of intercalation in the vascular system.

A reason why we do not see a lot of autocellular junctions in ISVs might be our observation that cells, which have intercalated undergo a cell self fusion process thereby eliminating their autocellular junctions; this ultimately results in seamless tubes with an intracellular lumen (Figure 6.16E, F, E', F', 6.17E, F and movie 16A, B and 17). Two adjacent cells in the *C. elegans* digestive tract have been shown to undergo cell self fusion to form seamless tubes (Rasmussen et al., 2008). These cells express so-called fusogenes such as *eff-1* and *aff-1*, which are essential for cell-cell or cell self fusion. Interestingly, because these two cells are adjacent to each other, they express different versions of fusogenes to avoid fusion between the two cells (Rasmussen et al., 2008). It will be interesting to find out whether ECs express similar proteins and especially how they are regulated. As all ECs appear to have a similar potential to undergo intercalation and cell self fusion, it is unlikely that all ECs express

fusogenic proteins as this would result in cross fusion of all ECs. It is reasonable to propose that autocellular junctions potentially trigger activation of fusogenic proteins. Obviously fusogenic proteins first have to be identified and potentially ECs might use a different mechanism, not involving fusogenic proteins for cell self fusion.

### 7.3 Conclusions

This study shows that ECs have a high degree of plasticity and can use a whole set of different cellular mechanism to form a lumenized functional vascular system. Cells can divide, rearrange or form an intracellular lumen. Molecular mechanisms driving these cellular mechanisms remain largely unknown. The high variance and unpredictability of behavior of ECs indicates that at least for a given vascular bed, no genetically unique ECs exist; this might be in sharp contrast to the tracheal system, in which specialized fusion cells exist. The only specialized cells, the tip cells, lose their identity upon contact formation (Leslie et al., 2007). Therefore ECs most likely use general molecular pathway to drive these cellular processes. This will make it difficult to sort out important components for a given mechanism as inactivating these components might disrupt general EC functions. Thus, advanced genetic techniques will be required to manipulate gene function in time and space such as the inducible CreERT-Lox system in combination with dominant negative factors. In addition new transgenic lines expressing different sets of fluorescently tagged markers such as apical markers will be required to unambiguously prove some of the concepts proposed in this study.

## 8 Acknowledgements

I would like to gratefully thank my supervisor Prof. Dr. Markus Affolter, who gave me the opportunity to do my PhD thesis in his lab. His encouragement and enthusiasm was always a driving force during my thesis. I always very much enjoyed the scientific and non-scientific discussions we had. Thanks

Sincere thanks goes to Lukas Herwig in the lab without his work much of this thesis would not have been possible. A large portion of this work arose as a fruitful collaboration with him spending days and nights at the confocal microscope. He became a true friend and celebrating groundbreaking results at parties was always a joy.

I would also like to thank all former and present members of the Affolter lab for an enjoyable atmosphere, for scientific support and scientific discussions, but also for enjoyable evenings and Friday afternoon jokes.

Last but not least, I would like to thank Claudia and my parents for emotional and financial support.

## 9 Appendix

### 9.1 Kleaveland et al., 2009

**Regulation of cardiovascular development and integrity by the heart of glass-cerebral cavernous malformation protein pathway.**

**Contribution:** I injected *heg1* and *ccm2* morpholinos and did Ab stainings of CDH5 on 2d wt and morphant embryos (see supplementary Figure 9A). I also did movies of QD injected wt and morphant *fli1:cdc42GFP* embryos (supplementary Figure 7E).

### 9.2 Li et al., 2010

**A noncoding antisense RNA in *tie-1* locus regulates *tie-1* function in vivo.**

**Contribution:** I injected *tie1* and *tie1AS*-lncRNA and did Ab stainings on 24 hpf wt and morphant embryos, thereby quantifying disintegrated junctions (see Figure 3B and C).

### 9.3 Review: Ellertsdottir et al., 2010

**Vascular morphogenesis in the zebrafish embryo**

**Contribution:** I wrote an initial draft on angiogenesis.

# Regulation of cardiovascular development and integrity by the heart of glass—cerebral cavernous malformation protein pathway

Benjamin Kleaveland<sup>1</sup>, Xiangjian Zheng<sup>1</sup>, Jian J Liu<sup>2</sup>, Yannick Blum<sup>3</sup>, Jennifer J Tung<sup>4</sup>, Zhiying Zou<sup>1</sup>, Shawn M Sweeney<sup>1</sup>, Mei Chen<sup>1</sup>, Lili Guo<sup>1</sup>, Min-min Lu<sup>1</sup>, Diane Zhou<sup>1</sup>, Jan Kitajewski<sup>4</sup>, Markus Affolter<sup>3</sup>, Mark H Ginsberg<sup>2</sup> & Mark L Kahn<sup>1</sup>

Cerebral cavernous malformations (CCMs) are human vascular malformations caused by mutations in three genes of unknown function: *KRIT1*, *CCM2* and *PDCD10*. Here we show that the heart of glass (HEG1) receptor, which in zebrafish has been linked to *ccm* gene function, is selectively expressed in endothelial cells. *Heg1*<sup>-/-</sup> mice showed defective integrity of the heart, blood vessels and lymphatic vessels. *Heg1*<sup>-/-</sup>; *Ccm2*<sup>lacZ/+</sup> and *Ccm2*<sup>lacZ/lacZ</sup> mice had more severe cardiovascular defects and died early in development owing to a failure of nascent endothelial cells to associate into patent vessels. This endothelial cell phenotype was shared by zebrafish embryos deficient in *heg*, *krit1* or *ccm2* and reproduced in *CCM2*-deficient human endothelial cells *in vitro*. Defects in the hearts of zebrafish lacking *heg* or *ccm2*, in the aortas of early mouse embryos lacking *CCM2* and in the lymphatic vessels of neonatal mice lacking HEG1 were associated with abnormal endothelial cell junctions like those observed in human CCMs. Biochemical and cellular imaging analyses identified a cell-autonomous pathway in which the HEG1 receptor couples to KRIT1 at these cell junctions. This study identifies HEG1-CCM protein signaling as a crucial regulator of heart and vessel formation and integrity.

CCMs are a common vascular malformation, with a prevalence of 0.1%–0.5% in the human population<sup>1</sup>. CCMs arise primarily in the brain as thin-walled, dilated blood vessels that cause seizures, headaches and stroke in midlife, often in association with focal hemorrhage<sup>1,2</sup>. Familial CCM shows an autosomal dominant pattern of inheritance and is caused by loss-of-function mutations in three genes: *KRIT1* (also known as *CCM1*)<sup>1,3,4</sup>, *CCM2* (also known as *malcalverin* and *osm*)<sup>5,6</sup> and *PDCD10* (also known as *CCM3*)<sup>7</sup>. The CCM proteins are putative adaptor proteins that interact biochemically<sup>8–10</sup> and participate in a signaling pathway that is not yet fully characterized. The mechanism by which loss of CCM protein signaling results in the development of vascular malformations is not known.

A clue to the role of CCM protein signaling in the cardiovascular system comes from genetic studies in zebrafish, which reveal that loss of *krit1*, *ccm2* or *heg* (encoding the type I transmembrane receptor heart of glass) results in a dilated heart phenotype early in development<sup>11,12</sup>. This phenotype is characterized by heart failure associated with enlarged cardiac chambers in which the endocardium is covered by a thin layer of myocardial cells. Expression of *heg*, *krit1* and *ccm2* mRNA has been detected in the endocardium, but not the

myocardium, of zebrafish embryos<sup>11,12</sup>, suggesting that these proteins operate in an endothelial cell-autonomous signaling pathway. An endothelial role for this pathway is also supported by studies of *KRIT1*-deficient mice, which show lethal vascular defects at embryonic day 9 (E9); however, these studies did not detect high-level *Krit1* or *Ccm2* gene expression in the mouse cardiovascular system, leading to the proposal of cell-nonautonomous mechanisms of CCM pathogenesis such as a requirement for CCM protein signaling in adjacent neuronal cells<sup>13,14</sup>.

Here we used mice and zebrafish lacking the HEG1 receptor and the *CCM2* adaptor to investigate the role of this pathway in the cardiovascular system. Our studies support an endothelial cell-autonomous mechanism in which the HEG1 receptor couples to *CCM* proteins to regulate endothelial cell-cell junctions required for the formation and maintenance of the heart and vessels. Complete loss of function in this pathway resulted in an inability of emerging endothelial cells to associate into a functional cardiovascular system in mouse and zebrafish embryos. Less-complete loss of function permitted heart and vessel development but resulted in integrity defects manifested by cardiac rupture, vascular hemorrhage and lymphatic leakage. These cardiovascular defects arose in conjunction with abnormal endothelial

<sup>1</sup>Department of Medicine and Cardiovascular Institute, University of Pennsylvania, 421 Curie Blvd., Philadelphia, Pennsylvania 19104, USA. <sup>2</sup>Department of Medicine, University of California, San Diego, 9500 Gilman Drive, MC 0726, La Jolla, California 92093-0726, USA. <sup>3</sup>Biozentrum, University of Basel, Klingelbergstrasse 50/70, CH-4056 Basel, Switzerland. <sup>4</sup>Department of Pathology and Department of Obstetrics and Gynecology, Institute of Cancer Genetics and Herbert Irving Comprehensive Cancer Center, Columbia University Medical Center, New York, New York 10032, USA. Correspondence should be addressed to M.L.K. (markkahn@mail.med.upenn.edu).

Received 8 October 2008; accepted 17 December 2008; published online 18 January 2009; corrected after print 12 February 2009; doi:10.1038/nm.1918



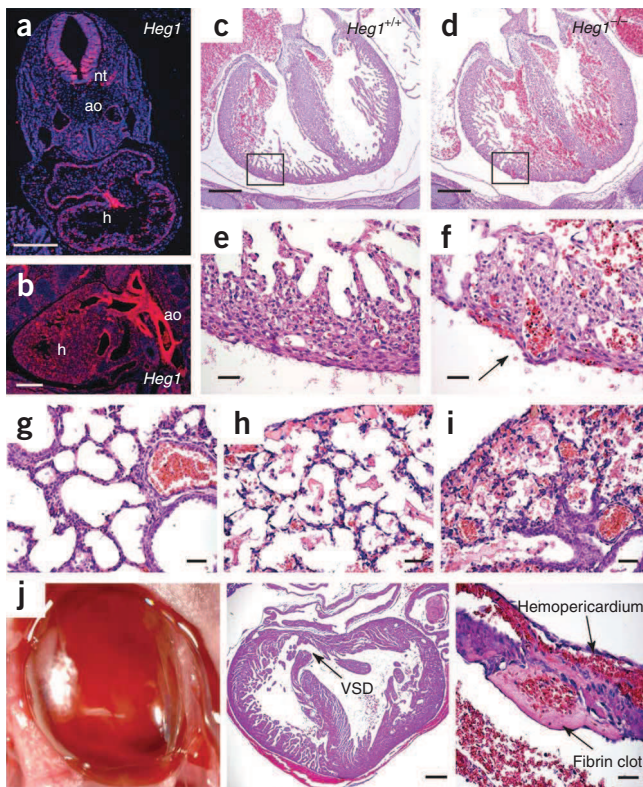


**Figure 1** Heart and blood vessel integrity defects in HEG1-deficient mouse embryos and neonates. (a,b) *Heg1* was selectively expressed in the developing cardiovascular system. Radioactive *in situ* hybridization revealed *Heg1* expression in the vascular endothelium, cardiac endocardium and neural tube at E10.5 (a). By E14.5, *Heg1* was expressed in both endothelial and smooth muscle cells in major arteries (b). ao, aorta; h, heart; nt, neural tube. (c–f) E15 *Heg1*<sup>-/-</sup> embryos showed deep invaginations of the ventricular chamber into the compact zone of the ventricular wall and into the septum, often associated with the presence of blood between the epicardial and myocardial cell layers of the heart (arrow in f). e,f show magnification of boxed regions in c,d. (g–i) Pulmonary hemorrhage in *Heg1*<sup>-/-</sup> neonates (h,i) but not in *Heg1*<sup>+/+</sup> littermates (g) was manifested by the presence of erythrocytes and fibrin in alveolar air spaces. (j) Cardiac rupture in P4 *Heg1*<sup>-/-</sup> neonate. Hemopericardium (left, middle) associated with cardiac rupture and formation of a transmural thrombus (right) was observed in *Heg1*<sup>-/-</sup> mice. VSD, ventricular septal defect. Scale bars, 200  $\mu$ m in a–d and j (middle), 20  $\mu$ m in e–i and j (right).

junctions similar to those observed in human CCMs<sup>15–17</sup> and associated with KRIT1 depletion in human endothelial cells *in vitro*<sup>18</sup>, suggesting a common mechanism by which loss of this signaling pathway confers a spectrum of vertebrate cardiovascular defects in developing and mature animals. Our studies indicate that the signaling pathway implicated in human CCM regulates endothelial cell-cell association and suggest that agents designed to promote endothelial cell association may be effective treatments for CCM.

## RESULTS

### *Heg1* is expressed in the developing cardiovascular system

It has been unclear how CCM proteins function in cardiovascular cell types and whether it is loss of CCM protein function in cardiovascular or other cell types that causes human vascular disease. To determine whether HEG1 receptors have a direct role in regulating CCM protein signaling, we cloned the mouse *Heg1* gene (Supplementary Fig. 1 online) and characterized *Heg1* mRNA expression in mice. Using *in situ* hybridization, we detected *Heg1* expression in the endothelium of the developing heart and aorta and in the neural tube at E10.5 (Fig. 1a), and in the arterial endothelium, smooth muscle, endocardium of the heart and brain vasculature at E14.5 (Fig. 1b and Supplementary Fig. 2 online). In contrast to *Heg1*, *Ccm2* expression was low and detected primarily in the developing neural tube at E10.5 (Supplementary Fig. 3 online).

### HEG1 deficiency results in lethal hemorrhage in mice

To address the role of the HEG1 receptor in mammals, we generated HEG1-deficient mice by targeting *Heg1* exon 1 in embryonic stem cells (Supplementary Fig. 4 online). In mice with genetic backgrounds of 50% SV129 and 50% C57Bl/6 or >95% C57Bl/6, HEG1 deficiency resulted in embryonic and postnatal lethality (Supplementary Table 1 online). Midgestation HEG1-deficient embryos

showed cardiac defects characterized by invagination of the ventricular cavity into, and often through, the compact layer of ventricular myocardium (Fig. 1c–f). The septal myocardium was similarly honeycombed by endothelial-lined extensions from the ventricular cavity (Fig. 1d), a defect accompanied by the presence of ventricular septal defects in most late-gestation embryos. TUNEL and Ki67 staining revealed that HEG1-deficient myocardial defects were not caused by an increase in myocardial apoptosis or a decrease in myocardial proliferation (Supplementary Fig. 5 online and data not shown). Although most HEG1-deficient mice survived to birth, approximately half died before weaning as a result of pulmonary hemorrhage (Fig. 1g–i). Neonatal HEG1-deficient mice also showed defective cardiac integrity manifested by a blood-filled pericardial sac, a phenotype that arose as a result of rupture of the low-pressure atrial chamber of the heart (Fig. 1j). Cardiac or pulmonary integrity defects were observed in 50% of HEG1-deficient mice. These findings indicate that HEG1 deficiency results in a loss of cardiac and pulmonary vascular integrity, resulting in lethality.

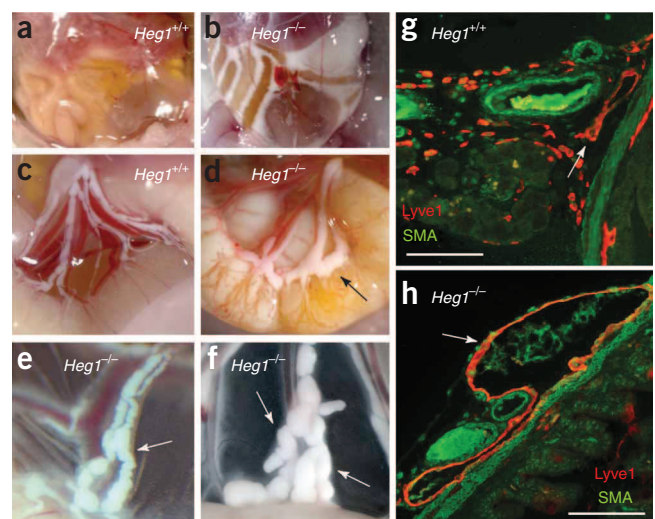


**Figure 2** Lymphatic vessel dilatation and leakage in *Heg1*<sup>-/-</sup> neonatal mice. (a,b) HEG1-deficient neonates showed chylous ascites, manifested by the accumulation of white chyle in the peritoneal space. (c–f) Lymphatic malformations in *Heg1*<sup>-/-</sup> mice. Neonatal mesenteric lymphatic vessels of *Heg1*<sup>-/-</sup> mice were dilated (arrows) and leaked chyle into the intestinal wall and peritoneum. (g,h) Immunostaining for LYVE1 confirmed the lymphatic identity of the dilated mesenteric vessels (arrows). SMA,  $\alpha$ -smooth muscle actin. Scale bars, 100  $\mu$ m.

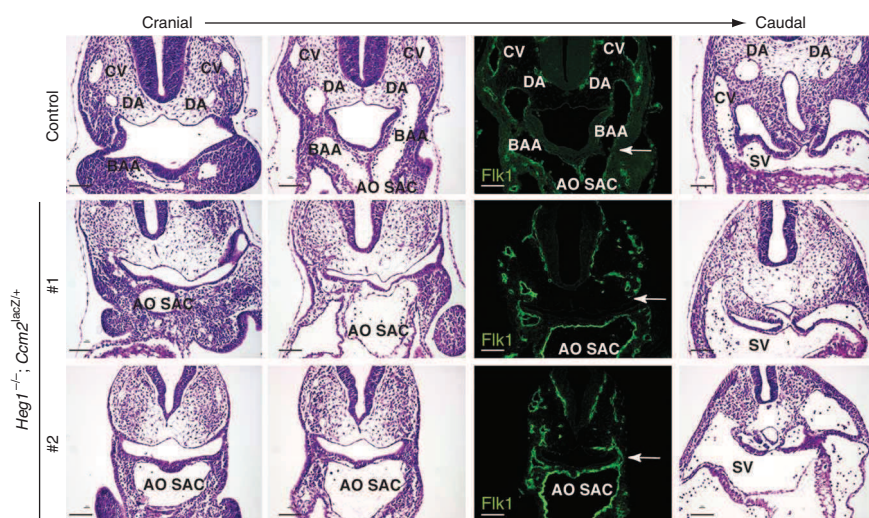


**Figure 3** *Heg1*<sup>-/-</sup>; *Ccm2*<sup>lacZ/+</sup> mouse embryos do not establish a patent blood vascular network. Transverse sections of E9 *Heg1*<sup>+/-</sup>; *Ccm2*<sup>+/+</sup> (control) and two *Heg1*<sup>-/-</sup>; *Ccm2*<sup>lacZ/+</sup> embryos at three levels are shown. H&E staining revealed the presence of blood-filled dorsal aortas (DA), cardinal veins (CV) and branchial arch arteries (BAA) of normal caliber in the *Heg1*<sup>+/-</sup>; *Ccm2*<sup>+/+</sup> control embryo (top) but not in *Heg1*<sup>-/-</sup>; *Ccm2*<sup>lacZ/+</sup> littermates (bottom). Staining for Flk1 in adjacent sections at the level of the first two branchial arch arteries is shown. Flk1<sup>+</sup> endothelial cells were present at the dorsal aortas, cardinal veins and branchial arch arteries (arrows) in *Heg1*<sup>-/-</sup>; *Ccm2*<sup>lacZ/+</sup> embryos, but these cells did not form vessels of normal caliber with patent lumens. AO SAC, aortic sac; SV, sinus venosus. Scale bars, 50 μm.

### HEG1 deficiency causes dilated lymphatic vessel malformations

Neonatal mammals transport absorbed fat through the intestinal and mesenteric lymphatic vessels in the form of white chyle. A distinct phenotype observed in approximately 10% of HEG1-deficient neonatal mice was the appearance of chylous ascites shortly after their first feeding (Fig. 2a,b). Chylous ascites was invariably associated with severely dilated intestinal and mesenteric lymphatic vessels that leaked chyle into the intestinal wall and peritoneal space (Fig. 2c–f). The dilated mesenteric lymphatic vessels were lined with endothelial cells that expressed the lymphatic molecular marker LYVE1 and were associated with smooth muscle cells typical of collecting lymphatic vessels (Fig. 2g,h). These findings indicate that loss of HEG1 receptors is associated with a loss of integrity of lymphatic vessels as well as of blood vessels and the heart. Because lymphatic vessels are not subject to the hemodynamic forces generated by the beating heart, these findings further suggest that loss of integrity arises as an intrinsic defect in the heart and vessels of HEG1-deficient mice.

### *Heg1* and *Ccm2* interact genetically in mice

Identical big-heart phenotypes arise in zebrafish embryos lacking *heg*, *krit1* (also known as *santa*) or *ccm2* (also known as *valentine*), and gene-knockdown experiments using morpholinos have shown strong interactions among these genes in zebrafish<sup>12</sup>. In contrast, human CCMs have been linked to loss-of-function mutations in *KRIT1* and *CCM2*, but not *HEG1*, and HEG1-deficient mice do not experience the early embryonic lethality reported for *KRIT1*-deficient mice<sup>13</sup>. To determine whether—and to what extent—*HEG1* interacts genetically with *CCM* genes in mammals, we intercrossed *Heg1*<sup>+/-</sup>; *Ccm2*<sup>lacZ/+</sup> mice. The *Ccm2*<sup>lacZ</sup> allele is predicted to be a null allele because the *Ccm2*<sup>lacZ</sup> mRNA transcript lacks the 3' half of the *Ccm2* mRNA (exons 6–10, Supplementary Fig. 6 online), and *Ccm2*<sup>lacZ/lacZ</sup> embryos experience early embryonic lethality that phenocopies *Krit1*<sup>-/-</sup> embryos (see below and ref. 13). In contrast to *Heg1*<sup>-/-</sup>; *Ccm2*<sup>+/+</sup>

mice, which showed no abnormalities before midgestation, both *Heg1*<sup>-/-</sup>; *Ccm2*<sup>lacZ/+</sup> and *Ccm2*<sup>lacZ/lacZ</sup> embryos died before E10 (Supplementary Table 2 online). *Heg1*<sup>-/-</sup>; *Ccm2*<sup>lacZ/+</sup> and *Ccm2*<sup>lacZ/lacZ</sup> embryos were indistinguishable from littermates of all other genotypes until E9, when the mutants showed identical phenotypes of growth retardation and marked pericardial edema despite the presence of a visibly normal heartbeat (data not shown). Histologic examination revealed normal development of the ventricular chamber and bulbus cordis (future right ventricle) but aberrant formation of a dilated aortic sac (Fig. 3 and Supplementary Fig. 7 online). Compared to control embryos, the paired dorsal aortas of E9 *Heg1*<sup>-/-</sup>; *Ccm2*<sup>lacZ/+</sup> and *Ccm2*<sup>lacZ/lacZ</sup> embryos were small or undetectable and completely

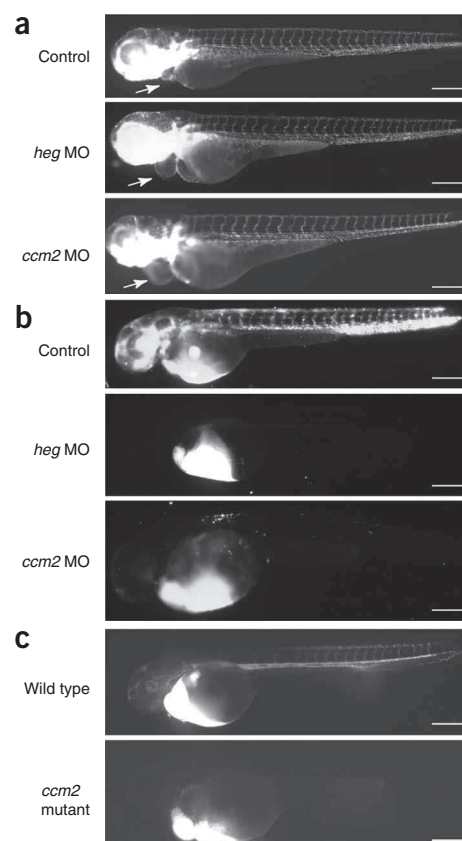


**Figure 4** Endothelial cells of zebrafish lacking *heg* or *ccm2* form vessels that are normally patterned but not patent. (a) Fli1-GFP-transgenic, *heg*- and *ccm2*-morphant (MO) embryos showed dilated hearts (arrows) and normal vascular patterning. (b) Angiography revealed a proximal circulatory block in *heg*- and *ccm2*-morphant zebrafish. Fluorescent microspheres were distributed throughout the vasculature of control, but not *heg*- or *ccm2*-morphant, zebrafish after venous injection. (c) FITC-dextran was distributed throughout the vasculature in wild-type, but not *ccm2*-mutant, zebrafish after venous injection. Scale bars, 250 μm.



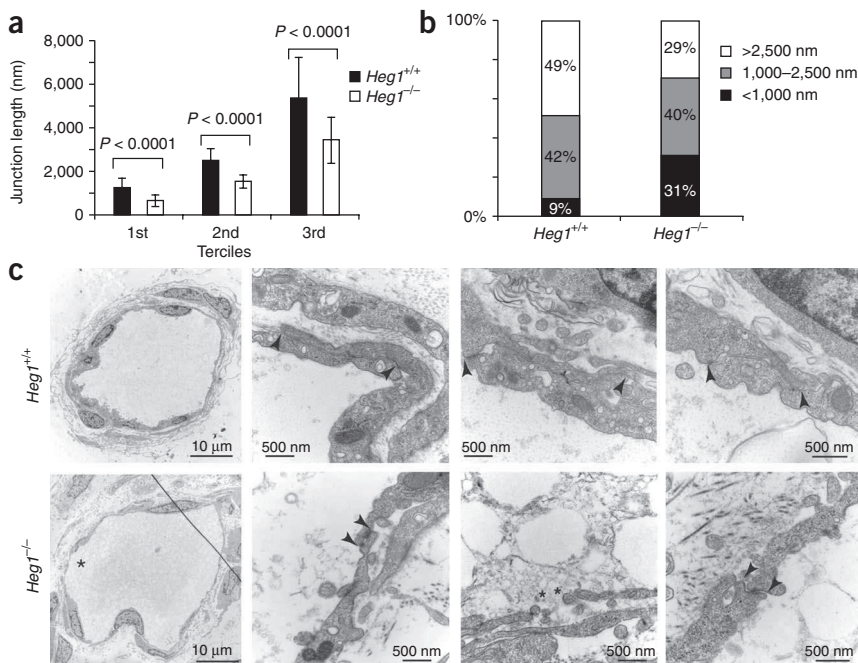


**Figure 5** HEG1 is required for normal endothelial junctions *in vivo*. Dilated mesenteric lymphatic vessels in *Heg1*<sup>-/-</sup> mice had severely shortened endothelial junctions and gaps between endothelial cells. (a) Endothelial cell junctions were measured as the length of two overlapping cell membranes. Junction lengths in *Heg1*<sup>+/+</sup> and *Heg1*<sup>-/-</sup> lymphatic vessels are shown divided into tertiles (1st, shortest third of junctions in each group; 2nd, middle third of junctions in each group; 3rd, longest third of junctions in each group; mean  $\pm$  s.d. for each tertile).  $n = 66$  *Heg1*<sup>+/+</sup> junctions and 123 *Heg1*<sup>-/-</sup> junctions. The data shown are from analysis of 6 vessel cross-sections from one animal of each genotype. (b) Percentage of endothelial junctions <1,000 nm, 1,000–2,500 nm and >2,500 nm. The same junctions were analyzed in panels a and b. (c) Representative low-magnification (far left) and high-magnification images of endothelial cells. Asterisks indicate sites of endothelial gaps, normally not present in collecting mesenteric lymphatics; arrowheads indicate endothelial junction limits. Endothelial gaps were present in *Heg1*<sup>-/-</sup> but not *Heg1*<sup>+/+</sup> vessels.

lacked luminal blood cells (Fig. 3 and Supplementary Fig. 7). Analysis of serial transverse sections revealed that the aortic sac did not connect to a lumenized first, second or third branchial arch artery in the mutant embryos, suggesting that blood in the heart did not enter the dorsal aortas despite the presence of a normal heartbeat (Fig. 3 and Supplementary Fig. 7). When visible, the cardinal veins of E9 *Heg1*<sup>-/-</sup>; *Ccm2*<sup>lacZ/+</sup> and *Ccm2*<sup>lacZ/lacZ</sup> embryos were also devoid of blood, except at the point where they connected to the sinus venosus of the heart (Fig. 3). In contrast to the lack of blood in the vessels, extravasated blood cells were frequently present in the dilated pericardial cavity (Fig. 3 and data not shown), a finding that may reflect a primary defect in the integrity of the heart; alternatively, this finding may arise from the heart beating against a closed circulatory system and/or from reduced embryonic viability at this point in development.

To determine whether the lack of blood-filled vessels in E9 *Heg1*<sup>-/-</sup>; *Ccm2*<sup>lacZ/+</sup> and *Ccm2*<sup>lacZ/lacZ</sup> embryos is due to a lack of endothelial cells, we used Flk1 immunostaining to identify endothelial cells. We found endothelial cells at sites where the branchial arch arteries and dorsal aortas are normally located, but in all *Heg1*<sup>-/-</sup>; *Ccm2*<sup>lacZ/+</sup> and *Ccm2*<sup>lacZ/lacZ</sup> embryos studied these cells were not organized into lumenized vessels as they were in control embryos (Fig. 3). Thus, circulation in *Heg1*<sup>-/-</sup>; *Ccm2*<sup>lacZ/+</sup> and *Ccm2*<sup>lacZ/lacZ</sup> embryos was blocked by an inability of mutant endothelial cells to form lumenized vessels capable of carrying blood. These findings indicate a strong genetic interaction between HEG1 receptors and the CCM protein signaling pathway during formation of the primary vasculature in mammals.

#### *heg* and *ccm2* are required for vessel patency in zebrafish

In contrast to E9 *Heg1*<sup>-/-</sup>; *Ccm2*<sup>lacZ/+</sup> and *Ccm2*<sup>lacZ/lacZ</sup> mouse embryos, zebrafish embryos lacking *heg* or *ccm2* show primarily cardiac defects<sup>11,12</sup>. To determine whether HEG1 and CCM proteins have differing roles in cardiovascular development in zebrafish and mice, we examined vascular patterning and function in *heg*-morphant, *ccm2*-morphant and *ccm2*-mutant zebrafish embryos at 48 hours post fertilization (h.p.f.). Morpholino knockdown of *heg* or *ccm2* in Fli1-GFP transgenic fish (which have GFP-labeled endothelium) resulted in

dilated heart chambers but no abnormalities in vessel patterning (Fig. 4a). However, we noted visually that blood cells in the hearts of *heg*- and *ccm2*-morphant zebrafish did not circulate despite detectable contraction of the dilated heart, a finding similar to the circulatory block we observed in E9 *Heg1*<sup>-/-</sup>; *Ccm2*<sup>lacZ/+</sup> and *Ccm2*<sup>lacZ/lacZ</sup> mouse embryos.

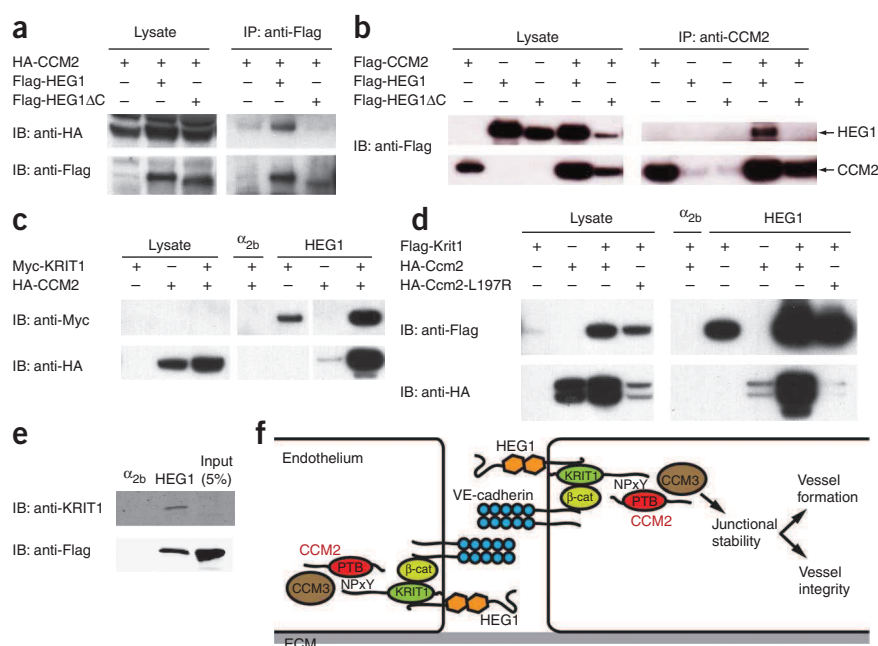
We used angiography to functionally test the patency of the vasculature of *heg*- and *ccm2*-morphant zebrafish. Fluorescent beads injected into the sinus venosus of zebrafish embryos treated with control morpholinos circulated throughout the body and outlined the developing vasculature of the head and tail (Fig. 4b). In contrast, injection of *heg*- or *ccm2*-morphant zebrafish revealed a complete or near-complete circulatory block immediately distal to the heart (Fig. 4b), the same point at which circulation was blocked in E9 *Heg1*<sup>-/-</sup>; *Ccm2*<sup>lacZ/+</sup> and *Ccm2*<sup>lacZ/lacZ</sup> mouse embryos. We also observed a complete circulatory block in all *ccm2*-mutant zebrafish embryos injected with FITC-dextran (Fig. 4c). These findings indicate a conserved role for HEG1 and CCM2 in the formation of a patent vertebrate circulatory system.

#### HEG1-CCM signaling regulates endothelial tube formation

The inability of nascent endothelial cells to form patent branchial arch vessels in *Heg1*<sup>-/-</sup>; *Ccm2*<sup>lacZ/+</sup> and *Ccm2*<sup>lacZ/lacZ</sup> mouse embryos and *heg*- or *ccm2*-morphant zebrafish embryos suggested that HEG1-CCM protein signaling is required for endothelial cells to form lumenized tubes during early vascular development. To assess the role of CCM2 in endothelial tube formation, we used a fibrin bead assay to examine the ability of human umbilical vein endothelial cells (HUVECs) expressing CCM2-specific or scrambled control small hairpin RNAs to form tubes<sup>19</sup>. CCM2-specific small hairpin RNA resulted in an 85%–90% reduction in CCM2 mRNA expression and had no effect on endothelial cell size, proliferation or migration (Supplementary Fig. 7 and data not shown). Although control HUVECs generated multicellular structures with clearly visible mature lumens at 10 d, CCM2-deficient HUVECs formed branched cords similar to those of control cells in length but were frequently unable to form visible lumens (Supplementary Fig. 7).

**Figure 6** HEG1 receptor intracellular tails associate with CCM2 through KRIT1.

(a,b) Coimmunoprecipitation of mouse HEG1 and mouse CCM2 required the HEG1 receptor intracellular tail. Hemagglutinin (HA)-tagged CCM2 or Flag-CCM2 was coexpressed with Flag-HEG1 or Flag-HEG1ΔC (a mutant lacking the terminal 106 amino acids of the HEG1 C-terminal tail) in HEK293T cells. Immunoprecipitation was done using antibodies to Flag (a) or CCM2 (b). The results shown are representative of >3 independent experiments. (c) The HEG1 intracellular tail interacted with KRIT1 and CCM2. HA-tagged mouse CCM2 and Myc-tagged mouse KRIT1 were expressed in HEK293T cells, and pull-down assays were done with affinity matrices containing the intracellular tail of either the human  $\alpha_{2b}$  integrin or human HEG1. The HEG1 tail efficiently pulled down KRIT1 in the absence of CCM2, but not *vice versa*. The results shown are representative of >3 independent experiments. (d) HEG1 interacted with ccm2 through krit1. Flag-tagged zebrafish krit1, HA-tagged zebrafish ccm2 and HA-tagged zebrafish ccm2-L197R were expressed in HEK293T cells, and pull-down assays were done using human  $\alpha_{2b}$  or human HEG1 intracellular tail affinity matrices as in c. ccm2-L197R did not associate with the HEG1 tail (far right lane). The results shown are representative of >3 independent experiments. (e) The HEG1 tail efficiently bound endogenous KRIT1. Pull-down assays using  $\alpha_{2b}$  or HEG1 tail affinity matrices were done using lysates from CHO cells transfected with Flag-tagged human CCM2. Endogenous KRIT1 was detected with monoclonal antibody to KRIT1 (top) and heterologous CCM2 with monoclonal antibody to Flag (bottom). The far right lane shows immunoblotting of cell lysate equivalent to 5% of the input for the pull-down assays. The results shown are representative of >3 independent experiments. (f) HEG1-CCM protein signaling at endothelial cell junctions. HEG1 receptors couple to KRIT1 and CCM2 through HEG1 tail-KRIT1 and KRIT1-CCM2 interactions, respectively. KRIT1 also interacts with the junctional proteins VE-cadherin and  $\beta$ -catenin ( $\beta$ -cat) and CCM2 also interacts with CCM3. HEG1-CCM protein signaling is proposed to regulate junction formation and function. ECM, extracellular matrix; NPXY, NPXY amino acid sequences; PTB, phosphotyrosine binding domain.



Studies of lumen formation by endothelial cells *in vitro* and in the intersegmental vessels (ISVs) of the zebrafish embryo *in vivo* have shown that endothelial cells can assemble lumenized vessels through the formation and fusion of intracellular vacuoles<sup>20–23</sup>. We assessed the formation of vacuole-like structures in the ISVs of morphant and control zebrafish embryos using transgenic zebrafish expressing GFP-Cdc42 fusion proteins that outline the intracellular vacuoles that form in endothelial cells<sup>22</sup>. Endothelial vacuole-like structures formed normally in the ISVs of zebrafish embryos lacking *heg* or *ccm2* (Supplementary Fig. 7 and Supplementary Movies 1–3 online). Injection of fluorescent quantum dots into the dorsal aorta of morphant zebrafish to bypass the block at the level of the branchial arch arteries confirmed that these vessels formed a patent lumen (Supplementary Fig. 7 and Supplementary Movies 4–6 online). These findings suggest that defects in endothelial tube formation observed in deficient endothelial cells do not arise because of loss of intracellular endothelial vacuole-like structures.

### HEG1-CCM signaling regulates endothelial junctions *in vivo*

An ultrastructural characteristic of human CCMs is the presence of abnormal endothelial cell-cell junctions and gaps between endothelial cells<sup>15–17</sup>, and a recent study showed a role for KRIT1 in the dynamic regulation of endothelial cell-cell junctions *in vitro*<sup>18</sup>. Thus, one mechanism by which HEG1-CCM protein signaling might regulate cardiovascular development and integrity is through regulation of endothelial cell association. To directly assess the role of HEG1 in regulating endothelial junctions *in vivo*, we used transmission electron microscopy to examine cell-cell junctions in the endothelium of neonatal mouse lymphatic vessels. The dilated mesenteric lymphatic

vessels of *Heg1*<sup>-/-</sup> neonatal mice showed markedly shortened endothelial junctions compared to vessels in control littermates (mean length of junctions, 1,769 ± 506 nm for *Heg1*<sup>-/-</sup> versus 3,355 ± 1,009 nm for *Heg1*<sup>+/+</sup>; *P* = 0.01; Fig. 5a,b) and were accompanied by endothelial gaps not present in control collecting mesenteric lymphatic vessels (Fig. 5c). Similarly shortened junctions were identified in the endocardium of *ccm2*-morphant zebrafish hearts (Supplementary Fig. 8 online). Finally, analysis of the constricted, bloodless aortas of E9 CCM2-deficient mouse embryos also revealed shortened endothelial junctions despite the fact that the caliber of these vessels was markedly reduced (Supplementary Fig. 8). These findings indicate that defective endothelial junctions characterize both the dilated and constricted cardiovascular phenotypes of animals lacking HEG1-CCM protein signaling as well as human CCMs. Notably, the levels of  $\beta$ -catenin, VE-cadherin and claudin-5, key components of endothelial junctions, were preserved in the lymphatic vessels of HEG1 deficient mice, in the hearts and vessels of zebrafish embryos lacking *heg* or *ccm2* and in CCM2-deficient HUVECs (Supplementary Fig. 9 online). These findings suggest that HEG1-CCM protein signaling may regulate the function of these proteins rather than their expression.

### HEG1 receptors couple to CCM proteins through KRIT1

Our findings suggest that HEG1 receptors interact with CCM proteins in an endothelial cell-autonomous signaling pathway: HEG1 is expressed in endothelial cells in zebrafish and mice; *Heg1*<sup>-/-</sup>; *Ccm2*<sup>lacZ/+</sup> and *Ccm2*<sup>lacZ/lacZ</sup> mouse embryos and *heg*- and *ccm2*-morphant zebrafish embryos show aberrant vessel formation at an early developmental time point when vessels are composed exclusively

of endothelial cells; and *CCM2*-knockdown HUVECs show defects in tube formation. In addition, we detected heterologously expressed mouse HEG1 at cell junctions in HUVECs (**Supplementary Fig. 10** online). To determine whether HEG1 can interact with intracellular *CCM2*, we coexpressed Flag-tagged, wild-type mouse HEG1 or mouse HEG1 lacking most of its intracellular tail (HEG1 $\Delta$ C) with hemagglutinin-tagged mouse *CCM2* in HEK293T cells and conducted coimmunoprecipitation experiments with antibodies to Flag and *CCM2*. *CCM2* coimmunoprecipitated with full-length HEG1 using antibodies to Flag (to pull down HEG1) or *CCM2* (**Fig. 6a,b**). In contrast, although HEG1 $\Delta$ C was expressed at the cell surface at levels similar to those of full-length HEG1 (**Supplementary Fig. 11** online), *CCM2* did not coprecipitate with HEG1 $\Delta$ C (**Fig. 6a,b**).

To further define how the HEG1 intracellular tail associates with *CCM* proteins, we used affinity matrices containing the intracellular tail of human HEG1 or of human  $\alpha_{2b}$  integrin to pull down hemagglutinin-tagged mouse *CCM2* and Myc-tagged mouse KRIT1 heterologously expressed in HEK293T cells. The intracellular tail of HEG1, but not that of  $\alpha_{2b}$  integrin, efficiently pulled down KRIT1 and both KRIT1 and *CCM2* when they were coexpressed (**Fig. 6c**). However, only small amounts of *CCM2* were pulled down when it was expressed alone (**Fig. 6c**), indicating that KRIT1 markedly facilitates *CCM2* interaction with the HEG1 intracellular tail.

To further assess the mechanism of *CCM2* association with HEG1, we compared the ability of human HEG1 to interact with zebrafish *krit1* coexpressed with wild-type zebrafish *ccm2* or with *ccm2*-L197R, a *ccm2* protein with an amino acid substitution in the phosphotyrosine binding domain that blocks its binding to *krit1* (ref. 8); the corresponding mutant allele of *CCM2* has been identified as a cause of human *CCM*<sup>6</sup>. Expression of wild-type *ccm2* efficiently rescued the big-heart phenotype of *ccm2*-deficient zebrafish embryos, but expression of *ccm2*-L197R did not (**Supplementary Fig. 12** online), indicating that this amino acid substitution leads to a loss of *ccm2* function in zebrafish and humans. As observed with the mouse proteins, the HEG1 receptor tail efficiently pulled down both *krit1* and wild-type *ccm2* when they were coexpressed in HEK293T cells, but only *krit1* was efficiently pulled down when *ccm2*-L197R was coexpressed (**Fig. 6d**). Finally, HEG1 receptor tails also efficiently pulled down endogenous KRIT1 in CHO cells, despite the fact that the levels of endogenous KRIT1 were so low that they could not be detected in 5% of the input cell lysate by immunoblotting with the same antibody (**Fig. 6e**). These findings support a model in which HEG1 receptors couple to *CCM* proteins primarily through interaction with KRIT1 at endothelial cell-cell junctions (**Fig. 6f**).

## DISCUSSION

Human genetic studies have revealed that *CCM* is caused by haploinsufficiency of *KRIT1*, *CCM2* or *PDCD10*, and genetic studies in mice and zebrafish have implicated these proteins in cardiovascular development. How the loss of this signaling pathway leads to these diverse cardiovascular defects has not been clear. Our studies of the expression and function of HEG1 and *CCM2* support a mechanism in which HEG1 receptor signaling through *CCM* proteins is required to regulate endothelial cell-cell association during formation of the cardiovascular system and for its integrity thereafter. We identified endothelial junction defects identical to those in human *CCMs* in the dilated hearts and vessels of zebrafish and mice deficient in HEG1 or *CCM2*, suggesting that *CCM* proteins regulate vertebrate cardiovascular development through control of endothelial cell association and that defects in this regulation leads to human *CCM* pathogenesis.

Several lines of evidence suggest that the vascular defects observed in zebrafish, mice and humans lacking HEG1 and *CCM* proteins reflect the loss of an endothelial cell signaling pathway. Although *Ccm2* gene expression was relatively low and not vascular specific, *Heg1* expression was detected specifically in vascular tissues and was restricted to endothelial cells at the stages at which deficient mouse and zebrafish embryos first develop cardiovascular defects. The vascular defects observed in E9 *Heg1*<sup>-/-</sup>; *Ccm2*<sup>lacZ/+</sup> and *Ccm2*<sup>lacZ/lacZ</sup> mouse embryos and 48-h.p.f. morphant zebrafish embryos lacking *Heg* or *Ccm2* arose before the appearance of other vascular cell types, such as pericytes or smooth muscle cells, in which HEG1 might indirectly regulate endothelial cell function. Consistent with these observations, mosaic analysis in zebrafish embryos has suggested that *krit1* functions cell autonomously during cardiovascular development<sup>24</sup>. Finally, *CCM2*-knockdown endothelial cells were defective in the formation of lumenized tubes, and biochemical studies showed that HEG1 receptors coupled to *CCM* proteins such as *CCM2* primarily through the KRIT1 protein. These findings strongly support a conserved cell-autonomous mechanism in which HEG1 receptors signal through *CCM* proteins to regulate endothelial cells during the formation and function of the heart and vessels.

Common ultrastructural defects in endothelial junctions suggest that the nonpatent branchial arch arteries that appear early in the development of mouse and zebrafish embryos lacking HEG1-*CCM* protein signaling, the diverse cardiovascular integrity defects in older HEG1-deficient mice, and the vascular defects in human *CCMs* can all be explained by varying degrees of loss of endothelial cell-cell association. In our studies, the most severe cardiovascular defects were observed in 48-h.p.f. morphant zebrafish embryos and E9 *Heg1*<sup>-/-</sup>; *Ccm2*<sup>lacZ/+</sup> and *Ccm2*<sup>lacZ/lacZ</sup> mouse embryos. In these animals, the differentiation and proliferation of early endothelial cells and their migration to sites of vessel formation (vessel patterning) were undisturbed (consistent with our observation that *CCM2* deficient HUVECs migrated normally *in vitro*), but endothelial cell assembly into a lumenized, patent circulatory system was blocked. Recent studies in zebrafish suggest that patent vessels arise either through the coalescence of vacuoles in single endothelial cells<sup>22</sup> (that is, a mechanism within endothelial cells) or through the circumferential arrangement of endothelial cells that are connected by cell-cell junctions<sup>21,23</sup> (a mechanism between endothelial cells). Our finding that endothelial cell vacuolization and lumenization were preserved in the ISVs of zebrafish embryos lacking the HEG1-*CCM* protein pathway is most consistent with a defect in endothelial cell-cell association.

The defects observed in the integrity of the heart, blood vessels and lymphatic vessels of HEG1-deficient mice also support the idea that impaired endothelial cell-cell association results from loss of HEG1-*CCM* protein signaling. The dilated, leaky lymphatic vessels of HEG1-deficient mice recapitulated many of the key structural and functional defects observed in human *CCMs* and *heg*-deficient zebrafish hearts, including shortened endothelial cell junctions, abnormal coverage of endothelial cells by adjacent cell types such as pericytes or cardiomyocytes, and vessel leakage and rupture. In addition, we observed dilated lymphatic vessels in *Heg1*<sup>+/-</sup>; *Ccm2*<sup>lacZ/+</sup> mice but not in *Heg1*<sup>+/-</sup> or *Ccm2*<sup>lacZ/+</sup> mice (data not shown), a result consistent with a genetic link between HEG1 and *CCM2* in the formation of *CCM*-like dilated vessels and in early vessel formation in embryos. Finally, KRIT1 was recently found to localize at and functionally regulate endothelial cell junctions<sup>18</sup>, and we found that heterologously expressed HEG1 receptors similarly colocalized with  $\beta$ -catenin at endothelial junctions. Thus, a unifying mechanism to explain these diverse vascular phenotypes is one in which HEG1 signaling



through CCM proteins is required for endothelial cells to associate with each other to create and maintain the vertebrate cardiovascular system.

A final question with important therapeutic implications is whether and how these studies advance our understanding of human CCM pathogenesis. Although molecular and genetic pathways are frequently postulated to link embryonic cardiovascular development and adult cardiovascular disease states, such links are often tenuous. It is therefore noteworthy that our studies of HEG1-CCM signaling in developing mice and zebrafish support conservation of the role of this pathway in both development and disease. Our findings suggest that the primary role of HEG1-CCM signaling is to control the association of endothelial cells to create and maintain cardiovascular structures. Thus, CCMs are predicted to be a disease of defective endothelial association, and agents that positively regulate endothelial junction formation might provide a means of stabilizing human CCMs or preventing their *de novo* formation. Alternatively, activation of HEG1-CCM signaling might provide a means of treating vascular diseases characterized by vascular leakage or defective vessel integrity, such as sepsis. Studies to define better the components and *in vivo* role of this signaling pathway may therefore identify new strategies for treating inherited and acquired vascular diseases.

## METHODS

**Mice.** We generated SV/129 embryonic stem cells heterozygous for the *Heg1* allele by deleting exon 1 using recombineering-based gene-targeting techniques, and we microinjected the stem cells into C57Bl/6 blastocysts. We intercrossed F<sub>1</sub>-generation *Heg1*<sup>+/-</sup> mice (50% 129, 50% C57Bl/6) and conducted phenotypic analysis on *Heg1*<sup>+/-</sup> and wild-type littermates. We generated *Heg1*<sup>+/-</sup> mice on a >95% C57Bl/6 background by backcrossing for 5 generations. We generated *Ccm2*<sup>lacZ/+</sup> mice from 129P2 embryonic stem cells in which an IRES-βGeo cassette had been inserted into *Ccm2* exon 6 using a retroviral gene trap (Bay Genomics clone RRG051; ref. 14). We obtained *Tg(Tek-cre)12Flv* and *Gt(ROSA)26Sor* transgenic mice from Jackson Research Laboratories. Unless otherwise specified, we maintained all mice on a mixed genetic background. The University of Pennsylvania Institutional Animal Care and Use Committee approved all animal protocols. Genotyping primer sequences are available in **Supplementary Methods** online.

**In situ hybridization and immunostaining.** Primer sequences used to generate *Heg1* and *Ccm2* *in situ* probes are available in **Supplementary Methods**. We carried out radioactive *in situ* hybridization, immunostaining and TUNEL staining on paraformaldehyde-fixed, paraffin-embedded sections. Detailed protocols are available at [http://www.med.upenn.edu/mcrc/histology\\_core/](http://www.med.upenn.edu/mcrc/histology_core/). We used the following antibodies for immunostaining of tissue sections: rabbit monoclonal antibody to Ki67 (1:250; Vector Laboratories), mouse monoclonal antibody to α-smooth muscle actin (1:100; 1A4, Sigma), rabbit polyclonal antibody to LYVE1 (1:2,000; ref. 25), mouse monoclonal antibody to β-catenin (1:100; BD Transduction), rat monoclonal antibody to Flk1 (1:50; Phar-Mingen) and rabbit polyclonal antibody to claudin-5 (1:50; Zymed).

**Zebrafish studies.** We maintained and bred Tuebingen long-fin wild-type zebrafish and *Tg(fli1a:EGFP)<sup>y1</sup>* (ref. 26), *Tg(kdr:EGFP)* (ref. 27), *Tg(fli1a:EGFP-cdc42)<sup>y48</sup>* (ref. 22) and *ccm2*<sup>hi296aTg</sup> (ref. 28) mutant zebrafish. We injected antisense morpholino oligonucleotides (Gene Tools) that interfere with the splicing of *ccm2* and *heg*<sup>11,12</sup> into the yolks of one-cell-stage embryos at a dose of 5 ng. To rescue the big-heart phenotype caused by the *ccm2* morpholino, we first injected the one-cell-stage embryos with 5 ng of the *ccm2* morpholino and then injected half of those embryos with 100 pg of cRNA encoding *ccm2* or *ccm2*-L197R. We carried out microangiography of zebrafish embryos as described<sup>29</sup>. We injected red fluorescent (580 and 605 nm) 0.02-μm carboxylate-modified FluoSphere beads (Invitrogen) or 10 mg ml<sup>-1</sup> 70-kDa FITC-dextran (Sigma) into the sinus venosus of 48-h.p.f. zebrafish embryos. We mounted the embryos laterally in 2% methylcellulose and acquired images using an Olympus MVX10 microscope.

**Immunoprecipitation and immunoblotting.** We subcloned full-length mouse HEG1 without endogenous signal peptide (amino acids 38–1,313) and C-terminally truncated HEG1 (amino acids 38–1,207) into pcDNA3.1 with a human interleukin-1 signal peptide, an N-terminal Flag epitope and a C-terminal v5 epitope (see **Supplementary Fig. 1b**). We cloned His<sub>6</sub>-recombinant human HEG1 intracellular tail containing an *in vivo* biotinylation peptide tag at the N terminus into pET15b as previously described for integrin intracellular-tail model proteins<sup>30</sup>. We expressed and purified tail proteins from *Escherichia coli*<sup>31</sup>.

For coimmunoprecipitation studies, we transfected plasmids driving expression of Flag-tagged full-length and truncated mouse HEG1 and hemagglutinin-tagged mouse CCM2 into HEK293T cells. After 48 h, we incubated the cells for 10 min in lysis buffer (50 mM Tris-HCl, 150 mM NaCl, 25 mM EDTA, 1% NP-40, 0.5% sodium deoxycholate, PhosStop (Roche) and complete protease inhibitor (Roche), pH 8) drawn through a 25-gauge needle and cleared by centrifugation. We conducted Flag immunoprecipitation with 2 μg ml<sup>-1</sup> antibody to Flag (M2, Sigma) and CCM2 immunoprecipitation with polyclonal antibody to CCM2 (2055, see **Supplemental Methods**) for >2 h and then incubated with protein G-agarose (Invitrogen) for 1 h. We detected proteins using the following antibodies: mouse monoclonal antibody to Flag (1:500; M2, Sigma), mouse monoclonal antibody to hemagglutinin (1:2,000; Abcam) and horseradish peroxidase-conjugated goat antibody to mouse IgG (1:5,000; Jackson ImmunoResearch).

For affinity matrix pull-down assays, we transfected HEK293T and CHO cells with plasmids driving expression of Myc-tagged mouse KRIT1, hemagglutinin-tagged mouse CCM2, Flag-tagged zebrafish krit1, hemagglutinin-tagged zebrafish *ccm2*, hemagglutinin-tagged zebrafish *ccm2*-L197R and Flag-tagged mouse CCM2. We incubated the cells for 10 min in lysis buffer (25 mM HEPES (pH 7.4), 100 mM NaCl, 0.5% NP-40 and complete protease inhibitor (Roche)). After clarification, we incubated 350 mg of lysate with 10 mg of immobilized human HEG1 tail overnight. We detected proteins using the following antibodies: mouse monoclonal antibody to Flag (1:2,000; M2, Sigma), mouse monoclonal antibody to Myc (1:2,000; Abcam), mouse monoclonal antibody to hemagglutinin (1:2,000; Abcam), polyclonal antibody to KRIT1 (1:1,000; 6832, ref. 18), horseradish peroxidase-conjugated goat antibody to mouse IgG (1:5,000; Jackson ImmunoResearch) and horseradish peroxidase-conjugated donkey antibody to rabbit IgG (1:5,000; Jackson ImmunoResearch). We carried out all steps at 4 °C.

**Electron microscopy and cell-cell junction quantitation.** We fixed neonatal mouse gut mesentery, 48-h.p.f. zebrafish embryos and E9.5 mouse embryos overnight, embedded them in Polybed 812 (Polysciences), sectioned them, stained them and examined them with a JEOL 1010 electron microscope fitted with a Hamamatsu digital camera. We imaged all identifiable endocardial cell-cell junctions from six *Heg1*<sup>+/+</sup> and five *Heg1*<sup>-/-</sup> lymphatic vessel cross-sections (66 and 123 junctions, respectively), and we quantitated junction lengths using ImageJ. We similarly imaged and quantitated endothelial cell-cell junctions from three control and four *ccm2* morpholino-injected zebrafish atria cross-sections (88 and 107 junctions, respectively) and four *Ccm2*<sup>+/+</sup> and six *Ccm2*<sup>lacZ/lacZ</sup> mouse dorsal aorta cross-sections (128 and 107 junctions, respectively). We ordered the junctions by length and determined the mean junction length for each tercile. We also calculated the percentage of junctions <1,000 nm, 1,000–2,500 nm and >2,500 nm. Lastly, we calculated the overall mean junction length from the mean junction lengths for each heart or vessel cross-section.

**Statistics.** We calculated *P* values using an unpaired two-tailed Student *t* test or  $\chi^2$  analysis as indicated.

*Note: Supplementary information is available on the Nature Medicine website.*

## ACKNOWLEDGMENTS

We thank C. Bertozzi, C. Chen, A. Granger, J. Lee, D. Li, P. Mericko, A. Schmaier, E. Sebзда, N. Shanbhag and K. Whitehead for valuable insights; M. Pack and J. He for assistance with zebrafish studies; R. Meade for preparation of the electron microscopy samples; and T. Branson for animal husbandry. This work was supported by the Swiss National Science Foundation, a Network of Excellence grant from the European Community (M.A.) and the US National Institutes of Health grants T32 HL07439 (to B.K.), T32 HL07971 (to X.Z.),

HL078784 and AR27214 (to M.G.), HL62454 (to J.K.) and HL075380 and HL095326 (to M.L.K.).

#### AUTHOR CONTRIBUTIONS

B.K. designed and performed all of the studies involving mutant mouse lines, contributed to endothelial cell culture and biochemical studies and wrote the manuscript; X.Z. designed and performed most of the zebrafish and biochemical studies; J.J.L., M.C., Z.Z., S.M.S. and L.G. contributed to the biochemical studies; Y.B. and M.C. contributed to the zebrafish studies; J.J.T. performed the endothelial cell culture studies; M.L. performed the immunohistochemistry studies; D.Z. contributed to the generation of mutant mouse lines; J.K. designed the endothelial cell culture studies and wrote the manuscript; M.A. designed some of the zebrafish studies and wrote the manuscript; M.H.G. designed some of the biochemical studies and wrote the manuscript; M.L.K. contributed to the design of mouse, zebrafish, endothelial and biochemical studies and wrote the manuscript.

Published online at <http://www.nature.com/naturemedicine/>

Reprints and permissions information is available online at <http://npg.nature.com/reprintsandpermissions/>

- Rigamonti, D. *et al.* Cerebral cavernous malformations. Incidence and familial occurrence. *N. Engl. J. Med.* **319**, 343–347 (1988).
- Revenu, N. & Vikkula, M. Cerebral cavernous malformation: new molecular and clinical insights. *J. Med. Genet.* **43**, 716–721 (2006).
- Sahoo, T. *et al.* Mutations in the gene encoding KRIT1, a Krev-1/rap1a binding protein, cause cerebral cavernous malformations (CCM1). *Hum. Mol. Genet.* **8**, 2325–2333 (1999).
- Eerola, I. *et al.* KRIT1 is mutated in hyperkeratotic cutaneous capillary-venous malformation associated with cerebral capillary malformation. *Hum. Mol. Genet.* **9**, 1351–1355 (2000).
- Liquori, C.L. *et al.* Mutations in a gene encoding a novel protein containing a phosphotyrosine-binding domain cause type 2 cerebral cavernous malformations. *Am. J. Hum. Genet.* **73**, 1459–1464 (2003).
- Denier, C. *et al.* Mutations within the MGC4607 gene cause cerebral cavernous malformations. *Am. J. Hum. Genet.* **74**, 326–337 (2004).
- Bergametti, F. *et al.* Mutations within the programmed cell death 10 gene cause cerebral cavernous malformations. *Am. J. Hum. Genet.* **76**, 42–51 (2005).
- Zawistowski, J.S. *et al.* CCM1 and CCM2 protein interactions in cell signaling: implications for cerebral cavernous malformations pathogenesis. *Hum. Mol. Genet.* **14**, 2521–2531 (2005).
- Voss, K. *et al.* CCM3 interacts with CCM2 indicating common pathogenesis for cerebral cavernous malformations. *Neurogenetics* **8**, 249–256 (2007).
- Zhang, J., Rigamonti, D., Dietz, H.C. & Clatterbuck, R.E. Interaction between krit1 and malcavernin: implications for the pathogenesis of cerebral cavernous malformations. *Neurosurgery* **60**, 353–359 (2007).
- Mably, J.D., Mohideen, M.A., Burns, C.G., Chen, J.N. & Fishman, M.C. Heart of glass regulates the concentric growth of the heart in zebrafish. *Curr. Biol.* **13**, 2138–2147 (2003).
- Mably, J.D. *et al.* Santa and valentine pattern concentric growth of cardiac myocardium in the zebrafish. *Development* **133**, 3139–3146 (2006).
- Whitehead, K.J., Plummer, N.W., Adams, J.A., Marchuk, D.A. & Li, D.Y. Ccm1 is required for arterial morphogenesis: implications for the etiology of human cavernous malformations. *Development* **131**, 1437–1448 (2004).
- Plummer, N.W. *et al.* Neuronal expression of the Ccm2 gene in a new mouse model of cerebral cavernous malformations. *Mamm. Genome* **17**, 119–128 (2006).
- Wong, J.H., Awad, I.A. & Kim, J.H. Ultrastructural pathological features of cerebrovascular malformations: a preliminary report. *Neurosurgery* **46**, 1454–1459 (2000).
- Clatterbuck, R.E., Eberhart, C.G., Crain, B.J. & Rigamonti, D. Ultrastructural and immunocytochemical evidence that an incompetent blood-brain barrier is related to the pathophysiology of cavernous malformations. *J. Neurol. Neurosurg. Psychiatry* **71**, 188–192 (2001).
- Tu, J., Stoodley, M.A., Morgan, M.K. & Storer, K.P. Ultrastructural characteristics of hemorrhagic, nonhemorrhagic, and recurrent cavernous malformations. *J. Neurosurg.* **103**, 903–909 (2005).
- Glading, A., Han, J., Stockton, R.A. & Ginsberg, M.H. KRIT1/CCM1 is a Rap1 effector that regulates endothelial cell cell junctions. *J. Cell Biol.* **179**, 247–254 (2007).
- Nakatsu, M.N. *et al.* Angiogenic sprouting and capillary lumen formation modeled by human umbilical vein endothelial cells (HUVEC) in fibrin gels: the role of fibroblasts and Angiopoietin-1. *Microvasc. Res.* **66**, 102–112 (2003).
- Folkman, J. & Haudenschild, C. Angiogenesis *in vitro*. *Nature* **288**, 551–556 (1980).
- Jin, S.W., Beis, D., Mitchell, T., Chen, J.N. & Stainier, D.Y. Cellular and molecular analyses of vascular tube and lumen formation in zebrafish. *Development* **132**, 5199–5209 (2005).
- Kamei, M. *et al.* Endothelial tubes assemble from intracellular vacuoles *in vivo*. *Nature* **442**, 453–456 (2006).
- Blum, Y. *et al.* Complex cell rearrangements during intersegmental vessel sprouting and vessel fusion in the zebrafish embryo. *Dev. Biol.* **316**, 312–322 (2008).
- Hogan, B.M., Bussmann, J., Wolburg, H. & Schulte-Merker, S. Ccm1 cell autonomously regulates endothelial cellular morphogenesis and vascular tubulogenesis in zebrafish. *Hum. Mol. Genet.* **17**, 2424–2432 (2008).
- Sebzda, E. *et al.* Syk and Slp-76 mutant mice reveal a cell-autonomous hematopoietic cell contribution to vascular development. *Dev. Cell* **11**, 349–361 (2006).
- Lawson, N.D. & Weinstein, B.M. *In vivo* imaging of embryonic vascular development using transgenic zebrafish. *Dev. Biol.* **248**, 307–318 (2002).
- Jin, S.W. *et al.* A transgene-assisted genetic screen identifies essential regulators of vascular development in vertebrate embryos. *Dev. Biol.* **307**, 29–42 (2007).
- Amsterdam, A. & Hopkins, N. Retroviral-mediated insertional mutagenesis in zebrafish. *Methods Cell Biol.* **77**, 3–20 (2004).
- Weinstein, B.M., Stemple, D.L., Driever, W. & Fishman, M.C. Gridlock, a localized heritable vascular patterning defect in the zebrafish. *Nat. Med.* **1**, 1143–1147 (1995).
- Lim, C.J. *et al.* Alpha4 integrins are type I cAMP-dependent protein kinase-anchoring proteins. *Nat. Cell Biol.* **9**, 415–421 (2007).
- Pfaff, M., Liu, S., Erle, D.J. & Ginsberg, M.H. Integrin beta cytoplasmic domains differentially bind to cytoskeletal proteins. *J. Biol. Chem.* **273**, 6104–6109 (1998).

---

**Erratum:** Regulation of cardiovascular development and integrity by the heart of glass–cerebral cavernous malformation protein pathway

Benjamin Kleaveland, Xiangjian Zheng, Jian J Liu, Yannick Blum, Jennifer J Tung, Zhiying Zou, Mei Chen, Lili Guo, Min-min Lu, Diane Zhou, Jan Kitajewski, Markus Affolter, Mark H Ginsberg & Mark L Kahn

*Nat. Med.* 15, 169–176 (2009); published online 18 January; corrected online 27 January 2009

In the version of the supplementary information for this article originally posted online, the descriptions of Supplementary Videos 1–6 were incorrect. The errors have been corrected as of 27 January 2009.

## CORRIGENDA

---

### Corrigendum: Regulation of cardiovascular development and integrity by the heart of glass—cerebral cavernous malformation protein pathway

Benjamin Kleaveland, Xiangjian Zheng, Jian J Liu, Yannick Blum, Jennifer J Tung, Zhiying Zou, Shawn M Sweeney, Mei Chen, Lili Guo, Minmin Lu, Diane Zhou, Jan Kitajewski, Markus Affolter, Mark H Ginsberg & Mark L Kahn

*Nat. Med.* 15, 169–176 (2009); published online 18 January 2009; corrected after print 12 February 2009

In the version of this article initially published, Shawn M. Sweeney was not included in the list of authors. The error has been corrected in the HTML and PDF versions of the article.

---

### Corrigendum: A pivotal role for galectin-1 in fetomaternal tolerance

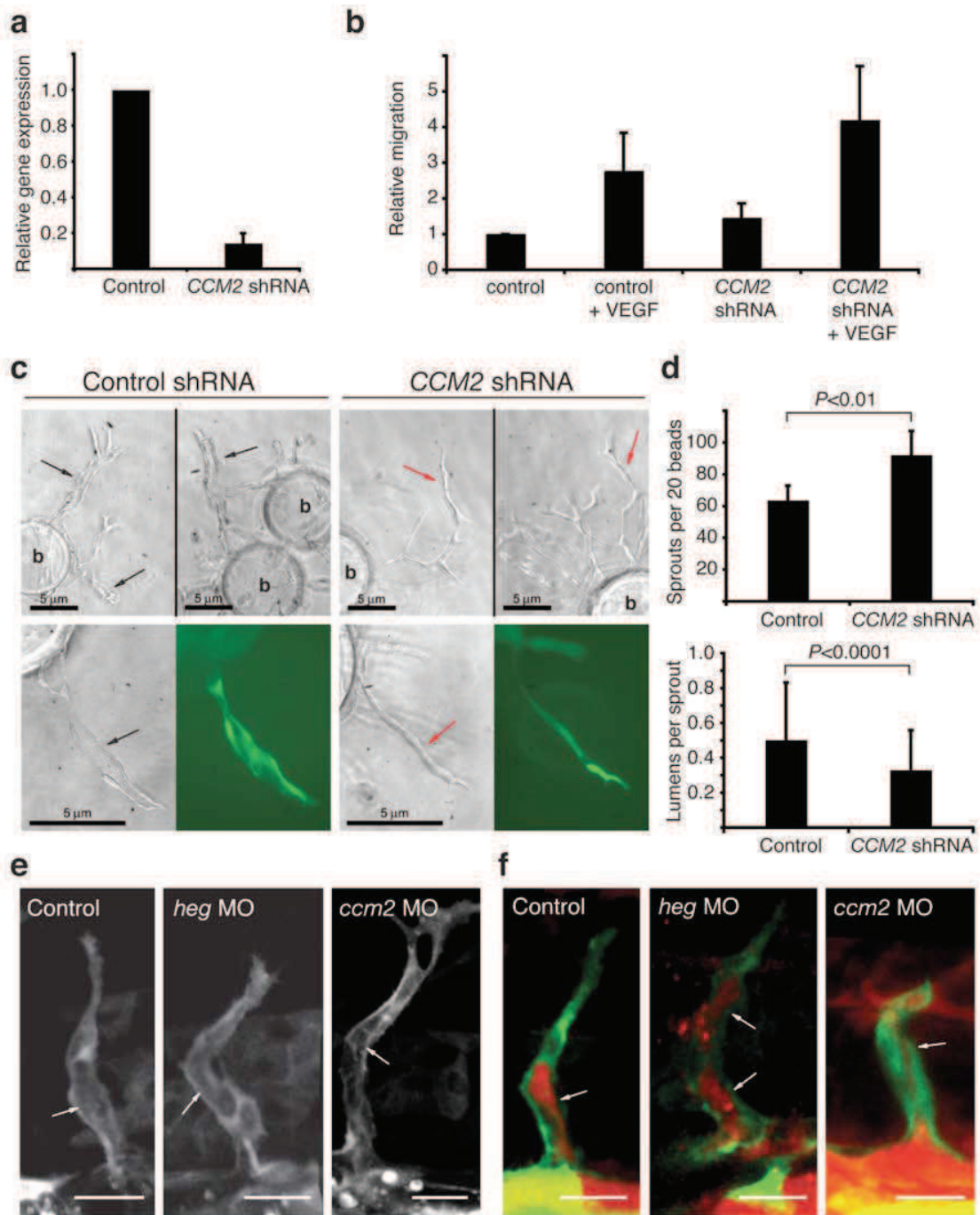
Sandra M Blois, Juan M Ilarregui, Mareike Tometten, Mariana Garcia, Arif S Orsal, Rosalia Cordo-Russo, Marta A Toscano, Germán A Bianco, Peter Kobelt, Bori Handjiski, Irene Tirado, Udo R Markert, Burghard F Klapp, Françoise Poirier, Julia Szekeres-Bartho, Gabriel A Rabinovich & Petra C Arck

*Nat. Med.* 13, 1450–1457 (2007); published online 18 November 2007; corrected after print 7 May 2009

In the version of this article initially published, the plot labeled “Stress + Gal-1” duplicated the plot labeled “Control” for the IL-12p70 staining in **Figure 2f**. The corrected plots have now been provided in the HTML and PDF versions of the article. Two sentences were omitted from the section on purification of uterine DCs in the Methods. The sentences should have read: “We obtained purified DCs from uterine tissue in very low numbers. Thus, we pooled isolated cells from each group and used this cell cocktail for the isotype control staining.” The error has been corrected in the HTML and PDF versions of the article. In **Figure 4f**, the lanes of the western blot were merged inappropriately. The properly presented blot, in which the gel lanes have been separated to indicate that the samples were not originally run side by side, has been provided in the PDF and HTML versions of the article. The standard curve of the cytometric bead array kit used to generate the cytokine data can be found in the revised Supplementary information available online.

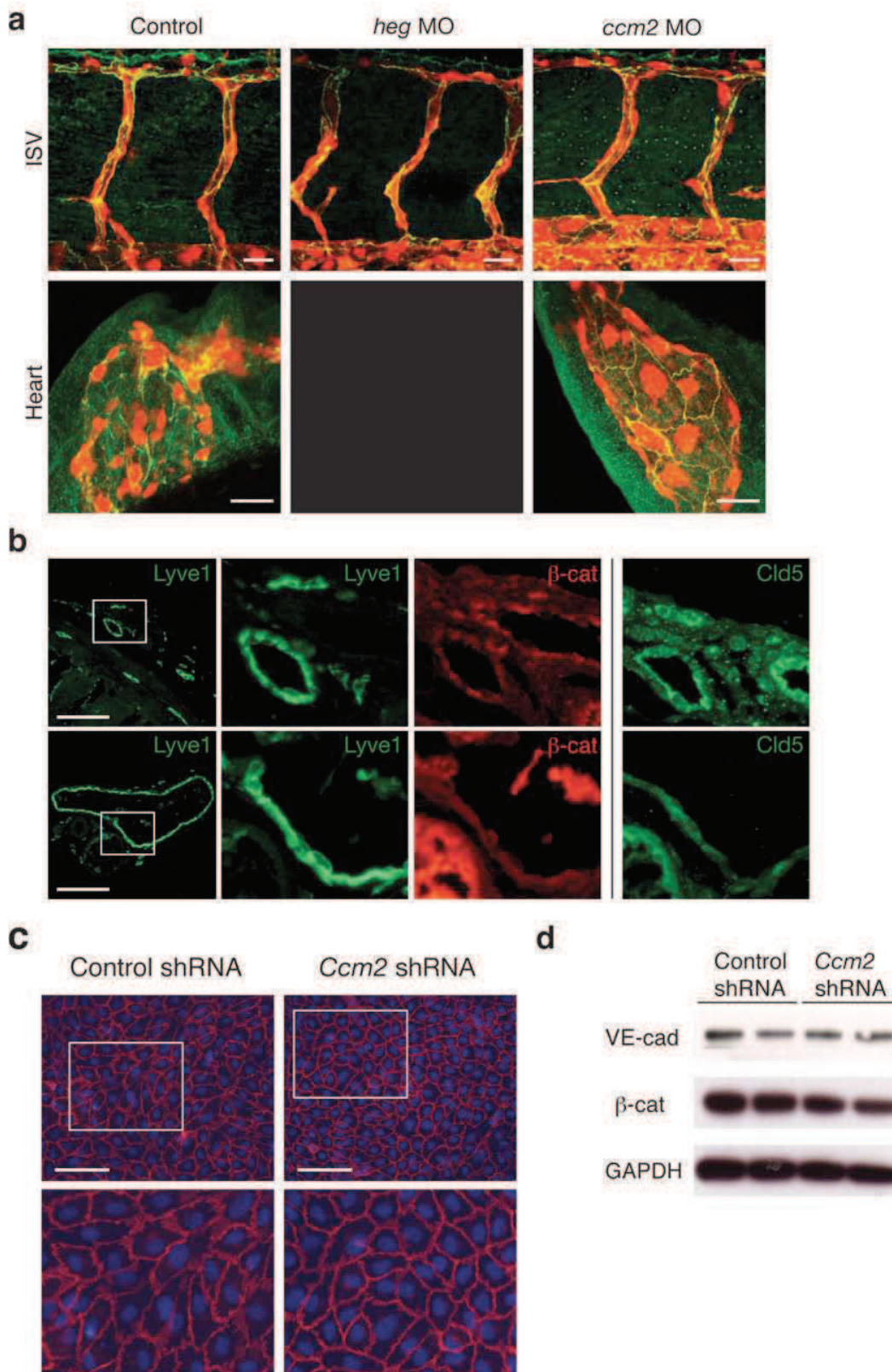


Supplemental Figure 7.



**Supplemental Figure 7. Endothelial cells lacking HEG1-CCM signaling exhibit defects in tube formation but not endothelial vacuolization.** (a–d) CCM2-deficient endothelial cells exhibit a cell autonomous defect in lumen formation. (a) *CCM2* mRNA levels were reduced by >85% in HUVEC expressing *CCM2*-specific but not scrambled (control) shRNA. (b) CCM2-deficient HUVEC migrate normally in response to VEGF in a modified Boyden chamber assay. No significant differences were observed ( $P$  values  $\geq 0.1$ ). (c) Control shRNA expressing endothelial cells formed tubes with visible lumens (black arrows), while CCM2-deficient endothelial cells formed cords that often lacked detectable lumens (red arrows). GFP is co-expressed with lentiviral shRNAs. (d) CCM2-deficient endothelial cells form more sprouts but fewer lumens. The number of sprouts per 20 beads and number of visible lumens per sprout for HUVEC stably expressing *CCM2* shRNA or control shRNA are shown.  $N = 100$  beads for each group; data shown are representative of four independent experiments. (e) Endothelial vacuole formation is preserved in zebrafish embryos lacking *heg* or *ccm2*. Shown are the intersegmental vessels of 24–26 hpf *fli1a:EGFP-cdc42* transgenic zebrafish embryos treated with scrambled morpholino (control) or morpholinos to block expression of *heg* or *ccm2*. The GFP-cdc42 fusion protein outlines the endothelial cell vacuoles that form and fuse during lumen formation (white arrows). (f) The intersegmental vessels of zebrafish embryos lacking *heg* or *ccm2* are patent. Red fluorescent quantum dots injected into the dorsal aorta of 24–26 hpf *fli1a:EGFP-cdc42* morphant embryos reveals patent intersegmental vessels lacking *heg* or *ccm2*. Note the presence of red quantum dots within the green endothelial lumens (white arrows) of all embryos. b, bead. Scale bars in c, 5  $\mu\text{m}$ ; in e and f, 20  $\mu\text{m}$ .

**Supplemental Figure 9.**



**Supplemental Figure 9. HEG1 or CCM2 deficiency does not reduce expression of endothelial junctional proteins.** (a) Immunostaining for VE-cadherin (green) in 48 hpf *kdr:EGFP* (red) transgenic zebrafish embryos treated with control morpholinos or morpholinos directed against *heg* or *ccm2* is shown. (b) Immunostaining for the lymphatic endothelial marker LYVE1 and junctional proteins beta-catenin and claudin-5 in serial sections of dilated lymphatic vessels from a neonatal HEG1-deficient mouse is shown. (c) Immunostaining for beta-catenin in CCM2-deficient and control HUVEC monolayers. (d) Immunoblotting for VE-cadherin, beta-catenin and GAPDH was performed using cell lysate from control and CCM2-deficient HUVEC. Scale bars in **a**, 20  $\mu$ m; in **b** and **c**, 100  $\mu$ m.

# blood

2010 115: 133-139  
Prepublished online October 30, 2009;  
doi:10.1182/blood-2009-09-242180

## A noncoding antisense RNA in *tie-1* locus regulates *tie-1* function in vivo

Keguo Li, Yannick Blum, Anjali Verma, Zhong Liu, Kallal Pramanik, Noah R. Leigh, Chang Z. Chun, Ganesh V. Samant, Baofeng Zhao, Maija K. Garnaas, Mark A. Horswill, Stephen A. Stanhope, Paula E. North, Robert Q. Miao, George A. Wilkinson, Markus Affolter and Ramani Ramchandran

---

Updated information and services can be found at:  
<http://bloodjournal.hematologylibrary.org/content/115/1/133.full.html>

Articles on similar topics can be found in the following Blood collections  
[Vascular Biology](#) (332 articles)

---

Information about reproducing this article in parts or in its entirety may be found online at:  
[http://bloodjournal.hematologylibrary.org/site/misc/rights.xhtml#repub\\_requests](http://bloodjournal.hematologylibrary.org/site/misc/rights.xhtml#repub_requests)

Information about ordering reprints may be found online at:  
<http://bloodjournal.hematologylibrary.org/site/misc/rights.xhtml#reprints>

Information about subscriptions and ASH membership may be found online at:  
<http://bloodjournal.hematologylibrary.org/site/subscriptions/index.xhtml>





## A noncoding antisense RNA in *tie-1* locus regulates *tie-1* function in vivo

Keguo Li,<sup>1</sup> Yannick Blum,<sup>2</sup> Anjali Verma,<sup>1</sup> Zhong Liu,<sup>3</sup> Kallal Pramanik,<sup>1</sup> Noah R. Leigh,<sup>1</sup> Chang Z. Chun,<sup>1</sup> Ganesh V. Samant,<sup>1</sup> Baofeng Zhao,<sup>3</sup> Maija K. Garnaas,<sup>1</sup> Mark A. Horswill,<sup>1</sup> Stephen A. Stanhope,<sup>4</sup> Paula E. North,<sup>5</sup> Robert Q. Miao,<sup>3,5</sup> George A. Wilkinson,<sup>1</sup> Markus Affolter,<sup>2</sup> and Ramani Ramchandran<sup>1</sup>

<sup>1</sup>Department of Pediatrics, Medical College of Wisconsin, Developmental Vascular Biology Program, Children's Research Institute, Milwaukee; <sup>2</sup>Biozentrum der Universität Basel, Basel, Switzerland; <sup>3</sup>Pediatric Surgery, Translational and Biomedical Research Center, Children's Research Institute, Milwaukee, WI; <sup>4</sup>University of Chicago, Biological Sciences Division, IL; and <sup>5</sup>Pediatric Pathology, Children's Research Institute, Milwaukee, WI

Recently, messenger RNAs in eukaryotes have shown to associate with antisense (AS) transcript partners that are often referred to as long noncoding RNAs (lncRNAs) whose function is largely unknown. Here, we have identified a natural AS transcript for tyrosine kinase containing immunoglobulin and epidermal growth factor homology domain-1 (*tie-1*), *tie-1AS* lncRNA in

zebrafish, mouse, and humans. In embryonic zebrafish, *tie-1AS* lncRNA transcript is expressed temporally and spatially in vivo with its native target, the *tie-1* coding transcript and in additional locations (ear and brain). The *tie-1AS* lncRNA selectively binds *tie-1* mRNA in vivo and regulates *tie-1* transcript levels, resulting in specific defects in endothelial cell con-

tact junctions in vivo and in vitro. The ratio of *tie-1* versus *tie-1AS* lncRNA is altered in human vascular anomaly samples. These results directly implicate noncoding RNA-mediated transcriptional regulation of gene expression as a fundamental control mechanism for physiologic processes, such as vascular development. (Blood. 2010;115:133-139)

### Introduction

Over the past few years, intensive unbiased analysis of transcriptome species has revealed that eukaryotic genomes contain a variety of RNA species. RNA molecules are essentially classified into 2 types, protein coding and nonprotein coding. The protein-coding transcripts or messenger RNA (mRNA) account for only approximately 2.3% of the human genome.<sup>1</sup> The majority of transcription appears to be nonprotein coding or noncoding, and the function of these noncoding transcripts is largely unknown.<sup>2</sup> Of the noncoding RNAs, the regulatory short noncoding RNAs, such as microRNAs, are well studied. The long noncoding RNAs (lncRNAs), which compose the largest portion of the mammalian noncoding transcriptome, are the least understood, especially its function.<sup>3,4</sup> lncRNAs are oriented in sense or antisense (AS) direction with respect to a protein coding locus, and located in intronic or intergenic regions.<sup>5</sup> In humans and mice, 61% to 72% of all transcribed regions possess lncRNAs in AS orientation,<sup>2,6</sup> and AS lncRNA transcripts play important roles in pathogenesis. For instance, the *BACE1-AS* transcript was elevated in subjects with Alzheimer disease and in amyloid precursor protein transgenic mice.<sup>7</sup> A growing body of evidence suggests that lncRNAs for most critical physiologic processes will be identified. Angiogenesis, the development of new vasculature from existing vasculature, is one of the fundamental developmental physiologic processes regulated in a developing vertebrate embryo.<sup>8</sup> Here, we identify a natural AS transcript for tyrosine kinase containing immunoglobulin and epidermal growth factor homology domain-1 (*tie-1*), *tie-1AS* lncRNA in zebrafish, mouse, and humans. *tie-1* is a cell-surface tyrosine kinase receptor for angiopoietin ligands that is known to play a role in vascular development in vertebrates.<sup>9-12</sup> In embryonic zebrafish, *tie-1AS* lncRNA transcript is expressed temporally and spatially in vivo with its native target, the *tie-1* coding transcript, and in additional locations (ear and brain). Its expression is controlled by a 3-kb genomic

fragment in the 3' region of *tie-1*, and the bioinformatic predicted hybrid structure between *tie-1:tie-1AS* was detected in vivo. Capped or uncapped *tie-1AS* lncRNA selectively binds *tie-1* mRNA in vivo and regulates *tie-1* transcript levels, resulting in specific defects in endothelial cell contact junctions in vivo and in vitro. Further, the ratio of *tie-1* versus *tie-1AS* lncRNA is altered in human vascular anomaly samples, suggesting that the imbalance of *tie-1* regulation by *tie-1AS* may be important in disease. This is the first report, to our knowledge, that identifies a long AS noncoding RNA in the *tie-1* locus that regulates proper vessel formation in vivo.

### Methods

#### Zebrafish and human studies

All zebrafish studies were performed according to Medical College of Wisconsin animal protocol guidelines under protocol no. 312-06-2. Research on human patient samples for this work was performed under the Medical College of Wisconsin–approved Institutional Review Board protocols. RNA from tissue sample was isolated by Trizol method.

#### Reagents

The transgenic Tg(*flk:EGFP*) line<sup>13</sup> was obtained from M.A.'s laboratory in Basel, Switzerland. Probes used in this study, *tie-1* and *tie-1AS* lncRNA, were generated by T3/T7 transcription on polymerase chain reaction (PCR) products of *tie-1AS*. T3 and T7 sequences were included into the PCR primers. Quantitative PCR for *tie-1* was performed as described previously<sup>14</sup> using gene-specific primer pairs for *tie-1*, *cd-31*, and zebrafish *actin*. All primer sequences are provided in supplemental Table 1 (available on the *Blood* website; see the Supplemental Materials link at the top of the online article).

Submitted September 4, 2009; accepted October 6, 2009. Prepublished online as *Blood* First Edition paper, October 30, 2009; DOI 10.1182/blood-2009-09-242180.

The online version of this article contains a data supplement.

The publication costs of this article were defrayed in part by page charge payment. Therefore, and solely to indicate this fact, this article is hereby marked "advertisement" in accordance with 18 USC section 1734.

© 2010 by The American Society of Hematology

### Molecular biology: cloning of *tie-1AS* lncRNA

Rapid amplification of cDNA ends (RACEs) was performed by the RLM-RACE Kit (Ambion) and SMART RACE cDNA Amplification Kit (Clontech). An embryo pool spanning 1 hour postfertilization (hpf) to 3 days old was used to prepare total RNA. The RNA was treated with DNase I for 30 minutes and recovered by RNeasy kit (QIAGEN). The RACE products were cloned into pCR4-TOPO vector (Invitrogen) and sequenced. RACE primers are listed in supplemental Table 1. The sequences have been deposited in GenBank ID number GU166385.

### MO and microinjections

Morpholino (MO) injections were performed as described previously.<sup>15</sup> Gene Tools Inc designed the *tie-1* splice MO: CATGTCTACTACAGATC-CAGATTG. For *tie-1* MO efficacy experiments, reverse-transcribed (RT)-PCR was performed using gene-specific primers in exons immediately flanking the targeted region on 24 hpf RNA isolated from uninjected and *tie-1* MO-injected (5 and 10 ng) embryos. The mMESSAGE MACHINE kit (Ambion) was used for generating sense RNA for *tie-1AS* lncRNA. For quantitative PCR, RNA was extracted via the Trizol method and quantitative PCR was carried out using DyNAmo HS SYBR Green qPCR Kit (New England Biolabs). For RNA Pol inhibitor studies, 8 hpf zebrafish embryos were injected with  $\alpha$ -amanitin and allowed to develop until 24 hpf. For tagetin, injections were performed at 1-cell stage. For *tie-1AS* lncRNA promoter cloning, the region 152648 to 149799 corresponding to clone CH211-286N19 in linkage group 7 (accession no. CR936976.15) was amplified using forward primer, TAAGGTACCGCGGGGACATCTAAAGACAC; and reverse primer, ATTGGATCCCTTGGTGGCCAGAAAAC. The 3-kb PCR product was purified, digested with *KpnI-Bam*HI, and cloned into the *KpnI-Bg*III site of pGL3-Basic (Promega) vector and is referred to as pGL3-zfNcrRNA-3kb construct. For microinjection, pGL3-hRobo4-3kb promoter construct<sup>16</sup> and pGL3 vector were linearized with *Sal*I, and pGL3-zfNcrRNA-3kb promoter construct was linearized with *Bam*HI; 100 pg of linearized DNA was injected into the cytoplasm of 1-cell stage zebrafish embryo, embryos were lysed at 26 hpf, and firefly luciferase activity was measured as per the instruction manual.

### Endothelial cell culture and electroporation

Human umbilical vascular endothelial cells (HUVECs; passage 3-6) were cultured in M199 medium with 20% fetal bovine serum (HyClone) and endothelial cell growth supplement (BD Biosciences). Plasmid DNA transfection was performed using the MicroPorator from NanoEnTek. Briefly, 1  $\mu$ g of plasmid DNA was mixed with  $10^5$  cells in 10  $\mu$ L of resuspension buffer, and electroporation was performed at 1000 V and 30 ms. After electroporation, cells were seeded in regular HUVEC growth medium with transfection efficiency reaching 80%. The expression of Tie-1, Hsp90, and actin was examined by Western blot analysis at 72 hours after electroporation. The 3-dimensional tube formation assay was performed at 48 hours, and tube formation was observed at 72 hours after electroporation.

## Results

### Identification of *tie-1AS* in multiple species

Using the zebrafish information network database<sup>17,18</sup> of in situ expression profile across embryonic developmental stages, we identified several novel expressed sequence tags (ESTs) that showed a vascular-specific expression profile. We focused on one EST (accession no. DU644726) that mapped to 73 bp downstream of the *tie-1* coding locus. Because the 3'-untranslated region (UTR) of the zebrafish *tie-1* gene was incomplete, we verified whether this EST represented the 3'-UTR of the *tie-1* coding transcript or represented a new transcript. A set of primers derived from the EST was used to perform rapid amplification of cDNA

ends (RACE) reaction (supplemental Figure 1A arrows). Interestingly, both the 5' and 3' RACE reactions in both directions generated end-extended products. The 3' RACE reaction provided a product that extends the 3'UTR of the *tie-1* gene to the polyA tail, whereas the 5' RACE reaction generated a product in the opposite direction of *tie-1* coding transcript, thus providing evidence for a novel transcript arising from the *tie-1* genomic locus in the AS direction. The noncoding and novel transcripts associated with *tie-1* have 456 bp of overlapped sequence with opposite transcriptional orientation. The 5'RACE transcript called "*tie-1AS*" was detected in the presence of RT from RNA isolated from an embryo pool of multiple stages (1-72 hpf; supplemental Figure 1B, +RT lane) and is 804 bp long. Sequencing of the *tie-1AS* revealed a 148-bp unique 5' sequence, followed by a 456-bp region that is complementary to *tie-1s*' last exon, and a 200-bp 3' region complementary to *tie-1s*' last intron-exon junction (supplemental Figure 1C). The single largest open reading frame predicted within this AS transcript, is 93 amino acids (data not shown). We performed additional RACE reactions and cDNA walking in the opposite orientation to multiple exons within the *tie-1* locus and found that indeed multiple AS transcripts or long noncoding RNA are generated from the *tie-1* locus (supplemental Figure 1D blue boxes). These data indicate that the *tie-1AS* represented by EST DU644726 is one of several noncoding RNAs transcribed from the *tie-1* locus. We only focused on the extreme 3'-UTR *tie-1AS* for further studies and from hereon will be referring to it as *tie-1AS* lncRNA. Both mouse (supplemental Figure 1E) and human (supplemental Figure 1F blue boxes) RNA indeed have similar *tie-1AS* lncRNA as zebrafish and the nucleotide conservation across the 3 species is 28.5%. These results suggest that the *tie-1* locus has evolutionarily conserved noncoding RNAs that may regulate *tie-1* transcripts by similar mechanisms.

### Expression profile of *tie-1AS* lncRNA and *tie-1*

To investigate developmental expression pattern of *tie-1AS* lncRNA and *tie-1*, we performed quantitative real-time PCR for both transcripts using sequence-specific primers (Figure 1A arrows) that will amplify each transcript independently across multiple stages in embryonic zebrafish development. Starting at 1 hpf and until 10 hpf, the levels of both transcripts are low. After gastrulation, both transcripts show remarkable concordance at every stage until 72 hpf (compare Figure 1B *tie-1* and Figure 1C *tie-1AS* lncRNA). The levels of *tie-1* transcript are a log higher at each stage (compare ordinate axis in Figure 1B-C) compared with *tie-1AS* lncRNA, suggesting that the low amount of *tie-1AS* lncRNA might be sufficient to regulate endogenous *tie-1* coding transcript levels.

Quantitative PCR analysis shows that the transcript levels of *tie-1AS* lncRNA and *tie-1* are remarkably congruent in development but do not indicate the spatial location of the *tie-1AS* lncRNA transcript in relation to the *tie-1* gene. To determine the expression pattern of *tie-1AS* lncRNA transcript, we performed in situ hybridization (ISH) for *tie-1AS* lncRNA using a digoxigenin-labeled *tie-1AS* lncRNA (or sense of *tie-1*) at 24 hpf and compared with *tie-1* expression pattern previously demonstrated at the same stage.<sup>19</sup> *Tie-1* is expressed in the axial vessels as indicated by arrows in Figure 1D and in intermediate cell mass (Figure 1D \*). Previous reports indicate *tie-1* expression in intersomitic vessels (ISVs),<sup>19</sup> which we have noticed in longer dark-stained embryos. *Tie-1AS* lncRNA is also expressed in the axial vessels, albeit weakly (Figure 1E arrow), but shows strong expression in the intermediate cell mass (Figure 1E \*), otic vesicles (Figure 1E #), and brain (Figure 1E brace). We have been unable to detect strong

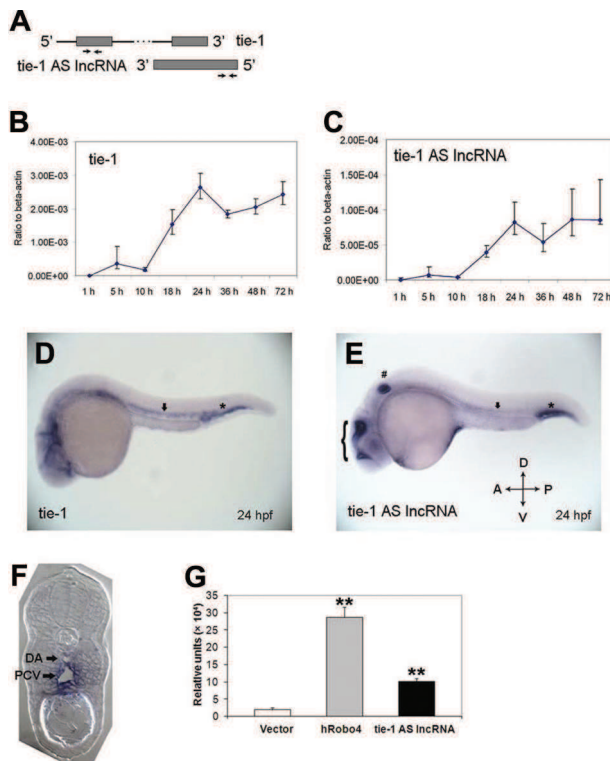


**Figure 1. Expression patterns of *tie-1AS* lncRNA.** (A) The primer pair locations for quantitative PCR. Developmental expression profile of *tie-1* (B) and *tie-1AS* (C) is shown. The total RNAs were extracted using Trizol followed by DNase I treatment. The RNAs were recovered by RNeasy kit (QIAGEN). (D) *Tie-1* is expressed in the axial vessels (↔) and blood islands (\*). (E) *Tie-1AS* lncRNA is expressed in the axial vessels (↔), intermediate cell mass (\*), otic vesicles (#), and brain (brace). (F) Transverse section of 24 hpf *tie-1AS* lncRNA embryo is shown. ♦ indicates the location of DA and PCV. (G) Luciferase activity in vivo (26 hpf) for a 3-kb fragment upstream of zebrafish *tie-1AS* lncRNA. The hRobo4 promoter is used as a positive control. \*\* $P < .01$ .

*tie-1AS* lncRNA expression in ISVs, but it is worth mentioning that the axial vessel ISH results are in agreement with quantitative PCR results that showed lower amounts of *tie-1AS* lncRNA expression compared with *tie-1* expression at any given stage, especially at 24 hpf. We have also performed ISH for *tie-1AS* lncRNA at other stages but did not notice any dramatic differences in spatial localization than at 24 hpf shown in Figure 1F. To fine-map the expression regions of *tie-1AS* lncRNA, we sectioned 24 hpf (Figure 1E) whole-mount stained embryos and mounted them as shown in Figure 1F. *Tie-1AS* lncRNA is expressed in both dorsal aorta (DA) and posterior cardinal vein (PCV) and at the junction of both structures (Figure 1F black arrows). The quantitative PCR and the ISH results together show that *tie-1AS* lncRNA and *tie-1* transcripts are found at the same location and time in embryonic development, arguing for a regulatory role of the *tie-1AS* lncRNA on the *tie-1* gene.

To investigate control of *tie-1AS* lncRNA transcription, we cloned a 3-kb genomic fragment downstream of *AS* to the *tie-1* coding locus into a pGL-3 basic vector that contains luciferase reporter gene. This vector is specifically designed to determine promoter activity of DNA fragments. We also obtained a human Roundabout4 (*Robo4*) promoter fragment cloned in the same vector that was shown previously to be active in endothelial cells as a positive control.<sup>16</sup> We injected wild-type zebrafish embryos with the empty pGL-3 vector, p*Robo4* promoter-luc, and *ptie-1AS* lncRNA promoter-luc at 1-cell stage. Injected embryos were assayed at 26 hpf when expression of *Robo4*<sup>15</sup> and *tie-1AS* lncRNA (Figure

1C) is high in the vasculature. Lysates from 26 hpf embryos were checked for luciferase activity. Compared with vector alone, the *ptie-1AS* lncRNA promoter-luc construct showed a 5-fold increase (Figure 1G black bar), whereas the p*Robo4* promoter-luc construct showed a 14-fold increase in luciferase activity (Figure 1G gray bar). This result suggests that a 3-kb DNA fragment downstream of *tie-1* gene is sufficient to drive transcription of *tie-1AS* lncRNA in vivo.

#### Hybrid *tie-1AS* lncRNA:*tie-1* RNA in vivo

We made use of the utilities RNAfold and RNAcifold from the Vienna RNA package<sup>20,21</sup> to determine whether hybridization between *tie-1AS* lncRNA and *tie-1* RNA was likely to occur. In our initial analysis, we set the temperature parameter to 28°C (representative of in vivo temperatures for zebrafish) and examined predicted RNA secondary structures and fold energies for *tie-1AS* lncRNA and *tie-1* RNA singularly as well as in a duplex. Predicted secondary structures for the *tie-1* RNA alone and in duplex with *tie-1AS* lncRNA are depicted in supplemental Figure 2A (the secondary structure for the *tie-1AS* lncRNA is omitted). The hybridization energies for *tie-1*, *tie-1AS* lncRNA, and their duplex are  $-1418.83$ ,  $-284.66$ , and  $-1885.96$ , respectively, implying that the *tie-1* and *tie-1AS* lncRNA are anticipated to duplex under in vivo conditions.

To determine the specificity of this prediction, 2 additional studies were performed. The first examined whether *tie-1AS* lncRNA could be anticipated to have specific correspondence to *tie-1* RNA, as opposed to other potential targets. We computed the ratio of the energy of the *tie-1AS* lncRNA/*tie-1* mRNA structure and the sum of the individual energies of the *tie-1AS* lncRNA and *tie-1* mRNA (1.107), and compared it with the analogous ratios for the *tie-1AS* lncRNA and each mRNA identified in the NCBI zebrafish reference sequence.<sup>22</sup> The distribution of energy ratios is depicted in supplemental Figure 2B with a marker representing that of *tie-1AS* lncRNA and *tie-1* mRNA. The ratio of *tie-1AS* lncRNA and *tie-1* mRNA duplex to singular energies is greater than 99.97% of that of all other zebrafish mRNAs, implying that, compared with other zebrafish mRNAs, *tie-1* mRNA represents a strong target for *tie-1AS* lncRNA.

Next, we studied whether the coding *tie-1* mRNA could be anticipated to have other targeting interfering RNA with similar characteristics in terms of transcript length and base composition as *tie-1AS* lncRNA by computing a distribution of duplex energies between *tie-1* mRNA and permuted *tie-1AS* lncRNA sequences, and then comparing the actual energy of the *tie-1AS* lncRNA and *tie-1* mRNA with those observed (supplemental Figure 2C). The energy of the *tie-1AS* lncRNA and *tie-1* mRNA duplex is substantially lower than that of any of the permuted *tie-1AS* lncRNAs, implying that, compared with other similar RNA molecules, *tie-1AS* lncRNA can be anticipated to particularly target *tie-1* mRNA.

To confirm the bioinformatic prediction, we performed ribonuclease protection assay and RT-PCR to determine whether the *tie-1AS* lncRNA exists in vivo as a RNA-RNA duplex with *tie-1* RNA (Figure 2A). RNA was isolated from 24 hpf wild-type zebrafish embryos, and the cytoplasmic (Figure 2A top panel) or nuclear (Figure 2A bottom panel) RNA fractions were isolated as described in supplemental Methods. Total RNA preparations were then digested with RNase A, which digests single-stranded RNA and not duplex RNA, plus DNase I (Figure 2A lanes 1-3) and DNase I alone (Figure 2A lanes 4-6). Using RT-PCR and primers specific to the overlapping region of *tie-1* RNA (Figure 2A P1-P2), we detected a protected RNA fragment in both cytoplasmic and nuclear fractions of RNA, indicating that *tie-1*:*tie-1AS* lncRNA RNA-RNA duplex



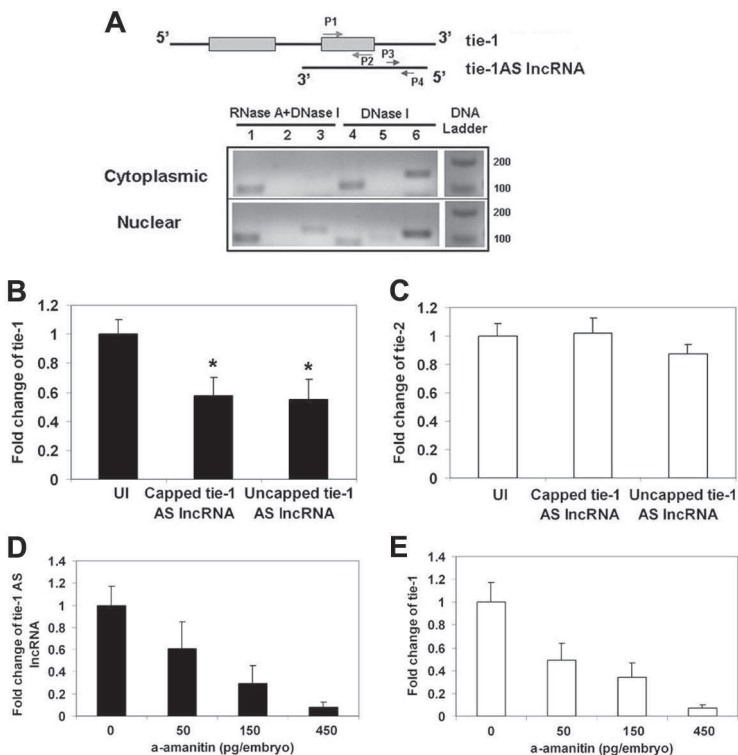


**Figure 2. Functional investigation of the *tie-1AS* lncRNA.** (A) The RNA duplex was examined by ribonuclease protection assay. The zebrafish embryos at 24 hpf were digested with 0.25% trypsin into single cells, from which cytoplasmic and nuclear RNA was extracted. The RNAs were treated with DNase I and RNase A followed by RT-PCR. Primers used are as follows: lanes 1 and 4, P1 and P2, amplicon size 114 bp; lanes 2 and 5, P3 and P4, amplicon size 133 bp; and lanes 3 and 6,  $\beta$ -actin, amplicon size 147 bp. (B) Overexpression of *tie-1AS* lncRNA down-regulates the expression of *tie-1*. \* $P < .05$ . (C) No effect on the expression of *tie-2*. The zebrafish embryos were injected at the 1-cell stage with 150 pg of *tie-1AS* mRNA, and quantitative PCR was performed at 24 hpf. (D) Chemical treatment of zebrafish embryos with  $\alpha$ -amanitin shows dose-dependent sensitivity to *tie-1AS* lncRNA and *tie-1* (E) transcription.

exists in vivo (Figure 2A lane 1). We did not observe a detectable signal (Figure 2A lane 2) using a second primer pair (Figure 2A P3-P4), specific to the nonoverlapping single-stranded region of *tie-1AS* lncRNA, although this sequence was amplified in nuclear DNase-treated extracts (Figure 2A lane 5 bottom panel), suggesting that indeed the lack of band in lane 2 and the presence of band in lane 1 is arising from a duplex species of *tie-1* RNA and *tie-1AS* lncRNA. We have sequenced the amplicon in lane 1 and lane 4 and confirmed its identity as *tie-1*. To confirm complete digestion by RNase A, we checked  $\beta$ -actin mRNA, which was protected in nuclear fraction (Figure 2A lane 3 bottom gel) but not in cytoplasmic (Figure 2A lane 3 top gel), fraction. Assuming partial cleavage of RNA in nuclear fraction based on  $\beta$ -actin result and the complete lack of protected band for *tie-1:tie-1AS* lncRNA in nuclear fraction, an argument could be made that the protected *tie-1:tie-1AS* lncRNA hybrid species exists exclusively in the cytoplasmic fraction of embryo lysates. This result is consistent with regulation of endogenous *tie-1* sense transcript by *tie-1AS* lncRNA at the posttranscriptional level.

#### Regulation of *tie-1* by *tie-1AS* lncRNA

To investigate whether *tie-1:tie-1AS* lncRNA hybrid has a functional role in regulating *tie-1* transcript levels in vivo, we injected the sense RNA of *tie-1AS* lncRNA in 1-cell zebrafish embryos and allowed embryos to develop to 24 hpf, at which point we harvested the RNA and performed quantitative PCR for *tie-1* (Figure 2B) and *tie-2* transcript levels (Figure 2C). We injected capped or uncapped sense RNA (100 pg) for *tie-1AS* lncRNA to determine whether *tie-1* levels were modulated in these embryos. Interestingly, injection of either capped and uncapped *tie-1AS* lncRNA sense RNA reduced *tie-1* expression at 24 hpf (Figure 2B, \* $P < .05$ ) without affecting *tie-2* transcript levels (Figure 2C), indicating that the hybridization of the *tie-1AS* lncRNA to *tie-1* RNA in vivo results in down-regulation of the endogenous *tie-1* transcript. Further, this effect is independent of the RNA capping process because both capped and

uncapped sense RNA showed the same effect arguing for RNA based hybridization mediated mechanistic regulation of *tie-1* transcript levels.

To investigate the RNA polymerase responsible for transcribing *tie-1AS* lncRNA in zebrafish, we performed the classic Pol II inhibitor ( $\alpha$ -amanitin) treatment of zebrafish embryos and checked for transcript levels of *tie-1* (Figure 2E) and *tie-1AS* lncRNA (Figure 2D) at 24 hpf. We observed a dose-dependent decrease in both *tie-1* and *tie-1AS* lncRNA transcripts in  $\alpha$ -amanitin-treated embryos starting at 50 pg, with robust inhibition observed at 450 pg. We also performed Pol III inhibitor (tagetin) treatment and did not observe any change in *tie-1* or *tie-1AS* lncRNA transcript levels. These results indicate that RNA polymerase II is responsible for transcribing *tie-1AS* lncRNA in zebrafish embryo, which is in concordance with a recent report that suggests that the majority of noncoding RNA are transcribed by Pol II.<sup>23</sup>

#### Endothelial junction defects in *tie-1AS* GOF

If *tie-1* gene levels were reduced in embryos injected with *tie-1AS* lncRNA-injected embryos, we would expect to observe phenotype in injected embryos similar to conventional loss-of-function experiments. As a positive control for *tie-1* knockdown, we chose the MO-mediated knockdown, which is routinely used in zebrafish research to determine the function of a given gene in development.<sup>24</sup> We designed splice MO that targets the transmembrane region of the Tie-1 receptor kinase (Figure 3A blue box). To determine MO efficacy, we performed RT-PCR using specific primers in the exons spanning across the targeted exons of Tie-1 TM region. Compared with the uninjected sample (Figure 3A lane UI), embryos injected with 5 ng of the *tie-1* MO (Figure 3A lane 5) show a second smaller transcript in addition to the native transcript. Indeed, increasing concentrations of *tie-1* splice MOs (10 ng) resulted in knockdown of endogenous *tie-1* transcript and replacement by an alternative transcript (Figure 3A, compare

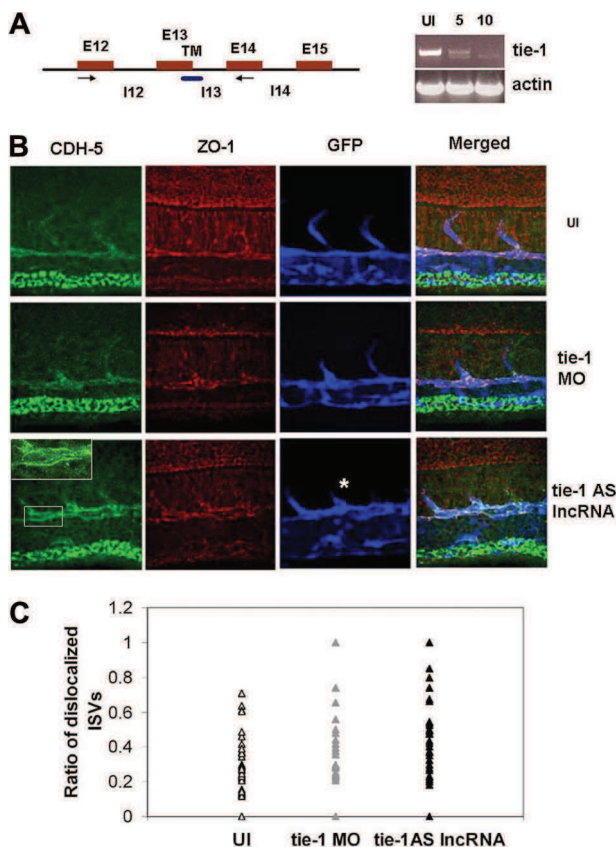


**Figure 3. The phenotype of zebrafish *tie-1AS* IncRNA overexpression.** (A) The MO targeting splice-site is complementary to the 13th exon-intron boundary. RT-PCR was performed to confirm MO-targeting effects. (B) Immunostaining of Tg(*flk*: EGFP) embryos injected with *tie-1AS* (150 pg) or *tie-1* MO (5–10 ng) at the 1-cell stage and fixed at 24 hpf. Staining was performed using CDH5, ZO-1, and anti-GFP antibodies. Most *tie-1AS* IncRNA-injected embryos showed an asymmetric distribution of Cdh-5 staining on endothelial cell membrane in vivo as shown in the enlarged inset. ISVs (white asterisk) also show a truncated phenotype. Details of image capture are available in supplemental Methods. (C) Quantification of the phenotype was performed as described in supplemental Methods, and the ratio of length of ISVs showing phenotype to an ISV with normal CDH-5 distribution is plotted. In general, the trend in *tie-1AS* IncRNA and *tie-1* MO-injected embryos shows higher ratios indicating more ISVs with asymmetric CDH-5 distribution per embryo.

lanes 5 and 10), indicating that the MO affects endogenous *tie-1* transcripts in a dose-dependent manner.

To investigate the possible phenotype of *tie-1* LOF, we followed the well-established function of Tie-1 in maintaining the integrity of the mammalian vasculature.<sup>12</sup> *Tie-1*-deficient mouse embryos show no perturbation of embryonic angiogenesis but loss of vessel integrity.<sup>9,10</sup> We injected *tie-1* MO or *tie-1AS* IncRNA into transgenic embryos where the vascular endothelial growth factor receptor-2 or *flk* promoter drives the expression of enhanced green fluorescent protein Tg(*flk*: EGFP)<sup>13</sup> in the vasculature and investigated vessel integrity at 24 hpf. Injected embryos were immunostained for tight junction and adherens junction proteins using antibodies to zona occludens (ZO-1; Figure 3B ZO-1 panels) and Ve-cadherin (CDH-5; Figure 3B CDH-5 panels), respectively. The ZO-1 protein<sup>25</sup> is present in all cell junctions, whereas the CDH-5 protein<sup>26</sup> is localized exclusively in endothelial cell junctions. Both proteins have been shown previously in zebrafish to be in similar location<sup>13</sup> as in mouse and humans.

We immunostained *tie-1AS* IncRNA injected, *tie-1* MO injected, and uninjected embryos for ZO-1 and CDH-5 proteins at 24 hpf. Uninjected embryos (Figure 3B UI) show ISVs that were properly patterned with well-organized contact with endothelial

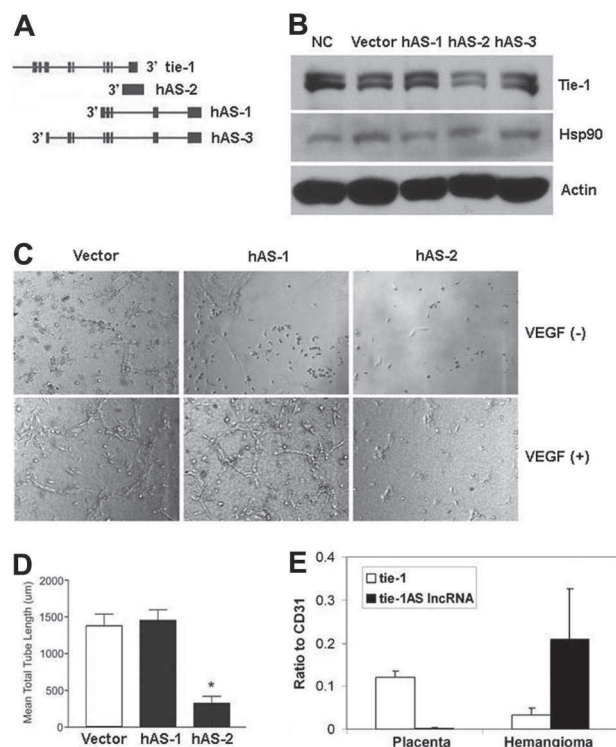


**Figure 4. Human IncRNA regulates Tie-1 expression in endothelial cells and is necessary for VEGF-induced tube formation and the disease connection.** (A) A schematic of the 3 human IncRNA AS (h-AS) *tie-1* transcripts is shown. (B) hAS-2 transfection in endothelial cells down-regulates Tie-1 protein levels compared with no-treatment control (NC), vector control (Vector), or hAS-1 or hAS-3 transfected lysates. (C) After transfection with empty vector and *tie-1* noncoding RNAs h-AS1 or h-AS2, HUVECs were suspended in type I collagen gels and treated with vehicle or 100 ng/mL VEGF. After 24 hours of incubation, cells were photographed using QCapture Program (QImaging Inc). Representative images are shown for 2 independent experiments. Details of image capture are available in supplemental Methods. (D) Quantification of mean lengths of tubes formed with VEGF-treated transfected HUVECs. \* $P < .05$ . (E) Tissues from patients diagnosed with vascular anomalies have aberrant levels of *tie-1AS* IncRNA transcript compared with *tie-1*. Interestingly, RNA from normal placenta tissue shows an exact reverse pattern with high levels of *tie-1* and low to nondetectable levels of *tie-1AS* IncRNA.

cell of the DA and cardinal vein (CV) for both ZO-1 (Figure 3B UI, ZO-1) and CDH-5 (Figure 3B UI, CDH-5). In contrast, both the *tie-1AS* IncRNA-injected and the *tie-1* MO-injected embryos showed aberrant ZO-1 staining (compare respective panels for *tie-1* MO and *tie-1AS* IncRNA in Figure 3B). The ZO-1 staining in both *tie-1* MO and *tie-1AS* IncRNA showed asymmetric distribution through the cell surface, whereas in uninjected embryos the ZO-1 staining was restricted to cell contact junctions. In terms of vascular-specific junctions, CDH-5 staining clearly shows asymmetric or uniform distribution of CDH-5 protein on all sides of the cell in *tie-1AS* IncRNA sample (Figure 3B), compared with the uninjected panel. The ISV structure in both *tie-1AS* IncRNA and the *tie-1* MO-injected embryos appears thinner, and the ISV length from DA to dorsal surface is shorter. Quantification of the percentage CDH-5 mislocalization along the length of a single ISV in each sample group is shown in Figure 3C. In general, more ISV cells show CDH-5 mislocalization along the ISV length in *tie-1* MO and *tie-1AS* IncRNA samples.

To investigate the effects of human *tie-1AS* IncRNA on endothelial tube formation in vitro, we electroporated HUVECs with AS transcripts encoding 3 different regions in the 3'-UTR of the human *tie-1* gene locus as indicated in Figure 4A. The 3 human AS (hAS) transcripts are called hAS-1, hAS-2, and hAS-3. The hAS-1



and hAS-3 encodes identical regions with the hAS-3–encompassing region further upstream of hAS-1 (Figure 4A). The hAS-2 spans the last exon of the *tie-1* gene and covers the last intron-exon junction. This AS contains both intron and exon sequences of *tie-1* in the reverse orientation, which is similar to the zebrafish AS used in all the experiments here. First, we electroporated HUVECs with the 3 hASs and generated lysates to detect Tie-1 protein levels via Western blot. Among the different sample groups, only hAS-2–transfected lysate (Figure 4B lane hAS-2) showed appreciable difference in Tie-1 protein levels compared with hAS-1 (Figure 4B lane hAS-1), hAS-3 (Figure 4B lane hAS-3), untransfected (Figure 4B lane NC), or empty vector transfected (Figure 4B lane vector) cells. No appreciable differences were noticed for housekeeping proteins Hsp90 or actin (Figure 4B Hsp90/actin). This result indicates that hAS-2 like zebrafish *tie-1AS* lncRNA selectively targets *tie-1* transcript, resulting in down-regulation of the Tie-1 protein.

We next performed an in vitro tubulogenesis assay in collagen gel in the presence and absence of vascular endothelial growth factor (VEGF). In both empty vector (Figure 4C vector) and hAS-1 (Figure 4C hAS-1) transfected endothelial cell panels, we notice tube formation in the presence of VEGF. However, in hAS-2–transfected endothelial cell (Figure 4C hAS-2), tube formation is absent in the presence of VEGF, indicating that down-regulation of Tie-1 protein results in disruption of endothelial tube formation in vitro. This result is in concordance with previous reports of Tie-1 function in modulating endothelial cell junctions and in turn stability of endothelial network.<sup>27,28</sup> Quantitation of the VEGF-induced tube formation (Figure 4D) shows a statistically significant difference ( $*P < .05$ ) between hAS-2 and vector or hAS-1–transfected cells.

#### ***Tie-1AS* lncRNA disease connection**

Mutations in Tie's have been previously implicated in patients with vascular malformations.<sup>29-33</sup> To investigate whether the human *tie-1AS* lncRNA levels are altered in vascular malformation, we performed quantitative PCR for *tie-1* and *tie-1AS* lncRNA on RNA isolated from vascular anomaly<sup>34</sup> tissue from 12 patients previously diagnosed for various anomalies and compared them with RNA from normal placenta. In general, placenta share several markers with hemangioma tissue<sup>35</sup> and therefore were used for comparisons. The quantitative PCR comparison was performed to the CD31 endothelial marker. We noticed that the *tie-1AS* lncRNA levels show a 5- to 10-fold increase (Figure 4E black bar, *tie-1AS* lncRNA) in vascular anomaly patient samples compared with normal placenta. Interestingly, normalized *tie-1* levels (Figure 4E white bar, *tie-1* panel) have not dramatically changed among the sample groups. Importantly, the ratio of *tie-1* versus *tie-1AS* lncRNA is opposite in normal placenta tissue compared with vascular anomaly tissue. These results suggest that the balance between *tie-1AS* lncRNA and *tie-1* is probably critical for regulation of *tie-1* levels, and diseases where vasculature is implicated may observe a shift in this regulation, arguing for a specific function for *tie-1AS* lncRNA in vascular conditions.

## **Discussion**

A growing body of evidence suggests that mammalian genomes encode many thousands of large intergenic transcripts. To date, the functional significance of these transcripts is poorly understood. In this study, we have identified a noncoding AS RNA in the 3'-UTR

of the *tie-1* gene locus that is expressed in the AS direction to the *tie-1* gene. The salient features of this study include (1) a vascular-specific noncoding RNA that is expressed in both previously known and unknown regions of native *tie-1* transcript expression in vivo, (2) selective targeting of *tie-1* transcript by direct interaction of the noncoding RNA with its cognate RNA in vivo that results in down-regulation of the *tie-1* transcript, (3) phenotypic consequences in vivo and in vitro of the noncoding RNA mediated down-regulation of *tie-1* transcripts, and (4) potential imbalance in *tie-1*/noncoding *tie-1AS* ratios in vascular-related disease states.

The noncoding *tie-1AS* lncRNA is expressed in the temporal and, for the most part, spatial location that matches the endogenous *tie-1* gene expression pattern. Interestingly, regions in the brain, such as the forebrain and hindbrain, and otic vesicles show strong expression of the noncoding species exclusively. This argues for a *tie-1* gene role previously unrecognized in the brain and ear function, perhaps in the vasculature of these organs. Indeed, 2 recent studies implicate angiopoietins, ligands for Tie's, in lymphatic vessel development in ear.<sup>36,37</sup> Whether the ear expression observed in the fish translates into a role for *tie-1* in inner ear development or vasculature associated with ear development in mouse remains to be seen. Because the noncoding RNA for *tie-1* is conserved in humans and mice, this paradigm of using noncoding RNA expression pattern to speculate putative novel gene function (simply based on expression alone) of well-studied genes is intriguing.

The presence of noncoding AS transcript at the same time and space as its native endogenous transcript suggests a regulatory paradigm; and based on our comprehensive zebrafish genome searches, it is clear that the energy of the *tie-1AS* lncRNA:*tie-1* RNA complex is substantially lower than what is typically observed, which argues for selective duplex formation with one another. Indeed, experimental data confirm this prediction in vivo. Hybridization of the AS long noncoding RNA to its target is predicted to destabilize it and in turn result in loss of protein.<sup>4</sup> This is probably the functional significance with the noncoding *tie-1AS* lncRNA both in vivo and in vitro. Both uncapped and capped noncoding *tie-1AS* lncRNA targets *tie-1*, suggesting that (1) the hybridization mediated down-regulation mechanism of target gene is independent of RNA capping and (2) this down-regulation is probably an RNA-mediated mechanism. However, definitive evidence is needed before reaching this conclusion.

Down-regulation of gene expression often leads to loss of function phenotypes, especially for haploinsufficient genes. *Tie-1* loss of function is established in the late angiogenesis phase<sup>38</sup> and is required cell autonomously for endothelial cell survival and vascular network extension during late embryogenesis.<sup>9</sup> In *tie-1AS* lncRNA-injected embryos, we have similarly noticed that endothelial cell junctions typified by Ve-cadherin are mislocalized, therefore arguing for loss or aberrant cell contacts. This phenotype also corresponds well to the expression of *tie-1AS* at the junction between PCV and DA as shown by ISH. Importantly, the human *tie-1AS* lncRNA also prevents tube formation of endothelial cells in response to VEGF stimulus, arguing that the aberrant cell contact observed in vivo results in loss of cell-cell adhesion necessary for tube formation in vitro. Both humans and zebrafish share the same 3'-UTR *tie-1AS* lncRNA region that targets the *tie-1* gene, which spans the exon-intron junction of the last *tie-1* exon in the AS direction and in essence behaves mechanistically as a splice MO. Therefore, this argues that noncoding AS RNA-mediated down-regulation of target gene may mimic other AS technology.

At present, the function of noncoding RNA in disease is still unclear<sup>4</sup>; and to date, mutations in noncoding RNA have not been reported in disease. Mutations in Tie, especially Tie-2, have been implicated in vascular malformation, in particular congenital venous malformations.<sup>29</sup> The imbalance in the ratio of *tie-1* and noncoding lncRNA in patients diagnosed with vascular malformations suggests aberrant gene regulation in disease, but whether this regulation is critical for the pathogenesis of disease is unknown.

In conclusion, we have identified a novel long noncoding AS transcript that regulates *tie-1* gene levels in vivo and in vitro, resulting in phenotypic consequences similar to mammals. To our knowledge, this is the first report on the identification of a long noncoding RNA that plays a functional regulatory role in vascular development.

## Acknowledgments

This work was supported in part by start-up funds from the Children's Research Institute at the Medical College of Wisconsin and the National Institutes of Health (HL090712 grant; R.R.). K.L. and C.Z.C. are supported partly by funds from Advancing Healthier

Wisconsin Grant (R.R.). G.V.S. is a recipient of the State of Wisconsin Breast Cancer Research postdoctoral fellowship.

## Authorship

Contribution: K.L., Y.B., A.V., Z.L., K.P., N.R.L., C.Z.C., G.V.S., B.Z., M.K.G., and M.A.H. performed experiments and analyzed data; K.L., Y.B., A.V., K.P., R.Q.M., G.A.W., and R.R. designed experiments; S.A.S. designed and performed bioinformatic analysis and analyzed data; P.E.N. provided human tissue samples; and G.A.W., M.A., and R.R. wrote the manuscript.

Conflict-of-interest disclosure: The authors declare no competing financial interests.

The current affiliation for M.K.G. is Harvard Graduate School, Boston, MA.

Correspondence: Ramani Ramchandran, Department of Pediatrics, Medical College of Wisconsin, Children's Research Institute Developmental Vascular Biology Program, CRI C3420, 8701 Watertown Plank Rd, PO Box 26509, Milwaukee, WI 53226; e-mail: ramchan@mcw.edu.

## References

- Ponting CP, Oliver PL, Reik W. Evolution and functions of long noncoding RNAs. *Cell*. 2009;136(4):629-641.
- Katayama S, Tomaru Y, Kasukawa T, et al. Antisense transcription in the mammalian transcriptome. *Science*. 2005;309(5740):1564-1566.
- Dinger ME, Pang KC, Mercer TR, Mattick JS. Differentiating protein-coding and noncoding RNA: challenges and ambiguities. *PLoS Comput Biol*. 2008;4(11):e1000176.
- Mercer TR, Dinger ME, Mattick JS. Long noncoding RNAs: insights into functions. *Nat Rev Genet*. 2009;10(3):155-159.
- Zhang Y, Liu XS, Liu QR, Wei L. Genome-wide in silico identification and analysis of cis natural antisense transcripts (cis-NATs) in ten species. *Nucleic Acids Res*. 2006;34(12):3465-3475.
- Cheng J, Kapranov P, Drenkow J, et al. Transcriptional maps of 10 human chromosomes at 5-nucleotide resolution. *Science*. 2005;308(5725):1149-1154.
- Faghihi MA, Modarresi F, Khalil AM, et al. Expression of a noncoding RNA is elevated in Alzheimer's disease and drives rapid feed-forward regulation of beta-secretase. *Nat Med*. 2008;14(7):723-730.
- Folkman J. Tumor angiogenesis: therapeutic implications. *N Engl J Med*. 1971;285(21):1182-1186.
- Puri MC, Partanen J, Rossant J, Bernstein A. Interaction of the TEK and TIE receptor tyrosine kinases during cardiovascular development. *Development*. 1999;126(20):4569-4580.
- Puri MC, Rossant J, Alitalo K, Bernstein A, Partanen J. The receptor tyrosine kinase TIE is required for integrity and survival of vascular endothelial cells. *EMBO J*. 1995;14(23):5884-5891.
- Sato TN, Qin Y, Kozak CA, Audus KL. Tie-1 and tie-2 define another class of putative receptor tyrosine kinase genes expressed in early embryonic vascular system. *Proc Natl Acad Sci U S A*. 1993;90(20):9355-9358.
- Sato TN, Tozawa Y, Deutsch U, et al. Distinct roles of the receptor tyrosine kinases Tie-1 and Tie-2 in blood vessel formation. *Nature*. 1995;376(6535):70-74.
- Blum Y, Belting HG, Ellertsdottir E, Herwig L, Luders F, Affolter M. Complex cell rearrangements during intersegmental vessel sprouting and vessel fusion in the zebrafish embryo. *Dev Biol*. 2008;316(2):312-322.
- Garnaas MK, Moodie KL, Liu ML, et al. Syx, a RhoA guanine exchange factor, is essential for angiogenesis in vivo. *Circ Res*. 2008;103(7):710-716.
- Bedell VM, Yeo SY, Park KW, et al. Roundabout4 is essential for angiogenesis in vivo. *Proc Natl Acad Sci U S A*. 2005;102(18):6373-6378.
- Okada Y, Yano K, Jin E, et al. A three-kilobase fragment of the human Robo4 promoter directs cell type-specific expression in endothelium. *Circ Res*. 2007;100(12):1712-1722.
- Westerfield M, Doerry E, Kirkpatrick AE, Douglas SA. Zebrafish informatics and the ZFIN database. *Methods Cell Biol*. 1999;60:339-355.
- Sprague J, Bayraktaroglu L, Bradford Y, et al. The Zebrafish Information Network: the zebrafish model organism database provides expanded support for genotypes and phenotypes. *Nucleic Acids Res*. 2008;36(Database issue):D768-D772.
- Lyons MS, Bell B, Stainier D, Peters KG. Isolation of the zebrafish homologues for the tie-1 and tie-2 endothelium-specific receptor tyrosine kinases. *Dev Dyn*. 1998;212(1):133-140.
- Hofacker IL. RNA secondary structure analysis using the Vienna RNA package. *Curr Protoc Bioinformatics*. 2004;Chapter 12:12.
- Gruber AR, Lorenz R, Bernhart SH, Neubock R, Hofacker IL. The Vienna RNA websuite. *Nucleic Acids Res*. 2008;36(Web Server issue):W70-W74.
- Pruitt KD, Tatusova T, Maglott DR. NCBI reference sequences (RefSeq): a curated non-redundant sequence database of genomes, transcripts and proteins. *Nucleic Acids Res*. 2007;35(Database issue):D61-D65.
- Guttman M, Amit I, Garber M, et al. Chromatin signature reveals over a thousand highly conserved large non-coding RNAs in mammals. *Nature*. 2009;458(7235):223-227.
- Nasevicius A, Ekker SC. Effective targeted gene 'knockdown' in zebrafish. *Nat Genet*. 2000;26(2):216-220.
- Fallon MB, Mennone A, Anderson JM. Altered expression and localization of the tight junction protein ZO-1 after common bile duct ligation. *Am J Physiol*. 1993;264(6):C1439-C1447.
- Navarro P, Caveda L, Breviaro F, Mandoteanu I, Lampugnani MG, Dejana E. Catenin-dependent and -independent functions of vascular endothelial cadherin. *J Biol Chem*. 1995;270(52):30965-30972.
- Tsiamis AC, Morris PN, Marron MB, Brindle NP. Vascular endothelial growth factor modulates the Tie-2:Tie-1 receptor complex. *Microvasc Res*. 2002;63(2):149-158.
- Ribatti D. Transgenic mouse models of angiogenesis and lymphangiogenesis. *Int Rev Cell Mol Biol*. 2008;266:1-2665.
- Limaye N, Wouters V, Uebelhoefer M, et al. Somatic mutations in angiotensin receptor gene TEK cause solitary and multiple sporadic venous malformations. *Nat Genet*. 2009;41(1):118-124.
- Vikkula M, Boon LM, Carraway KL III, et al. Vascular dysmorphogenesis caused by an activating mutation in the receptor tyrosine kinase TIE2. *Cell*. 1996;87(7):1181-1190.
- Wang H, Zhang Y, Toratani S, Okamoto T. Transformation of vascular endothelial cells by a point mutation in the Tie2 gene from human intramuscular haemangioma. *Oncogene*. 2004;23(53):8700-8704.
- Bhandarkar SS, Jaconi M, Fried LE, et al. Full-length 5 potentially inhibits NADPH oxidase 4 and blocks the growth of endothelial tumors in mice. *J Clin Invest*. 2009;119(8):2359-2365.
- Perry B, Banyard J, McLaughlin ER, et al. AKT1 overexpression in endothelial cells leads to the development of cutaneous vascular malformations in vivo. *Arch Dermatol*. 2007;143(4):504-506.
- Mulliken JB, Glowacki J. Hemangiomas and vascular malformations in infants and children: a classification based on endothelial characteristics. *Plast Reconstr Surg*. 1982;69(3):412-422.
- North PE, Waner M, Brodsky MC. Are infantile hemangioma of placental origin? *Ophthalmology*. 2002;109(2):223-224.
- Dellinger M, Hunter R, Bernas M, et al. Defective remodeling and maturation of the lymphatic vasculature in Angiopoietin-2 deficient mice. *Dev Biol*. 2008;319(2):309-320.
- Kim KE, Cho CH, Kim HZ, Baluk P, McDonald DM, Koh GY. In vivo actions of angiopoietins on quiescent and remodeling blood and lymphatic vessels in mouse airways and skin. *Arterioscler Thromb Vasc Biol*. 2007;27(3):564-570.
- Partanen J, Puri MC, Schwartz L, Fischer KD, Bernstein A, Rossant J. Cell autonomous functions of the receptor tyrosine kinase TIE in a late phase of angiogenic capillary growth and endothelial cell survival during murine development. *Development*. 1996;122(10):3013-3021.



## Review

## Vascular morphogenesis in the zebrafish embryo

Elín Ellertsdóttir, Anna Lenard, Yannick Blum, Alice Krudewig, Lukas Herwig, Markus Affolter, Heinz-Georg Belting\*

Department of Cell Biology, Biozentrum der Universität Basel, Klingelbergstrasse 70, CH-4056 Basel, Switzerland

## ARTICLE INFO

## Article history:

Received for publication 11 September 2009

Revised 28 October 2009

Accepted 28 October 2009

Available online 3 November 2009

## Keywords:

Angiogenesis  
Vasculogenesis  
Branching morphogenesis  
Cell migration  
Lumen formation  
Development  
Zebrafish

## ABSTRACT

During embryonic development, the vertebrate vasculature is undergoing vast growth and remodeling. Blood vessels can be formed by a wide spectrum of different morphogenetic mechanisms, such as budding, cord hollowing, cell hollowing, cell wrapping and intussusception. Here, we describe the vascular morphogenesis that occurs in the early zebrafish embryo. We discuss the diversity of morphogenetic mechanisms that contribute to vessel assembly, angiogenic sprouting and tube formation in different blood vessels and how some of these complex cell behaviors are regulated by molecular pathways.

© 2009 Elsevier Inc. All rights reserved.

## Introduction

Branched tubular organs, such as the insect tracheal system or the vertebrate cardiovascular system, kidney or lung, are found throughout the animal kingdom. Formation of such tubular networks from precursor cells or tissues involves a variety of morphogenetic processes, such as tube formation, elongation, branching and fusion. These processes are brought about by complex cellular behaviors, which include cell polarization, cell migration, cell rearrangements, cell shape changes and cell division. Although tubular organs are extremely diverse in anatomy and function, the cellular activities that govern tube formation and branching morphogenesis appear to be quite similar (Baer et al., 2009; Andrew and Ewald, 2010). In this review, we describe the current understanding of blood vessel formation in the early zebrafish embryo. We are placing special emphasis on the morphogenetic processes that contribute to vascular development and discuss the regulatory components that accompany these events.

In vertebrates, the cardiovascular system constitutes a highly ramified network of tubes that transports gas, nutrients, hormones and metabolites throughout the body. It also has important roles in the regulation of homeostasis and wound healing and is involved in the pathology of numerous diseases including cancer and inflammation (Carmeliet, 2003). The cardiovascular system emerges as one of the first organs during embryonic development and retains morpho-

genetic plasticity in adult life. Blood vessels are an integral component of all organs and are vital not only for their function but also for their formation during embryonic development (Nikolova and Lammert, 2003; Red-Horse et al., 2007; Sakaguchi et al., 2008). Blood vessels are highly diverse: they differ in size and are specialized depending on their function and the tissue or organ they are embedded in (Aird, 2007; Rocha and Adams, 2009). In general, they consist of an inner epithelium (endothelium) lining the lumen; depending on the type of vessel, this endothelium is surrounded by a basal lamina and by mural cells, such as pericytes and smooth muscle cells, which both support and regulate the function of the endothelium (Armulik et al., 2005).

Over the last decade, the molecular pathways controlling vascular development have attracted much attention, and a large number of key molecules has been identified that regulate different aspects of blood vessel morphogenesis. The basic frameworks of the vascular anatomy are conserved among vertebrates, which makes it possible to assign homologies between distinct blood vessels and to directly compare the formation of these vessels in different vertebrate species (Isogai et al., 2001; see Fig. 1). The zebrafish embryo has proven to be a useful model to study vascular morphogenesis in vivo. The vasculature can be easily visualized using a variety of labeling techniques, such as endothelial specific expression of fluorescent protein or by microangiography (Fig. 1). Its small size, experimental accessibility, optical clarity and rapid development allow to observe cellular activities, such as cell migration, cellular rearrangements and cell divisions, as they occur during blood vessel reformation in the embryo. It is also possible to follow cardiovascular mutant phenotypes for several days because oxygenation of the early zebrafish embryo does

\* Corresponding author.

E-mail address: [heinz-georg.belting@unibas.ch](mailto:heinz-georg.belting@unibas.ch) (H.-G. Belting).



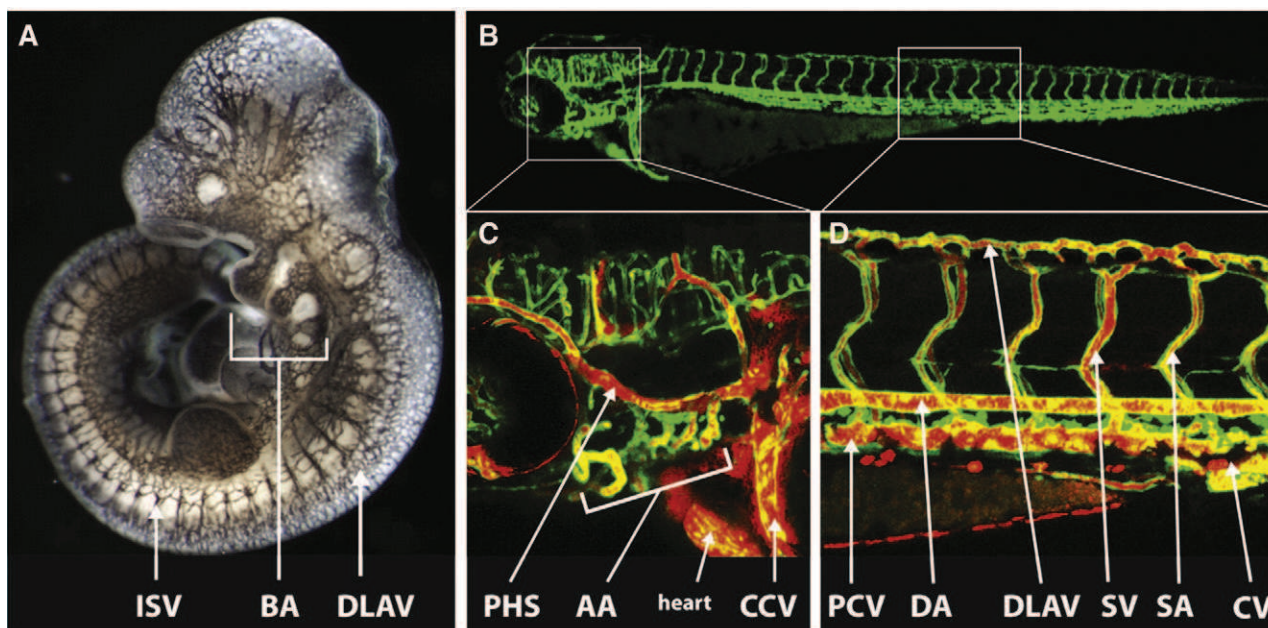


**Fig. 1.** The vascular system in mouse and fish embryos. (A) Visualization of the vascular system by immunohistochemical localization of PECAM-1 in a day 10 mouse embryo (photo courtesy of Ralf Adams, MPI, Münster, Germany). Owing to the opacity of the mouse embryo, only superficial blood vessels can be seen. BA: branchial arches (1st and 2nd); ISV: intersegmental vessel; DLAV: dorsal longitudinal anastomotic vessel. (B–D) The vascular system in a 3-day-old zebrafish embryo visualized by reporter gene analysis (*TG:flk1:EGFP* in green) and by microangiography using quantum dots (red in panels C and D). Some blood vessels are indicated according to Isogai et al. (2001). AA: aortic arches (1–6); CV: caudal vein; CCV: common cardinal vein; DA: dorsal aorta; PCV: posterior cardinal vein; PHS: primary head sinus; SA: segmental artery; SV: segmental vein. At these stages, anatomical similarities between the two species are best observed in the branchial arches and in the ISV of the trunk. ISV and DLAV form quite similarly in both species (Isogai et al., 2003; Walls et al., 2008).

not rely on blood circulation. Furthermore, functional studies by forward and reverse genetics have shown that the molecular components that regulate vascular development are conserved between mammals and fish (Beis and Stainier, 2006; Lawson and Weinstein, 2002b; Thisse, 2002). Thus, the zebrafish embryo presents a unique system in which live imaging can be combined with functional studies to gain a more complete insight into how the molecular and morphogenetic mechanisms are integrated at the (sub)cellular level to shape the vascular tree.

### Vasculogenesis

The formation of vertebrate blood vessels is commonly subdivided into two distinct morphogenetic processes, called vasculogenesis and angiogenesis. Vasculogenesis is defined by in situ aggregation of angioblasts into a blood vessel (Coffin and Poole, 1988; Poole and Coffin, 1989; Risau, 1995; Risau et al., 1988), while further sprouting of vessels from existing vessels occurs via a process called angiogenesis (Risau, 1995).

#### Origin and specification of endothelial cells

Angioblasts are precursors of endothelial cells not yet incorporated into blood vessels. They originate from the ventrolateral mesoderm (Kimmel et al., 1995; Stainier et al., 1995). Analyses of genes expressed in the hematopoietic and endothelial cell lineages have revealed a remarkable conservation between vertebrate species. In particular, transcription factors belonging to the ETS, GATA and LMO families have been shown to control specification of these lineages in mammals as well as fish (De Val et al., 2008; Detrich et al., 1995; Liu and Patient, 2008; Thompson et al., 1998; Zon et al., 1991). At the beginning of somitogenesis, transcription factors, such as *scl/tal1* and *lmo2*, which specify angioblasts and hematopoietic cells, are expressed in two domains along the body axis, the anterior and the posterior lateral mesoderm (Dooley et al., 2005; Liao et al., 1998; Patterson et al., 2007). During somitogenesis these cell populations

acquire unique gene expression profiles. For example, *flk1*-positive/*scl*-positive precursor cells differentiate into *flk1*-positive/*scl*-negative and *flk1*-negative/*scl*-positive cells, which will give rise to endothelial and hematopoietic cells, respectively (Gering et al., 1998). There seems to be no transcriptional factor regulating exclusively the endothelial specification but a combination of multiple factors with overlapping expression patterns (reviewed by De Val and Black, 2009).

#### Formation of the dorsal aorta and the cardinal vein

The basic anatomy of the initial embryonic circulatory system is quite similar among vertebrates. In addition, the first embryonic vessels to appear, the dorsal aorta (DA) and the posterior cardinal vein (PCV), are formed by a distinct morphogenetic mechanism called vasculogenesis in all vertebrates (Isogai et al., 2001). In zebrafish, angioblasts are specified well before the first blood vessels are formed. Expression of molecular markers such as *fli1a* shows that angioblasts are located in two lateral stripes at 12–14 hpf. By 28–30 hpf, the DA and the PCV can be discerned and are fully lumenized (Roman et al., 2002). In vivo imaging, using a *Tg(fli1a:EGFP)* reporter fish line, has shown that angioblasts migrate as individual cells towards the embryonic midline where they coalesce (Lawson and Weinstein, 2002b). During recent years, a considerable amount of research has focused on how this migration process is regulated, how these cells form the axial vessels and how DA and PCV are specified. As indicated in Fig. 2, the PCV forms subsequently to the DA (Eriksson and Löfberg, 2000; Herbert et al., 2009; Jin et al., 2005), and this relationship appears to be conserved among vertebrates (Coffin and Poole, 1988; Hirakow and Hiruma, 1981; Meier, 1980).

Formation of the DA in zebrafish has been studied by transmission electron microscopy (TEM) (Eriksson and Löfberg, 2000; Meier, 1980) and more recently by analysis of transgenic zebrafish embryos (Herbert et al., 2009; Jin et al., 2005; Lawson and Weinstein, 2002b). During vasculogenesis, angioblasts are attracted towards the midline by guidance cues thought to emanate from the endoderm



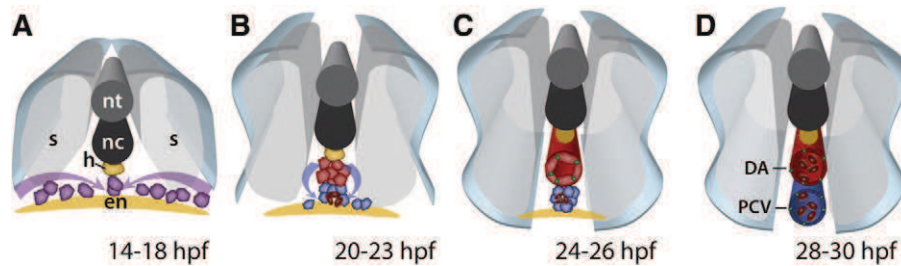


**Fig. 2.** Phases of vasculogenesis in the zebrafish embryo. Schematic cross sections of the trunk region at representative stages of development (according to Herbert et al., 2009 and Jin et al., 2005). (A) Medial migration. From 14 hpf onward, angioblasts (purple) that originate in the lateral plate mesoderm migrate over the endoderm towards the midline just below the hypochord, where they aggregate to form a vascular cord (B). (B) Arterio-venous segregation and ventral sprouting. At around 17 hpf, angioblasts start to express markers of arterio-venous differentiation, such as *ephrin-b2a* in arterial cells (marked in red). These cells are located in the dorsal portion of the vascular rod and will give rise to the DA, whereas *ephb4a* expressing cells are located more ventrally and will contribute to the PCV and CV. At 21 hpf, angioblasts located in the ventral part of the vascular cord start migrating ventrally and accumulate below the forming DA (B, C). (C) Lumen formation. The DA forms and lumenizes prior to the PCV and CV in the absence of blood cells (brown) by cord hollowing. Venous angioblasts aggregate and coalesce around the blood cells to ultimately form a tube. (D) Functional Vasculature. At 30 hpf, both vessels are fully formed and carry blood flow. Endothelial cell junctions are indicated in green.

(Jin et al., 2005; Fig. 2A). Once the angioblasts have reached the embryonic midline, they form aggregates and tube formation commences (Fig. 2B). TEM studies have shown that angioblasts initially form “aggregates of tightly packed cells” between hypochord and the underlying mesoderm (Eriksson and Löfberg, 2000). These aggregates are discontinuous along the anterior–posterior axis and the cells are spherical at the beginning of the process. At around the 17-somite stage (17.5 hpf), more flattened tube forming cells are found posterior to the 7th–9th somite in the fish embryo. From analysis of transgenic zebrafish, it has been suggested that endothelial cells migrate in two waves to the midline and it has been suggested that the first wave contributes to the DA while the cells of the second wave will form the primary vein (Jin et al., 2005). Alternatively, endothelial cells from both migratory waves may join in a single medial cord and segregate independently from this structure. The latter possibility has recently gained strong support from *in vivo* time-lapse analyses, which showed that the precursor cells of the caudal vein dissociate from the primordium of the DA by a process termed ventral sprouting (Herbert et al., 2009). Ventral sprouting is initiated around 20 h post-fertilization shortly before the emergence of dorsal sprouts, which will give rise to segmental arteries (SA) (see below) at a time when the DA is not yet lumenized. This finding together with the observation that the expression of the arterial marker *ephrinb2a* (*efnb2a*) is restricted to a subpopulation within the vascular cord suggested that the primary arteries and veins are derived from a common primordium that contains a mixed population of arterial as well as venous angioblasts (Herbert et al., 2009; Jin et al., 2005).

Specification of arterial versus venous fates has been shown to depend on the interaction of the VEGF and Notch signaling pathways (reviewed by Lawson and Weinstein, 2002a; Siekmann et al., 2008). Sonic hedgehog (SHH) signals from the notochord lead to an activation of *vegfa* expression in ventral somites (Lawson et al., 2002). VEGF-A is sensed by the angioblasts via VEGF-receptor-2/KDR/FLK1 (KDR-Like/KDRL in zebrafish), which leads to the activation of Notch signaling and the transcriptional activation of other factors which results in arterial differentiation in a subset of angioblasts (Cermenati et al., 2008; Lawson et al., 2003; Pendeville et al., 2008; Zhong et al., 2001). In contrast to arterial development, specification of venous fates is independent of VEGF-A signaling (Covassin et al., 2006; Lawson et al., 2003). In agreement with these concepts, modification of VEGF or Notch signaling levels influences the segregation and ventral sprouting behavior. Angioblasts showed excessive ventral migration, when VEGF-A and Notch signals were blocked, whereas downregulation of FLT4 led to a reduction in ventral sprouting (Herbert et al., 2009).

Arterial and venous specification of angioblasts is reflected by particular gene expressions (Lawson and Weinstein, 2002a). Notably,

two members of the Eph-ephrin subclass of the receptor tyrosine kinase family are differentially expressed in arteries (*EphrinB2/Efnb2*) and veins (*EphB4*) (Adams et al., 1999; Lawson et al., 2001). Genetic analyses in mouse have demonstrated an important role for bidirectional EphB4-Efnb2 signaling for vascular morphogenesis (reviewed by Adams and Alitalo, 2007). In mouse and fish, EPHB4-Efnb2 signaling has been shown to be involved in sorting of neuronal cells, which leads to their segregation into adjacent hindbrain segments (Kemp et al., 2009; Mellitzer et al., 1999). To test whether these factors also play a role in the segregation of arterial and venous angioblasts in the primary vascular cord, Herbert and colleagues (2009) modified EPHB4a and EfnB2a levels and interfered with forward and reverse properties of EPHB4a-EfnB2a signaling. Either overexpression or knockdown of EPHB4a/EfnB2a function caused aberrant migration of transplanted angioblasts consistent with defects in arterio-venous segregation. Taken together, these findings show that repulsive EPH4a-EfnB2 signaling regulates arterio-venous segregation, thereby controlling the directionality of angioblast sprouting.

#### *Anterior–posterior differences in artery formation*

While the process of vasculogenesis has been best described in the dorsal aorta of the trunk, there is increasing evidence of regional differences in the way the primary vessels form and it has been proposed that distinct cues guide endothelial cells in different domains of the body (Coffin and Poole, 1991; Eriksson and Löfberg, 2000). In agreement with this view, several zebrafish mutants have been isolated that exhibit vascular defects in particular regions of the body (Jin et al., 2007).

Some experiments have shed light on the differences that regulate the formation of the DA of the trunk and the paired lateral dorsal aortae (LDA), which is located in anterior body regions. In an earlier study, the role of the endoderm for formation of the DA was examined in *casanova* (*sox32*) mutants that lack endoderm (Jin et al., 2005). In these embryos, medial migration of angioblasts was slowed but the DA formed normally, suggesting that endoderm is dispensable for DA formation. However, it has more recently been shown that the endoderm plays an essential role for LDA formation in the anterior region of the embryo (Siekmann et al., 2009). Strikingly, mutants for the chemokine receptor *cxc4a*, which is expressed in the LDA, lack the LDA. CXCR4 is known to bind to CXCL12, which is specifically expressed in the anterior endoderm underlying the developing LDA. Furthermore, loss of CXCL12 function phenocopies the *cxc4a* deficiency. These findings illustrate the molecular diversity in endothelial cells and the importance of local extrinsic cues for the formation and patterning of the primary aorta.

### *Transforming a cord into a tube: lumen formation in the primary blood vessels*

The morphogenesis of biological tubes has been a longstanding interest in developmental biology and it has been shown that tubes can form in very different ways (Baer et al., 2009; Lubarsky and Krasnow, 2003). After angioblasts have aggregated into a cord-like structure, they ultimately have to assemble a tube. This could in principal occur by different morphogenetic processes, including (i) cell hollowing, where cells form vacuoles that fuse between cells to form a continuous intracellular lumen; (ii) wrapping, where cells migrate in a polarized state and surround the future lumen; (iii) cord hollowing, where cells within the cord attain apical–basal polarity and the lumen is formed by membrane separation and fluid influx; or by (iv) cavitation, where cells in the middle of the rod undergo apoptosis leaving a luminal space behind (Hogan and Kolodziej, 2002; Kucera et al., 2007; Lubarsky and Krasnow, 2003).

Tube formation of the DA has been studied at the cellular level by transgenic and immunofluorescent analyses in zebrafish embryos (Jin et al., 2005). Shortly after angioblasts have formed a cord, the DA begins to lumenize (21 hpf; Figs. 2B, C). Analysis of proteins involved in apical–basal polarization, such as fibronectin or  $\beta$ -catenin, has shown that this process is preceded by endothelial polarization and the formation of junctions between ECs, suggesting that a cord hollowing process forms the lumen of the DA. At the 20-somite stage (19 hpf), cell junctions, as visualized by ZO-1 and Claudin5, are discernable between the cells forming the dorsal aorta (Jin et al., 2005). The mechanisms of lumen formation in the zebrafish dorsal aorta and caudal vein have recently been examined by in vivo time-lapse analyses (Herbert et al., 2009). These studies confirmed a cord hollowing mechanism in the DA, whereas the lumen of the CV is formed by ventrally sprouting venous angioblasts that coalesce around resident blood cells. This mode of lumen formation has not been described before and it is likely to be different from cell wrapping as described above because the sprouting angioblast do not seem to migrate as an epithelial sheet of cells.

In a recent, comprehensive study, lumen formation of the paired dorsal aortae has been examined in the mouse embryo (Strilić et al., 2009). By anatomical and immunofluorescent analyses, Strilić and colleagues show that the lumen of the dorsal aortae forms in discrete steps similar to those observed in the zebrafish and, for the first time, they were able to decipher the molecular mechanisms involved in this process. Consistent with observations in zebrafish, the first steps of lumen formation are initiated upon formation of intercellular adherens junctions between angioblasts. Junctional remodeling then leads to an apical interface between adjacent ECs, followed by an accumulation of anti-adhesive CD34-sialomucins, such as CD34 and Podocalyxin (PODXL). Proper localization of these proteins to the apical surface depends on the presence of VE-cadherin. The subsequent formation of the aortic lumen is driven by a VEGF-A-dependent constriction of the apical surfaces as well as EC elongation induced by the F-actin cytoskeleton. These cell shape changes apparently rely on interactions between Moesin with CD34-sialomucins, which lead to an apical localization of F-actin. This view is supported by the analysis of Moesin and of *Podxl* mutants which both exhibit reduced levels of apical F-actin and a delay in aortic lumen formation. Furthermore, loss of *Podxl* leads to a reduction of Moesin at the sites of endothelial contacts, suggesting that PODXL connects with Moesin in order to recruit F-actin.

In summary, these studies indicate that the morphogenetic mechanisms that drive lumen formation in the dorsal aorta/aortae have been conserved between teleosts and mammals. In either case, coalescence of ECs and subsequent apical–basal polarization of a vascular cord appear to be the primary steps. The lumen is then formed between apical surfaces of apposing ECs by a cord hollowing process. Whether the molecular mechanisms that underlie lumen

formation are conserved between fish and mouse remains to be determined. Furthermore, it will be interesting to learn about the morphogenetic processes that may be required to further inflate the lumen.

### **Angiogenesis**

While the primary axial vessels are formed by vasculogenesis, elaboration of the vasculature, i.e. the formation of secondary blood vessels, occurs via angiogenesis, a process by which new blood vessels are generated from a pre-existing one. However, with respect to morphogenetic cell behaviors, angiogenesis can occur in quite different ways. Originally, it has been described as a sprouting process, by which a new vessel is branching off a primary vessel (reviewed by Patan, 2000). In addition to sprouting, a considerably different mode of angiogenesis called intussusception has been described in mammals (reviewed by Makanya et al., 2009). During intussusceptive angiogenesis, a vessel splits along its longitudinal axis into two new branches, thus effectively enlarging the vascular surface area. This process plays an important role in vascular remodeling during plexus formation. In zebrafish, angiogenesis by intussusception has not yet been described and therefore we focus our discussion on sprouting angiogenesis.

#### *Sprouting angiogenesis*

Sprouting angiogenesis was described as a general mechanism of microvascular growth during the 1970s, and its relevance for tumor growth and metastasis was soon recognized (Folkman, 1982). Early on angiogenesis was studied in a variety of in vivo and tissue culture systems such as the chorion allantoic membrane of the chick or the corneal pocket (reviewed by Patan, 2000). As an outcome of these studies, sprouting angiogenesis was described as a sequence of events that include (i) migration of ECs toward the angiogenic stimulus, (ii) alignment of ECs in a bipolar mode, (iii) lumen formation and cell divisions distant to the tip of the sprout and (iv) connection of individual sprouts to initiate circulation (Ausprunk and Folkman, 1977; Patan, 2000).

In recent years, much progress has been made in establishing systems in which angiogenic processes can be followed in detail. These include the retinal vasculature of the mouse, which develops postnatally, and the zebrafish embryo, in which all aspects of angiogenesis can be followed in vivo. Embryonic vasculogenesis and angiogenesis in zebrafish occur in ways very similar to those in mammals. In contrast to the latter, zebrafish embryos do not require extra-embryonic vasculogenesis due to their extrauterine development. This greatly facilitates the analysis of embryonic blood vessel formation, as it is not influenced by prior extra-embryonic events. Although all major blood vessels are easily accessible in the zebrafish embryo, the intersegmental blood vessels (ISV) have been most thoroughly studied because of their metameric organization and relatively simple anatomy.

#### *ISV formation in the zebrafish embryo*

Formation of ISVs in the zebrafish embryos involves two waves of angiogenic sprouting (Isogai et al., 2003). ECs of the primary wave form the segmental arteries (SA). During the primary wave, ECs sprout from the DA at ~22 hpf. These sprouts grow dorsally and – once they have reached the level of the dorsal neural tube – connect with their neighbors from anterior and posterior segments to form the future dorsal longitudinal anastomotic vessel (DLAV). The second wave, which starts at 32 hpf, involves ECs from the PCV (Yaniv et al., 2006). These sprouts will either connect to an existing SA, thereby transforming it into a vein (SV), or, alternatively, they will grow up to the level of the horizontal myoseptum and form a population of cells

named parachordal lymphangioblasts (PLs) (Hogan et al., 2009; Isogai, 2003). The majority of these cells eventually migrates away from the horizontal myoseptum and contributes to the lymphatic vasculature (Hogan et al., 2009).

Formation of the SA has been described in detail by *in vivo* time-lapse and immunofluorescent analyses (Blum et al., 2008; Childs et al., 2002; Isogai et al., 2003; Lawson and Weinstein, 2002b). These studies have led to several models of SA morphogenesis. While earlier studies suggested that the SA is made up by 3 cells that are arranged serially in a head to tail fashion (Childs et al., 2002), mosaic analyses and the analysis of endothelial cell junctions showed that SAs are composed of 4–6 cells that extensively overlap along the proximodistal axis of the vessel (Blum et al., 2008). Taken together, these findings suggest a model of SA formation, as shown in Fig. 3. Initially, one or two cells migrate out of the epithelium of the DA forming the sprout (Fig. 3A). During dorsal outgrowth, this sprout consists usually of 3–4 cells, one tip cell and two or three stalk cells (Fig. 3B). When the tip cell has made contacts with its anterior and posterior neighbors, the basic scaffold of the SA is formed (Fig. 3C). Because of cell divisions that occur at varying time points, the stalk can consist of a variable number of cells generating a large degree of morphological heterogeneity, which is illustrated by the variation of junctional patterns (Blum et al., 2008). However, further cell divisions and cellular rearrangements during vessel assembly lead to a paired configuration of cells along the proximodistal extent of the SA, which then forms a lumen. In the following section, we discuss some of the morphogenetic and molecular mechanisms that govern the different aspects of SA formation. Since much progress has also been made in other angiogenesis models, we will discuss them in comparison with SA formation.

Sprouting of SA and SV appears to be triggered by different signals. For example, VEGF-A is critical for SA formation, while it appears dispensable for SV formation, since SV sprout normally in embryos that are mutant for phospholipase C- $\gamma$  (*plc- $\gamma$* ), which is a downstream mediator of VEGF-A/VEGFR-2 signaling; Bahary et al., 2007; Habeck et al., 2002; Lawson et al., 2003; Nasevicius et al., 2000; Covassin et al., 2009; Covassin et al., 2006). Here, we will focus on the morphogenesis of the SA. The regulation of angiogenesis by VEGFs and their receptors has been studied in many previous publications in great detail (reviewed by Cébe-Suarez et al., 2006; Matsumoto and Mugishima, 2006; Olsson et al., 2006; Shibuya and Claesson-Welsh, 2006; Yamazaki and Morita, 2006). While early studies focused on general pro-angiogenic functions of VEGF signaling, more specific roles for VEGF signaling in patterning of angiogenic sprouts have recently been revealed (Covassin et al., 2006; Gerhardt et al., 2003; Ruhrberg et al., 2002). Upon VEGF-A/VEGFR-2 signals, ECs initiate the angiogenic

program, which entails the loosening of junctional connections with neighboring cells, migratory behavior towards the angiogenic stimulus and cell division (reviewed by Lampugnani and Dejana, 2007). Cells within the nascent sprout respond in different ways to the VEGF-A. Whereas cells located at the base (termed stalk cells) show increased rates of proliferation, the leading cell (termed tip cell) sends long and dynamic filopodia into the surrounding environment to guide the growing sprout towards the stimulus (Gerhardt et al., 2003). Endothelial tip and stalk cells do not only have different functions and behaviors (discussed below), they also show differences in gene expression. For example, Platelet derived growth factor B (*Pdgfb*) and *Flt4* are expressed at higher levels in the tip cell than in the stalk cell (Gerhardt et al., 2003; Siekmann and Lawson, 2007).

Patterning and angiogenic behavior of sprouts are regulated by the cooperation of the Notch and VEGFR-2 signaling pathways (Hellström et al., 2007; Siekmann et al., 2008; Siekmann and Lawson, 2007; Suchting et al., 2007; reviewed by Phng and Gerhardt, 2009; Siekmann et al., 2008). The tip cell, receiving the highest level of VEGFR-2 signal, responds with an upregulation of the Notch ligand Delta-like-4 (*DLL4*), which leads to increased intracellular Notch signaling in the neighboring stalk cells (Hellström et al., 2007). In zebrafish, loss of *DLL4* function leads to prolonged angiogenic activity in the ISVs, whereas over-activation of *Notch* signaling leads to a quiescent phenotype (Leslie et al., 2007; Siekmann and Lawson, 2007). *DLL4* also regulates angiogenesis by suppressing VEGF-C dependent FLT4 (VEGFR-3) signaling in endothelial cells in mouse and fish (Hogan et al., 2009; Tammela et al., 2008). In zebrafish, VEGF-C/FLT4 signaling is required for venous and lymphatic development (Covassin et al., 2006; Küchler et al., 2006). However, a “kinase-dead” allele of FLT4 is able to rescue the hyperbranching phenotype caused by the loss of *DLL4* function (Hogan et al., 2009). Furthermore, in the absence of *DLL4*, arterial cells become more sensitive to varying levels of VEGF-C in the embryo (Hogan et al., 2009). These experiments point out a mechanism for how different endothelial lineages can respond specifically to sources of VEGF-C in the trunk. Venous and lymphatic cells, which do not express *dll4*, are able to respond to VEGF-C/FLT4, whereas in arterial cells this pathway is inhibited by *DLL4* (Hogan et al., 2009).

Although the molecular mechanisms that control angiogenic behavior in the sprout may not be identical in fish and mouse, there is a common theme in that differences in intracellular Notch signaling confer different cell behaviors along the proximodistal axis of the sprout. Tip cells (low Notch) extend numerous filopodia, are highly migratory and thus display the strongest angiogenic behavior while the proximal stalk cells (high Notch) appear less migratory. It has

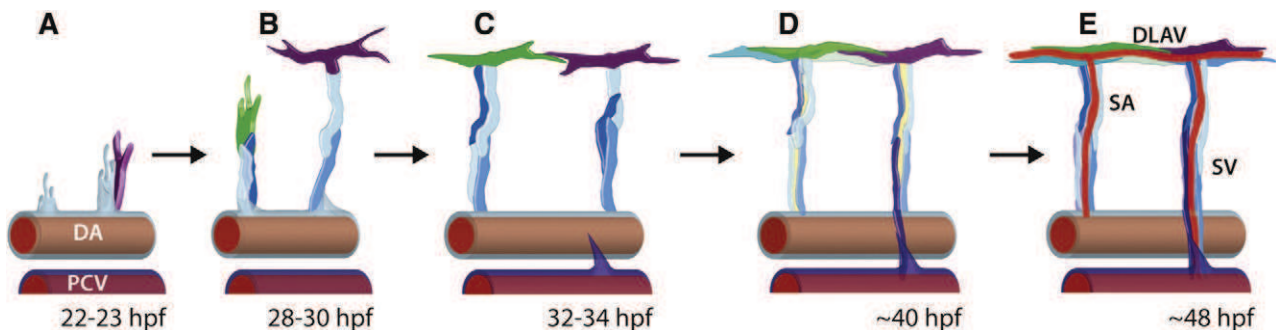


**Fig. 3.** A model for the morphogenetic events that lead to the formation of ISV and DLAV in the Trunk. Two neighboring sprouts are depicted as representative examples. The leading cells are indicated in green and purple, respectively. At 22 hpf ECs of the DA form sprouts (A) that grow along the somite boundaries up to the dorsal roof of the neural tube (B). During these stages, the sprout consists of 2 to 4 cells that are stabilized by interendothelial junctions (not indicated). At the dorsal side of the embryo, the tip cells send extensions toward their anterior and posterior neighbors to establish connections. During this phase, the ECs establish a scaffold consisting of a vascular cord that is not yet lumenized (B, C). Further cell rearrangements and cell divisions lead to formation of a continuous apical surface that may surround initial luminal spaces (yellow) (D). At around 32 hpf, a secondary wave of angiogenic sprouts emerges from the PCV. These sprouts either generate a group of lymphatic cells, called parachordal lymphangioblasts (not shown), or connect with the adjacent primary vessel (D, on the right), which will become a segmental vein. Blood flow in ISVs commences after SA, SV and DLAV have been established (E).



been proposed that the reduced migratory behavior of stalk cells is important to maintain sprout integrity and connection to the DA (Siekmann et al., 2008).

While the general aspects of angiogenesis in the ISVs of the fish and the postnatal vasculature of the mouse retina are very similar, there appear to be differences in gene expression and pattern of cell proliferation. While in the mouse retina cell proliferation is largely restricted to the stalk (Gerhardt et al., 2003), in fish similar rates can be observed in stalk and tip cells (Blum et al., 2008). Furthermore, based on gene expression—intersegmental sprouts in the fish appear not as polarized as those in the mouse retina. In contrast to the mouse retina, the tip cell markers *dll4* and *flt4* are quite uniformly expressed in tip and stalk cells of the sprouting SA (Hogan et al., 2009; Leslie et

al., 2007; Siekmann and Lawson, 2007). Similar to zebrafish, ISV sprouts in the mouse embryo show a relatively even distribution of DLL4 protein (Tammela et al., 2008). These differences between distinct types of blood vessels raise the possibility that, compared to the mouse retina, the state of the tip cell in ISV is less defined. It will be interesting to see whether these differences are due to different interpretations of VEGF/Notch signals or whether they are connected to different morphogenetic processes occurring in the two systems (see below).

How the angiogenic sprout lumenizes is still controversial. Different morphogenetic behaviors and cellular configurations in the sprout can have significant impact on how a vessel is formed. In principle, there are at least 3 different morphogenetic processes of tubulogenesis that may occur in an angiogenic sprout: budding, cord hollowing or cell hollowing (see Fig. 4A). When a novel tube is formed by budding, the ECs that follow the tip cells maintain their epithelial character with a defined apical–basal polarity. During budding, the luminal space of the sprout remains continuous with that of the parent vessel, extending up to the tip cell. Tube branching by budding has been described in many experimental systems including the tracheal system in *Drosophila* and several branched organs in mammals (Baer et al., 2009). Vessel branching by budding appears to occur in larger caliber capillaries that are constantly perfused. In the mouse retina, the lumen is located immediately adjacent to the tip cell (see Fig. 4B). In addition, in vivo time-lapse recording of blood vessels in the zebrafish brain appears consistent with such morphogenetic mode of tubular branching (Huisken and Stainier, 2009).

Formation of ISV does not occur by budding since the initial sprouts do not contain a lumen continuous with the DA (Fig. 4C). Rather, the lumen becomes patent at the time when SA, DLAV and SV have formed proper connections. After labeling circulating blood with fluorescent tracer dyes, it was observed that (from the perspective of the DA) the lumen opens up in a stepwise manner from proximal to

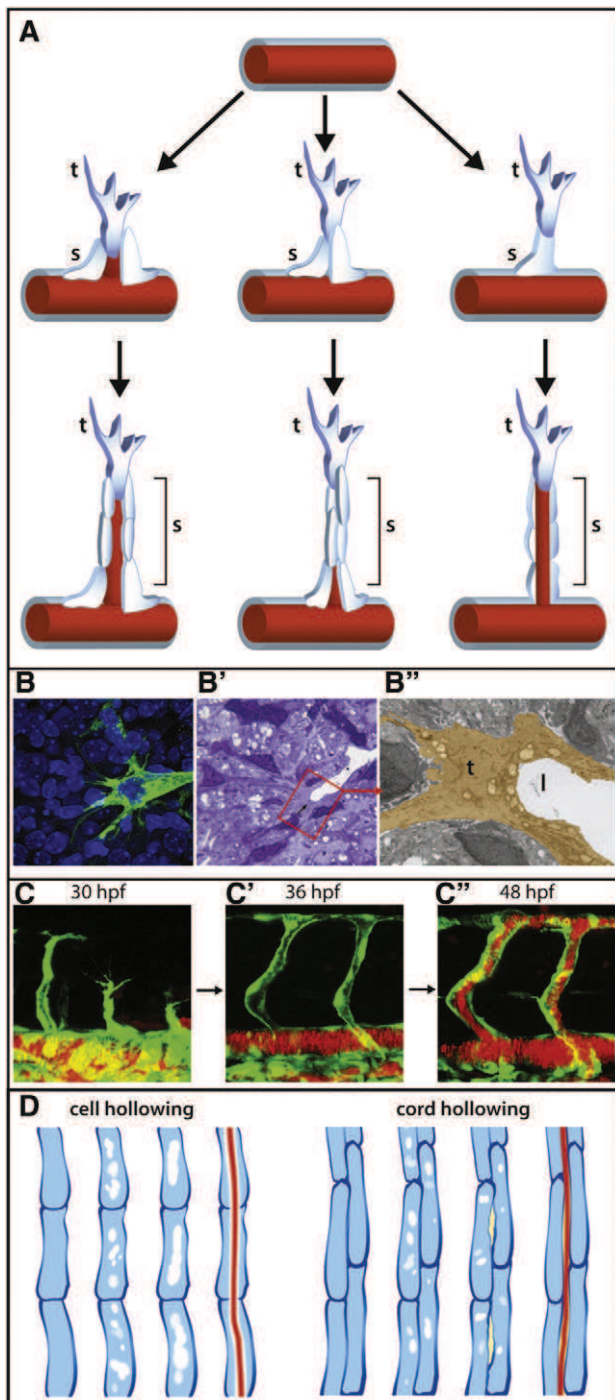


**Fig. 4.** Different morphogenetic mechanisms that underlie sprouting angiogenesis. (A) Three examples for the cellular organization of an angiogenic sprout. Depending on how the cells are arranged in the sprout, different types of vessels may form. Left: Branching morphogenesis by budding. ECs remain epithelial, while the sprout grows via cell division within the stalk. The lumen remains open and continuous at all times. Middle: Formation of a multicellular tube by cord hollowing. This shows an example, where cells grow in a paired configuration maintaining an apical surface in between. The lumen remains open at the base but is closed in distal region. Close to the tip, cells may be of a more mesenchymal character and undergo cell divisions. Cellular rearrangements will then lead to a continuous apical surface and open up the luminal space. Right: Formation of a unicellular tube with an intracellular lumen. At the tip of a capillary, the lumen may also form within a string of cells. The cells hollow out by vacuole formation followed by exocytosis. This mode of lumen formation will generate a so-called intracellular lumen. (B) Lumen formation behind the leading tip cell in the mouse retina. The lumen of the nascent sprout extends to the tip of the growing sprout. This situation is in agreement with the configuration shown in panel A. Isolectin B4 labeling (green) of an endothelial tip cell projecting long filopodia. Nuclei, Dapi, blue (B). Semithin (B') and close up of ultrathin (B'') en face section of the sprouting front in the retina illustrating continuous lumen formation (l) just behind the tip cell (t). The endothelial tip cell in panel C is pseudocolored brown. Figure courtesy of Denise Stenzel and Holger Gerhardt, London Research Institute—Cancer Research UK. © Gerhardt et al., 2003. Originally published in *J. Cell Biol.* doi:10.1083/jcb.200302047. (C) Lumen formation in the ISV and DLAV of a zebrafish embryo. During scaffold formation, neither ISV nor DLAV are perfused, suggesting that the lumen is formed subsequently. Blood flow is initiated after subsequent remodeling and establishment of the intersegmental veins (compare to Fig. 3). Confocal still pictures from an in vivo time-lapse movie of a transgenic zebrafish embryo (*TG:fl1a:EGFP<sup>fl1</sup>;gata1:DsRed<sup>sd2</sup>*). ECs are labeled in green; erythrocytes are labeled in red. (D) Alternate models of lumen formation in the zebrafish ISV. Depending on the cellular arrangement of cells in an angiogenic sprout, de novo lumen formation can occur in at least two different ways. If cells are arranged in a serial fashion, the lumen may be generated by cell hollowing (left, see also A). In this process, ECs pinocytose solutes from extracellular space and form vacuoles that coalesce and fuse to give rise to an intracellular lumen. Eventually intracellular vacuoles of neighboring cells will fuse by exocytosis and form a patent lumen (see Kamei et al., 2006). Alternatively, if cells are arranged in a paired fashion, they may form a lumen by cord hollowing (right, see also A). This process requires establishment of a continuous apical surface that is bounded by at least two ECs. Vacuoles can then be exocytosed into this intercellular space, which will eventually become the vascular lumen.



distal (Kamei et al., 2006). Because vacuole formation and fusion has long been considered an important component of lumen formation, the stepwise expansion of luminal space was interpreted as a succession of vacuolar fusion events that generate a unicellular tube containing an intracellular lumen (Kamei et al., 2006; Fig. 4D). Capillaries that contain intracellular lumens have indeed been described (Bar et al., 1984) and have been called “seamless tubes” because they are characterized by the absence of cell junctions along the longitudinal axis of the vessel. More recently, analyses of cell junctions within nascent sprouts and patent ISVs showed that the cells in the stalk overlap extensively along the proximodistal axis and that ISVs are multicellular tubes containing an extracellular lumen (Blum et al., 2008). This cellular configuration is more consistent with a lumen formation process by cord hollowing (Fig. 4D). In this model, cells in the stalk rearrange to form a continuous apical surface. The lumen is then formed by a process, in which small pre-luminal spaces (rather than vacuoles) are formed by exocytosis and/or paracellular influx of liquids. The stepwise opening of the lumen from the direction of the aorta would then be consistent with the completion of cell rearrangements in the stalk. The events described here would be quite comparable to those described above for the lumen formation in the dorsal aorta.

The three mechanisms discussed here are not necessarily mutually exclusive. For example, it is possible that sprouting angiogenesis contains aspects of both, budding and chord hollowing, depending on the extent to which apical–basal polarity is maintained in the stalk cells. Likewise, it is possible that a single blood vessel contains regions of intracellular as well as regions of extracellular lumen. Taken together, it is clear that different vessels can form by various morphogenetic mechanisms. It remains to be explored what the decisive factors are that determine which mechanism is used. It is likely that parameters such as vessel caliber, blood pressure of the parental vessel as well as cell number within the sprout play important roles.

#### *Guidance cues along the way—endothelial pathfinding*

To effectively oxygenate a given organ, blood vessels have to be evenly distributed within this tissue. This can be achieved in different ways, for example by controlling the number of angiogenic sprouts that are generated (e.g. ISV) or by the formation of a plexus (e.g. retinal vasculature in the mouse), which is then remodeled by a pruning process. In recent years, a number of ligands (and their respective receptors) that provide endothelial guidance cues have been described, including the Semaphorin, Netrin, Ephrin and Slit systems (reviewed by Larrivée et al., 2009). Interestingly, these signals were originally described as cues for axonal growth cones (reviewed by Eichmann et al., 2005). It has become clear since that many of the signaling pathways that act during axonal pathfinding are also employed for guidance of angiogenic sprouts.

In the zebrafish, the guidance of angiogenic sprouts is best studied during SA formation. Segmental arteries sprout from the DA at the intersomitic boundary; as they grow out, they follow the intersomitic fissure up to the horizontal myoseptum, from where they change their path to grow more or less straight to the dorsal roof of the neural tube. The exit point of intersegmental sprouts is regulated by molecular guidance cues. In *out of bounds* (*obd*) mutants, angiogenic sprouts form ectopically along the ventral somite border (Childs et al., 2002). Furthermore, these sprouts no longer avoid the ventral somite and the ISVs take on a plexus-like organization. Molecular analyses showed that *obd* encodes the receptor PlexinD1 that is expressed in ECs and interacts with the ligands SEMA3A1/2, which is expressed in ventral somites. Upon ligand binding, a repulsive signal is activated in the ECs prohibiting them from moving into the somite region (Torres-Vázquez, 2004). Recently, it has been shown that the interaction of different Plexins and Semaphorins is also important for the timing of SA sprout formation (Lamont et al., 2009).

Analyses in mouse have uncovered an additional and quite different molecular mechanism that limits the number of sprouts. Bautch and coworkers have shown that a soluble form of FLT-1 (VEGFR-1), sFLT-1, is secreted from ECs adjacent to the forming sprout (Chappell et al., 2009). This isoform is able to bind VEGF, thereby removing it from the environment surrounding the sprout. It is thought that sFLT-1 serves two purposes: it ensures the ordered formation of sprouts from an activated endothelium and it prevents the early sprout to connect back to its original vessel.

The sharing of attracting and repulsive signaling pathways by neurons and ECs appears to be a common theme. In fact, it has been shown that growing neurons and nascent capillaries can walk the same tracks (Mukouyama et al., 2002). It will be interesting to see whether in these instances neurons and ECs simply use the same cues provided by the stromal cells or whether they also navigate by direct cell–cell interactions. It is noteworthy that not only the tip cell but also stalk cells appear to express guidance receptors albeit at lower levels (Larrivée et al., 2009). In zebrafish, for example, the guidance receptor *PlexinD1* is expressed at comparable levels in the tip and the stalk of nascent SA (Torres-Vázquez et al., 2004). This raises the possibility that also stalk cells are involved in angiogenic pathfinding. Indeed, it appears that the tip cell fate is not fixed and that cells at the stalk can become tip cells and vice versa. In murine allantoic explant cultures, migratory ECs are passing each other at the tip (Perryn et al., 2008). In a similar fashion, ECs are changing lead during the outgrowth of vascular cords that sprout from differentiating murine embryonic stem cells (Holger Gerhardt, personal communication). It has been suggested that these tip cell turnovers are regulated by oscillations in Notch signaling along the vascular sprout (Phng and Gerhardt, 2009). It should be noted that these vascular cords are not perfused during early outgrowth and are, in that respect, similar to developing SAs rather than vessels in the postnatal mouse retina.

#### *Cell–cell adhesion during sprouting angiogenesis*

The above observations indicate that the angiogenic sprout is highly plastic with regard to signaling events and cell–cell interactions and that cellular rearrangements play an important role in blood vessel morphogenesis. It is generally believed that cellular rearrangements involve remodeling of intercellular junctions (Baer et al., 2009). In *Drosophila*, adherens junctions play an important role for cellular rearrangement during various processes, such as border cell migration or tracheal morphogenesis (Pacquelet and Rørth, 2005; Ribeiro et al., 2004). In the case of border cell migration very different cell behaviors, invasive cell migration and cell adhesion require DE-cadherin. These distinct cellular activities are mediated by homophilic interactions of DE-cadherin between different cell types: interactions among border cells maintain cohesion of the migratory cells while interactions between border cells and nurse cells allow invasive migration into the substratum (Niewiadomska et al., 1999). The role of VE-cadherin during vertebrate angiogenesis is less clear. Mice that are mutant for VE-cadherin die at mid-gestation exhibiting vascular defects that are consistent with a role for VE-cadherin in maintaining vascular integrity (Carmeliet et al., 1999; Crosby, 2005). Further in vitro analyses have also emphasized a role of VE-cadherin in endothelial cell survival and stabilizing the endothelium, in part by antagonizing VEGFR-2 signaling (reviewed by Lampugnani and Dejana, 2007; Vestweber et al., 2009). Recent organotypic cell culture and knockdown experiments in zebrafish point at a role of VE-cadherin in angiogenic sprouting (Abraham et al., 2009). In these studies, quiescent endothelial tubes did not respond to VEGF stimulation unless VE-cadherin function was reduced. They further showed that VE-cadherin suppresses sprouting by inhibiting VEGFR-2/RAC1 signaling. In the zebrafish ISV, knockdown of VE-cadherin led to the formation of ectopic “branch points” along the proximo-

distal axis of the ISV, which were interpreted as prolonged angiogenic behavior of the ECs within the ISV.

While the above results suggest an anti-angiogenic function, other studies indicate a more pro-angiogenic role for VE-cadherin. As discussed above, blood vessel formation is a very dynamic process involving cell rearrangements and cell migration. These dynamics have been studied using murine allantoic explant cultures, which allow to measure the migration of individual and groups of ECs in a process called vasculogenic sprouting, which involves the outgrowth of multicellular sprouts from a primary plexus (Perryn et al., 2008; Rupp et al., 2004). ECs actively migrate over the substrate, frequently passing each other during outgrowth of the vascular rod. These rearrangements are effectively inhibited by addition of a VE-cadherin blocking antibody (Perryn et al., 2008), indicating that VE-cadherin is required for cellular rearrangements as they occur during vasculogenic sprouting. In zebrafish, we have observed that VE-cadherin is also essential for cellular rearrangements during SA formation (H.-G. Belting and M. Affolter, unpublished observation). Therefore, it appears that in addition to functions in vascular integrity and cell survival, VE-cadherin is also involved in sprouting angiogenesis. One can easily imagine that, analogous to the role of DE-cadherin in border cell migration, VE-cadherin may fulfill dual functions at the same time: maintenance of cell–cell contacts and cellular rearrangements.

### Conclusions and perspectives

Blood vessel formation includes a spectrum of different morphogenetic processes such as budding, cord hollowing, cell hollowing, cell wrapping and intussusception. The genetic and molecular bases, which initiate and control these different processes is not known. It is clear, however, that ECs of different vascular beds are different in their gene expression profile and that blood vessels are anatomically highly diverse (Rocha and Adams, 2009). Morphogenesis may also be influenced by extraneous factors such as diverse extracellular matrices and signals, shear stress due to blood pressure or differences in cell number (Aird, 2007; Nguyen et al., 2006; Sottile, 2004).

The morphogenetic events that underlie blood vessel formation are likely to determine the way a vessel ultimately lumenizes. During sprouting angiogenesis, larger vessels appear to extend their lumens in conjunction with the outgrowing sprout, while small capillaries may form their lumens de novo by cell hollowing or cord hollowing. The respective contribution to lumen formation in different vessels remains to be determined.

Elaboration of the vascular tree requires additional processes, such as vessel fusion and pruning. How these processes occur at the morphogenetic level has not yet been described in much detail. With regard to vessel fusion, one can envisage that cellular remodeling plays a major role. Furthermore, it is likely that the fusion process occurs differently depending on vessel type. In the zebrafish, the DLAVs form in a non-perfused state and blood circulation commences subsequently. Recently, VE-cadherin localization during DLAV formation revealed that cells from adjacent sprouts undergo extensive rearrangements (Blum et al., 2008). Initial contacts between neighboring sprouts require VE-cadherin, as knockdown of VE-cadherin function leads to slowed-down formation of cell–cell contacts (Montero-Balaguer et al., 2009). It will be interesting to examine the exact cellular mechanisms that drive vessel fusion during DLAV formation and compare them with those occurring in perfused vessels.

### Acknowledgments

The authors wish to thank Ralf Adams, Victoria Bautch, Holger Gerhardt, Eckhard Lammert, Stefan Schulte-Merker and Arndt Siekmann for interesting discussions and two anonymous referees for very helpful comments on the original manuscript. This work has

been supported by the Kantons Basel-Stadt and Basel-Land, and by the Swiss National Science Foundation. A.L. and A.K. are supported by fellowships from the Werner Siemens-Foundation (Zug).

### References

- Abraham, S., Yeo, M., Montero-Balaguer, M., Paterson, H., Dejana, E., Marshall, C.J., Mavria, G., 2009. VE-cadherin-mediated cell–cell interaction suppresses sprouting via signaling to MLC2 phosphorylation. *Curr. Biol.* 19, 1–7.
- Adams, R.H., Alitalo, K., 2007. Molecular regulation of angiogenesis and lymphangiogenesis. *Nat. Rev., Mol. Cell Biol.* 8, 464–478.
- Adams, R.H., Wilkinson, G.A., Weiss, C., Diella, F., Gale, N.W., Deutsch, U., Risau, W., Klein, R., 1999. Roles of ephrinB ligands and EphB receptors in cardiovascular development: demarcation of arterial/venous domains, vascular morphogenesis, and sprouting angiogenesis. *Genes Dev.* 13, 295–306.
- Aird, W.C., 2007. Phenotypic heterogeneity of the endothelium: II. Representative vascular beds. *Circ. Res.* 100, 174–190.
- Andrew, D., Ewald, A., 2010. Morphogenesis of epithelial tubes: Insights into tube formation, elongation, and elaboration. *Dev. Biol.* 341, 66–83.
- Armulik, A., Abramsson, A., Betsholtz, C., 2005. Endothelial/pericyte interactions. *Circ. Res.* 97, 512–523.
- Ausprunk, D.H., Folkman, J., 1977. Migration and proliferation of endothelial cells in preformed and newly formed blood vessels during tumor angiogenesis. *Microvasc. Res.* 14, 53–65.
- Baer, M.M., Chanut-Delalande, H., Affolter, M., 2009. Cellular and molecular mechanisms underlying the formation of biological tubes. *Curr. Top. Dev. Biol.* 89, 137–162.
- Bahary, N., Goishi, K., Stuckenzol, C., Weber, G., Leblanc, J., Schafer, C.A., Berman, S.S., Klagsbrun, M., Zon, L.I., 2007. Duplicate VegfA genes and orthologues of the KDR receptor tyrosine kinase family mediate vascular development in the zebrafish. *Blood* 110, 3627–3636.
- Bar, T., Guldner, F.H., Wolff, J.R., 1984. “Seamless” endothelial cells of blood capillaries. *Cell Tissue Res.* 235, 99–106.
- Beis, D., Stainier, D.Y.R., 2006. In vivo cell biology: following the zebrafish trend. *Trends Cell Biol.* 16, 105–112.
- Blum, Y., Belting, H.-G., Ellertsdóttir, E., Herwig, L., Lüders, F., Affolter, M., 2008. Complex cell rearrangements during intersegmental vessel sprouting and vessel fusion in the zebrafish embryo. *Dev. Biol.* 316, 312–322.
- Carmeliet, P., 2003. Angiogenesis in health and disease. *Nat. Med.* 9, 653–660.
- Carmeliet, P., Lampugnani, M.G., Moons, L., Brevario, F., Compernelle, V., Bono, F., Balconi, G., Spagnuolo, R., Oosthuysen, B., Dewerchin, M., Zanetti, A., Angellilo, A., Matot, V., Nuyens, D., Lutgens, E., Clotman, F., de Ruiter, M.C., Gittenberger-de Groot, A., Poelmann, R., Lupu, F., Herbert, J.M., Collen, D., Dejana, E., 1999. Targeted deficiency or cytosolic truncation of the VE-cadherin gene in mice impairs VEGF-mediated endothelial survival and angiogenesis. *Cell* 98, 147–157.
- Cébe-Suarez, S., Zehnder-Fjällman, A., Ballmer-Hofer, K., 2006. The role of VEGF receptors in angiogenesis; complex partnerships. *Cell. Mol. Life Sci.* 63, 601–615.
- Cermenati, S., Moleri, S., Cimbro, S., Corti, P., Del Giacco, L., Amodeo, R., Dejana, E., Koopman, P., Cotelli, F., Beltrame, M., 2008. Sox18 and Sox7 play redundant roles in vascular development. *Blood* 111, 2657–2666.
- Chappell, J.C., Taylor, S.M., Ferrara, N., Bautch, V., 2009. Local guidance of emerging vessel sprouts requires soluble Flt-1 (VEGFR-1). *Dev. Cell* 1–40.
- Childs, S., Chen, J.-N., Garrity, D.M., Fishman, M.C., 2002. Patterning of angiogenesis in the zebrafish embryo. *Development* 129, 973–982.
- Coffin, J.D., Poole, T.J., 1988. Embryonic vascular development: immunohistochemical identification of the origin and subsequent morphogenesis of the major vessel primordia in quail embryos. *Development* 102, 735–748.
- Coffin, J.D., Poole, T.J., 1991. Endothelial cell origin and migration in embryonic heart and cranial blood vessel development. *Anat. Rec.* 231, 383–395.
- Covassin, L.D., Villefranc, J.A., Kacergis, M.C., Weinstein, B.M., Lawson, N.D., 2006. Distinct genetic interactions between multiple Vegf receptors are required for development of different blood vessel types in zebrafish. *Proc. Natl. Acad. Sci. U. S. A.* 103, 6554–6559.
- Covassin, L.D., Siekmann, A.F., Kacergis, M.C., Laver, E., Moore, J.C., Villefranc, J.A., Weinstein, B.M., Lawson, N.D., 2009. A genetic screen for vascular mutants in zebrafish reveals dynamic roles for Vegf/Plc1 signaling during artery development. *Dev. Biol.* 329, 212–226.
- Crosby, C.V., 2005. VE-cadherin is not required for the formation of nascent blood vessels but acts to prevent their disassembly. *Blood* 105, 2771–2776.
- De Val, S., Black, B.L., 2009. Transcriptional control of endothelial cell development. *Dev. Cell* 16, 180–195.
- De Val, S., Chi, N.C., Meadows, S.M., Minovitsky, S., Anderson, J.P., Harris, I.S., Ehlers, M.L., Agarwal, P., Visel, A., Xu, S.-M., Pennacchio, L.A., Dubchak, I., Krieg, P.A., Stainier, D.Y.R., Black, B.L., 2008. Combinatorial regulation of endothelial gene expression by ETS and forkhead transcription factors. *Cell* 135, 1053–1064.
- Detrich, H.W., Kieran, M.W., Chan, F.Y., Barone, L.M., Yee, K., Rundstadler, J.A., Pratt, S., Ransom, D., Zon, L.I., 1995. Intraembryonic hematopoietic cell migration during vertebrate development. *Proc. Natl. Acad. Sci. U.S.A.* 92, 10713–10717.
- Dooley, K., Davidson, A., Zon, L., 2005. Zebrafish functions independently in hematopoietic and endothelial development. *Dev. Biol.* 277, 522–536.
- Eichmann, A., Yuan, L., Moyon, D., Lenoble, F., Pardanauer, L., Breat, C., 2005. Vascular development: from precursor cells to branched arterial and venous networks. *Int. J. Dev. Biol.* 49, 259–267.
- Eriksson, J., Löfberg, J., 2000. Development of the hypochord and dorsal aorta in the zebrafish embryo (*Danio rerio*). *J. Morphol.* 244, 167–176.

- Folkman, J., 1982. Angiogenesis: initiation and control. *Ann. N.Y. Acad. Sci.* 401, 212–227.
- Gerhardt, H., Golding, M., Fruttiger, M., Ruhrberg, C., Lundkvist, A., Abramsson, A., Jeltsch, M., Mitchell, C., Alitalo, K., Shimada, D., Betsholtz, C., 2003. VEGF guides angiogenic sprouting utilizing endothelial tip cell filopodia. *J. Cell Biol.* 161, 1163–1177.
- Gering, M., Rodaway, A.R., Göttgens, B., Patient, R.K., Green, A.R., 1998. The SCL gene specifies haemangioblast development from early mesoderm. *EMBO J.* 17, 4029–4045.
- Habeck, H., Odenthal, J., Walderich, B., Maischein, H., Schulte-Merker, S., consortium, T.s., 2002. Analysis of a zebrafish VEGF receptor mutant reveals specific disruption of angiogenesis. *Curr. Biol.* 12, 1405–1412.
- Hellström, M., Phng, L.-K., Hofmann, J.J., Wallgard, E., Coultas, L., Lindblom, P., Alva, J., Nilsson, A.-K., Karlsson, L., Gaiano, N., Yoon, K., Rossant, J., Iruela-Arispe, M.L., Kalén, M., Gerhardt, H., Betsholtz, C., 2007. Dll4 signalling through Notch1 regulates formation of tip cells during angiogenesis. *Nature* 445, 776–780.
- Herbert, S.P., Huisken, J., Kim, T.N., Feldman, M.E., Houseman, B.T., Wang, R.A., Shokat, K.M., Stainier, D.Y.R., 2009. Arterial-venous segregation by selective cell sprouting: an alternative mode of blood vessel formation. *Science* 326, 294–298.
- Hirakow, R., Hiruma, T., 1981. Scanning electron microscopic study on the development of primitive blood vessels in chick embryos at the early somite-stage. *Anat. Embryol. (Berl.)* 163, 299–306.
- Hogan, B.L., Kolodziej, P.A., 2002. Organogenesis: molecular mechanisms of tubulogenesis. *Nat. Rev., Genet.* 3, 513–523.
- Hogan, B.M., Bos, F.L., Bussmann, J., Witte, M., Chi, N.C., Duckers, H.J., Schulte-Merker, S., 2009. Ccbe1 is required for embryonic lymphangiogenesis and venous sprouting. *Nat. Genet.* 41, 396–398.
- Hogan, B.M., Robert, H., Witte, M., Heloterä, H., Alitalo, K., Duckers, H.J., Schulte-Merker, S., 2009. Vegfc/Flt4 signalling is suppressed by Dll4 in developing zebrafish intersegmental arteries. *Development* 136, 4001–4009.
- Huisken, J., Stainier, D.Y.R., 2009. Selective plane illumination microscopy techniques in developmental biology. *Development* 136, 1963–1975.
- Isogai, S., 2003. Angiogenic network formation in the developing vertebrate trunk. *Development* 130, 5281–5290.
- Isogai, S., Horiguchi, M., Weinstein, B.M., 2001. The vascular anatomy of the developing zebrafish: an atlas of embryonic and early larval development. *Dev. Biol.* 230, 278–301.
- Isogai, S., Lawson, N.D., Torrealday, S., Horiguchi, M., Weinstein, B.M., 2003. Angiogenic network formation in the developing vertebrate trunk. *Development* 130, 5281–5290.
- Jin, S., Herzog, W., Santoro, M., Mitchell, T., Frantsve, J., Jungblut, B., Beis, D., Scott, I., Damico, L., Ober, E., 2007. A transgene-assisted genetic screen identifies essential regulators of vascular development in vertebrate embryos. *Dev. Biol.* 307, 29–42.
- Jin, S.-W., Beis, D., Mitchell, T., Chen, J.-N., Stainier, D.Y.R., 2005. Cellular and molecular analyses of vascular tube and lumen formation in zebrafish. *Development* 132, 5199–5209.
- Kamei, M., Saunders, W.B., Bayless, K.J., Dye, L., Davis, G.E., Weinstein, B.M., 2006. Endothelial tubes assemble from intracellular vacuoles in vivo. *Nature* 442, 453–456.
- Kemp, H.A., Cooke, J.E., Moens, C.B., 2009. EphA4 and EfnB2a maintain rhombomere coherence by independently regulating intercalation of progenitor cells in the zebrafish neural keel. *Dev. Biol.* 327, 313–326.
- Kimmel, C.B., Ballard, W.W., Kimmel, S.R., Ullmann, B., Schilling, T.F., 1995. Stages of embryonic development of the zebrafish. *Dev. Dyn.* 203, 253–310.
- Kucera, T., Eglinger, J., Strlic, B., Lammert, E., 2007. Vascular lumen formation from a cell biological perspective. *Novartis Found. Symp.* 283, 46–56 discussion 56–60, 238–241.
- Küchler, A.M., Gjini, E., Peterson-Maduro, J., Cancilla, B., Wolburg, H., Schulte-Merker, S., 2006. Development of the zebrafish lymphatic system requires VEGFC signaling. *Curr. Biol.* 16, 1244–1248.
- Lamont, R., Lamont, E., Childs, S., 2009. Antagonistic interactions among Plexins regulate the timing of intersegmental vessel formation. *Dev. Biol.* 331, 199–209.
- Lampugnani, M.G., Dejana, E., 2007. Adherens junctions in endothelial cells regulate vessel maintenance and angiogenesis. *Thromb. Res.* 120 (Suppl 2), S1–S6.
- Larivière, B., Freitas, C., Suchting, S., Brunet, I., Eichmann, A., 2009. Guidance of vascular development: lessons from the nervous system. *Circ. Res.* 104, 428–441.
- Lawson, N.D., Weinstein, B.M., 2002a. Arteries and veins: making a difference with zebrafish. *Nat. Rev., Genet.* 3, 674–682.
- Lawson, N.D., Weinstein, B.M., 2002b. In vivo imaging of embryonic vascular development using transgenic zebrafish. *Dev. Biol.* 248, 307–318.
- Lawson, N.D., Scheer, N., Pham, V.N., Kim, C.H., Chitnis, A.B., Campos-Ortega, J.A., Weinstein, B.M., 2001. Notch signaling is required for arterial-venous differentiation during embryonic vascular development. *Development* 128, 3675–3683.
- Lawson, N.D., Vogel, A.M., Weinstein, B.M., 2002. Sonic hedgehog and vascular endothelial growth factor act upstream of the Notch pathway during arterial endothelial differentiation. *Dev. Cell* 3, 127–136.
- Lawson, N.D., Mugford, J.W., Diamond, B.A., Weinstein, B.M., 2003. Phospholipase C gamma-1 is required downstream of vascular endothelial growth factor during arterial development. *Genes Dev.* 17, 1346–1351.
- Leslie, J.D., Ariza-Mcnaughton, L., Bermange, A.L., Mcadow, R., Johnson, S.L., Lewis, J., 2007. Endothelial signalling by the Notch ligand Delta-like 4 restricts angiogenesis. *Development* 134, 839–844.
- Liao, E.C., Paw, B.H., Oates, A.C., Pratt, S.J., Postlethwait, J.H., Zon, L.L., 1998. SCL/Tal-1 transcription factor acts downstream of cloche to specify hematopoietic and vascular progenitors in zebrafish. *Genes Dev.* 12, 621–626.
- Liu, F., Patient, R., 2008. Genome-wide analysis of the zebrafish ETS family identifies three genes required for hemangioblast differentiation or angiogenesis. *Circ. Res.* 103, 1147–1154.
- Lubarsky, B., Krasnow, M.A., 2003. Tube morphogenesis: making and shaping biological tubes. *Cell* 112, 19–28.
- Makanya, A., Hlushchuk, R., Djonov, V., 2009. Intussusceptive angiogenesis and its role in vascular morphogenesis, patterning, and remodeling. *Angiogenesis* 12, 113–123.
- Matsumoto, T., Mugishima, H., 2006. Signal transduction via vascular endothelial growth factor (VEGF) receptors and their roles in atherosclerosis. *J. Atheroscler. Thromb.* 13, 130–135.
- Meier, S., 1980. Development of the chick embryo mesoblast: pronephros, lateral plate, and early vasculature. *J. Embryol. Exp. Morphol.* 55, 291–306.
- Mellitzer, G., Xu, Q., Wilkinson, D.G., 1999. Eph receptors and ephrins restrict cell intermingling and communication. *Nature* 400, 77–81.
- Montero-Balaguer, M., Swirsding, K., Orsenigo, F., Cotelli, F., Mione, M., Dejana, E., 2009. Stable vascular connections and remodeling require full expression of VE-cadherin in zebrafish embryos. *PLoS ONE* 4, e5772.
- Mukoyama, Y.-s., Shin, D., Britsch, S., Taniguchi, M., Anderson, D.J., 2002. Sensory nerves determine the pattern of arterial differentiation and blood vessel branching in the skin. *Cell* 109, 693–705.
- Nasevicius, A., Larson, J., Ekker, S.C., 2000. Distinct requirements for zebrafish angiogenesis revealed by a VEGF-A morphant. *Yeast* 17, 294–301.
- Nguyen, T.-H., Eichmann, A., Le Noble, F., Fleury, V., 2006. Dynamics of vascular branching morphogenesis: the effect of blood and tissue flow. *Phys. Rev., E, Stat. Nonlinear Soft Matter Phys.* 73, 061907.
- Niewiadomska, P., Godt, D., Tepass, U., 1999. DE-cadherin is required for intercellular motility during *Drosophila* oogenesis. *J. Cell Biol.* 144, 533–547.
- Nikolova, G., Lammert, E., 2003. Interdependent development of blood vessels and organs. *Cell Tissue Res.* 314, 33–42.
- Olsson, A.-K., Dimberg, A., Kreuger, J., Claesson-Welsh, L., 2006. VEGF receptor signalling—in control of vascular function. *Nat. Rev., Mol. Cell Biol.* 7, 359–371.
- Pacquelet, A., Rørth, P., 2005. Regulatory mechanisms required for DE-cadherin function in cell migration and other types of adhesion. *J. Cell Biol.* 170, 803–812.
- Patan, S., 2000. Vasculogenesis and angiogenesis as mechanisms of vascular network formation, growth and remodeling. *J. Neuro-oncol.* 50, 1–15.
- Patterson, L.J., Gering, M., Eckfeldt, C.E., Green, A.R., Verfaillie, C.M., Ekker, S.C., Patient, R., 2007. The transcription factors Scl and Lmo2 act together during development of the hemangioblast in zebrafish. *Blood* 109, 2389–2398.
- Pendeville, H., Winandy, M., Manfroid, I., Nivelles, O., Motte, P., Pasque, V., Peers, B., Struman, I., Martial, J.A., Voz, M.L., 2008. Zebrafish Sox7 and Sox18 function together to control arterial-venous identity. *Dev. Biol.* 317, 405–416.
- Perryn, E.D., Czirik, A., Little, C.D., 2008. Vascular sprout formation entails tissue deformations and VE-cadherin-dependent cell-autonomous motility. *Dev. Biol.* 313, 545–555.
- Phng, L.-K., Gerhardt, H., 2009. Angiogenesis: a team effort coordinated by Notch. *Dev. Cell* 16, 196–208.
- Poole, T.J., Coffin, J.D., 1989. Vasculogenesis and angiogenesis: two distinct morphogenetic mechanisms establish embryonic vascular pattern. *J. Exp. Zool.* 251, 224–231.
- Red-Horse, K., Crawford, Y., Shojai, F., Ferrara, N., 2007. Endothelium-microenvironment interactions in the developing embryo and in the adult. *Dev. Cell* 12, 181–194.
- Ribeiro, C., Neumann, M., Affolter, M., 2004. Genetic control of cell intercalation during tracheal morphogenesis in *Drosophila*. *Curr. Biol.* 14, 2197–2207.
- Risau, W., 1995. Differentiation of endothelium. *FASEB J.* 9, 926–933.
- Risau, W., Sariola, H., Zerwes, H.G., Sasse, J., Ekblom, P., Kemler, R., Doetschman, T., 1988. Vasculogenesis and angiogenesis in embryonic-stem-cell-derived embryoid bodies. *Development* 102, 471–478.
- Rocha, S., Adams, R., 2009. Molecular differentiation and specialization of vascular beds. *Angiogenesis* 12, 139–147.
- Roman, B.L., Pham, V.N., Lawson, N.D., Kulik, M., Childs, S., Lekven, A.C., Garrity, D.M., Moon, R.T., Fishman, M.C., Lechleider, R.J., Weinstein, B.M., 2002. Disruption of acvr1l1 increases endothelial cell number in zebrafish cranial vessels. *Development* 129, 3009–3019.
- Ruhrberg, C., Gerhardt, H., Golding, M., Watson, R., Ioannidou, S., Fujisawa, H., Betsholtz, C., Shima, D.T., 2002. Spatially restricted patterning cues provided by heparin-binding VEGF-A control blood vessel branching morphogenesis. *Genes Dev.* 16, 2684–2698.
- Rupp, P.A., Czirik, A., Little, C.D., 2004. alpha5beta3 integrin-dependent endothelial cell dynamics in vivo. *Development* 131, 2887–2897.
- Sakaguchi, T.F., Sadler, K.C., Crosnier, C., Stainier, D.Y.R., 2008. Endothelial signals modulate hepatocyte apical-basal polarization in zebrafish. *Curr. Biol.* 18, 1565–1571.
- Shibuya, M., Claesson-Welsh, L., 2006. Signal transduction by VEGF receptors in regulation of angiogenesis and lymphangiogenesis. *Exp. Cell Res.* 312, 549–560.
- Siekmann, A.F., Lawson, N.D., 2007. Notch signalling limits angiogenic cell behaviour in developing zebrafish arteries. *Nature* 445, 781–784.
- Siekmann, A.F., Covassin, L., Lawson, N.D., 2008. Modulation of VEGF signalling output by the Notch pathway. *BioEssays* 30, 303–313.
- Siekmann, A.F., Standley, C., Fogarty, K.E., Wolfe, S.A., Lawson, N.D., 2009. Chemokine signaling guides regional patterning of the first embryonic artery. *Genes Dev.* 23, 2272–2277.
- Sottile, J., 2004. Regulation of angiogenesis by extracellular matrix. *Biochim. Biophys. Acta* 1654, 13–22.
- Stainier, D.Y., Weinstein, B.M., Detrich III, H.W., Zon, L.L., Fishman, M.C., 1995. Cloche, an early acting zebrafish gene, is required by both the endothelial and hematopoietic lineages. *Development* 121, 3141–3150.

- Strilić, B., Kucera, T., Eglinger, J., Hughes, M.R., McNagny, K.M., Tsukita, S., Dejana, E., Ferrara, N., Lammert, E., 2009. The molecular basis of vascular lumen formation in the developing mouse aorta. *Dev. Cell* 17, 505–515.
- Suchting, S., Freitas, C., Le Noble, F., Benedito, R., Bréant, C., Duarte, A., Eichmann, A., 2007. The Notch ligand Delta-like 4 negatively regulates endothelial tip cell formation and vessel branching. *Proc. Natl. Acad. Sci. U.S.A.* 104, 3225–3230.
- Tammela, T., Zarkada, G., Wallgard, E., Murtomäki, A., Suchting, S., Wirzenius, M., Waltari, M., Hellström, M., Schomber, T., Peltonen, R., Freitas, C., Duarte, A., Isoniemi, H., Laakkonen, P., Christofori, G., Ylä-Herttuala, S., Shibuya, M., Pytowski, B., Eichmann, A., Betsholtz, C., Alitalo, K., 2008. Blocking VEGFR-3 suppresses angiogenic sprouting and vascular network formation. *Nature* 454, 656–660.
- Thisse, C., 2002. Organogenesis—heart and blood formation from the zebrafish point of view. *Science* 295, 457–462.
- Thompson, M.A., Ransom, D.G., Pratt, S.J., MacLennan, H., Kieran, M.W., Detrich, H.W., Vail, B., Huber, T.L., Paw, B., Brownlie, A.J., Oates, A.C., Fritz, A., Gates, M.A., Amores, A., Bahary, N., Talbot, W.S., Her, H., Beier, D.R., Postlethwait, J.H., Zon, L.L., 1998. The cloche and spadetail genes differentially affect hematopoiesis and vasculogenesis. *Dev. Biol.* 197, 248–269.
- Torres-Vazquez, J., 2004. Semaphorin-plexin signaling guides patterning of the developing vasculature. *Dev. Cell* 7, 117–123.
- Torres-Vázquez, J., Gitler, A.D., Fraser, S.D., Berk, J.D., Pham, V.N., Fishman, M.C., Childs, S., Epstein, J.A., Weinstein, B.M., 2004. Semaphorin-plexin signaling guides patterning of the developing vasculature. *Dev. Cell* 7, 117–123.
- Vestweber, D., Winderlich, M., Cagna, G., Nottebaum, A.F., 2009. Cell adhesion dynamics at endothelial junctions: VE-cadherin as a major player. *Trends Cell Biol.* 19, 8–15.
- Walls, J.R., Coultas, L., Rossant, J., Henkelman, R.M., 2008. Three-dimensional analysis of vascular development in the mouse embryo. *PLoS ONE* 3, e2853.
- Yamazaki, Y., Morita, T., 2006. Molecular and functional diversity of vascular endothelial growth factors. *Mol. Divers.* 10, 515–527.
- Yaniv, K., Isogai, S., Castranova, D., Dye, L., Hitomi, J., Weinstein, B.M., 2006. Live imaging of lymphatic development in the zebrafish. *Nat. Med.* 12, 711–716.
- Zhong, T.P., Childs, S., Leu, J.P., Fishman, M.C., 2001. Gridlock signalling pathway fashions the first embryonic artery. *Nature* 414, 216–220.
- Zon, L.L., Mather, C., Burgess, S., Bolce, M.E., Harland, R.M., Orkin, S.H., 1991. Expression of GATA-binding proteins during embryonic development in *Xenopus laevis*. *Proc. Natl. Acad. Sci. U. S. A.* 88, 10642–10646.



## 10 References

**Abraham, S., Yeo, M., Montero-Balaguer, M., Paterson, H., Dejana, E., Marshall, C. J. and Mavria, G.** (2009). VE-Cadherin-mediated cell-cell interaction suppresses sprouting via signaling to MLC2 phosphorylation. *Curr Biol* **19**, 668-74.

**Adams, R. H. and Alitalo, K.** (2007). Molecular regulation of angiogenesis and lymphangiogenesis. *Nat Rev Mol Cell Biol* **8**, 464-78.

**Andrew, D. J. and Ewald, A. J.** (2010). Morphogenesis of epithelial tubes: Insights into tube formation, elongation, and elaboration. *Dev Biol* **341**, 34-55.

**Armer, H. E., Mariggi, G., Png, K. M., Genoud, C., Monteith, A. G., Bushby, A. J., Gerhardt, H. and Collinson, L. M.** (2009). Imaging transient blood vessel fusion events in zebrafish by correlative volume electron microscopy. *PLoS One* **4**, e7716.

**Asakawa, K., Suster, M. L., Mizusawa, K., Nagayoshi, S., Kotani, T., Urasaki, A., Kishimoto, Y., Hibi, M. and Kawakami, K.** (2008). Genetic dissection of neural circuits by Tol2 transposon-mediated Gal4 gene and enhancer trapping in zebrafish. *Proc Natl Acad Sci U S A* **105**, 1255-60.

**Augustin, H. G., Koh, G. Y., Thurston, G. and Alitalo, K.** (2009). Control of vascular morphogenesis and homeostasis through the angiopoietin-Tie system. *Nat Rev Mol Cell Biol* **10**, 165-77.

**Ausprunk, D. H. and Folkman, J.** (1977). Migration and proliferation of endothelial cells in preformed and newly formed blood vessels during tumor angiogenesis. *Microvasc Res* **14**, 53-65.

**Baer, M. M., Chanut-Delalande, H. and Affolter, M.** (2009). Cellular and molecular mechanisms underlying the formation of biological tubes. *Curr Top Dev Biol* **89**, 137-62.

**Baker, J. and Garrod, D.** (1993). Epithelial cells retain junctions during mitosis. *J Cell Sci* **104** ( Pt 2), 415-25.

**Bar, T., Guldner, F. H. and Wolff, J. R.** (1984). "Seamless" endothelial cells of blood capillaries. *Cell Tissue Res* **235**, 99-106.

**Bayless, K. J. and Davis, G. E.** (2002). The Cdc42 and Rac1 GTPases are required for capillary lumen formation in three-dimensional extracellular matrices. *J Cell Sci* **115**, 1123-36.

**Bayless, K. J., Salazar, R. and Davis, G. E.** (2000). RGD-dependent vacuolation and lumen formation observed during endothelial cell morphogenesis in three-dimensional fibrin matrices involves the alpha(v)beta(3) and alpha(5)beta(1) integrins. *Am J Pathol* **156**, 1673-83.

**Bazzoni, G. and Dejana, E.** (2004). Endothelial cell-to-cell junctions: molecular organization and role in vascular homeostasis. *Physiol Rev* **84**, 869-901.

- Blum, Y., Belting, H. G., Ellertsdottir, E., Herwig, L., Luders, F. and Affolter, M.** (2008). Complex cell rearrangements during intersegmental vessel sprouting and vessel fusion in the zebrafish embryo. *Dev Biol* **316**, 312-22.
- Bryant, D. M., Datta, A., Rodriguez-Fraticelli, A. E., Peranen, J., Martin-Belmonte, F. and Mostov, K. E.** (2010). A molecular network for de novo generation of the apical surface and lumen. *Nat Cell Biol* **12**, 1035-45.
- Bryant, D. M. and Mostov, K. E.** (2008). From cells to organs: building polarized tissue. *Nat Rev Mol Cell Biol* **9**, 887-901.
- Carmeliet, P.** (2005). Angiogenesis in life, disease and medicine. *Nature* **438**, 932-6.
- Carmeliet, P., Ferreira, V., Breier, G., Pollefeyt, S., Kieckens, L., Gertsenstein, M., Fahrig, M., Vandenhoek, A., Harpal, K., Eberhardt, C. et al.** (1996). Abnormal blood vessel development and lethality in embryos lacking a single VEGF allele. *Nature* **380**, 435-9.
- Carmeliet, P., Lampugnani, M. G., Moons, L., Breviario, F., Compernelle, V., Bono, F., Balconi, G., Spagnuolo, R., Oosthuysen, B., Dewerchin, M. et al.** (1999). Targeted deficiency or cytosolic truncation of the VE-cadherin gene in mice impairs VEGF-mediated endothelial survival and angiogenesis. *Cell* **98**, 147-57.
- Caussinus, E., Colombelli, J. and Affolter, M.** (2008). Tip-cell migration controls stalk-cell intercalation during *Drosophila* tracheal tube elongation. *Curr Biol* **18**, 1727-34.
- Chappell, J. C., Taylor, S. M., Ferrara, N. and Bautch, V. L.** (2009). Local guidance of emerging vessel sprouts requires soluble Flt-1. *Dev Cell* **17**, 377-86.
- Childs, S., Chen, J. N., Garrity, D. M. and Fishman, M. C.** (2002). Patterning of angiogenesis in the zebrafish embryo. *Development* **129**, 973-82.
- Cleaver, O. and Krieg, P. A.** (1998). VEGF mediates angioblast migration during development of the dorsal aorta in *Xenopus*. *Development* **125**, 3905-14.
- Colas, J. F. and Schoenwolf, G. C.** (2001). Towards a cellular and molecular understanding of neurulation. *Dev Dyn* **221**, 117-45.
- Coultas, L., Chawengsaksophak, K. and Rossant, J.** (2005). Endothelial cells and VEGF in vascular development. *Nature* **438**, 937-45.
- Covassin, L. D., Villefranc, J. A., Kacergis, M. C., Weinstein, B. M. and Lawson, N. D.** (2006). Distinct genetic interactions between multiple Vegf receptors are required for development of different blood vessel types in zebrafish. *Proc Natl Acad Sci U S A* **103**, 6554-9.
- Davis, G. E. and Bayless, K. J.** (2003). An integrin and Rho GTPase-dependent pinocytotic vacuole mechanism controls capillary lumen formation in collagen and fibrin matrices. *Microcirculation* **10**, 27-44.

- Davis, G. E. and Camarillo, C. W.** (1996). An alpha 2 beta 1 integrin-dependent pinocytic mechanism involving intracellular vacuole formation and coalescence regulates capillary lumen and tube formation in three-dimensional collagen matrix. *Exp Cell Res* **224**, 39-51.
- Dejana, E., Tournier-Lasserre, E. and Weinstein, B. M.** (2009). The control of vascular integrity by endothelial cell junctions: molecular basis and pathological implications. *Dev Cell* **16**, 209-21.
- Del Toro, R., Prahst, C., Mathivet, T., Siegfried, G., Kaminker, J. S., Larrivee, B., Breant, C., Duarte, A., Takakura, N., Fukamizu, A. et al.** (2010). Identification and functional analysis of endothelial tip cell-enriched genes. *Blood* **116**, 4025-33.
- Djonov, V. G., Kurz, H. and Burri, P. H.** (2002). Optimality in the developing vascular system: branching remodeling by means of intussusception as an efficient adaptation mechanism. *Dev Dyn* **224**, 391-402.
- Dong, B., Horie, T., Denker, E., Kusakabe, T., Tsuda, M., Smith, W. C. and Jiang, D.** (2009). Tube formation by complex cellular processes in *Ciona intestinalis* notochord. *Dev Biol* **330**, 237-49.
- Dyson, S. E., Jones, D. G. and Kendrick, W. L.** (1976). Some observations on the ultrastructure of developing rat cerebral capillaries. *Cell Tissue Res* **173**, 529-42.
- Eichmann, A., Le Noble, F., Autiero, M. and Carmeliet, P.** (2005). Guidance of vascular and neural network formation. *Curr Opin Neurobiol* **15**, 108-15.
- Ellertsdottir, E., Lenard, A., Blum, Y., Krudewig, A., Herwig, L., Affolter, M. and Belting, H. G.** (2010). Vascular morphogenesis in the zebrafish embryo. *Dev Biol* **341**, 56-65.
- Fantin, A., Vieira, J. M., Gestri, G., Denti, L., Schwarz, Q., Prykhodzhiy, S., Peri, F., Wilson, S. W. and Ruhrberg, C.** (2010). Tissue macrophages act as cellular chaperones for vascular anastomosis downstream of VEGF-mediated endothelial tip cell induction. *Blood* **116**, 829-40.
- Ferrara, N., Carver-Moore, K., Chen, H., Dowd, M., Lu, L., O'Shea, K. S., Powell-Braxton, L., Hillan, K. J. and Moore, M. W.** (1996). Heterozygous embryonic lethality induced by targeted inactivation of the VEGF gene. *Nature* **380**, 439-42.
- Ferrara, N., Gerber, H. P. and LeCouter, J.** (2003). The biology of VEGF and its receptors. *Nat Med* **9**, 669-76.
- Fischer, R. S., Gardel, M., Ma, X., Adelstein, R. S. and Waterman, C. M.** (2009). Local cortical tension by myosin II guides 3D endothelial cell branching. *Curr Biol* **19**, 260-5.
- Fish, J. E., Santoro, M. M., Morton, S. U., Yu, S., Yeh, R. F., Wythe, J. D., Ivey, K. N., Bruneau, B. G., Stainier, D. Y. and Srivastava, D.** (2008). miR-126 regulates angiogenic signaling and vascular integrity. *Dev Cell* **15**, 272-84.
- Folkman, J.** (1971). Tumor angiogenesis: therapeutic implications. *N Engl J Med* **285**, 1182-6.

- Folkman, J.** (1982). Angiogenesis: initiation and control. *Ann N Y Acad Sci* **401**, 212-27.
- Fong, G. H., Rossant, J., Gertsenstein, M. and Breitman, M. L.** (1995). Role of the Flt-1 receptor tyrosine kinase in regulating the assembly of vascular endothelium. *Nature* **376**, 66-70.
- Fraisl, P., Mazzone, M., Schmidt, T. and Carmeliet, P.** (2009). Regulation of angiogenesis by oxygen and metabolism. *Dev Cell* **16**, 167-79.
- Gaengel, K., Genove, G., Armulik, A. and Betsholtz, C.** (2009). Endothelial-mural cell signaling in vascular development and angiogenesis. *Arterioscler Thromb Vasc Biol* **29**, 630-8.
- Gerhardt, H., Golding, M., Fruttiger, M., Ruhrberg, C., Lundkvist, A., Abramsson, A., Jeltsch, M., Mitchell, C., Alitalo, K., Shima, D. et al.** (2003). VEGF guides angiogenic sprouting utilizing endothelial tip cell filopodia. *J Cell Biol* **161**, 1163-77.
- Gering, M., Rodaway, A. R., Gottgens, B., Patient, R. K. and Green, A. R.** (1998). The SCL gene specifies haemangioblast development from early mesoderm. *Embo J* **17**, 4029-45.
- Gibson, M. C., Patel, A. B., Nagpal, R. and Perrimon, N.** (2006). The emergence of geometric order in proliferating metazoan epithelia. *Nature* **442**, 1038-41.
- Gu, C., Yoshida, Y., Livet, J., Reimert, D. V., Mann, F., Merte, J., Henderson, C. E., Jessell, T. M., Kolodkin, A. L. and Ginty, D. D.** (2005). Semaphorin 3E and plexin-D1 control vascular pattern independently of neuropilins. *Science* **307**, 265-8.
- Gupta, S., Zhu, H., Zon, L. I. and Evans, T.** (2006). BMP signaling restricts hemato-vascular development from lateral mesoderm during somitogenesis. *Development* **133**, 2177-87.
- Hanze, J., Weissmann, N., Grimminger, F., Seeger, W. and Rose, F.** (2007). Cellular and molecular mechanisms of hypoxia-inducible factor driven vascular remodeling. *Thromb Haemost* **97**, 774-87.
- Hellstrom, M., Phng, L. K., Hofmann, J. J., Wallgard, E., Coultas, L., Lindblom, P., Alva, J., Nilsson, A. K., Karlsson, L., Gaiano, N. et al.** (2007). Dll4 signalling through Notch1 regulates formation of tip cells during angiogenesis. *Nature* **445**, 776-80.
- Herbert, S. P., Huisken, J., Kim, T. N., Feldman, M. E., Houseman, B. T., Wang, R. A., Shokat, K. M. and Stainier, D. Y.** (2009). Arterial-venous segregation by selective cell sprouting: an alternative mode of blood vessel formation. *Science* **326**, 294-8.
- Hiratsuka, S., Nakao, K., Nakamura, K., Katsuki, M., Maru, Y. and Shibuya, M.** (2005). Membrane fixation of vascular endothelial growth factor receptor 1 ligand-binding domain is important for vasculogenesis and angiogenesis in mice. *Mol Cell Biol* **25**, 346-54.



- Hogan, B. M., Bos, F. L., Bussmann, J., Witte, M., Chi, N. C., Duckers, H. J. and Schulte-Merker, S.** (2009a). *Ccbe1* is required for embryonic lymphangiogenesis and venous sprouting. *Nat Genet* **41**, 396-8.
- Hogan, B. M., Herpers, R., Witte, M., Helotera, H., Alitalo, K., Duckers, H. J. and Schulte-Merker, S.** (2009b). *Vegfc/Flt4* signalling is suppressed by *Dll4* in developing zebrafish intersegmental arteries. *Development* **136**, 4001-9.
- Hotta, K., Yamada, S., Ueno, N., Satoh, N. and Takahashi, H.** (2007). Brachyury-downstream notochord genes and convergent extension in *Ciona intestinalis* embryos. *Dev Growth Differ* **49**, 373-82.
- Isogai, S., Horiguchi, M. and Weinstein, B. M.** (2001). The vascular anatomy of the developing zebrafish: an atlas of embryonic and early larval development. *Dev Biol* **230**, 278-301.
- Isogai, S., Lawson, N. D., Torrealday, S., Horiguchi, M. and Weinstein, B. M.** (2003). Angiogenic network formation in the developing vertebrate trunk. *Development* **130**, 5281-90.
- Jakobsson, L., Franco, C. A., Bentley, K., Collins, R. T., Ponsioen, B., Aspalter, I. M., Rosewell, I., Busse, M., Thurston, G., Medvinsky, A. et al.** (2010). Endothelial cells dynamically compete for the tip cell position during angiogenic sprouting. *Nat Cell Biol* **12**, 943-53.
- Jazwinska, A., Ribeiro, C. and Affolter, M.** (2003). Epithelial tube morphogenesis during *Drosophila* tracheal development requires Piopio, a luminal ZP protein. *Nat Cell Biol* **5**, 895-901.
- Jin, S. W., Beis, D., Mitchell, T., Chen, J. N. and Stainier, D. Y.** (2005). Cellular and molecular analyses of vascular tube and lumen formation in zebrafish. *Development* **132**, 5199-209.
- Kakihara, K., Shinmyozu, K., Kato, K., Wada, H. and Hayashi, S.** (2008). Conversion of plasma membrane topology during epithelial tube connection requires Arf-like 3 small GTPase in *Drosophila*. *Mech Dev* **125**, 325-36.
- Kamei, M., Saunders, W. B., Bayless, K. J., Dye, L., Davis, G. E. and Weinstein, B. M.** (2006). Endothelial tubes assemble from intracellular vacuoles in vivo. *Nature* **442**, 453-6.
- Kametani, Y. and Takeichi, M.** (2007). Basal-to-apical cadherin flow at cell junctions. *Nat Cell Biol* **9**, 92-8.
- Karkkainen, M. J., Haiko, P., Sainio, K., Partanen, J., Taipale, J., Petrova, T. V., Jeltsch, M., Jackson, D. G., Talikka, M., Rauvala, H. et al.** (2004). Vascular endothelial growth factor C is required for sprouting of the first lymphatic vessels from embryonic veins. *Nat Immunol* **5**, 74-80.
- Kim, Y. H. and Raphael, Y.** (2007). Cell division and maintenance of epithelial integrity in the deafened auditory epithelium. *Cell Cycle* **6**, 612-9.

- Lalor, P. F., Lai, W. K., Curbishley, S. M., Shetty, S. and Adams, D. H.** (2006). Human hepatic sinusoidal endothelial cells can be distinguished by expression of phenotypic markers related to their specialised functions in vivo. *World J Gastroenterol* **12**, 5429-39.
- Lamont, R. E., Lamont, E. J. and Childs, S. J.** (2009). Antagonistic interactions among Plexins regulate the timing of intersegmental vessel formation. *Dev Biol* **331**, 199-209.
- Lampugnani, M. G., Orsenigo, F., Gagliani, M. C., Tacchetti, C. and Dejana, E.** (2006). Vascular endothelial cadherin controls VEGFR-2 internalization and signaling from intracellular compartments. *J Cell Biol* **174**, 593-604.
- Lawson, N. D., Scheer, N., Pham, V. N., Kim, C. H., Chitnis, A. B., Campos-Ortega, J. A. and Weinstein, B. M.** (2001). Notch signaling is required for arterial-venous differentiation during embryonic vascular development. *Development* **128**, 3675-83.
- Lawson, N. D., Vogel, A. M. and Weinstein, B. M.** (2002). sonic hedgehog and vascular endothelial growth factor act upstream of the Notch pathway during arterial endothelial differentiation. *Dev Cell* **3**, 127-36.
- Lawson, N. D. and Weinstein, B. M.** (2002a). Arteries and veins: making a difference with zebrafish. *Nat Rev Genet* **3**, 674-82.
- Lawson, N. D. and Weinstein, B. M.** (2002b). In vivo imaging of embryonic vascular development using transgenic zebrafish. *Dev Biol* **248**, 307-18.
- Lee, S. and Kolodziej, P. A.** (2002). Short Stop provides an essential link between F-actin and microtubules during axon extension. *Development* **129**, 1195-204.
- Lejmi, E., Leconte, L., Pedron-Mazoyer, S., Ropert, S., Raoul, W., Lavalette, S., Bouras, I., Feron, J. G., Maitre-Boube, M., Assayag, F. et al.** (2008). Netrin-4 inhibits angiogenesis via binding to neogenin and recruitment of Unc5B. *Proc Natl Acad Sci U S A* **105**, 12491-6.
- Leslie, J. D., Ariza-McNaughton, L., Bermange, A. L., McAdow, R., Johnson, S. L. and Lewis, J.** (2007). Endothelial signalling by the Notch ligand Delta-like 4 restricts angiogenesis. *Development* **134**, 839-44.
- Leung, D. W., Cachianes, G., Kuang, W. J., Goeddel, D. V. and Ferrara, N.** (1989). Vascular endothelial growth factor is a secreted angiogenic mitogen. *Science* **246**, 1306-9.
- Liao, E. C., Paw, B. H., Oates, A. C., Pratt, S. J., Postlethwait, J. H. and Zon, L. I.** (1998). SCL/Tal-1 transcription factor acts downstream of cloche to specify hematopoietic and vascular progenitors in zebrafish. *Genes Dev* **12**, 621-6.
- Liao, W., Bisgrove, B. W., Sawyer, H., Hug, B., Bell, B., Peters, K., Grunwald, D. J. and Stainier, D. Y.** (1997). The zebrafish gene cloche acts upstream of a flk-1 homologue to regulate endothelial cell differentiation. *Development* **124**, 381-9.
- Liu, Y., Cox, S. R., Morita, T. and Kourembanas, S.** (1995). Hypoxia regulates vascular endothelial growth factor gene expression in endothelial cells. Identification of a 5' enhancer. *Circ Res* **77**, 638-43.

- Lobov, I. B., Renard, R. A., Papadopoulos, N., Gale, N. W., Thurston, G., Yancopoulos, G. D. and Wiegand, S. J.** (2007). Delta-like ligand 4 (Dll4) is induced by VEGF as a negative regulator of angiogenic sprouting. *Proc Natl Acad Sci U S A* **104**, 3219-24.
- Lohela, M., Bry, M., Tammela, T. and Alitalo, K.** (2009). VEGFs and receptors involved in angiogenesis versus lymphangiogenesis. *Curr Opin Cell Biol* **21**, 154-65.
- Lu, X., Le Noble, F., Yuan, L., Jiang, Q., De Lafarge, B., Sugiyama, D., Breant, C., Claes, F., De Smet, F., Thomas, J. L. et al.** (2004). The netrin receptor UNC5B mediates guidance events controlling morphogenesis of the vascular system. *Nature* **432**, 179-86.
- Lubarsky, B. and Krasnow, M. A.** (2003). Tube morphogenesis: making and shaping biological tubes. *Cell* **112**, 19-28.
- Lucitti, J. L., Jones, E. A., Huang, C., Chen, J., Fraser, S. E. and Dickinson, M. E.** (2007). Vascular remodeling of the mouse yolk sac requires hemodynamic force. *Development* **134**, 3317-26.
- Makanya, A. N., Hlushchuk, R. and Djonov, V. G.** (2009). Intussusceptive angiogenesis and its role in vascular morphogenesis, patterning, and remodeling. *Angiogenesis* **12**, 113-23.
- Metzger, R. J., Klein, O. D., Martin, G. R. and Krasnow, M. A.** (2008). The branching programme of mouse lung development. *Nature* **453**, 745-50.
- Montero-Balaguer, M., Swirsding, K., Orsenigo, F., Cotelli, F., Mione, M. and Dejana, E.** (2009). Stable vascular connections and remodeling require full expression of VE-cadherin in zebrafish embryos. *PLoS One* **4**, e5772.
- Nicoli, S., Standley, C., Walker, P., Hurlstone, A., Fogarty, K. E. and Lawson, N. D.** (2010). MicroRNA-mediated integration of haemodynamics and Vegf signalling during angiogenesis. *Nature* **464**, 1196-200.
- Olsson, A. K., Dimberg, A., Kreuger, J. and Claesson-Welsh, L.** (2006). VEGF receptor signalling - in control of vascular function. *Nat Rev Mol Cell Biol* **7**, 359-71.
- Park, K. W., Crouse, D., Lee, M., Karnik, S. K., Sorensen, L. K., Murphy, K. J., Kuo, C. J. and Li, D. Y.** (2004). The axonal attractant Netrin-1 is an angiogenic factor. *Proc Natl Acad Sci U S A* **101**, 16210-5.
- Parker, L. H., Schmidt, M., Jin, S. W., Gray, A. M., Beis, D., Pham, T., Frantz, G., Palmieri, S., Hillan, K., Stainier, D. Y. et al.** (2004). The endothelial-cell-derived secreted factor Egfl7 regulates vascular tube formation. *Nature* **428**, 754-8.
- Perryn, E. D., Czirok, A. and Little, C. D.** (2008). Vascular sprout formation entails tissue deformations and VE-cadherin-dependent cell-autonomous motility. *Dev Biol* **313**, 545-55.
- Phng, L. K., Potente, M., Leslie, J. D., Babbage, J., Nyqvist, D., Lobov, I., Ondr, J. K., Rao, S., Lang, R. A., Thurston, G. et al.** (2009). Nrarp coordinates endothelial Notch and Wnt signaling to control vessel density in angiogenesis. *Dev Cell* **16**, 70-82.

- Proulx, K., Lu, A. and Sumanas, S.** (2010). Cranial vasculature in zebrafish forms by angioblast cluster-derived angiogenesis. *Dev Biol* **348**, 34-46.
- Rasmussen, J. P., English, K., Tenlen, J. R. and Priess, J. R.** (2008). Notch signaling and morphogenesis of single-cell tubes in the *C. elegans* digestive tract. *Dev Cell* **14**, 559-69.
- Ribeiro, C., Neumann, M. and Affolter, M.** (2004). Genetic control of cell intercalation during tracheal morphogenesis in *Drosophila*. *Curr Biol* **14**, 2197-207.
- Riesen, F. K., Rothen-Rutishauser, B. and Wunderli-Allenspach, H.** (2002). A ZO1-GFP fusion protein to study the dynamics of tight junctions in living cells. *Histochem Cell Biol* **117**, 307-15.
- Risau, W. and Flamme, I.** (1995). Vasculogenesis. *Annu Rev Cell Dev Biol* **11**, 73-91.
- Ruhrberg, C., Gerhardt, H., Golding, M., Watson, R., Ioannidou, S., Fujisawa, H., Betsholtz, C. and Shima, D. T.** (2002). Spatially restricted patterning cues provided by heparin-binding VEGF-A control blood vessel branching morphogenesis. *Genes Dev* **16**, 2684-98.
- Saharinen, P., Bry, M. and Alitalo, K.** (2010). How do angiopoietins Tie in with vascular endothelial growth factors? *Curr Opin Hematol* **17**, 198-205.
- Samakovlis, C., Hacohen, N., Manning, G., Sutherland, D. C., Guillemin, K. and Krasnow, M. A.** (1996a). Development of the *Drosophila* tracheal system occurs by a series of morphologically distinct but genetically coupled branching events. *Development* **122**, 1395-407.
- Samakovlis, C., Manning, G., Steneberg, P., Hacohen, N., Cantera, R. and Krasnow, M. A.** (1996b). Genetic control of epithelial tube fusion during *Drosophila* tracheal development. *Development* **122**, 3531-6.
- Satchell, S. C. and Braet, F.** (2009). Glomerular endothelial cell fenestrations: an integral component of the glomerular filtration barrier. *Am J Physiol Renal Physiol* **296**, F947-56.
- Senger, D. R., Galli, S. J., Dvorak, A. M., Perruzzi, C. A., Harvey, V. S. and Dvorak, H. F.** (1983). Tumor cells secrete a vascular permeability factor that promotes accumulation of ascites fluid. *Science* **219**, 983-5.
- Siekman, A. F. and Lawson, N. D.** (2007). Notch signalling limits angiogenic cell behaviour in developing zebrafish arteries. *Nature* **445**, 781-4.
- Siekman, A. F., Standley, C., Fogarty, K. E., Wolfe, S. A. and Lawson, N. D.** (2009). Chemokine signaling guides regional patterning of the first embryonic artery. *Genes Dev* **23**, 2272-7.
- Stone, C. E., Hall, D. H. and Sundaram, M. V.** (2009). Lipocalin signaling controls unicellular tube development in the *Caenorhabditis elegans* excretory system. *Dev Biol* **329**, 201-11.



- Strilic, B., Eglinger, J., Krieg, M., Zeeb, M., Axnick, J., Babal, P., Muller, D. J. and Lammert, E.** (2010). Electrostatic Cell-Surface Repulsion Initiates Lumen Formation in Developing Blood Vessels. *Curr Biol*.
- Strilic, B., Kucera, T., Eglinger, J., Hughes, M. R., McNagny, K. M., Tsukita, S., Dejana, E., Ferrara, N. and Lammert, E.** (2009). The molecular basis of vascular lumen formation in the developing mouse aorta. *Dev Cell* **17**, 505-15.
- Suchting, S., Freitas, C., le Noble, F., Benedito, R., Breant, C., Duarte, A. and Eichmann, A.** (2007). The Notch ligand Delta-like 4 negatively regulates endothelial tip cell formation and vessel branching. *Proc Natl Acad Sci U S A* **104**, 3225-30.
- Swift, M. R. and Weinstein, B. M.** (2009). Arterial-venous specification during development. *Circ Res* **104**, 576-88.
- Takai, Y., Miyoshi, J., Ikeda, W. and Ogita, H.** (2008). Nectins and nectin-like molecules: roles in contact inhibition of cell movement and proliferation. *Nat Rev Mol Cell Biol* **9**, 603-15.
- Tammela, T., Zarkada, G., Wallgard, E., Murtomaki, A., Suchting, S., Wirzenius, M., Waltari, M., Hellstrom, M., Schomber, T., Peltonen, R. et al.** (2008). Blocking VEGFR-3 suppresses angiogenic sprouting and vascular network formation. *Nature* **454**, 656-60.
- Tanaka-Matakatsu, M., Uemura, T., Oda, H., Takeichi, M. and Hayashi, S.** (1996). Cadherin-mediated cell adhesion and cell motility in *Drosophila* trachea regulated by the transcription factor Escargot. *Development* **122**, 3697-705.
- Tawk, M., Araya, C., Lyons, D. A., Reugels, A. M., Girdler, G. C., Bayley, P. R., Hyde, D. R., Tada, M. and Clarke, J. D.** (2007). A mirror-symmetric cell division that orchestrates neuroepithelial morphogenesis. *Nature* **446**, 797-800.
- Torres-Vazquez, J., Gitler, A. D., Fraser, S. D., Berk, J. D., Van, N. P., Fishman, M. C., Childs, S., Epstein, J. A. and Weinstein, B. M.** (2004). Semaphorin-plexin signaling guides patterning of the developing vasculature. *Dev Cell* **7**, 117-23.
- Uemura, T., Oda, H., Kraut, R., Hayashi, S., Kotaoka, Y. and Takeichi, M.** (1996). Zygotic *Drosophila* E-cadherin expression is required for processes of dynamic epithelial cell rearrangement in the *Drosophila* embryo. *Genes Dev* **10**, 659-71.
- van Hinsbergh, V. W. and Koolwijk, P.** (2008). Endothelial sprouting and angiogenesis: matrix metalloproteinases in the lead. *Cardiovasc Res* **78**, 203-12.
- Vogeli, K. M., Jin, S. W., Martin, G. R. and Stainier, D. Y.** (2006). A common progenitor for haematopoietic and endothelial lineages in the zebrafish gastrula. *Nature* **443**, 337-9.
- Walls, J. R., Coultas, L., Rossant, J. and Henkelman, R. M.** (2008). Three-dimensional analysis of vascular development in the mouse embryo. *PLoS One* **3**, e2853.
- Wang, H. U., Chen, Z. F. and Anderson, D. J.** (1998). Molecular distinction and angiogenic interaction between embryonic arteries and veins revealed by ephrin-B2 and its receptor Eph-B4. *Cell* **93**, 741-53.

- Wang, S., Aurora, A. B., Johnson, B. A., Qi, X., McAnally, J., Hill, J. A., Richardson, J. A., Bassel-Duby, R. and Olson, E. N.** (2008). The endothelial-specific microRNA miR-126 governs vascular integrity and angiogenesis. *Dev Cell* **15**, 261-71.
- Wang, Y., Kaiser, M. S., Larson, J. D., Nasevicius, A., Clark, K. J., Wadman, S. A., Roberg-Perez, S. E., Ekker, S. C., Hackett, P. B., McGrail, M. et al.** (2010). Moesin1 and Ve-cadherin are required in endothelial cells during in vivo tubulogenesis. *Development* **137**, 3119-28.
- Warga, R. M., Kane, D. A. and Ho, R. K.** (2009). Fate mapping embryonic blood in zebrafish: multi- and unipotential lineages are segregated at gastrulation. *Dev Cell* **16**, 744-55.
- Wolff, J.** (1964). [on the Possibilities of Capillary Stricture in the Central Nervous System. Electron-Microscopic Study on the Cerebral Cortex of the Rabbit.]. *Z Zellforsch Mikrosk Anat* **63**, 593-611.
- Wolff, J. R. and Bar, T.** (1972). 'Seamless' endothelia in brain capillaries during development of the rat's cerebral cortex. *Brain Res* **41**, 17-24.
- Yana, I., Sagara, H., Takaki, S., Takatsu, K., Nakamura, K., Nakao, K., Katsuki, M., Taniguchi, S., Aoki, T., Sato, H. et al.** (2007). Crosstalk between neovessels and mural cells directs the site-specific expression of MT1-MMP to endothelial tip cells. *J Cell Sci* **120**, 1607-14.
- Yaniv, K., Isogai, S., Castranova, D., Dye, L., Hitomi, J. and Weinstein, B. M.** (2006). Live imaging of lymphatic development in the zebrafish. *Nat Med* **12**, 711-6.
- You, L. R., Lin, F. J., Lee, C. T., DeMayo, F. J., Tsai, M. J. and Tsai, S. Y.** (2005). Suppression of Notch signalling by the COUP-TFII transcription factor regulates vein identity. *Nature* **435**, 98-104.
- Zeng, G., Taylor, S. M., McColm, J. R., Kappas, N. C., Kearney, J. B., Williams, L. H., Hartnett, M. E. and Bautch, V. L.** (2007). Orientation of endothelial cell division is regulated by VEGF signaling during blood vessel formation. *Blood* **109**, 1345-52.
- Zhang, Y., Singh, M. K., Degenhardt, K. R., Lu, M. M., Bennett, J., Yoshida, Y. and Epstein, J. A.** (2009). Tie2Cre-mediated inactivation of plexinD1 results in congenital heart, vascular and skeletal defects. *Dev Biol* **325**, 82-93.
- Zhong, T. P., Childs, S., Leu, J. P. and Fishman, M. C.** (2001). Gridlock signalling pathway fashions the first embryonic artery. *Nature* **414**, 216-20.
- Zhong, T. P., Rosenberg, M., Mohideen, M. A., Weinstein, B. and Fishman, M. C.** (2000). gridlock, an HLH gene required for assembly of the aorta in zebrafish. *Science* **287**, 1820-4.

# Curriculum Vitae

Yannick Ernst Henri Blum

Email: [yannick.blum@stud.unibas.ch](mailto:yannick.blum@stud.unibas.ch)

## PERSONAL INFORMATION

Date of Birth: 01. Dezember 1981

Place of Birth: Basel

Citizenship: Schwitzerland

## EDUCATION

- 2006-2010 PhD student in Markus Affolter's lab at the Biocentre University of Basel. Title of Thesis: Cellular Mechanisms During Vascular Development
- 2005-2006 Master of Science in Molecular Biology at the Biocentre University of Basel (supervised by Prof. Markus Affolter) Title: Development of the intersegmental vessel in the zebrafish: an analysis at the cellular level.
- 2003-2005 Bachelor of Science in Biology (Major in Integrative Biology)
- 2001-2003 Chemistry study at the ETH in Zürich with completion of two pre-degrees
- 1992-2001 Higher education entrance qualification Type C at GKG (Gymnasium Kirschgarten)

## CERTIFICATE AND QUALIFICATIONS

LTK Modul1: Einführung in die Labortierkunde (animal course). Successfully completed at the Institut für Labortierkunde der Univeristät Zürich.

## Languages

German: fluently

French: fluently

English: fluently

## Computer skills

Windows XP, Vista, 7  
MS Office  
Adobe Illustrator, Photoshop

## PUBLICATIONS

Complex cell rearrangements during intersegmental vessel sprouting and vessel fusion in the zebrafish embryo.

**Blum Y**, Belting HG, Ellertsdottir E, Herwig L, Lüders F, Affolter M.

Regulation of cardiovascular development and integrity by the heart of glass-cerebral cavernous malformation protein pathway.

Kleaveland B, Zheng X, Liu JJ, **Blum Y**, Tung JJ, Zou Z, Sweeney SM, Chen M, Guo L, Lu MM, Zhou D, Kitajewski J, Affolter M, Ginsberg MH, Kahn ML.

A noncoding antisense RNA in tie-1 locus regulates tie-1 function in vivo.

Li K, **Blum Y**, Verma A, Liu Z, Pramanik K, Leigh NR, Chun CZ, Samant GV, Zhao B, Garnaas MK, Horswill MA, Stanhope SA, North PE, Miao RQ, Wilkinson GA, Affolter M, Ramchandran R.

Vascular morphogenesis in the zebrafish embryo.

Ellertsdóttir E, Lenard A, **Blum Y**, Krudewig A, Herwig L, Affolter M, Belting HG.